SECRET
Un clas

Studies in Radar Cross - Sections - XVIII

Airborne Passive Measures and Countermeasures (Offense with, and Defense Against, Bomber Decoys (S))

by K. M. Siegel, M. L. Barasch, J. W. Crispin, R. F. Goodrich, A. H. Halpin, A. L. Maffett, W. C. Orthwein, C. E. Schensted, and C. J. Titus.

Contract AF 33 (616) - 2531
December 1955
2260-29-F

2260-29-F = RL-2047

The University of Michigan
Engineering Research Institute
Willow Run Laboratories
Willow Run Airport
Ypsilanti, Michigan

Un clas
SECRET

STUDIES IN RADAR CROSS-SECTIONS

I Scattering by a Prolate Spheroid, F.V. Schultz (UMM-42, March 1950), W(038)-ac-14222. UNCLASSIFIED

II The Zeros of the Associated Legendre Functions $P_n^m(\mu')$ of Non-Integral Degree, K.M. Siegel, D.M. Brown, H.E. Hunter, H.A. Alperin, and C.W. Quillen (UMM-82, April 1951), W-33(038)-ac-14222. UNCLASSIFIED

III Scattering by a Cone, K.M. Siegel and H.A. Alperin (UMM-87, January 1952), AF 30(602)-9. UNCLASSIFIED

IV Comparison Between Theory and Experiment of the Cross-Section of a Cone, K.M. Siegel, H.A. Alperin, J.W. Crispin, H.E. Hunter, R.E. Kleinman, W.C. Orthwein, and C.E. Schensted (UMM-92, February 1953), AF 30(602)-9. UNCLASSIFIED

V An Examination of Bistatic Early Warning Radars, K.M. Siegel (UMM-98, August 1952), W-33(038)-ac-14222. SECRET

VI Cross-Sections of Corner Reflectors and Other Multiple Scatterers at Microwave Frequencies, R.R. Bonkowski, C.R. Lubitz, and C.E. Schensted (UMM-106, October 1953), AF 30(602)-9. SECRET (UNCLASSIFIED when Appendix is removed)

VII Summary of Radar Cross-Section Studies Under Project Wizard, K.M. Siegel, J.W. Crispin, and R.E. Kleinman (UMM-108, November 1952), W-33(038)-ac-14222. SECRET

VIII Theoretical Cross-Sections as a Function of Separation Angle Between Transmitter and Receiver at Small Wavelengths, K.M. Siegel, H.A. Alperin, R.R. Bonkowski, J.W. Crispin, A.L. Maffett, C.E. Schensted, and I.V. Schensted (UMM-115, October 1953), W-33(038)-ac-14222. UNCLASSIFIED

IX Electromagnetic Scattering by an Oblate Spheroid, L.M. Rauch (UMM-116, October 1953), AF 30(602)-9. UNCLASSIFIED

X The Radar Cross-Section of a Sphere, H. Weil (2144-6-T, to be published), DA 36(039)SC-52654. UNCLASSIFIED

XI The Numerical Determination of the Radar Cross-Section of a Prolate Spheroid, K.M. Siegel, B.H. Gere, I. Marx, and F.B. Sleator (UMM-126, December 1953), AF 30(603)-9. UNCLASSIFIED

XII Summary of Radar Cross-Section Studies Under Project MIRO, K.M. Siegel, M.E. Anderson, R.R. Bonkowski, and W.C. Orthwein (UMM-127, December 1953), AF 30(602)-9. SECRET

XIII Description of a Dynamic Measurement Program, K.M. Siegel and J.M. Wolf (UMM-128, May 1954) W-33(038)-ac-14222. CONFIDENTIAL

XIV Radar Cross-Section of a Ballistic Missile, K.M. Siegel, M.L. Barasch, J.W. Crispin, I.V. Schensted, W.C. Orthwein, and H. Weil (UMM-134, September 1954), W-33(038)-ac-14222. SECRET

XV Radar Cross-Sections of B-47 and B-52 Aircraft, C.E. Schensted, J.W. Crispin, and K.M. Siegel (2260-1-T, August 1954), AF 33(616)-2531. CONFIDENTIAL

XVI Microwave Reflection Characteristics of Buildings, H. Weil, R.R. Bonkowski, T.A. Kaplan, and M. Leichter (2255-12-T, May 1955), AF 30(602)-1070. SECRET

XVII Complete Scattering Matrices and Circular Polarization Cross-Sections for the B-47 Aircraft at S-Band, A.L. Maffett, M.L. Barasch, W.E. Burdick, R.F. Goodrich, W.C. Orthwein, C.E. Schensted, and K.M. Siegel (2260-6-T, June 1955), AF 33(616)-2531. CONFIDENTIAL

XVIII Airborne Passive Measures and Countermeasures (Offense with, and Defense Against, Bomber Decoys (s)), K.M. Siegel, M.L. Barasch, J.W. Crispin, R.F. Goodrich, A.H. Halpin, A.L. Maffett, W.C. Orthwein, C.E. Schensted, and C.J. Titus (2260-29-F, December 1955), AF 33 (616)-2531. SECRET

PREFACE

In the series of Studies in Radar Cross-Sections, this paper, Studies XVIII, is the first report which is a final report for the contract under which it was written. As a result its style and approach are different from the rest of the series.

It contains many analyses which are incomplete—such being the intent of both the United States Air Force and The University of Michigan. This situation, and indeed the very nature of any report dealing with the employment of bomber decoys (because they are not operational today), has fostered the inclusion of discussions which are both philosophical and factual. However, considerable care has been taken by the authors to document statements of fact with figures, appendices, and references to other existent work. It is intended, therefore, that this paper should serve as a summary of our thinking as well as an introduction for future investigations by others relative to the decoy problem.

This paper is the eighteenth in a series of reports growing out of Studies in Radar Cross-Sections at the Engineering Research Institute of The University of Michigan. The primary aims of this program are:

1. To show that radar cross-sections can be determined analytically.
2. To elaborate means for computing cross-sections of objects of military interest.
3. To demonstrate that these theoretical cross-sections are in agreement with experimentally determined values.

Intermediate objectives are:

1. To compute the exact theoretical cross-sections of various simple bodies by solution of the appropriate boundary-value problems arising from Maxwell's equations.

2. To examine the various approximations possible in this problem and determine the limits of their validity and utility.

3. To find means of combining the simple body solutions in order to determine the cross-sections of composite bodies.

4. To tabulate various formulas and functions necessary to enable such computations to be done quickly for arbitrary objects.

5. To collect, summarize, and evaluate existing experimental data.

Titles of the papers already published or presently in process of publication are listed on the back of the title page.

K. M. Siegel

TABLE OF CONTENTS

TABLE OF CONTENTS (Continued)

TABLE OF CONTENTS (Concluded)

LIST OF FIGURES

LIST OF FIGURES (Continued)

LIST OF FIGURES (Continued)

LIST OF TABLES

I

INTRODUCTION AND SUMMARY

On 1 May 1954 The University of Michigan commenced an investigation directed toward the determination of the proper electromagnetic characteristics of decoys. Bomber decoys are vehicles with performance similar to a bomber during one flight only; these vehicles are much smaller and cheaper than a bomber yet simulate the electromagnetic characteristics of a bomber to a probing search radar. The philosophy of the offense was that, when a main offensive thrust was being made at a given location, the need for the bombers and pilots in a diversionary raid at a different location should be eliminated if at all possible. In other words, it was highly desirable to save the lives and bombers lost from such diversionary efforts and simultaneously it was also desirable to increase the probability of success of the main mission. It was conceived by the Rand Corporation (Ref. 1) and others that if some of our large bombers could carry decoys, then this unnecessary loss of life and bombers from a diversionary raid could be avoided. It was also foreseen that since a bomber could carry many decoys, the probability of success of the prime effort could be increased. As a result the United States Air Force made an effort to have decoys designed so that they could be carried by a B-36 (the Duck vehicle) and a B-47 and B-52 (the Quail vehicle) and so that these decoys, since they are carried by the bomber, could be used against the local defense radars of the USSR. It was also foreseen that long-range decoys (the Goose vehicle) with the capability of fooling the enemy's long-range search radars should be based in the United States or in friendly bases.

In our defensive picture, we can foresee that the Russians could use decoys similar to the Goose vehicles to fool our DEW Line and other radar fences in Canada, while vehicles similar to Quail and Duck vehicles could be designed to fool the local radar fences of the Air Defense Direction Centers and the Control Centers within the interior of the United States.

The role of The University of Michigan was to investigate the overall electromagnetic properties required for these vehicles and suggest passive means for obtaining these properties. The first input in such a study was a priority of the distribution of the Russian radar frequencies. The United States Air Force under this contract stated that the priorities in our investigation should be (1) S-band, 2600 - 3300 Mc, and (2) 65 - 300 Mc.[1]

They suggested the third priority be L-band. Since it became desirable, and possible, to consider the problem for all frequencies higher than S-band, all at once, we concentrated on S-band and higher band radiations first. If time had permitted we would also have made a precise study of L-band, when we began concentrating on Goose. We agree with The Johns Hopkins University that for long range search radars affecting Goose, L-band is probably much more important than X-band. On the other hand for Quail it was felt that the third priority frequency for local Russian defense radars should be X-band.

Since the effort on decoys for the B-36 had already started and since it was felt that the B-36 bomber should assume lower priority in the study than the B-47 and B-52, these latter two bombers were considered the prime ones upon which The University of Michigan should focus its attention. The first thing needed was the electromagnetic scattering properties of the B-47 and B-52 for monostatic linearly-polarized Russian radars at the above frequencies. This information was obtained and reported in one of our radar cross-section series (Ref. 2). We then focussed our attention on the design of corner reflectors and similar devices to go into the decoys. We found that it was quite easy to design decoys which had the reflection characteristics of the B-47 and B-52 at S-band (Sec. II). When we found that this design problem was an easy one, we questioned ourselves as to what

---

[1]For the reasons given in Section II passive devices like corner reflectors could not be used for this range. It was agreed almost at the start of the study that The Johns Hopkins University would be responsible for advising the USAF on active equipment for the 65 - 300 Mc range.

defenses we in the United States could and should use against similar devices. As a result, we designed possible defenses (Sec. III) against our offensive decoys. In Section IV, we make use of our study in a defense against decoys to again re-design the passive reflectors of the decoys, so that they will have a better chance to be interpreted as bombers by the Russian radars.

Many aspects of the above study are of course not completed, but we do feel that the framework exists so that the Department of Defense should be able to make significant use of our investigations to design useful decoys on the one hand, and to have a practical defense against Russian decoys on the other hand.

II

OFFENSE WITH DECOYS

2.1 OFFENSIVE DECOYS FOR A B-36, B-47, AND B-52

Initial investigations by others reveal that there are many types of vehicles that could fit into the B-47 and B-52 which could have the flight characteristics of a B-47 and B-52 for one flight of 200 mile range capability. The only questions to be asked in this section are associated with what are the best passive devices[1] to be put into decoys in order to fool Russian S-band monostatic linearly-polarized radars. It was foreseen at the start that decoys which work at S-band would probably work equally well or better at X-band against the above radars, and that passive devices would be of no use in decoys against radars in the 65 - 300 Mc ball park.

In Figure 1, we present a decoy with appropriate corner reflectors such that the scattering pattern of the decoy simulates that of the B-47 at S-band, except primarily broadside, as shown.

Considerable effort was made to design radar reflectors to be used by Convair on Duck . A quick and dirty tabulation of the B-36 cross-section obtained is given in Table 1. In Figure 2a, a comparison is made between the Duck cross-section and the B-36 cross-section. In order

---

[1]By a passive device is meant a device whose source of energy is furnished by the enemy, whose reflection characteristics are dependent upon the wavelength of the enemy's sources and the polarization of the enemy's sources and antennas, and whose reflection properties are dependent solely upon the characteristics of its geometry and conductivity. In other words we do not include devices such that the enemy's radiation is used to pulse our equipment which then uses its own source to blanket, either geographically or frequency-band-wise, the enemy's receiver or receivers.

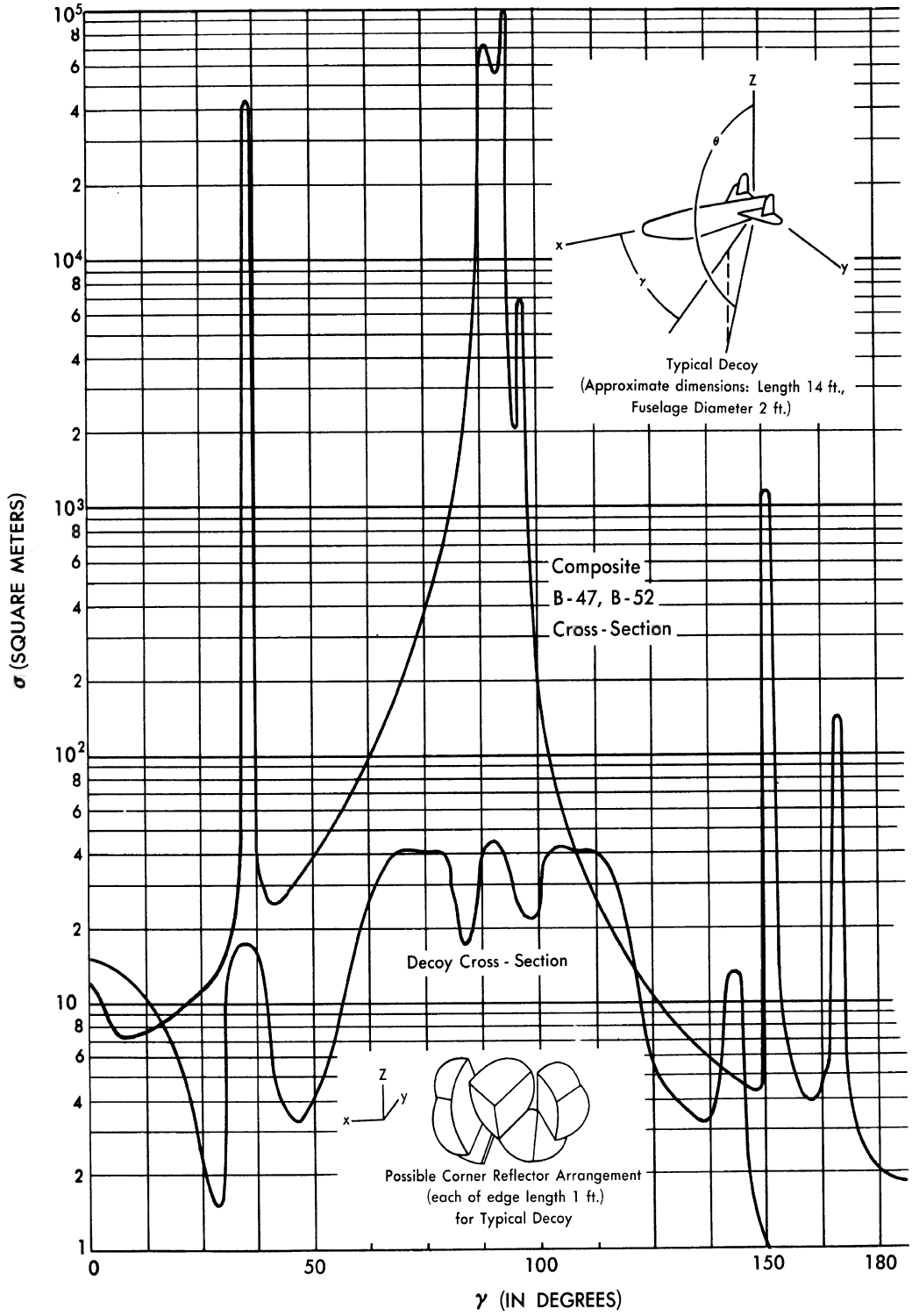

FIG. 1 CROSS-SECTION CURVE OF COMPOSITE (db AVERAGE) B-47, B-52 AS COMPARED WITH CROSS-SECTION CURVE OF TYPICAL DECOY FOR 0° ELEVATION AT S-BAND

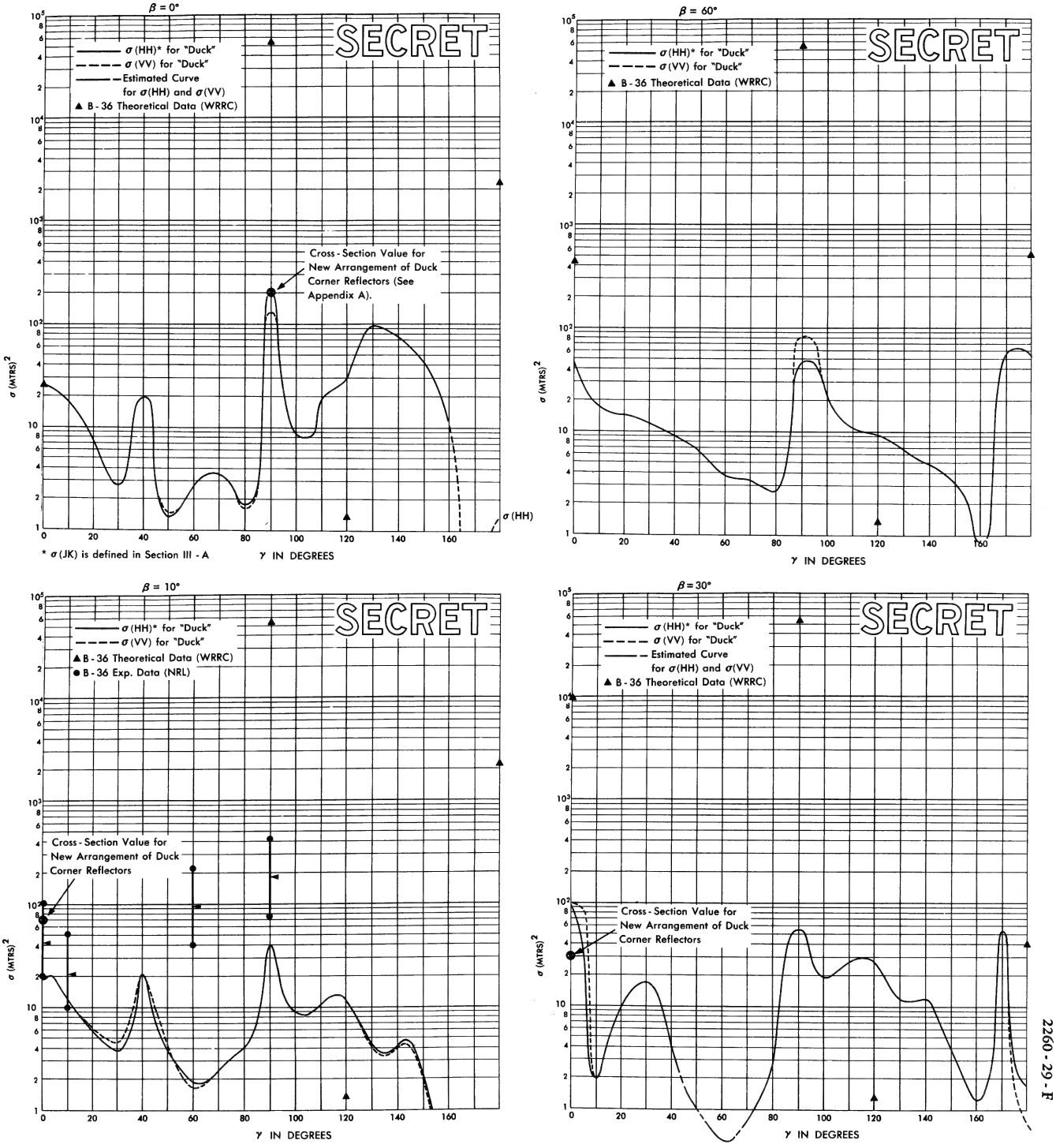

FIG. 2a CROSS-SECTION OF DUCK AS COMPARED WITH THEORETICAL AND EXPERIMENTAL CROSS-SECTION OF B-36

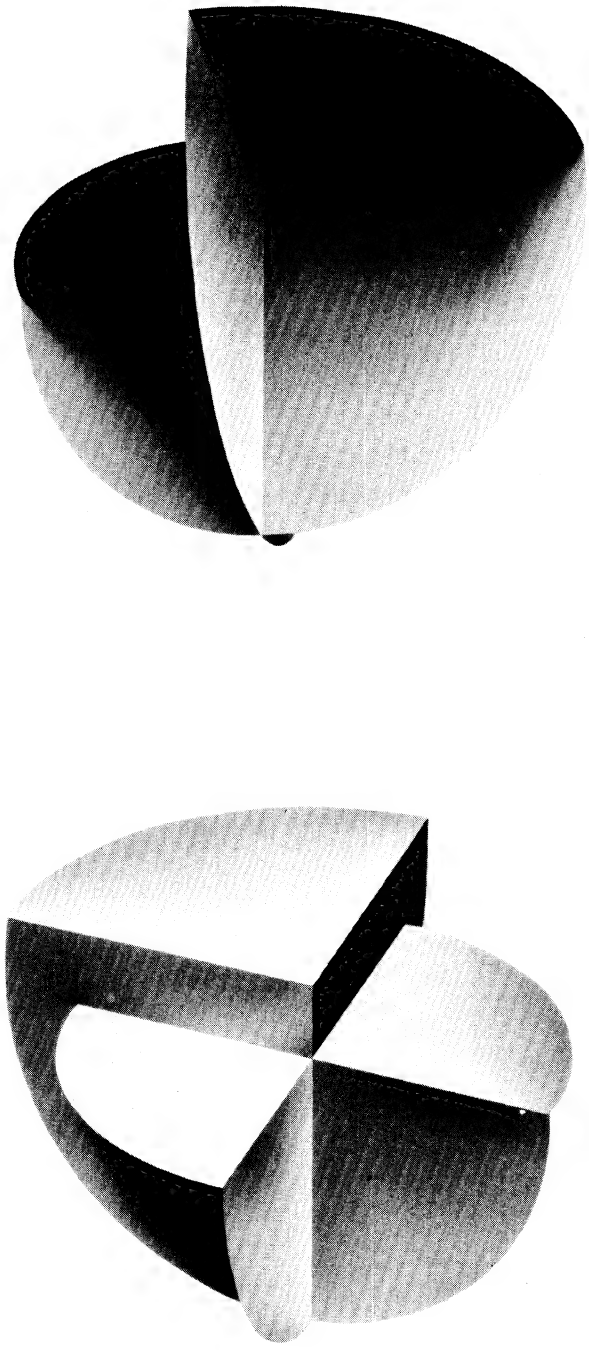

FIG. 2b SUGGESTED NEW ARRANGEMENT
FOR NOSE REFLECTORS IN DUCK
(CF. FIG. A - 2)

TABLE I

CONTRIBUTORS TO THE B-36 CROSS-SECTION

(numbers in contributing parts columns are cross-sections in sq. meters; angle values are in degrees)

γ	β	Wing	Recip. Engines	Jet Eng.	Jet Supp.	Fuselage Cylinder	Vert. Tail	Hor. Tail	Pro-pellers	Prolate Spheroid	Tail Cone	Tail Spheroid
0	0	1.75	- - -	21.2	Negl	0	.0131	Negl	2.40	1.94	0	- - -
0	10	1.90	- - -	21.2	.00704	Negl	.0097	Negl	2.40	2.06	Negl	- - -
0	30	3.67	Negl	Negl	.00011	Negl	965	Negl	Negl	3.19	Negl	- - -
0	60	400	Negl	Negl	.206	Negl	.0131	Negl	Negl	16.1	Negl	- - -
0	90	3720	105 m^2	Negl	Negl	1.35×10^5	0.0275	Negl	Negl	53.0	- - -	- - -
90	0	0.184	Negl	83.6	695	5.0×10^4	2690 m^2	Negl	Negl	53.0	0.54	0.63
90	10	0.289	Negl	83.6	695	5.0×10^4	Negl	Negl	Negl	53.0	0.76	0.63
90	30	2.14	Negl	83.6	695	5.0×10^4	Negl	Negl	Negl	53.0	1.81	0.63
90	60	33.8	Negl	83.6	695	5.0×10^4	Negl	Negl	Negl	53.0	11.4	0.63
120	0	.000458	Negl	Negl	Negl	Negl	Negl	Negl	Negl	Negl	0.051	1.26
120	10	.000519	Negl	Negl	Negl	Negl	Negl	0.00255	Negl	Negl	.00431	1.26
120	30	.000996	Negl	Negl	Negl	Negl	Negl	.00157	Negl	Negl	.0211	1.26
120	60	.00736	0.0054	Negl	Negl	Negl	Negl	.00322	Negl	Negl	.0265	1.26
180	0	2160	Negl	21.2	Negl	Negl	.0256	.0344	2.40	Negl	Negl	1.26
180	10	2160	Negl	21.2	Negl	0	.2742	.0454	2.40	0	Negl	1.26
180	30	40	Negl	Negl	Negl	0	.1239	.0980	Negl	0	.008	- - -
180	60	500	Negl	Negl	Negl	0	.0009	.155	Negl	0	.0377	- - -

γ	β	Total
0	0	25.55
0	10	25.57
0	30	971.
0	60	416.1
0	90	1.388×10^5
90	0	53521
90	10	53521
90	30	53521
90	60	53521

γ	β	Total
120	0	1.31
120	10	1.30
120	30	1.28
120	60	1.29
180	0	2196
180	10	2196
180	30	40
180	60	500

to illustrate the method used to compute the cross-section of Duck, we present in Appendix A the breakdown used for the Duck vehicle as originally designed and the associated computation. On the basis of this analysis a suggested new arrangement for the Duck corner reflectors is given (Fig. 2b) and in Figure 2a we also present the essential contributions of our suggested new arrangement.

In Reference 2 we presented the cross-section of the B-47 and B-52. Since that investigation was completed, new experimental checks have been obtained and one of these is a comparison for low frequencies (Fig. 3). The total experimental data are presented in Appendix B. In Appendix C we present the experimental results obtained by a subcontract to the Microwave Radiation Company, Inc., on the parts of the B-47 needed for checks of theoretical work. Since the comparisons in Figures 1 and 2a are considered by us to be excellent when one considers the properties of present-day radars and their display systems, it was foreseen that most decoys to which a little thought has been given would be successful in fooling Russian S-band linearly-polarized monostatic radars. It was thus foreseen that a study should be started to determine what were the best means of defending against decoys. It also seemed reasonable to assume that the United States was doing the defending,so the outputs of our study can become the inputs of our United States Air Defense programs.

In the course of our study on decoys, it became necessary to obtain the properties of elliptical and circular corner reflectors. In Appendix D we present the theoretical characteristics of elliptical and circular corner reflectors. In many of our investigations we have found that the work required to check the computations is of a greater order of magnitude than the work required to do the computations the first time. Thus, if we were going to save money and time, it became expedient to design a method of obtaining order-of-magnitude checks on computations involving corner reflectors. In Appendix E we present such a method.

It was also foreseen that if fuel tanks could become efficient

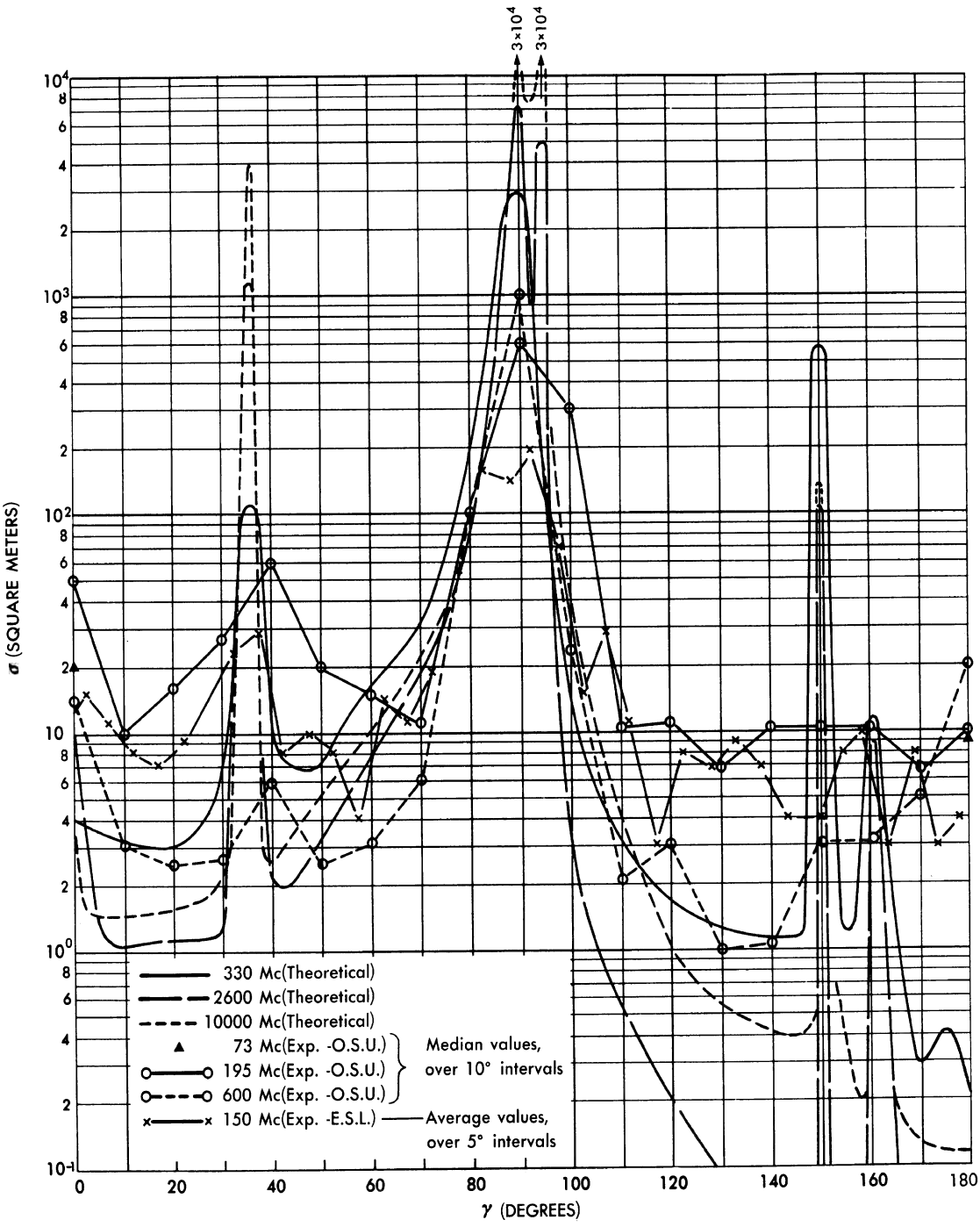

FIG. 3 CROSS-SECTIONS (σ (HH)) OF THE B-47 AIRCRAFT AT 0° ELEVATION
Theoretical: The University of Michigan
Experimental: The Ohio State University
& Evans Signal Laboratory

reflectors, a good deal of space could be saved in the decoy. In Appendix F it is shown that this, in fact, is the case and a comparison between theoretical and experimental results for the fuel tank is discussed.

Considerable work has been done both theoretically and experimentally on the bistatic cross-sections of corner reflectors and other multiple scatterers (Ref. 3). Theoretical and some experimental results of this kind of work are given in this reference. The Armed Forces have similarly carried through the analysis of corner reflectors, and military specifications now exist (Ref. 4).

Considerable work has been done in the decoy area associated with making smaller aircraft look like larger aircraft. For example, attempts have been made to simulate B-17 characteristics by the mounting of corner reflectors on a F-4U. The results are quite good. However, the F-4U is too small an aircraft to do a really excellent job (Ref. 5). Reference 5 concerns considerable work and measurements on angular noise and it seems feasible, if one deemed it necessary, that angular noise could have been duplicated.

Many means have been devised and investigated to make objects like decoys with no attempt to duplicate the flight characteristics of the aircraft. The best known of these is chaff (Sec. 2.2). Other types of radar reflectors have been designed for similar purposes. For example, the United States Air Force let a contract to develop eight-pound, 10-foot-diameter spherical reflectors to be attached to a balloon and borne aloft in a collapsed condition with the ability to automatically become corner reflectors after a certain amount of time had elapsed. Four hours was the time used in the study by the Fairchild Engine and Airplane Corporation (Ref. 6).

The Air Defense Command has analyzed the offensive potentiality of electronic countermeasures carried by meteorological-type balloons borne by the wind into the radar net. Some thought has been given to offensive problems by the defense and some recommendations are given in Reference 7. The offensive problem has been analyzed and a discussion

has been made on using ground-launched balloon reflectors drifting east into enemy dominated areas for use as decoys against enemy tracking and gun laying radars. Preliminary thinking involves the location of 40 sites about 15 miles apart from southern England to northern Scotland and about 20 more sites in central western Norway. These sites, it is believed, could maintain 200 targets on most surveillance radars in the potentially enemy-dominated areas between 50 and 63 degrees north latitude (Ref. 8).

2.2 CHAFF

John Hult of the Rand Corporation and others (Refs. 1 and 9) have suggested that an investigation should be made of the possibility of having the B-47 and the decoy both drop chaff. Assumed in the study is the fact that the cross-section of the chaff will dominate the return and as a result the two vehicles will look alike. Another idea involving chaff was the seeding or laying of chaff corridors which aircraft could fly through undetected. Many analyses have been made of chaff since and during World War II. However, there have been some recent studies which may have bearing upon the use of chaff in the bomber-decoy program. The tactical employment of chaff from 860 to 3000 Mc has been tested at Eglin Air Force Base (Ref. 10), especially towards obtaining optimum dispensing techniques.

At Radiation, Incorporated (Ref. 11),echo amplitudes of chaff were analyzed for three different experimental chaff types.

Recent theoretical investigations at The Johns Hopkins University (Ref. 12) indicate that the amount of chaff necessary to confuse the enemy is approximately equal to that necessary to hide both bomber and decoy (a lesser quantity obscures only the decoy). Their study yields numbers of units of chaff necessary to sow a trail 50 to 225 miles in length against radars of 1 to 10 μsec pulse durations for aircraft with radar cross-section areas of 100 to 1200 square feet. In particular,for the B-47 their estimated sowing rate compares favorably with the 30 units per minute obtained in recent field tests at Eglin Air Force Base for a B-47 dropping chaff at the rate of 10 ft/min. Reference 12 also contains a

discussion of investigations of active equipment which would work in the 50 to 300 Mc frequency range. The second priority frequency range (Sec. I) can be covered with a pulse barrage simulator which would weigh about 100 pounds. This seems to be the most important device yet considered for the low frequency range. As this report was being written, information was received concerning a General Electric device to be used for the same range being built at Utica, New York. Considerable analysis would probably be required to decide what the right characteristics should be for either a barrage jammer or an amplifier with its own power supply which would respond only to the frequency that excited it. It is obvious that important future work in the offensive problem must take place in the low frequency range.

Passive devices cannot be used in lower frequency ranges because it has been found that passive devices under consideration which would fit into small vehicles are usually highly wavelength dependent. In fact in most cases their cross-sections are proportional to $1/\lambda^2$. We find that aircraft cross-sections are not significantly frequency dependent (see Figure 3 for the B-47 and Figure 4 for the F-86). As a result, since the cross-section of the corner reflector decreases with an increase in wavelength and since the bomber cross-section is a slowly varying function of wavelength above 75 Mc, it becomes clear that if we can obtain a good matching cross-section at high frequencies L- through X-band, this same collection of corner reflector-like devices will be of no use at much lower frequencies. In this neighborhood active devices must be used.

Chu (Ref. 13) analyzed the question of when to use corner reflectors and when to use half-wave dipoles to simulate radar echoes for jamming. He found that at λ = 10 cm, the corner reflector is best; at λ = 53 cm, half-wave dipoles are superior; and at 300 cm, half-wave dipoles are the only means to simulate echoes by passive devices.

We find Chu's conclusions are equally valid today.

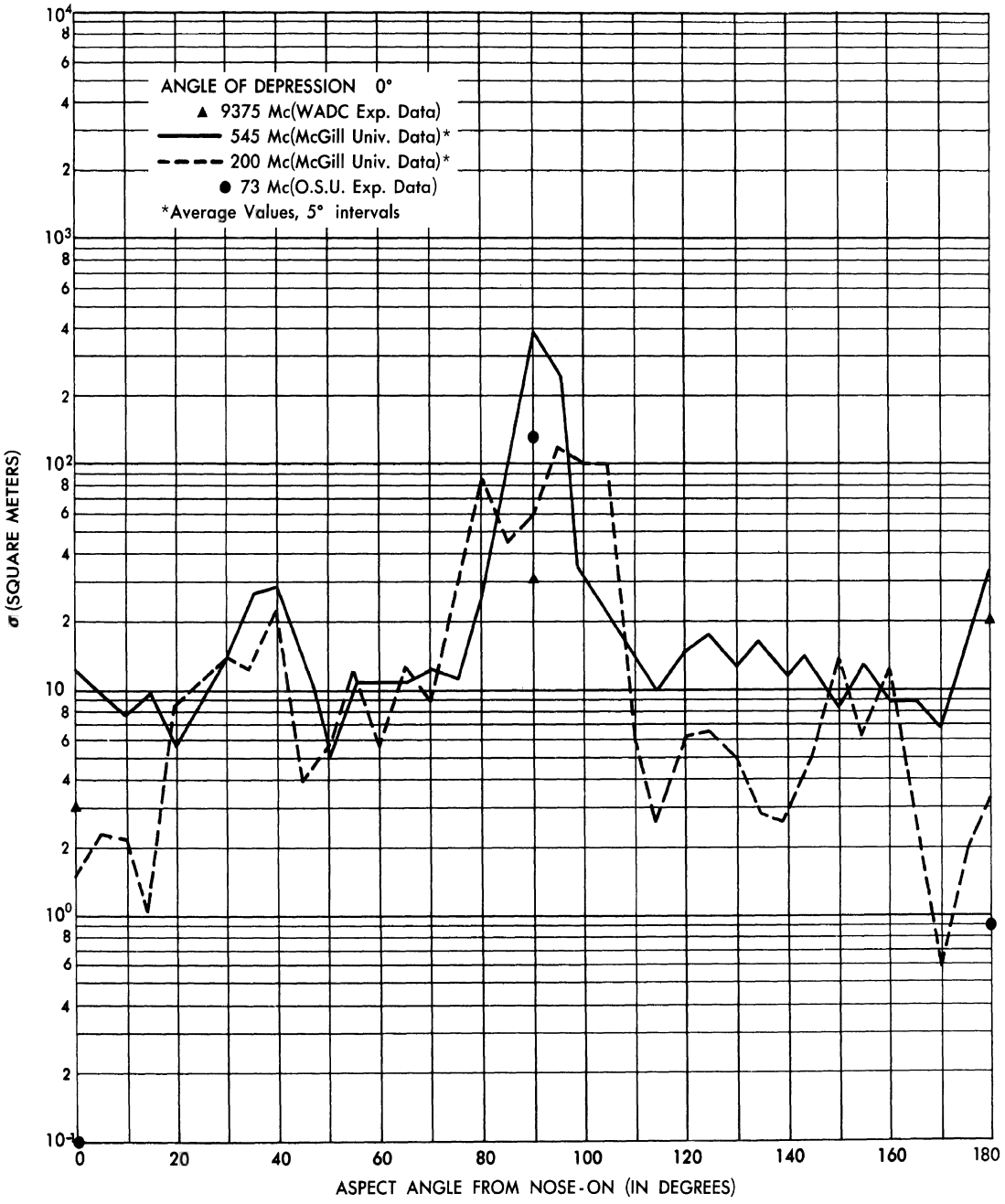

FIG. 4 CROSS-SECTION OF THE F-86 AIRCRAFT
(Experimental - Horizontal Polarization)

III

DEFENSE AGAINST DECOYS

Five methods of defense against decoys have suggested themselves to us:

A. The Circular Polarization Method

B. The Bistatic Radar Method

C. The Frequency Comparison Method

D. The Broadside Discrimination Method

E. The Scintillation and Glint Method

Each one of these methods is worthy of a separate investigation in a separate report. However, since the amount of work we have done on each one of these methods is sufficient only to prove whether the method would or would not work (because this was the only type of effort justified in this regard under the present contract), we limit ourselves to approximate numbers and general discussions.

3.1 THE CIRCULAR POLARIZATION METHOD

It was believed that major complex reflectors with wing-like structures might reflect as much energy in single and triple reflections as in even multiple reflections. Of course it was recognized that at some aspects, double reflections could dominate and at other aspects, single or triple reflections could dominate. Thus it was believed that if we took an average over a few seconds of time, equivalent in a typical case to an average over 10° - 20° in aspect, and if we transmitted right-circularly-polarized energy and received with two receivers (one receiving energy polarized to the right, the other receiving energy polarized to the left), we would find the ratio of energy for aircraft from the two receivers would be between 1/2 and 2. Corner reflectors, on the other hand, have the property, even when edge effects and multiple reflection

between edges and other corners and other gadgets in the decoy are included, that the reflection is either primarily odd or primarily even reflection at any particular aspect. After averaging over 10^{o} - 20^{o} in aspect we find that the energy ratio for decoys from the two receivers would be between 1/20 and 20. The instantaneous decoy returns would be at the extremities of this ratio (App. G), while it is expected that the aircraft instantaneous cross-sections would be near the middle of the range of ratios, with a slight preference towards single reflections. Thus it becomes obvious that we may use two receivers and one transmitter at one radar site to distinguish the difference between aircraft and corner reflector. It has been pointed out that if a corner reflector mounted on an aircraft is presented to a casual radar operator, this method of detection might be defeated. However, to an experienced operator, the tremendous increase in energy observed would clearly indicate that the cross-section was that of an aircraft plus a corner reflector. This is because, although the ratios might be in the wrong ball park, the level of energy in both receivers would be sufficiently high to guarantee the vehicle being seen as an aircraft. In order to prove these points, a study was made to determine the reflection characteristics of a B-47 at all polarizations for a monostatic probing radar at S-band (Ref. 14). In Reference 14 we discussed the experimental results of Raytheon, Hughes and others which showed that our theoretical conclusions are in the right ball park. We have determined in Appendix G the radar reflection properties of a corner reflector for circular polarization. This information, although not complete in the corner reflector case, does exhibit that the above method of detection of decoys will work.

In our analysis on the cross-section of aircraft for different combinations of monostatic polarizations (Ref. 14) only experimental data of a confidential and unclassified nature were discussed. Of importance in cross-polarization radar problems is the considerable work of the British (Refs. 15 and 16) concerning the Lincoln, Wayfarer, and Canberra type aircraft.

Some comparisons of results for these three aircraft (linear polarization results from Ref. 15 and circular polarization results

from Ref. 16) are made below with theoretical results obtained by us for the B-47 in Reference 14. For approximately nose-on incidence σ (HV) is down[1]

from σ (HH) by	from σ (VV) by	
7.7 db	7.9 db	for Lincoln,
9.8 db	9.7 db	for Wayfarer,
8.8 db	10.9 db	for Canberra,
5 to 6 db	5 to 6 db	for B-47;

σ (RR) is down from σ (LR) by

3.1 db	for Lincoln,
2.9 db	for Canberra,
3 db	for B-47.

For approximately broadside incidence σ (HV) is down

from σ (HH) by	from σ (VV) by	
7.9 db	9.9 db	for Lincoln,
8.1 db	7.0 db	for Wayfarer,
7 to 15 db	7 to 15 db	for B-47;

σ (RR) is down from σ (LR) by

2.1 db	for Lincoln,
0 db	for B-47.

[1]The letters, H, V, R, L indicate horizontal, vertical, right circular, and left circular polarizations. In σ (JK), J indicates transmitter polarization, K indicates receiver polarization. For the B-47, the numbers are obtained for an elevation of 4^{o}.

3.2 BISTATIC RADAR METHOD

We are able in the case of decoys at S-band to duplicate the reflection characteristics of much larger vehicles by passive devices at most aspects. This is because of the nature of the passive device being used. That is, the aircraft was not designed to be an efficient scatterer in the direction from whence the incident radiation came. Since the passive device being used, namely a corner reflector, is an extremely efficient scatterer in the direction from whence the radiation came, we can use the high efficiency of a small device (corner reflector) to duplicate the inefficiency of a large device (bomber). If we use this very property of the corner reflector, that is its high efficiency to concentrate its energy in the forward quadrants, to detect it, we find that the method to be employed is to use bistatic radars. In other words, if a transmitter-receiver looks at a decoy and finds the energy primarily reflected in the forward quadrants, then the amount of energy which goes off into the backward quadrants is negligible. As a result, if we have a transmitter-receiver and a remote receiver, we would find the cross-section of the decoy to be very much larger in the transmitter-receiver site than in the remote receiver site for all aspects. However, for the bomber,the cross-section at the remote site compared with the cross-section at the transmitter-receiver site would for some aspects be larger, other aspects equivalent, and still other aspects smaller. Thus a comparison of the energy at the two receivers would show, when corner reflectors had allowed the decoy to have a cross-section equivalent to the bomber cross-section at the transmitting site, that the ratio of the bomber cross-section to the corner reflector cross-section at the remote receiver site would be extremely high. A direct comparison over several degrees in aspect would always show whether the cross-section of the vehicle was coming primarily from corner reflectors or primarily from a bomber-like vehicle. Corner reflectors might be added to the aircraft to attempt to fool the casual observer, but again the level of energy in the remote receiver should clearly indicate that the vehicle is a bomber. In Appendix H the bistatic radar cross-sections of a B-47 at S-band have been obtained. Since it has been found that the scattering from the edges of the corner reflector is negligible (Refs. 17 and 18), it is clear that the above method of

detection of decoys will work. Similar analysis has been made for the bistatic cross-sections of an F-84 and the data is presented in the table of Figure 5.

Forward Scatter and Back Scatter from a F-84F (Modified) Airplane[1]

	20,000 feet		28,000 feet		36,000 feet	
Miles from Base Line	Back Scatter	Forward Scatter	Back Scatter	Forward Scatter	Back Scatter	Forward Scatter
1.9	10	7	12	14	0	17
3.8	6	3	5	- 3	0	- 6
5.8	0	- 6	-3 1/2	noise	-10	- 7
7.7	- 6	noise (- 15)	- 1	noise	- 4	- 4
9.6	0	- 3	- 5	noise	- 5	-10
11.5	- 9	noise	- 9	- 8	-1 1/2	- 6

All values are in db. Reference level at 0 db is the back scatter from a 1 1/2" sphere, "noise" is in each case at least 15 db. True frequency is of the order of 330 Mc.

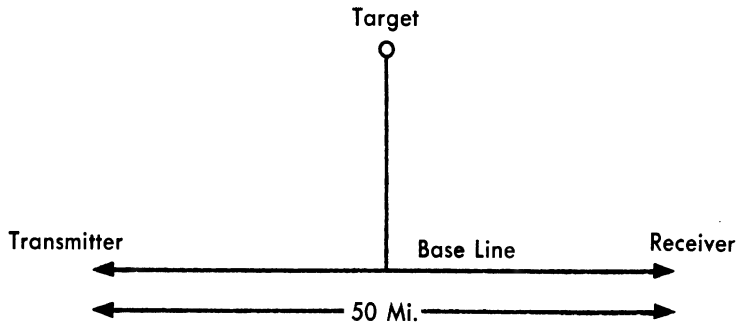

FIGURE 5

[1]Personal correspondence, Nelson Logan, Air Force Cambridge Research Center.

3.3 THE FREQUENCY COMPARISON METHOD

Since the cross-sections of bombers are slowly varying[1] functions of frequency in the high frequency range, and since corner reflectors vary rapidly (as $1/\lambda^2$), two radars operating at a factor of 10 separation in frequency would obtain cross-sections differing by a factor of 100. As a result, a frequency comparison method, where the radars are close together and the antennas have overlapping patterns, should indicate the difference between decoys and bombers. The difficulty arising from this method is simply that this is the only method which requires two transmitters. It also requires a good deal more power than the other methods.

3.4 THE BROADSIDE DISCRIMINATION METHOD

The Johns Hopkins University has recommended that the United States Air Force investigate the possibility of having a system which looks at the broadside returns of both bomber and decoy. The difficulty of matching large broadside radar cross-section returns with a small vehicle is obvious. However, the problem has been recently studied by The Johns Hopkins University (Ref. 12). They have been successful to the extent that, with a small increase in decoy diameter, the broadside bomber return (for X- and S-bands) can be simulated reasonably well by using a double corner (dihedral) reflector in a decoy.

3.5 SCINTILLATION AND GLINT METHOD

The scintillation and glint method is based on the fact that there are other observables in the radar returns from a scatterer in flight which the aforementioned decoys have not been designed to duplicate. A method may be proposed which is based on rapid fluctuation in the echo of the

[1]By slowly varying is meant that the amplitude of the return signal, although it fluctuates rapidly with frequency, remains within a small variation in amplitude. In other words, with a particular aspect average the cross-section of a B-47 in the high frequency range is not expected to vary over 10 db. Despite the fact that it might fluctuate rapidly with frequency anywhere between these limits, we call radar cross-section a slowly varying function of frequency.

aircraft which might be considerably different from the rapid fluctuation to be obtained from the decoy. For example, the return of a propeller-driven decoy would have frequencies (of the number of propeller blades times the number of engine revolutions per second divided by gear ratio between blades and engine) not present in a jet bomber return. If the bomber is propeller-driven and the decoy is not, the same conclusion exists.

One of the difficulties in analyzing scintillation and glint effects for propeller-driven aircraft in the United States occurs in the fact that we use 60 cycle per second power sources in this country. Since the frequency in cycles per second is equal to the revolutions per second times the number of blades divided by the gear ratio from engine to propeller, we find that typical aircraft, i.e., the F-4U, the F-8U, the SNB, and the DC-3, would yield frequencies within one cycle of 60 cycles per second. Thus it is clear that if we are trying to detect propeller-driven aircraft we must think very carefully of the expected modulation frequency and choose the source accordingly. Examples of the above numbers for other propeller-driven aircraft are given in Reference 19.

A great deal of work was done at the Radiation Laboratory of Massachusetts Institute of Technology (Ref. 20) on the detection of propeller modulation and the effect of trying to camouflage propeller modulation by adding layers of special material to the props. It was found that one could actually display prop modulations at ranges up to 2/3 of the normal tracking range of an aircraft. It is believed that the important conclusion reached as far as this study is concerned is that, in general, the patterns of received echo intensity as a function of target-aircraft propeller-rotation angle are extremely complex. Again, however, the analyses of that reference show that it would be difficult to design a system which determined the difference between flying vehicles, i.e., difference between a B-36 and a decoy, by angular or amplitude noise (scintillation and glint). This is especially true if we make attempts in the designing of the decoy to have motion in the decoy which is close in frequency to the modulation frequency of the propellers of the B-36.

Since bombers are subject to vibration and strain, and since a decoy is a much smaller vehicle, there is a possibility that the low frequency vibration of the two vehicles might be quite different, expecially since the bomber is made of a metal and the decoy is probably made of a plastic material. If these vibrations result in perceptible changes in the frequency distribution of the returned echo, then again it would be possible to distinguish between the bomber and the decoy. Although the authors believe that there could easily be large differences between the two devices if acoustical means of detection are used, the authors do not feel this strongly about present day devices used to measure the frequency spectra of radar returns. Power spectra of aircraft in radar experiments (when the method of propulsion is the same) are so similar that it would at this time be difficult to design equipment to measure differences. The one third scale model of a V2 missile which was dropped from a B-29 at the Holloman Air Development Center showed a power spectrum not much different from those obtained from aircraft[1]. Since a larger difference is expected between a missile and an aircraft than between a decoy and an aircraft (because of the difference in wings), it is felt that this is a very difficult means of discrimination to instrument. The authors are thoroughly familiar with the tremendous differences in patterns obtained for the same aircraft and with the tremendous fluctuations present over relatively small changes in aspect. However, the experiments made on spheres indicate that the source of this fluctuation is often in the ground equipment itself and is more a property of the ground equipment than of the vehicle.

Many measurements of the scintillation and glint of the target have been attempted. Despite our experiences concerning spheres we wish to point out some counter experiences of others, e.g., Hughes Aircraft Company, (Ref. 21). The results of scintillation measurements for a B-47 are given in this reference. Since the results the Hughes Aircraft Company obtained for scintillation noise from a corner reflector were

[1]The experiments and their results are described in Studies in Radar Cross-Sections XIII and XIV. (See list of Studies at front of this report.)

found to be a negligible amount at all frequencies, it was concluded by Hughes that their experimental equipment was such that the noise obtained from the aircraft target was a function of the target only. Although we feel that the data obtained by Hughes on scintillation for a B-47 is not the type for which it would be easy to instrument a means of detection of aircraft versus decoys, we feel that the above reference is a significant starting point for future analyses.

Analysis has been made of scintillation and glint of the B-47 aircraft as well as the effect of adding fuel additives to the exhaust of the B-47 so that this exhaust may serve as a radar countermeasure similar to chaff. The results of these type studies have been pretty much negative. An excellent source of the available information is Reference 22.

The University of Texas under Air Force Contract AF 33(616)-2842 is doing some research on the characteristics of gases which cause reflections. They may be able some time in the future to develop gases which can be used for chaff (Ref. 23).

Theoretical analyses have been made by the Rand Corporation (Ref. 24) for fluctuating targets and conclusions have been drawn from four cases. Two specific probability densities were assumed for each of the following: (1) pulse-to-pulse type fluctuations and (2) scan-to-scan type fluctuations. Further analysis of experimental data should be made to investigate the physical meaning of the above models. However, preliminary results certainly show that the above models warrant further study.

3.6 CONCLUSIONS

The conclusions reached here are that the circular polarization method, the bistatic radar method, and the frequency comparison method are worthy of further investigation. As pointed out in Section 3.4, extensive work on the broadside echo method has been done recently by The Johns Hopkins University. Their recommendations for handling this method appear in Reference 12. The difficulty with the scintillation

and glint method is the lack of existing equipment to take care of spectral identification. Too much time and expense are required to design new equipment and too much time is required to operate present day equipment (Ref. 25) during a raid, even if the idea turned out to be feasible enough to warrant further work at the present time. The methods deemed worthy of further study have been investigated a little further in order to suggest methods of varying the offense to counter these expected possible defenses. These investigations are described in the next section.

IV

COUNTERMEASURES TO THE ENEMY'S DEFENSE

4.1 CIRCULAR POLARIZATION METHOD

Since it has been found that, in decoys of feasible size, it is possible to place corner reflectors which will give echoes at most aspects of interest larger than those needed at the same aspect from the aircraft, two methods suggest themselves for countering the circular polarization detection scheme. The first is the use of 1/2 wavelength protuberances on one surface of the decoy corner reflector. This would allow for the scattering from one face to be almost randomly polarized and as a result it would reduce the return from the 95 percent - 5 percent energy ratio in the two receivers to possibly a 70 percent - 30 percent or a 60 percent - 40 percent relationship. A better scheme for doing this has been suggested by the Ohio State University (App. I). A study of the Poincaré sphere indicates that a double layer of dielectric material can be placed over one of the faces of the corner reflector so that the ray picture remains unchanged but the polarization picture changes in such a way as to return to the 60 percent - 40 percent energy relationship. This method looks better than the protuberance one because it does not reduce the efficiency of the corner reflector.

4.2 BISTATIC RADAR CROSS-SECTION METHOD

The bistatic radar cross-section method is the more difficult to counter; it requires the defense to have data processing equipment of sufficient magnitude in remote regions so that they can tie together the return from the receivers at the transmitter site to the returns at the remote receiver site. There is a possibility that the bistatic offensive situation could be improved and at the same time the circular polarization method countered. This would be possible if a face of the corner reflector, instead of having protuberances, were made from wire mesh with the spacings such as to change the polarization picture more towards the 60 percent - 40 percent ball park, yet at the same time

improve the bistatic return. Possibly a loaded dielectric material could be used as the third face so that, by compromising slightly the efficiency of the corner reflector, the bistatic return could be improved. This is not as impossible as it might seem on first sight for the following reason. Since the decoy is smaller than the bomber, it intercepts less radiation and as a result scatters less energy. The bomber scatters this energy into all quadrants by the nature of its geometry. The requirement on the decoy is to scatter the energy in the downward quadrants and there is no necessity of any energy in the quadrants above the decoy. As a result, although it seems impossible to match the bistatic returns at all the lower aspects, it may be possible to scatter enough energy bistatically to confuse the enemy.

Another possibility is the reflector shown in the sketch below.

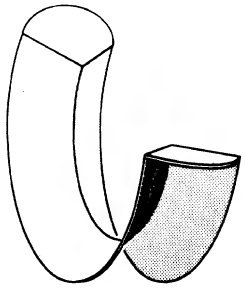

This reflector is a biconical reflector with added flat plates. An analysis has not been carried out, but it appears as if this reflector would concentrate the reflected energy in a fanshaped beam. A dielectric lens could be added for further control of the reflected energy.

4.3 THE FREQUENCY COMPARATOR METHOD

The difficulty with the frequency comparator method is the need for two transmitters and receivers with frequency separation of the order of magnitude of at least 3 to 1. The enemy's distribution of radars

suggests their use of S- and X-band as the two logical frequency bands in a frequency comparator mechanism (Sec. I). Since corner reflectors which easily match (except at broadside) the return of the B-47 can be used at S-band, it is clear that at X-band these corner reflectors will give radar cross-sections a factor of 10 larger than the bomber. It then seems possible to introduce holes in the corner reflector of circumference of 18 cm which have insulation material around the inner edge of the circular aperture and have a metallic material on the outer (back) edge of the circular aperture[1]. This then would allow for transmission of the X-band radiation through the aperture and at the same time would allow for reflection of the S-band radiation. In this way it is possible to make the returns to a monostatic radar equivalent at S- and X-band. Thus, as the quality and quantity of Russian radars are primarily in the S-, L-, and X-band range for those frequencies above 300 Mc, it seems clear that this method might be successful in overcoming the frequency comparison method, might help in overcoming the circular polarization method, and would also help out in the bistatic X-band radar return. Another and probably better method to overcome the frequency comparison method is given in the next section.

4.3.1 Use of Corner Reflectors With Curved Faces to Obtain Frequency Independent Cross-Section

Let us suppose that we desire a scatterer with the following properties:

1. The scatterer is to be small enough to fit into a sphere of a given radius.
2. At some fixed frequency it is to have as large a monostatic cross-section as is feasible over a fairly large solid angle.

[1]This scheme would have been analyzed further if time had been available.

3. At frequencies higher than that given in requirement 2, it is to have a reasonably constant cross-section[1].

The first two requirements are well met by a corner reflector, but the third is not. In order to keep the cross-section from increasing rapidly at higher frequencies, we can curve the faces of the corner reflector. If the faces are made of pieces of a sphere, then, for very high frequencies, the cross-section approaches some constant multiplied by the square of the radius of the sphere. If this limiting cross-section is chosen to be about the same as the cross-section of the corner reflector with flat faces at the fixed frequency mentioned in the second requirement, then the cross-section will be relatively independent of frequency above this fixed frequency. Actually it is probably desirable to make the limiting cross-section somewhat larger than (say twice as large as) the corner reflector cross-section at the fixed frequency in order not to degrade the cross-section at the fixed frequency.

No calculations have been made for the cross-section of the corner reflector with three curved faces. However, calculations have been made for some simpler but similar cases. For the bispherical reflector of Figure 6 where the faces meet at 90 degrees the cross-section in the plane perpendicular to the axis of rotation approaches $\pi a^2/3$, where a is the radius of the spheres, for high frequencies. For the bispherical reflector of Figure 7 where the faces meet at an angle of less than 90 degrees, the limiting cross-section is $\pi a^2/4$. If the faces were to meet at an angle greater than 90 degrees, then the limiting cross-section would be zero. From the slight difference between the cross-sections of the reflectors of Figure 6 and 7 we see that an error in the angle at which the faces meet is not as critical as it is for reflectors with plane faces.

[1]It is clear that if the decoy has a high enough cross-section at L-band, then everything said previously would hold for all higher frequencies than L-band. As a result, the following method might easily apply to Project Goose as well as Project Quail.

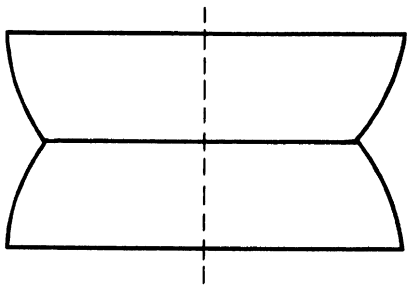

FIG. 6 BISPHERICAL REFLECTOR

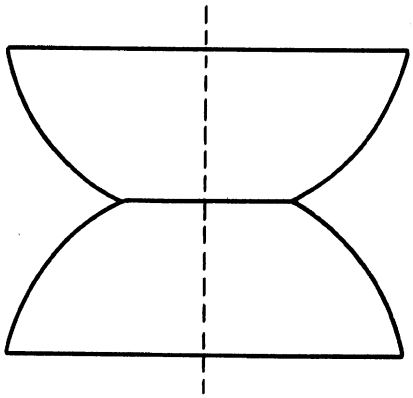

FIG. 7 BISPHERICAL REFLECTOR

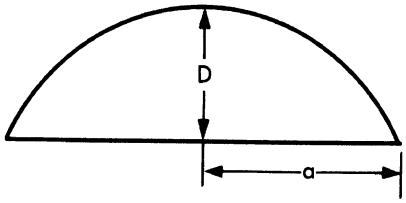

FIG. 8 SPHERICAL CAP

Numerical results are also available for the single scattering case. Figure 9 gives the cross-sections for a sphere of radius a and for a disk of radius a (at normal incidence). Also given are the high frequency limits as given by physical optics for the disk and by geometric optics for the sphere and a spherical cap (Fig. 8). It is reasonable to assume that the cross-section of a spherical cap with fairly large a/D would roughly follow the disk curve up to the geometric optics value, at which point the curve would level off. A similar conclusion would hold for the corner reflector with curved faces.

The cross-section of the shape in Figure 6 was calculated using the method outlined in Section 3.2 of Reference 3. For Figure 7 the results are given in Section 3.2 of Reference 3. The disk cross-section of Figure 9 was taken from Reference 26.

It should be noted that though we have been talking of spherical faces the corner could be constructed with either three cylindrical faces or with two cylindrical and one flat face provided the axes of the cylinders are not parallel. In fact, these latter arrangements might well be more efficient than spherical faces.

An approach similar to that discussed above is considered in Reference 27. There the suggestion is to use deliberate errors in the angles at which the faces of the corners meet, instead of curved faces. With three equal errors they obtain a curve for the cross-section which rises to a maximum and then decreases to zero with increasing frequency, rather than leveling off at a limiting value as the curved face reflector does (see Fig. V-7 of Ref. 27). Also, the angles between the faces would be more critical in the deliberate error approach than in the curved face approach. On the other hand, the curved faces would be more difficult to fabricate than flat faces.

4.4 CONCLUSIONS

If intelligence analysis concludes that the three major defensive methods are 4.1, 4.2, and 4.3 above, and if the conclusions bear out that

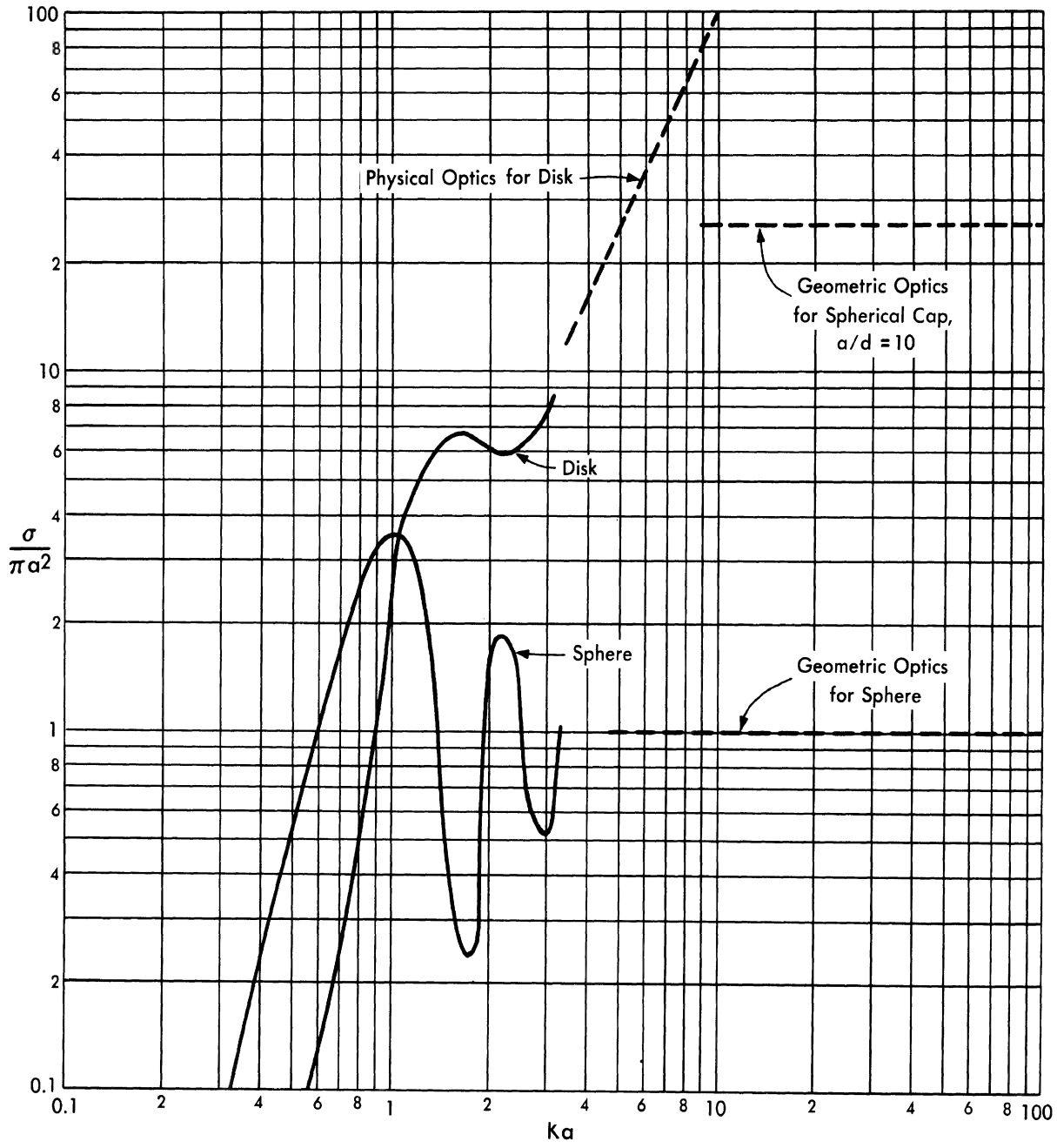

FIG. 9 CROSS-SECTIONS FOR A SPHERE OF RADIUS a AND FOR A DISK OF RADIUS a (AT NORMAL INCIDENCE)

the primary Russian radars are at S-band and the secondary high frequency (above 300 mc/s) radars are at X-band, then it seems that the offense may counter the circular polarization method and the frequency comparison method and improve its bistatic capability somewhat. Nevertheless, bistatic detection looks like the best method for the defense to use. This assumes they have sufficient data gathering and processing equipment at their disposal.

V

CONCLUSION

This analysis shows that decoys can be made to duplicate the electromagnetic properties of B-47 and B-52 aircraft. This report further suggests to the Air Defense Command three methods which it is felt the United States should investigate to augment our defense against Russian decoys. This report further discusses means of countering Russian defenses specifically designed for decoy discrimination. In no way is the solution of the problem complete, but sufficient analysis has been made to permit those in charge of our offense and defense to make adequate decisions and to put into practice those requirements of this report deemed worth augmenting.

APPENDIX A

MONOSTATIC RADAR CROSS-SECTIONS FOR THE B-36 AND THE DUCK VEHICLE

The monostatic radar cross-sections of the original Duck vehicle (Ref. 28) are presented in this appendix for the S-band wavelength $\lambda = 10$ cm. These results have been extrapolated to X-band so that comparisons could be made with X-band B-36 data of the Hughes Aircraft Co. (Ref. 29) and the Naval Research Laboratory. The results of these comparisons are very unsatisfactory especially in the range of broadside azimuths. However, it must be pointed out that the experiments of the Hughes Aircraft Co. are not very reliable at X-band for the B-36 and can be shown to be inconsistent. (These inconsistencies, with the exception of one point, do not occur for the Hughes Aircraft Co. B-47 data.) In addition, the Naval Research Laboratory (Ref. 30) experimental data for the B-36 are known to be very unreliable. We have, however, computed a few values of cross-section for the B-36 at a few aspects for comparison purposes with the Duck. The results verified our feeling that the comparison between the Duck and B-36 is not very good at certain frequency ranges and aspects. The Duck cross-section is definitely too small at azimuth angles of 90° and 180°.

In this light, a final section has been included in this appendix to indicate a possible nose corner reflector arrangement that would augment the cross-section of Duck.

In the following we outline the computations which we did on Duck and on the B-36 and then present graphically the results of this computation.

A.1 DUCK

For the Duck the cross-sections[1] σ(HH) and σ(VV) were computed

[1]The letters in parentheses refer respectively to the polarization of transmitted and received energy.

for azimuths $\gamma = 0^o$, 5^o, 10^o, 20^o, 30^o, 40^o, 50^o, 60^o, 70^o, 80^o, 90^o, 100^o, 110^o, 120^o, 130^o, 140^o, 150^o, 160^o, 170^o, 180^o and elevations $\beta = -4^o$, 0^o, 4^o, 10^o, 30^o, 60^o, 90^o. We thus obtain cross-sections for a large range of aspects. Comparisons with rough theoretical computations for the B-36 have been made for the aspects $\gamma = 0^o$, 90^o, 120^o, 180^o and $\beta = 0^o$, 10^o, 30^o, 60^o, 90^o. Comparison with dynamic experimental data from the Naval Research Laboratory will be limited to elevations $3^o \leq \beta \leq 12^o$ for azimuths $\gamma = 0^o$, 5^o, 10^o, 90^o.

For computational purposes, the Duck was approximated by the following simple contributing shapes:

1. Two circular corner reflectors in transparent housing were oriented as in the specifications[1].
2. The fuselage was considered to be a circular cylinder.
3. The wings were replaced by truncated elliptic cones, with a thin-wire trailing edge.
4. The top section of the vertical tail was considered an elliptic cylinder. It was faired into a rear wedge. The lower section of the vertical tail was simulated in the same manner.
5. The horizontal tail was considered an elliptic cone.
6. The fences were considered semi-circular flat plates.
7. The rear of the fuselage, with the exhaust opening, was considered an annulus. The rear of the fuselage-cylinder was treated as a wire loop. For the autopilot, a rectangular parallelepiped was used.

---

[1]The front reflector consisted of eight corners oriented with one lobe pointing directly forward; the rear reflector consisted of four corners oriented so its reflection pattern to the rear was symmetric relative to the horizontal and vertical planes.

8. The shell around the rocket motor was taken to be a truncated circular cone.

The following approximations were employed:

a. The circular cylinder was considered only at $\gamma = 90^{\circ}$.

b. Flat plates were considered only at normal incidence. Their edges are in reality rounded, so that edge contributions were neglected.

c. For wedges and elliptic cones, the contribution near normal was obtained until aspects were reached at which it became negligible. For off-normal, bodies of this type could be neglected.

d. The effect of shadowing was determined from the plan views. This determination was necessarily crude.

The list of cross-section expressions used in computation for the Duck are:

I. The triple-reflection cross-section of the circular reflector was obtained from the relation

$$\sigma = \frac{4\pi A^2}{\lambda^2},$$

where λ is wavelength and A is given as a function of the direction cosines ℓ, m, and n of the direction of incidence with the edges of the reflector, by Equations (D. 4-1) and (D. 4-2) in Appendix D. The values of A were obtained from Figure D. 4-1 in Appendix D.

II. The circular cylinder which represents the central portion of the fuselage has a cross-section at normal incidence given by

$$\sigma = \frac{2\pi L^2 b}{\lambda},$$

where L is the length and b the radius of the cylinder. For peak widths, the sum of the two off-normal components becomes equal to a fraction β of the peak height for an angle θ, given by

$$\frac{\sin\theta}{\cos^2\theta} = \beta \times 8\pi^2 \left(\frac{L}{\lambda}\right)^2 ,$$

where θ is measured from the cylinder axis. It followed from this that the circular cylinder could be neglected for off-normal aspects.

III. The wings were considered to be truncated elliptic cones except from the rear. For such a shape the cross-section at normal incidence is

$$\sigma = \frac{8\pi \left(L_2^{3/2} - L_1^{3/2}\right)^2 \tan^4 a}{9\lambda \eta^2 \left|\cos\theta\right|^3} ,$$

where a is the half cone angle, η is a/b for the ellipse, and where the cone is truncated by the planes $z = L_1$ and $z = L_2$, $z = 0$ being its vertex. θ is the angle between the direction of incidence and the z-axis. Off-normal, there are contributions for $z = L_1$ and $z = L_2$ given by

$$\sigma = \frac{\lambda z \eta^3 \tan a}{8\pi \sin\theta \sqrt{\sin^2\phi + \eta^2\cos^2\phi}} \left[\frac{\dfrac{\sin\theta}{\sqrt{\sin^2\phi + \eta^2\cos^2\phi}} - \dfrac{1}{\eta}\cos\theta\tan a}{\sin\theta\tan a\sqrt{\sin^2\phi+\eta^2\cos^2\phi}+\eta\cos\theta} \right]^2 .$$

Here the x-axis is the semi-major axis of the ellipse. ϕ is the usual spherical coordinate.

The horizontal tail was also considered an elliptic cone when viewed from below.

IV. Wedges were used for the rear edges of the vertical and horizontal tails. Let the edge-length be L, the half-angle be α, and the z-axis be perpendicular to the edge, but in the plane which contains the edge and bisects the angle. For incidence in the normal plane, where θ is the angle with the z-axis, $0 \leq \theta \leq \alpha$,

$$\sigma = \frac{\pi L^2}{(\pi-\alpha)^2} f(\vec{p}) + \frac{L^2 \sin^2 2\alpha}{4\pi \cos^2(\alpha - \theta) \cos^2(\alpha + \theta)} .$$

Here $f(\vec{p}) = 1$ for polarization parallel to the edge of the wedge and = 0 for perpendicular polarization.

For incidence in the normal plane, and for $\alpha \leq \theta \leq \pi/2 - \alpha$, the cross-section is

$$\sigma = \frac{\pi L^2}{(\pi - \alpha)^2} f(\vec{p}) + \frac{L^2}{4\pi} \tan^2 (\alpha + \theta) .$$

The wedge contributions were not significant enough to necessitate employment of a peak-width formula for off-normal incidence.

V. The top half of the vertical tail was taken to be an elliptic cylinder except from the rear. For such a body, of length L with semi-axis a, the cross-section at normal incidence is

$$\sigma = \frac{2\pi L^2 a^2 b^2}{\lambda (a^2 \cos^2 \phi + b^2 \sin^2 \phi)^{3/2}} ,$$

where ϕ is measured from the major axis. The cross-section of such a body was negligible, as expected, except near broadside.

VI. The fences were represented by flat plates. The cross-section at normal incidence was, therefore,

$$\sigma = \frac{4\pi A^2}{\lambda^2},$$

where A is the area of the plate. Since the edges of the fences are not too sharp, off-normal contributions were neglected.

The battery and autopilot boxes have flat sides which were treated similarly as flat plates. Likewise, the corner reflectors presented flat plates at some aspects.

VII. The rear edge of the cylindrical fuselage was taken as a wire loop, visible only directly tail-on. Its cross-section, which is small, is $\sigma = \pi a^2$ (a is the cylinder radius).

VIII. A small annulus is formed by the exhaust nozzle of the rear of the fuselage. Its flat-plate contribution at normal (tail-on) incidence was computed as

$$\sigma = \frac{4\pi}{\lambda^2}\left[\pi(R_2^2 - R_1^2)\right]^2,$$

where R_1 and R_2 are the inner and outer radii. It was found to be negligible.

IX. Dihedral contributions were present at aspects for the corner reflectors for which one direction cosine vanishes. In this case, if m is intermediate in value of the three cosines the contribution is

$$\sigma = \frac{4\pi A^2 \cos^2 2\gamma}{\lambda^2},$$

where A is $(\pi/2)a^2$ m N, where N is the number of quadrants of the circle visible. Here a is the radius, and γ the angle between the polarization vector and the edge of the dihedral.

X. The shell housing the rocket motor was represented by a truncated circular cone. The formulas for this may be obtained by setting $\eta = 1$ in those for the truncated elliptic cone.

A.2 B-36 RADAR CROSS-SECTION COMPUTATION

Rough computations of the monostatic radar cross-section of the B-36 bomber are herein presented for some aspects. The assumed configuration was that of the B-36H, gun turrets retracted. No account was taken of interior cross-sections of the objects visible to the radar through the transparent nose or through radome material.

The formulas used were taken exclusively from References 2 and 31 and the configuration was simulated as follows:

Fuselage	half of a prolate spheroid, a cylinder, and a truncated cone capped by a hemisphere
Wing and Horizontal Tail	a truncated elliptic cone and a wedge
Vertical Tail	a cylinder, a flat plate, and a wedge
Reciprocating Engines (nacelles)	ogives faired into the "wing wedges"
Jet Engines (nacelles)	two tori and a cylinder for each engine
Vertical Jet Support	an inclined cylinder and a wedge
Inclined Jet Support	a thin wire.

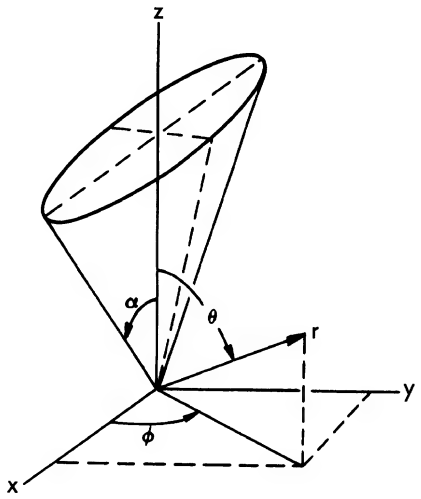

FIG. A-1 ELLIPTIC CONE GEOMETRY

Throughout the above, the wedge contributions were modeled by a thin wire when the radar illumination was incident in or near the plane of the wedge.

The prolate spheroid contribution was calculated from Formula A. 3-2 of Reference 2 by replacing θ by γ and ϕ by $\pi/2 - \beta$. At the broadside and vertical aspects the value used was one-half the value predicted by A. 3-2 (Ref. 2), i. e.,

$$\sigma = \frac{\pi b^4 c^2}{(b^2 \sin^2 \gamma + c^2 \cos^2 \gamma)^2} ,$$

where b = 7. 0, c = 20, since the "stationary phase point" may be considered as "split" between the two halves of the prolate spheroid.

Estimation of the cylinder contribution was obtained from the formula

$$\sigma = \frac{R \lambda \sin \theta}{2 \pi \cos^2 \theta} \sin^2 \left[\frac{2 \pi L}{\lambda} \cos \theta \right] ,$$

where R = 7 ft and L = 60 ft, which may be derived from Formula A. 1-11 of Reference 2. At broadside this gives

$$\sigma = \frac{2 \pi R L^2}{\lambda} .$$

At the vertical aspect, L was taken as 100 ft.

Tail cone contributions were obtained from Formula A. 3-8 of Reference 2.

$$\sigma = \frac{\lambda L \tan \alpha}{8 \pi \sin \theta} \tan^2 (\theta - \alpha) ,$$

where $L = 40$ ft and $\alpha = 5.5^{o}$. The geometry appears in Figure A-1. For aspects between broadside and tail-on the hemisphere contribution is given by Formula A. 3-3 of Reference 2 as

$$\sigma = \pi a^2 .$$

For the B-36, it was assumed that $a = 2$ ft.

Estimated cross-section for the truncated elliptic cone used to simulate the wing leading edge was obtained from A. 3-6 of Reference 2 using the following dimensions (in the terminology of Reference 2):

$L = 132$ feet

$\eta = a/b = 3.67$

a = semi-major axis

b = semi-minor axis

$\tan \alpha = 5/33$, and

$$\sigma = \frac{\lambda L \eta^3 \tan \alpha}{8 \pi B \sin \theta} \left[\frac{\frac{\sin \theta}{B} - \frac{1}{\eta} \cos \theta \tan \alpha}{B \sin \theta \tan \alpha + \eta \cos \theta} \right]^2$$

$$B^2 = \sin^2 \phi + \eta^2 \cos^2 \phi,$$

where θ and ϕ are again as defined in Figure A-1.

The thin wire formula is Formula (5) of Reference 31 after averaging over all polarizations and defining $L = 2\ell$. Since the precision of the calculations for our purposes need not be as great as for Reference 31, the objections to the thin wire formula are not serious, so that

$$\sigma = \frac{6\pi L^2 \sin^2\theta \left[\dfrac{\sin\left(\frac{2\pi L}{\lambda}\cos\theta\right)}{\frac{2\pi L}{\lambda}\cos\theta}\right]^2}{\pi^2 + \left[\ln\dfrac{\lambda}{1.78\,\pi a \sin\theta}\right]^2} .$$

The dimensions used were L = 110 ft and a = 1/40 ft. In the case of the horizontal tail, L = 35 ft and a = 1/40 ft.

The dominant contributions of the vertical tail were due to a cylinder 10 in. long corresponding to the essentially straight section of the leading edge, the trailing wedge 20 ft long and modeled by a wire 1/40 ft in radius and a flat plate 30 ft long and 1/2 ft wide. The flat plate contribution was assumed to be given by

$$\sigma = \frac{4\pi A^2}{\lambda^2} .$$

The jet engines were modeled by tori in the nose-on and tail-on regions and by a cylinder at broadside, for which R = 1.2 ft and L = 6 ft. The torus cross-section is given by

$$\sigma = \frac{8\pi^3 ab^2}{\lambda} ,$$

where a = 0.001 ft and b = 1 ft.

The jet engine support and brace were found to have negligible cross-sections at the aspects herein considered. All of the above dimensions are approximate, so that while the computed cross-section is not exact, it is of the right order of magnitude.

It was noted in the rough computations that for the B-36 a peak of $\sigma = 2.3 \times 10^4$ m^2 from the leading edge of the wing occured for azimuth 15.5^o and elevation 0^o. There was no matching peak for Duck since a peak of $\sigma = 1.5$ m^2 from the leading edge of the wing occured at azimuth 4^o and elevation 0^o.

A.3 EXPERIMENTAL DATA

The Naval Research Laboratory (NRL) S-band results shown in Figure 2a of the main text are taken from the data of the Naval Research Laboratory report previously referenced. Since this data covers only elevations from 3^o to 12^o, a comparison is made only at the 10^o elevation for each azimuth except 30^o.

Due to the saturation effects (Ref. 30) this data is somewhat scattered and fragmentary. The medians were not measured directly but were determined from the measured 75th percentile and the characteristics of the distribution of amplitudes.

No NRL values are shown in Figure 2.2 for an azimuth of 30^o because of the wide disagreement of experimental data in this region.

A.4 NEW ARRANGEMENT OF NOSE REFLECTORS FOR DUCK

A possible new arrangement for the corner reflectors for Duck is as follows:

In the nose of Duck place a circular corner reflector C of edge a = 18 in. with vertex abutting on battery installation 2-1/2 in. above longitudinal axis of Duck and with symmetry axis of C pointing forward at an elevation $\beta = 10^o$.

Let $\hat{i}$, $\hat{j}$, $\hat{k}$ be unit vectors in the directions of the usual right-handed xyz-aircraft-coordinate system (x-axis forward out of the nose, z-axis upward).

Take $\hat{e}_1^C$, $\hat{e}_2^C$, $\hat{e}_3^C$ to be a right-handed system describing the edges of C with $\hat{e}_1$ in the vertical plane of symmetry of Duck . Put

$$\alpha = 10^{\circ} + \cos^{-1} \frac{1}{\sqrt{3}} = 64.74^{\circ} .$$

Then $\hat{e}_1^C$, $\hat{e}_2^C$, $\hat{e}_3^C$ are given in the $\hat{i}$, $\hat{j}$, $\hat{k}$ system by

$$\hat{e}_1^C = \cos\alpha\,\hat{i} - \sin\alpha\,\hat{k} ,$$

$$\hat{e}_2^C = \frac{1}{\sqrt{2}} (\sin\alpha\,\hat{i} + \hat{j} + \cos\alpha\,\hat{k}) .$$

$$\hat{e}_3^C = \frac{1}{\sqrt{2}} (\sin\alpha\,\hat{i} - \hat{j} + \cos\alpha\,\hat{k}) .$$

To the right and left[1] of C place two circular corner reflectors, each of edge 14.4 in., with vertices coincident on the $\hat{e}_1^C$ - axis 3.6 in. from the vertex of C (Fig. A-2).

Describe the right reflector R with the system $\hat{e}_1^R$, $\hat{e}_2^R$, $\hat{e}_3^R$ and the left reflector L with the system $\hat{e}_1^L$, $\hat{e}_2^L$, $\hat{e}_3^L$. Then

$$\hat{e}_1^R = \hat{e}_1^C, \quad \hat{e}_2^R = -\hat{e}_3^C, \quad \hat{e}_3^R = \hat{e}_2^C , \quad \text{and}$$

$$\hat{e}_1^L = \hat{e}_1^C, \quad \hat{e}_2^L = \hat{e}_3^C, \quad \hat{e}_3^L = -\hat{e}_2^C .$$

In the direction of the axis of symmetry of the forward-looking corner reflector C(0° azimuth, 10° elevation),

$$\sigma_C = \frac{15.61\,a^4}{\lambda^2} = \frac{(15.61)(18)^4(2.54)^4}{(10^2)(10^4)} = 68.2\ m^2 .$$ [2]

---

[1] Considered while facing C.

[2] This is σ(HH) or σ(VV). σ(RR) = 27.8 m^2; σ(HV) = 16.55 m^2 .

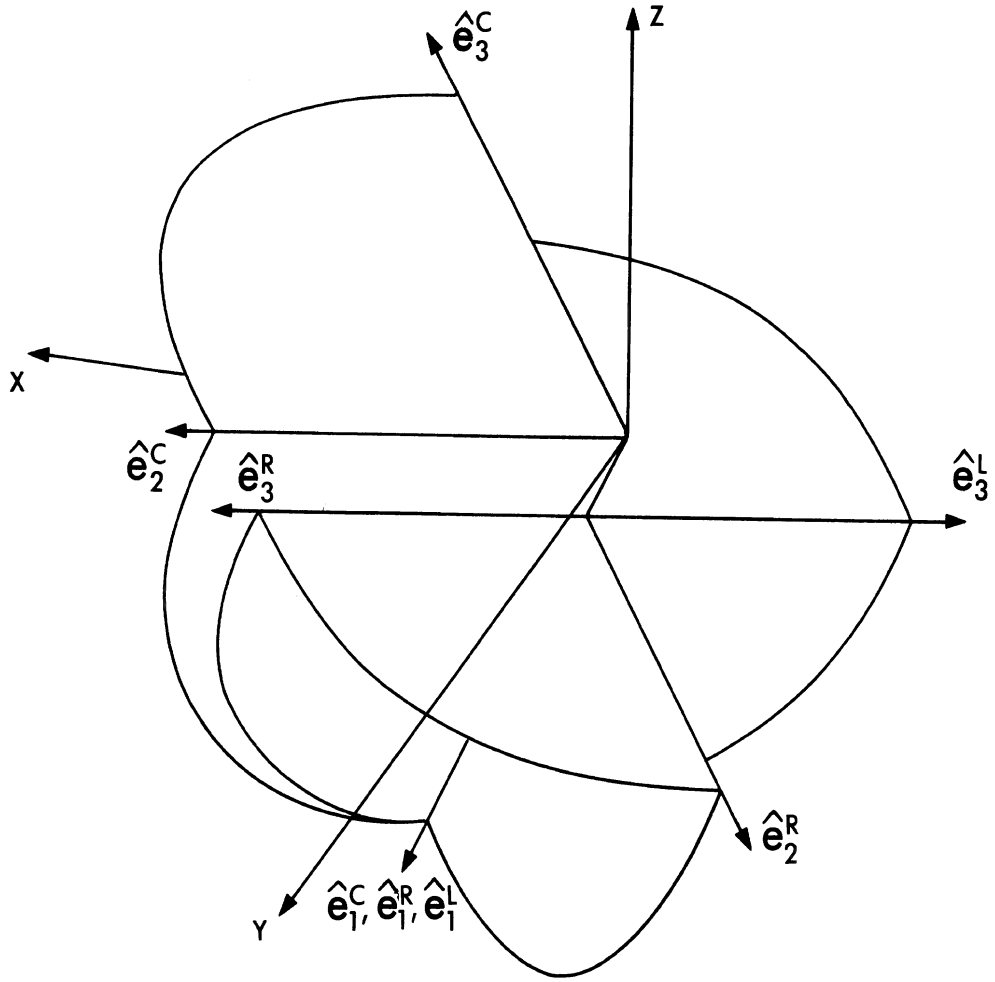

FIG. A-2 SUGGESTED NEW ARRANGEMENT FOR NOSE REFLECTORS IN DUCK

Broadside (direction of incidence $\hat{r} = \hat{j}$) a dihedral contribution is obtained from reflector R. The cross-section is

$$\sigma = \frac{\pi^3}{\lambda^2} (m^R)^2 \; a^4 \left[\frac{2(e_{1z}{}^R)^2}{\sin^2 \theta^*} - 1 \right]^2 ,$$

where $$m^R = \hat{e}_2{}^R \cdot \hat{r} = - \hat{e}_3{}^C \cdot \hat{j} = \frac{1}{\sqrt{2}} ,$$

$$e_{1z}^R = \hat{e}_1{}^R \cdot \hat{k} = - \sin \alpha ,$$

$$\theta^* = 90^\circ ;$$

hence, $$\sigma = 11.25 \text{ sq. m}^1$$

For nose-on incidence (0° azimuth, 0° elevation), the cross-section is computed by

$$\sigma = \frac{4 \pi A^2}{\lambda^2} ;$$

here[2] A = .202 sq. m and λ = .1 m; so that

---

[1]This is σ(HH) or σ(VV). σ(RR) = 27.8 sq. m; σ(HV) = 16.55 sq. m.

[2]The expression for A for a circular corner reflector of edge r with edges making direction cosines ℓ, m, n with the direction of incidence is given by

$$\frac{A}{r^2} = \ell \tan^{-1} \frac{1-2\ell^2}{4\ell^2 mn} + m \tan^{-1} \frac{1-2m^2}{4\ell^2 mn} + n \tan^{-1} \frac{1-2n^2}{4\ell^2 mn} \quad \text{for } \ell^2 \leq \frac{1}{2}$$

$$\frac{A}{r^2} = m \tan^{-1} \frac{2\ell n}{1-2n^2} + n \tan^{-1} \frac{2\ell m}{1-2m^2} \quad \text{for } \ell^2 \geq \frac{1}{2} .$$

For a more detailed discussion, see Appendix D.

σ = 51.3 sq. m .

For 0^{o} azimuth, 30^{o} elevation, the cross-section has dropped off to

σ = 21.6 sq. m .

TABLE A-1

COMPARATIVE CROSS-SECTION, OLD AND NEW ARRANGEMENTS FOR DUCK

	σ (new arrangement)	σ (original arrangement)
γ = 0, β = 10	68.2 sq. m	25.9 sq. m
γ = 90, β = 0	11.25 sq. m	11.1 sq. m
γ = 0, β = 30	21.6 sq. m	94.6 sq. m

An alternative possibility might be to place a circular flat plate forward of the battery and auto-pilot with its normal having 0^{o} azimuth and 10^{o} elevation. Place another flat plate perpendicular to the first. This yields a cluster of four corner reflectors (Fig. A-3).

The 0^{o} azimuth, 10^{o} elevation contribution would of course be from the circular flat plate and would be σ = 169 sq. m. The broadside contribution would be due to an almost semi-circular flat plate and would be $\sigma \cong 50$ sq. m.

The situation here of course is that the desired large contribution is obtained in exactly two particular directions with rapid drop-offs near these directions.

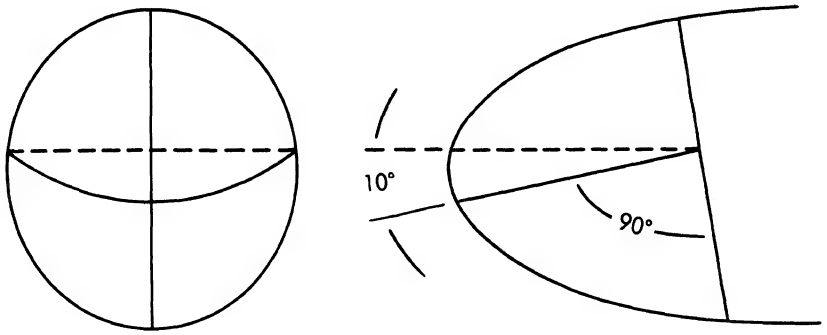

FIG. A-3 AN ALTERNATIVE REFLECTOR ARRANGEMENT

APPENDIX B

EVANS SIGNAL LABORATORIES EXPERIMENTAL DATA ON THE RADAR CROSS-SECTION OF THE B-47 AIRCRAFT

The Antenna and Microwave Circuitry Branch of the Evans Signal Laboratories conducted a series of radar back-scattering cross-section measurements from a model of the B-47. The measurements were performed at an actual frequency of 3000 Mc which corresponded to a "full-scale" frequency of 150 Mc.

Figure B-1 shows the coordinate system used in the measurements and gives meaning to the θ and ϕ which appear in later figures. Figures B-2a through f are graphs of cross-section σ vs. θ.

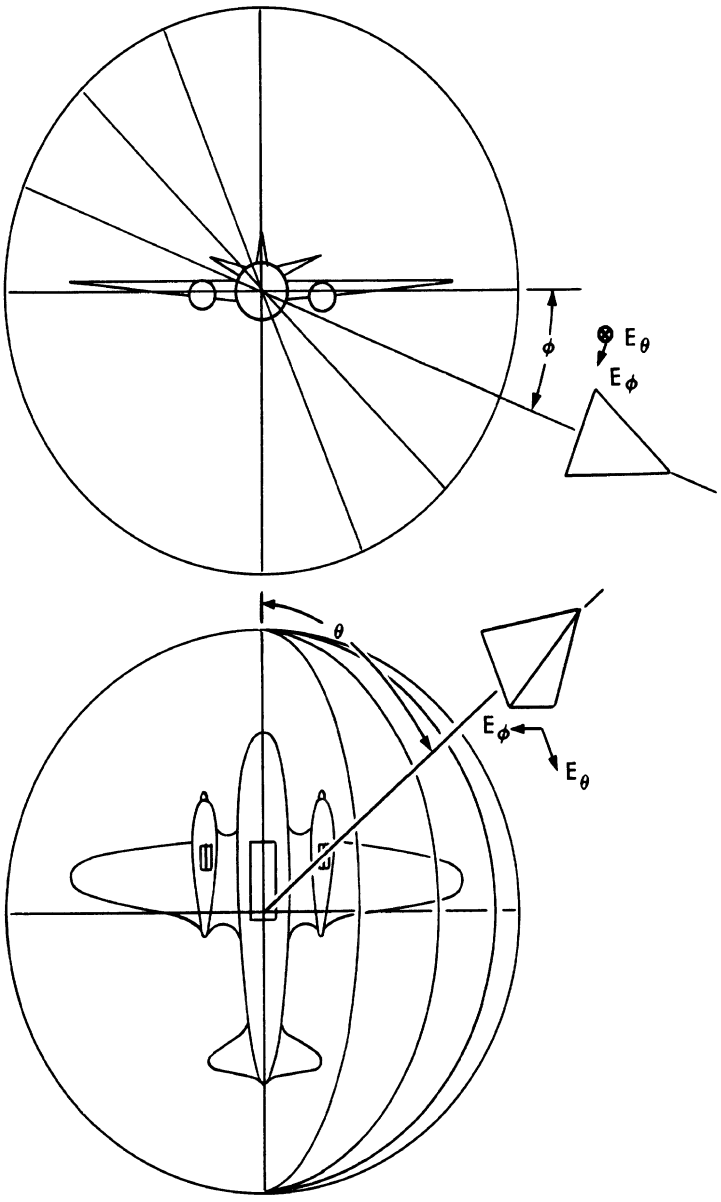

FIG. B-1 COORDINATE SYSTEM FOR AIRPLANE REFLECTION COEFFICIENT PATTERNS (as used by the Evans Signal Laboratory)

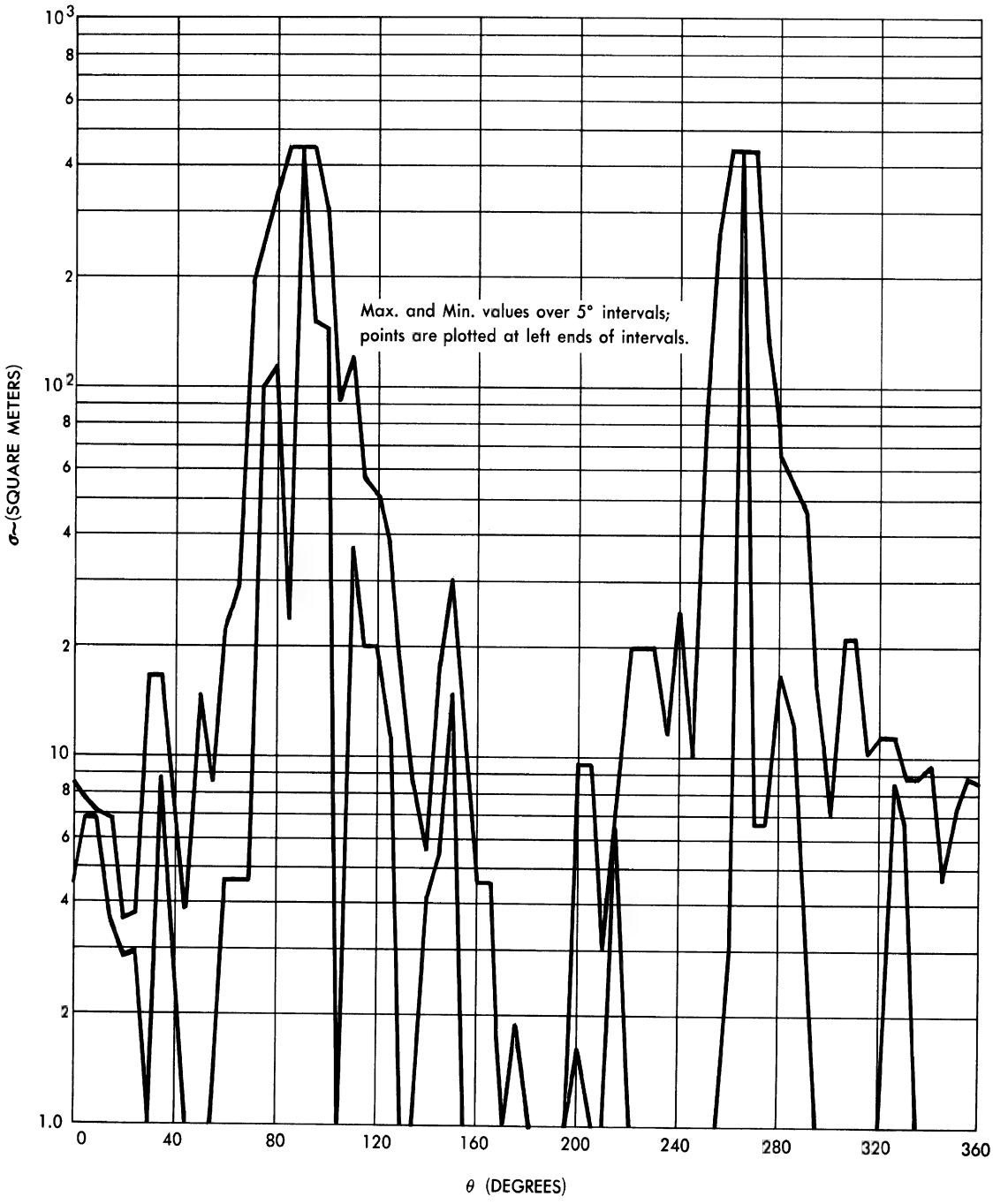

FIG. B-2a CROSS-SECTION OF THE B-47 AIRCRAFT AT 150 MC. - EVANS SIGNAL LABORATORY DATA ($\phi = 90°$; E_θ)

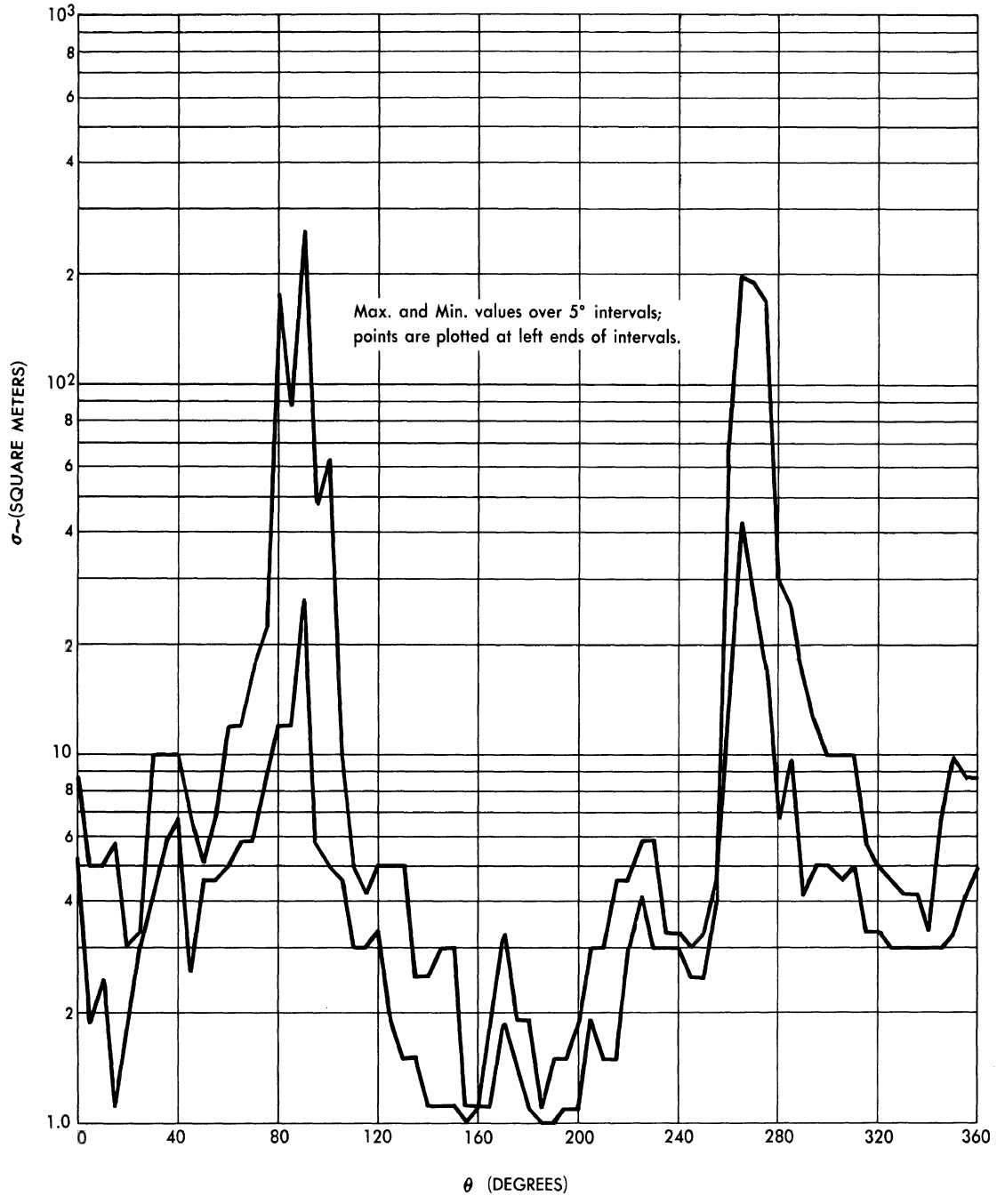

FIG. B-2b CROSS-SECTION OF THE B-47 AIRCRAFT AT 150 MC. - EVANS SIGNAL LABORATORY DATA (ϕ = 0°; E_ϕ)

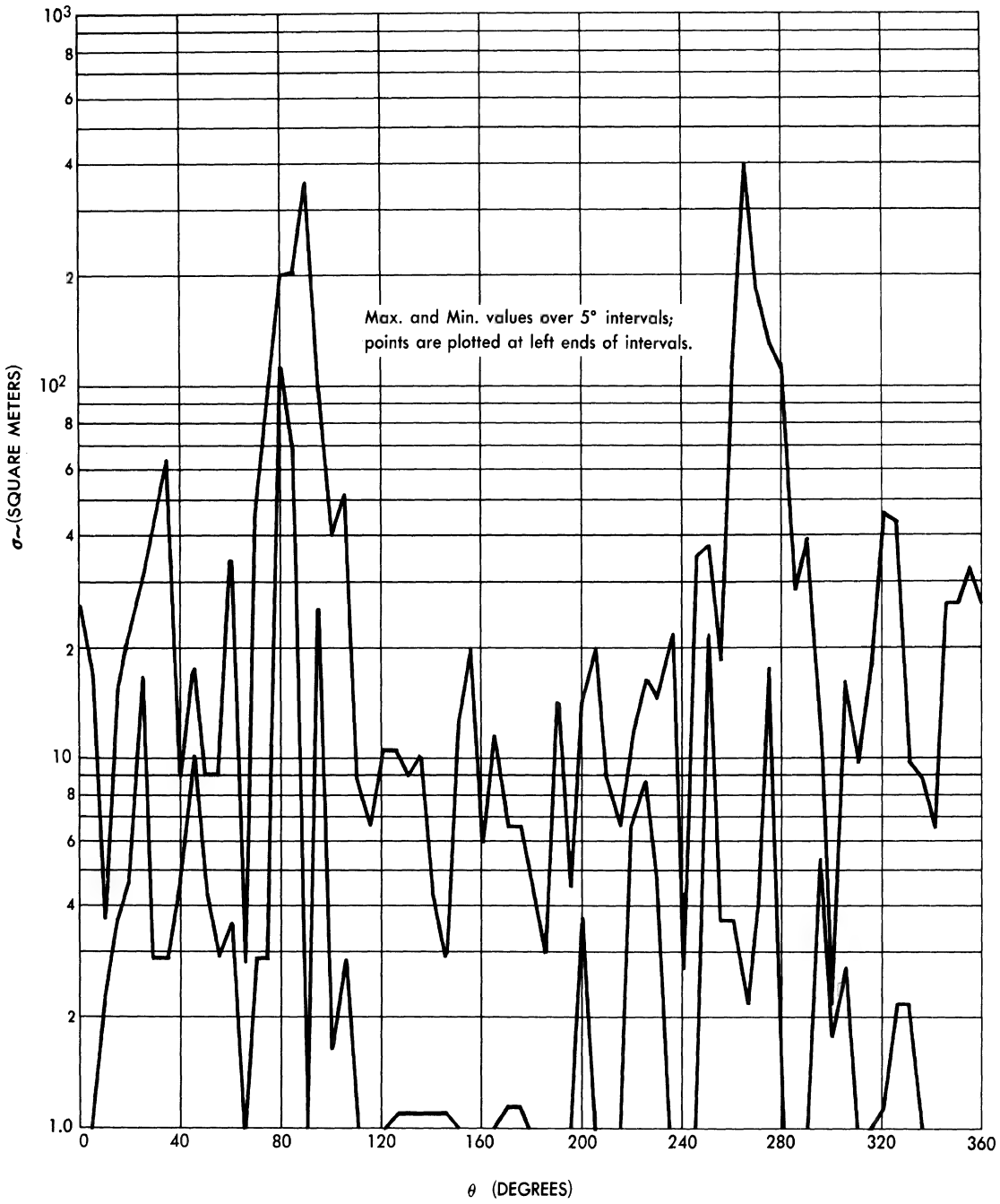

FIG. B-2c CROSS-SECTION OF THE B-47 AIRCRAFT
AT 150 MC. - EVANS SIGNAL LABORATORY DATA
($\phi = 0°$; E_θ)

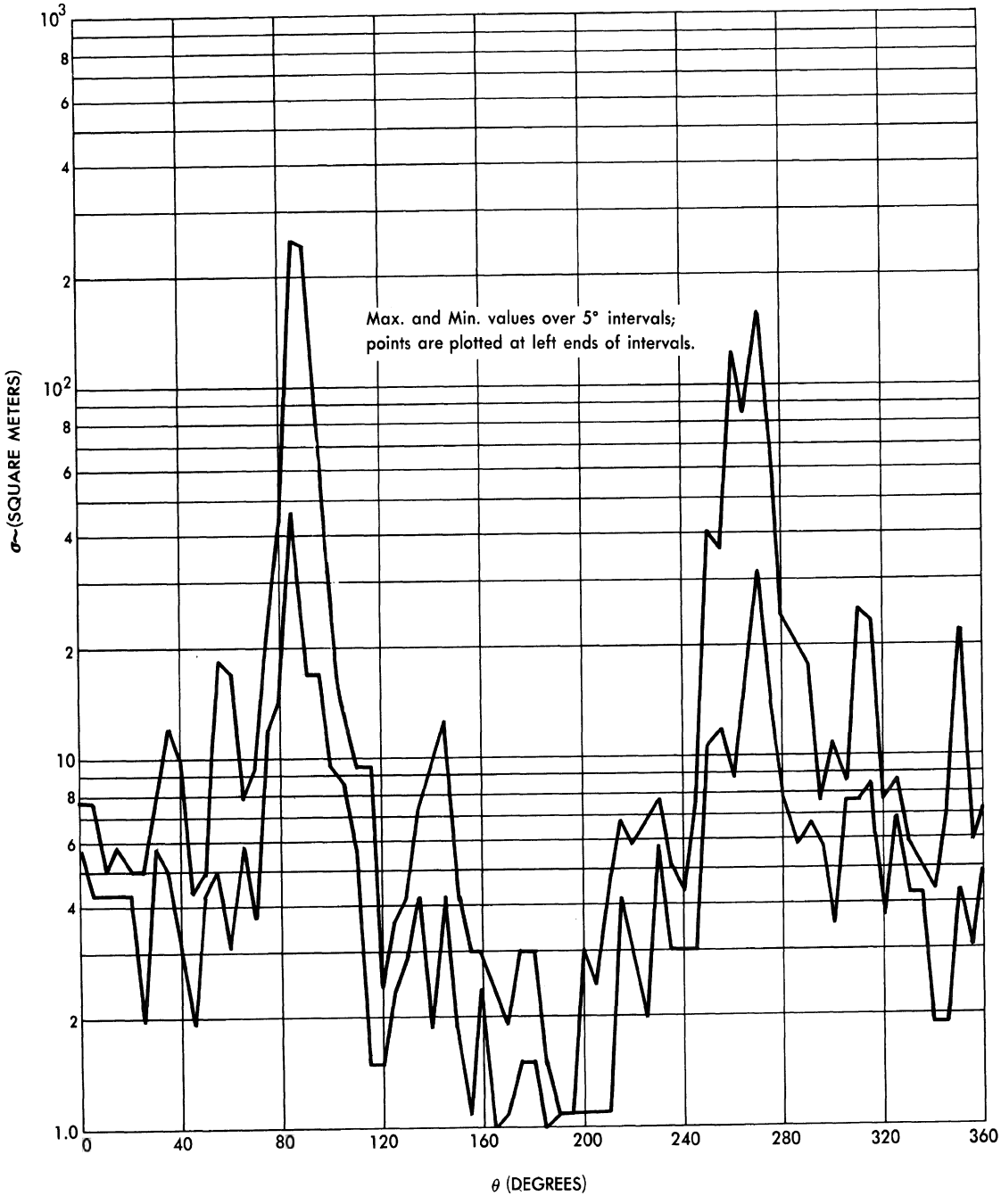

FIG. B-2d CROSS-SECTION OF THE B-47 AIRCRAFT AT 150 MC. - EVANS SIGNAL LABORATORY DATA ($\phi = 45°$; E_ϕ)

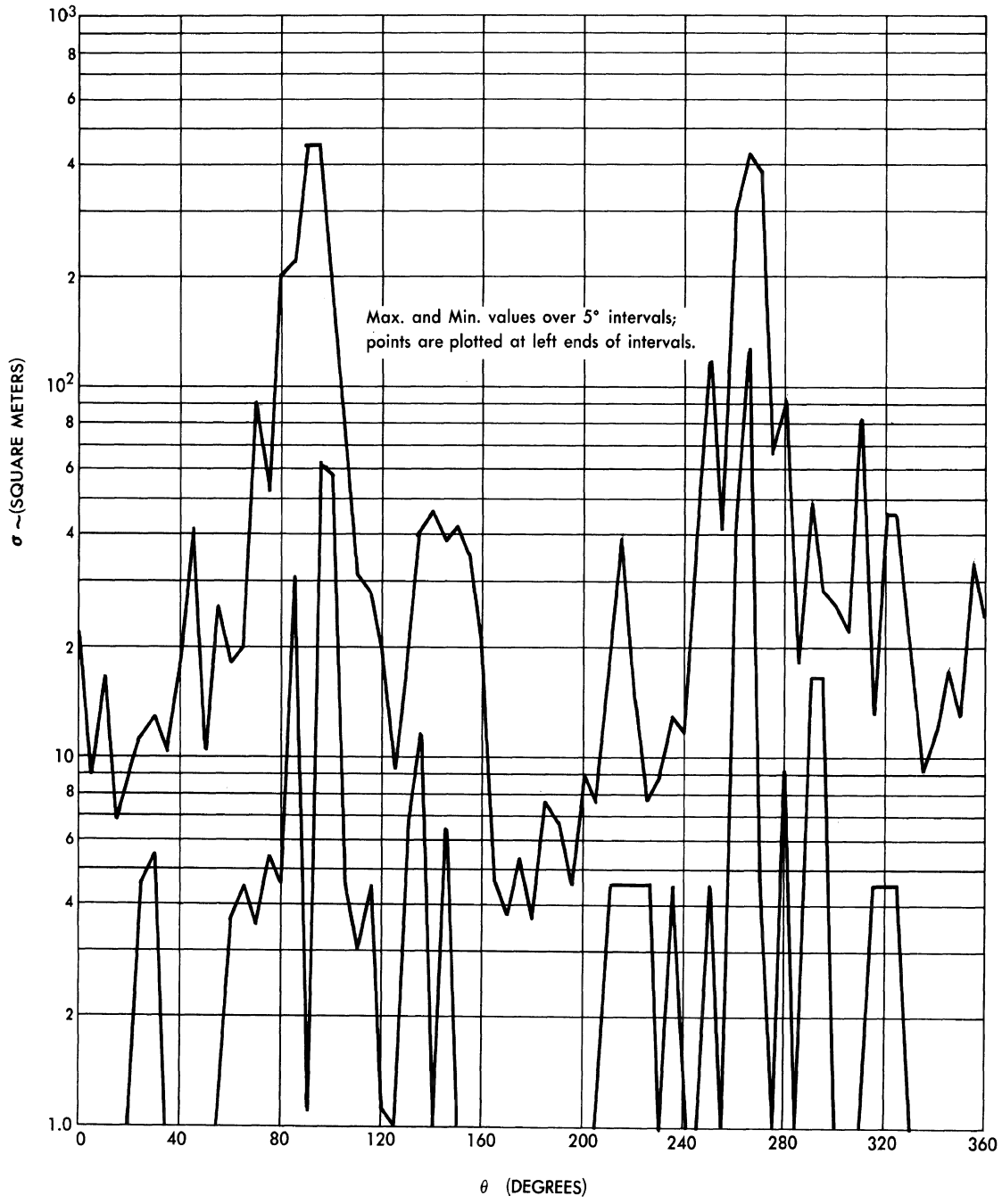

FIG. B-2e CROSS-SECTION OF THE B-47 AIRCRAFT AT 150 MC. - EVANS SIGNAL LABORATORY DATA ($\phi = 45°$; E_ϕ)

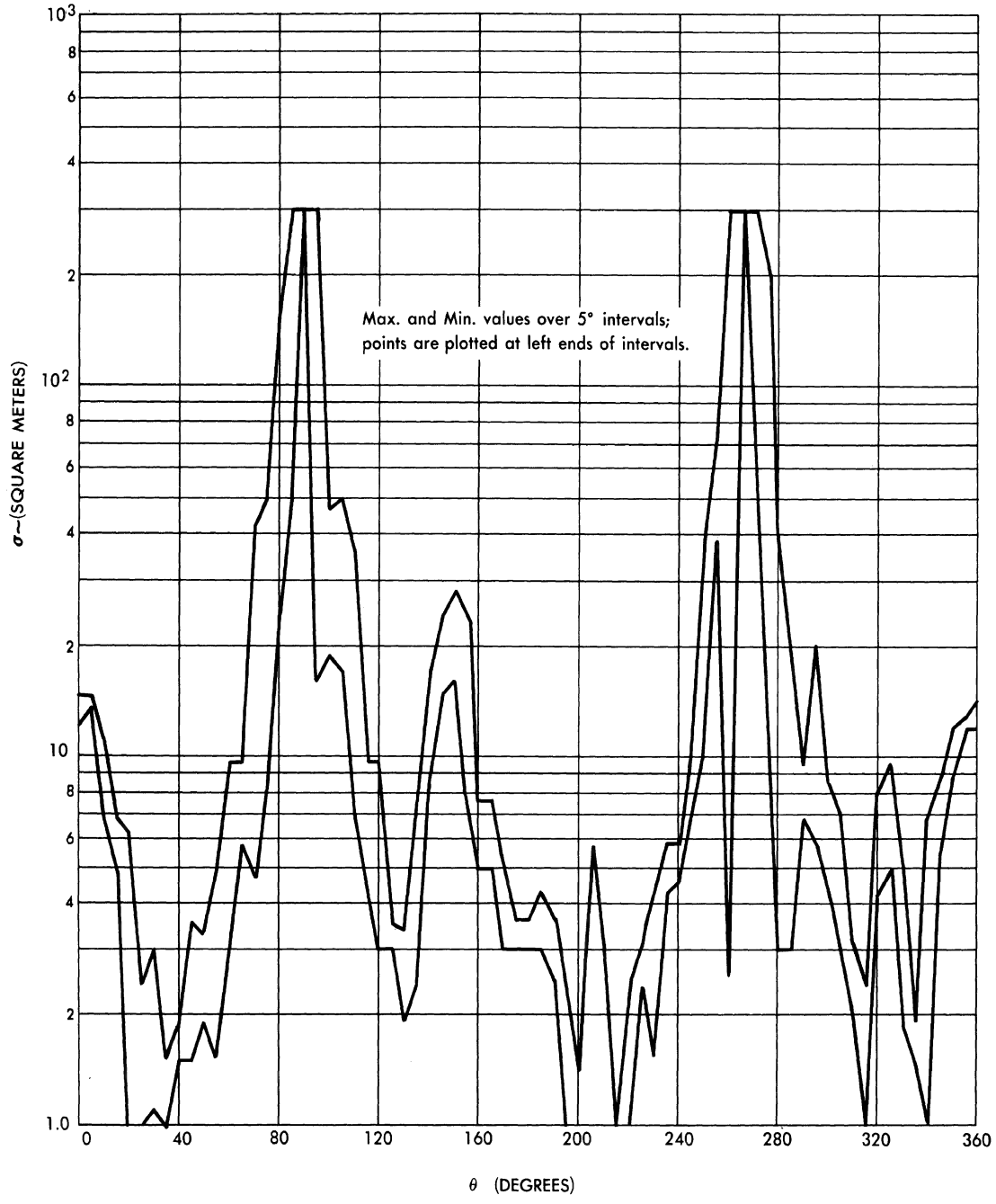

FIG. B-2f CROSS-SECTION OF THE B-47 AIRCRAFT
AT 150 MC. - EVANS SIGNAL LABORATORY DATA
(ϕ = 90° ; E_ϕ)

APPENDIX C

EXPERIMENTAL SCATTERING DATA OBTAINED BY MICROWAVE RADIATION COMPANY, INC.

In order to set a foundation for the theoretical discussion of repolarization we have had performed a number of radar scattering experiments. Under subcontract to the Microwave Radiation Company, Inc., the back scattering cross-sections of various geometrical configurations were to be measured for a range of linear polarizations. The combinations are as follows:

	Transmit	Receive
1.	vertical	vertical
2.	horizontal	horizontal
3.	horizontal	$+45^{o}$
4.	horizontal	-45^{o}
5.	$+45^{o}$	-45^{o}
6.	$+45^{o}$	$+45^{o}$
7.	vertical	$+45^{o}$

In addition, the back-scattering cross-sections were to be measured for various geometrical configurations when circular polarization combinations are used. The combinations are as follows:

	Transmit	Receive
1.	right hand	right hand
2.	right hand	left hand

The geometrical configurations to be measured are as follows:

1. Ten elliptic cylinders whose semi-major axes are equal and of 5 λ magnitude and whose semi-minor axes are 0.15 λ, 0.30 λ, 0.45 λ, 0.60 λ, 0.75 λ, 1.10 λ, 1.45 λ, 1.80 λ, 2.15 λ, and 2.5 λ. The length of the elliptic cylinders is primarily determined by far zone considerations of phase front uniformity. It is assumed that an aspect ratio comparable to that of the B-47 or B-52 wing would be a reasonable value. The length, L, would then be approximately 30 λ to 40 λ. The cylinders are fitted with smooth end caps.

2. Three ogival cylinders whose semi-major axes are 5 λ and whose semi-minor axes have the values 0.30 λ, 0.45 λ, and 1.0 λ. The ogival cylinders are fitted with smooth end caps.

3. A wing and body scatterer simulated by a right circular cylinder fuselage and two sets of wings. The diameter of the right circular cylinder is 10 λ. The first set of wings are elliptic cylinders of semi-minor axis 0.45 λ. The second set are ogival cylinders of semi-minor axis 0.45 λ. Both sets of wings are to be fitted in two positions, high wing and intermediate wing, and for two sweep-back angles of 30^{o} and 45^{o}.

4. Two rectangular plates whose center lines are separated by a spacing "d" and which are inclined at an angle, θ, with respect to each other (used as a model for diffraction repolarization studies). The three values of d to be used are 10 λ, 15 λ, and 20 λ, and θ has values 0^{o}, 15^{o}, 30^{o}, 45^{o}, 60^{o}, 75^{o}, and 90^{o}.

Measurements to be made on the configurations are as follows:

1. Elliptic Cylinder. The back-scattering cross-section is measured at intervals of 5^{o} from 0^{o} to 50^{o} and at intervals of 10^{o} from 50^{o} to 90^{o} in the principal plane for each of the nine polarization combinations. The major axis defines the zero angle of incidence, and the plane of rotation is the plane transverse to the cylinder axis.

2. Ogival Cylinder. Measurements are made at the same points as for the elliptic cylinder.

3. Wing-body Assembly. Measurements are made to furnish the back-scattering cross-section of the right circular cylinder fuselage alone for the points specified by the conical cuts θ = 30°, 45°, 70°, and 90°, where θ is measured with respect to the vertical z-axis of the cylinder. The cylinder axis is aligned along the x-direction. Measurements are made at 10° intervals in ϕ from 0° to 90°. When $\theta = 90^{\circ}$, the values of ϕ are determined for which the back-scattering cross-section is 1/3 and 1/10 the peak value. The "fuselage" is fitted with "wings", and back-scattering cross-section is determined for $\theta = 70^{\circ}$, 90°, 110°, 135°, and 150° in 10° steps for $\phi = 0^{\circ}$ to 180°. The measurements are repeated for the two wing positions. For the high and intermediate vertical positioning of the wings for both wing sets and both sweep-backs $\theta = 70^{\circ}$, 90°, 110°, 135°, and 150°, and for each $\theta, 0 \leq \phi \leq 180^{\circ}$ in steps of 10°. For the intermediate vertical positioning of the wings for both wing sets and both sweep-backs $\theta = 30^{\circ}$, 45°, 70°, 90°, 110°, 135°, 150°, and for each $\theta, 0 \leq \phi \leq 180^{\circ}$ in steps of 10°. A polar coordinate system is defined in which the polar angle α is measured from the x-axis and the azimuthal angle β is measured from the z-axis in the yz-plane. For both wing sets, vertical positioning, and both sweep-backs $\alpha = 90^{\circ}$, $90^{\circ} \pm \phi_{1/3}$, $90^{\circ} \pm \phi_{1/10}$, and for each $\alpha, 0^{\circ} \leq \beta \leq 180^{\circ}$ in steps of 10°.

4. Parallel Planes. Measurements are made at 15° intervals from 0° to 360° for all values of spacing and plate angle for the nine polarization combinations.

5. Single Plane. Measurements are made at 15° intervals from 0° to 360°.

At the completion date of the subcontract only the results for the elliptic and ogival cylinders and the flat plates had been received and these only for the polarization combinations:

	Transmitted	Received
1.	vertical	vertical
2.	horizontal	horizontal
3.	$+45^{o}$	$+45^{o}$
4.	$+45^{o}$	-45^{o}
5.	right hand	left hand
6.	right hand	right hand.

In order to interpret the scattering data from the various cylinders we consider the formulation of the back-scattering problem in terms of the scattering matrix (Ref. 14, Sec. II) notation. Since the back-scattering properties of a given object are specified to within an arbitrary phase degeneracy by five independent cross-sections (Ref. 14, Sec. II), the six polarization experiments should specify the scattering matrix and in addition give a consistency check among the various quantities.

In the notations of Reference 14,the S-matrix for a scatterer with cylindrical symmetry is of the form

$$S = \begin{pmatrix} S(hh) & 0 \\ 0 & S(vv) \end{pmatrix} \qquad (C\text{-}1)$$

where the polarization directions are along the cylinder axis $(S(hh))$ and perpendicular to the cylinder axis $(S(vv))$. The transformation to other polarization bases is of the form

$$S' = U^{t} S V \qquad (C\text{-}2)$$

where U^{t} is the transpose of U, U and V are unitary, V is the transformation from the hv system to the new incident system, and U is the transformation from the hv system to the new emergent system. From this we see that, for example, in the circular polarization basis where

$$U = V = \frac{1}{\sqrt{2}} \begin{pmatrix} 1 & i \\ i & 1 \end{pmatrix}$$

$$\sigma(r\,\ell) = \sigma(\ell\,r) \sim \frac{1}{4}\left|S_1 + S_2\right|^2$$
$$\sigma(r\,r) = \sigma(\ell\,\ell) \sim \frac{1}{4}\left|S_1 - S_2\right|^2, \qquad \text{(C-3)}$$

where we write $S_1 = S\,(hh)$, $S_2 = S\,(vv)$.

In an orthogonal linear basis inclined at an angle of 45° with the hv basis, $U = V = \frac{1}{\sqrt{2}}\begin{pmatrix} 1 & 1 \\ -1 & 1 \end{pmatrix}$,

$$\sigma(++) = \sigma(--) \sim \frac{1}{4}\left|S_1 + S_2\right|^2$$
$$\sigma(+-) = \sigma(-+) \sim \frac{1}{4}\left|S_1 - S_2\right|^2 . \qquad \text{(C-4)}$$

As we noted above the scattering matrix is specified by a knowledge of any five independent cross-sections $\sigma(hh)$, $\sigma(vv)$, $\sigma(r\,\ell)$, $\sigma(rr)$, $\sigma(++)$, $\sigma(+-)$. Since these six were measured in the course of the experiments we can, in principle, specify the S-matrix as well as check the consistency of the results. In particular, if ϕ is the phase difference between the horizontal and vertical fields,

$$\sigma(r\ell) = \sigma(++) = \frac{1}{4}\left[\sigma(hh) + \sigma(vv) + 2\sqrt{\sigma(hh)\,\sigma(vv)}\,\cos\phi\right],$$
$$\sigma(rr) = \sigma(+-) = \frac{1}{4}\left[\sigma(hh) + \sigma(vv) - 2\sqrt{\sigma(hh)\,\sigma(vv)}\,\cos\phi\right], \qquad \text{(C-5)}$$

etc.

From the results it was hoped that an approach to the problem might be found in terms of a phenomenological theory. This theory would be expected to predict the repolarization effects or, what is the same thing in the S-matrix notation, the behavior of the phase difference ϕ above as well as the magnitudes of say $\sigma(hh)$ and $\sigma(vv)$. However, the experimental results are inconsistent to such an extent (ranging upward to 30 db) that it must be concluded that to base any theory or even supposition of repolarization results on these experimental data would be untoward.

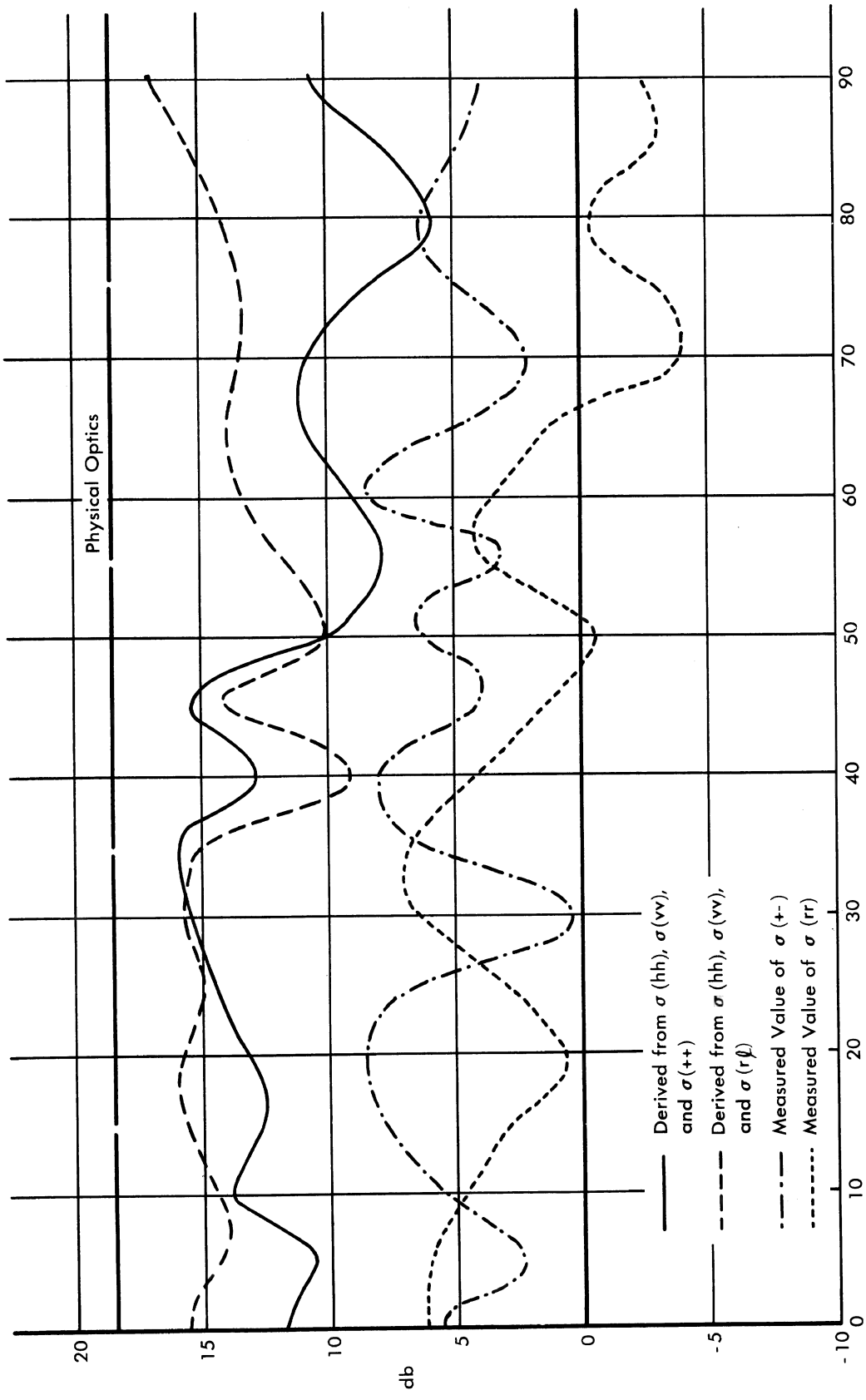

FIG. C-1 ELLIPTIC CYLINDER NO. 10, b = 2.5 λ

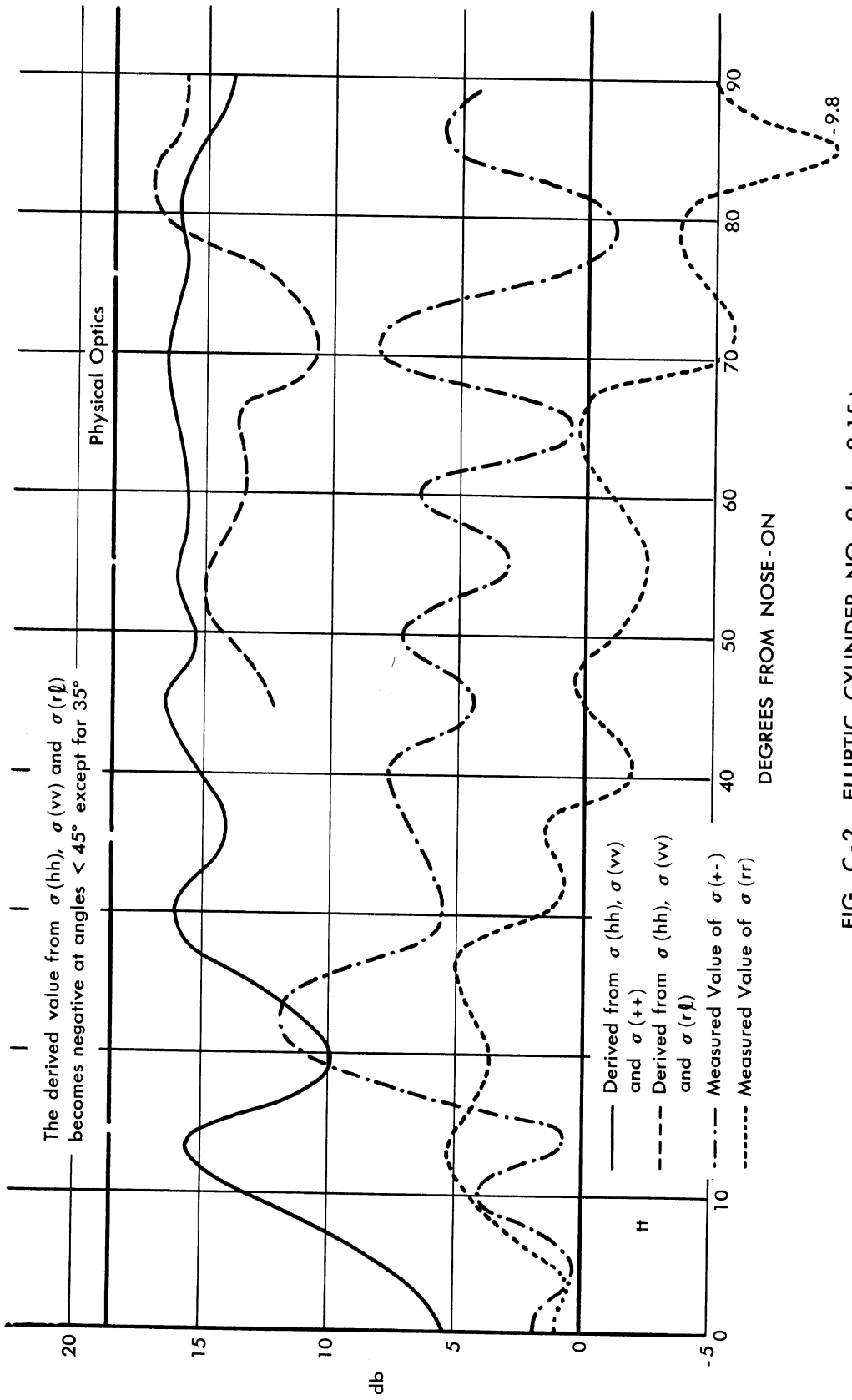

FIG. C-2 ELLIPTIC CYLINDER NO. 9, b= 2.15λ

An immediate check on the consistency is available from the comparison of the measured value of $\sigma(r\ell)$ vs. $\sigma(++)$ and $\sigma(rr)$ vs. $\sigma(+-)$. Since we found large discrepancies we considered the possibility that the errors might have arisen from the departures of the polarization sense from strict circularity in the measurements of $\sigma(rr)$ and $\sigma(r\ell)$. For this reason the measured values of $\sigma(+-)$ and $\sigma(rr)$ are compared with the corresponding values derived from $\sigma(hh)$, $\sigma(vv)$, and $\sigma(++)$ or $\sigma(r\ell)$. These four quantities should be identical. This follows from (C-5) on eliminating the angle ϕ:

$$\sigma(+-) = \sigma(rr) = \frac{1}{2}\left(\sigma(hh) + \sigma(vv)\right) - \sigma(++)$$
$$= \frac{1}{2}\left(\sigma(hh) + \sigma(vv)\right) - \sigma(r\ell) \ . \qquad \text{(C-6)}$$

To illustrate that the departure from circularity is not the source of error, these four quantities will be shown graphically for the two best results, those for the elliptic cylinders of semi-minor axis 2.5λ and 2.15λ. The graphs of these four quantities appear in Figures C-1 and C-2. The various cross-sections are normalized by a factor proportional to the physical optics result and appear plotted against the angle of incidence as measured from the semi-major axis of the elliptic cylinders. The values used in Figures C-1 and C-2 are the average cross-sections as determined from the measured noise level under the assumption that the phase difference between the target return and all extraneous signals be random (Ref. 35, App. 2).

The curves of Figure C-2 indicate a greater degree of consistency at the smaller angles, i.e., for aspects at which the return is smallest, since the radius of curvature at the specular reflection point is smaller for a smaller angle. For this reason the apparent consistency may be spurious since the background discrimination would of course be less at the smaller angles.

In the flat plate experiments the radar cross-section was found to be very small except in the regions of specular reflection. Because of this we present the cases of largest return, namely, those in which the

two flat plates are perpendicular and their centers separated by a distance of 10λ. In particular, since the same symmetry obtains as for the cylinders, i.e., the vertical polarization direction lies along axes of the flat plates so that in the horizontal-vertical polarization basis the S-matrix is of the form

$$S = \begin{pmatrix} S(hh) & 0 \\ 0 & S(vv) \end{pmatrix}$$

as in Equation (C-1) above, we can again make use of the relationships (C-6). However, in this case we exhibit the cross-sections

$$\begin{aligned} \sigma(r\ell) &= \sigma(++) \\ &= \frac{1}{2}\left(\sigma(hh) + \sigma(vv)\right) - \sigma(rr) \\ &= \frac{1}{2}\left(\sigma(hh) + \sigma(vv)\right) - \sigma(+-) \end{aligned} \qquad \text{(C-7)}$$

in Figure C-3, as well as the same set of cross-sections obtained for the cylinders in Figure C-4.

We include both sets in this case to illustrate a point in the consistency test. We note that in the side-lobe regions, about $90^{\circ} \pm 30^{\circ}$, $\sigma(++)$ and $\sigma(r\ell)$ are much smaller than $\sigma(hh)$ and $\sigma(vv)$. Hence, in the derived values of $\sigma(rr)$ or $\sigma(+-)$ there is actually no critical check on the consistency of either $\sigma(++)$ or $\sigma(r\ell)$ since the process involves subtracting these small values from the average of $\sigma(hh)$ and $\sigma(vv)$. For this reason a more apt set to use in the consistency check is the set $\sigma(+-)$, $\sigma(r\ell)$. This does involve a subtraction of numbers of the same order of magnitude and hence a more critical measure of the consistency.

Figures C-3 and C-4 indicate that the flat plate results are also inconsistent to a considerable degree. In fact, derived values of $\sigma(+-)$ and $\sigma(rr)$ are found to be negative in the angular range 0° to 45°, and those of $\sigma(r\ell)$ are found to be negative over most of the range 0° to 150°. No

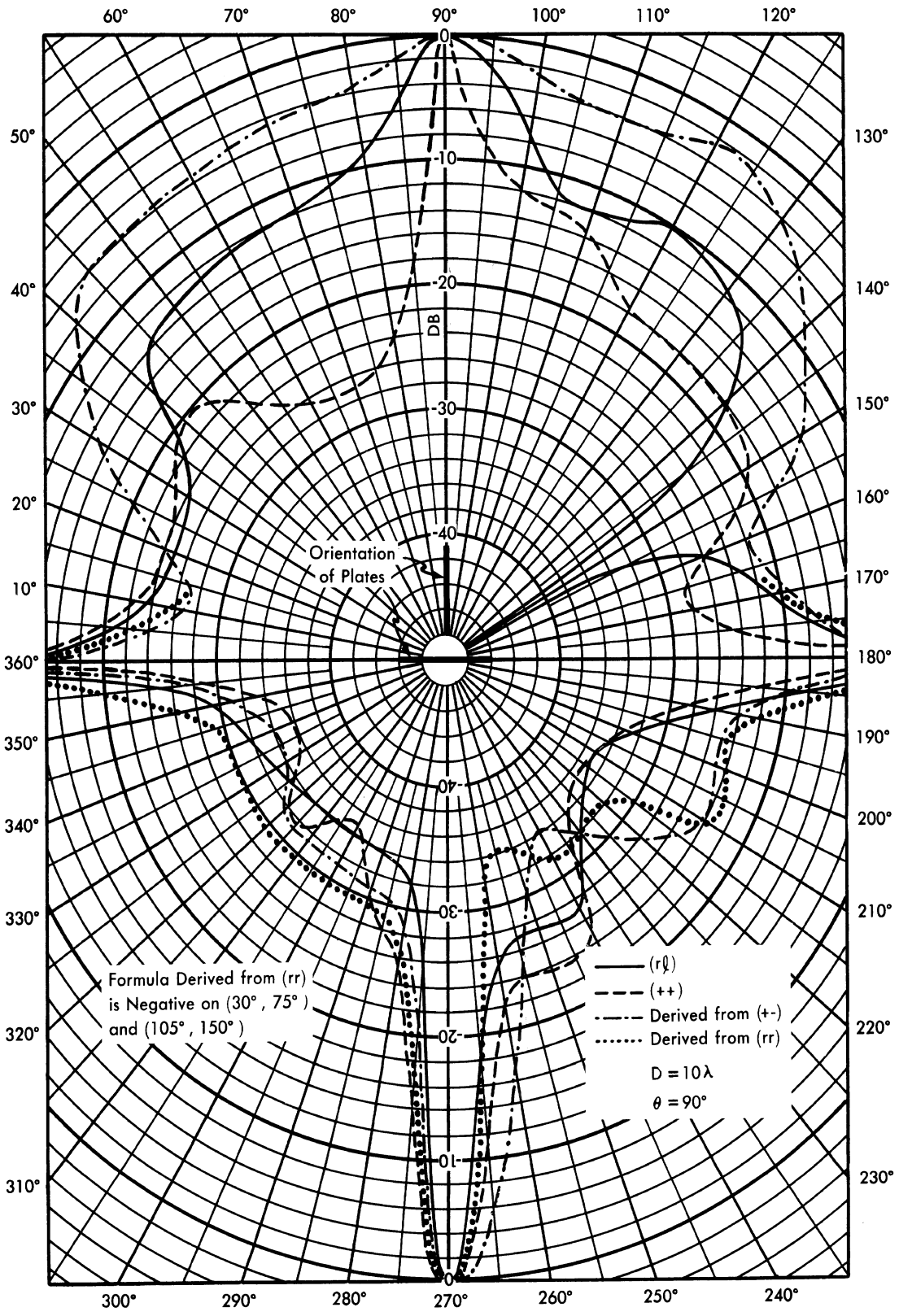

FIG. C-3 POLAR PLOT OF CROSS-SECTION OF PERPENDICULAR FLAT PLATES

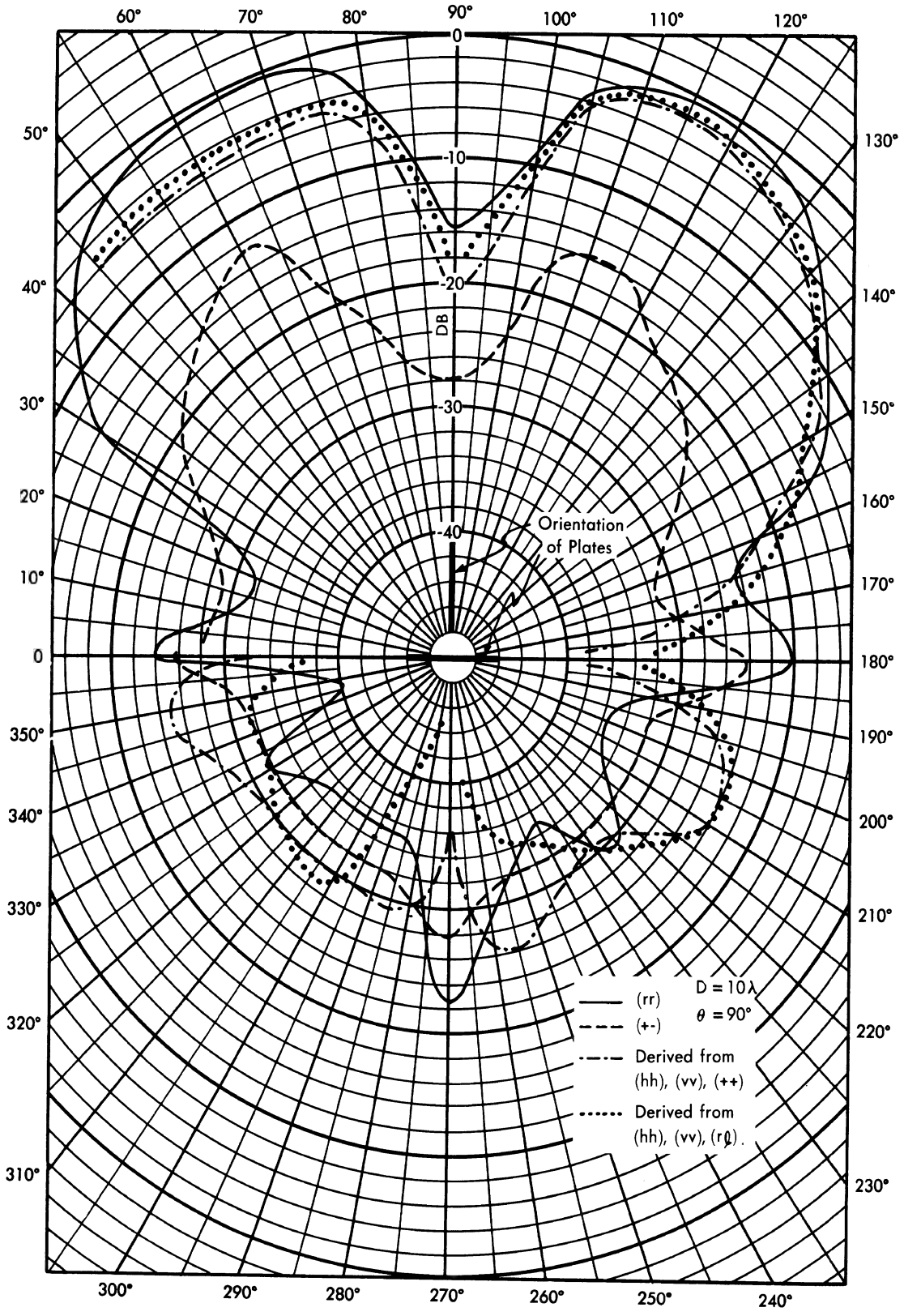

FIG. C-4 POLAR PLOT OF CROSS-SECTION OF PERPENDICULAR FLAT PLATES

experimental error analysis was available for the flat plate results at this writing.

The experimental procedure used is similar to that described in Reference 35. The equipment there described, however, has been modified to obtain the various transmitter and receiver polarizations. A diagram of the experimental arrangement appears in Figure C-5. An analysis of the source of errors in terms of the experimental equipment lies beyond the scope of this report.

In conclusion, we wish to emphasize the importance of such polarization experiments despite the present inconsistent results. For such relatively complex scatterers (complex in the sense that the exact theoretical solution of the scattering problem is extremely difficult) as elliptic cylinders, the available theoretical check on the experimental results is very crude. However, a polarization experiment in which enough independent cross-sections are measured so that the S-matrix is specified and, in addition, there is a consistency check, i.e., at least six independent cross-sections are known, will furnish an excellent measure of the validity of the experimental results.

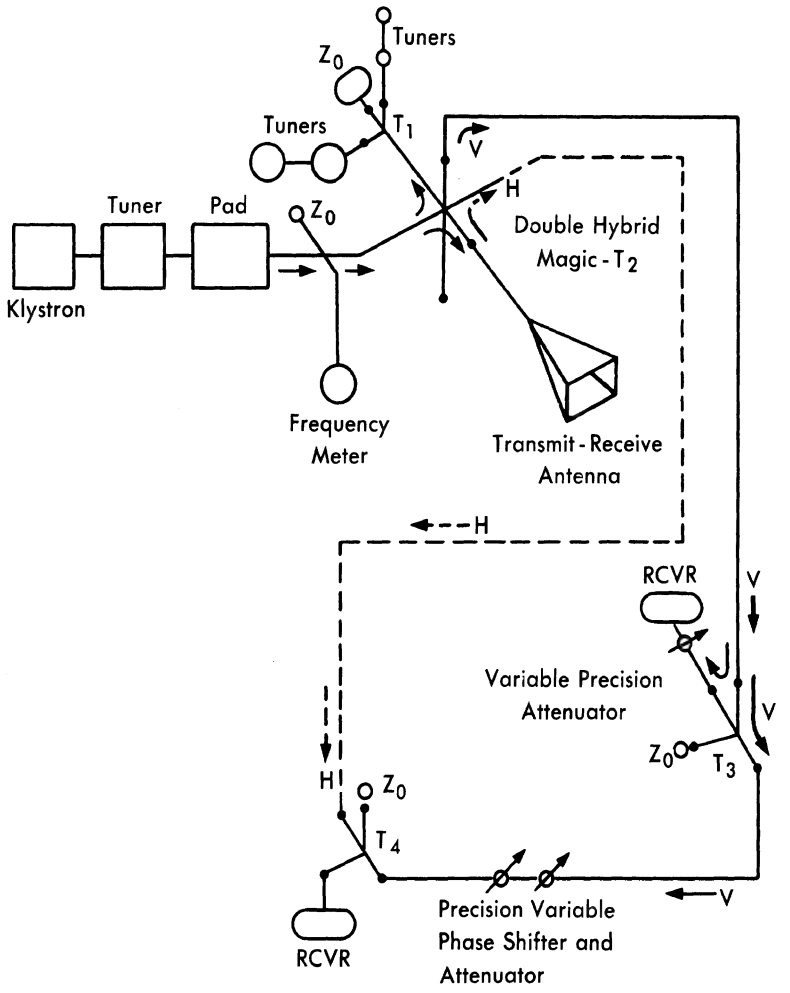

FIG. C-5a

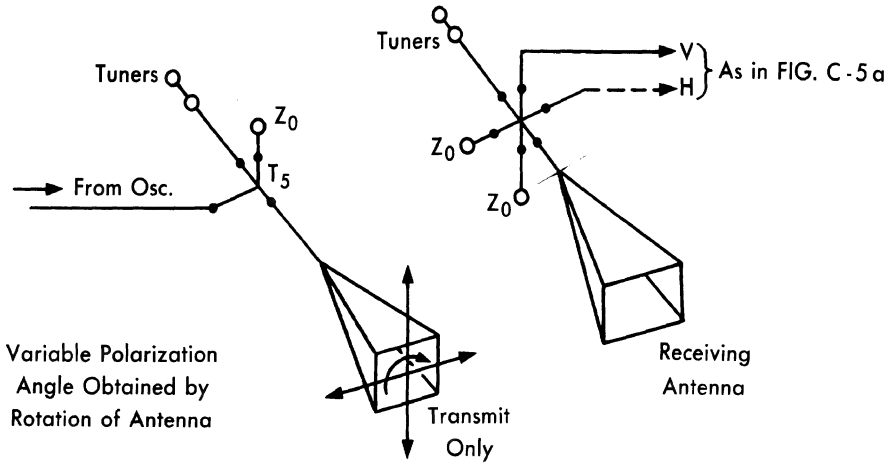

FIG. C-5b

FIG. C-5 EXPERIMENTAL ARRANGEMENT

APPENDIX D

MONOSTATIC RADAR CROSS-SECTION OF THE ELLIPTICAL CORNER REFLECTOR

D.1 INTRODUCTION

As discussed in Reference 3 the monostatic radar cross-section of a corner reflector is given by

$$\sigma = \frac{4\pi A^2}{\lambda^2} , \qquad \text{(D.1-1)}$$

in which A is the area of the projection of an equivalent aperture on a plane normal to the direction of incidence. A convenient aperture, as described in Reference 3, may be constructed by cutting out of each of the four quadrants of each coordinate plane an aperture of the same shape as the leaf of the corner reflector associated with that plane. This A will be determined here for the elliptical corner reflector, a shape frequently employed in asymmetric and limited volumes; as a special case, the area A will also be given for the circular corner reflector. Only triply-reflected radiation will be considered.

D.2 PROJECTION OF THE EQUIVALENT APERTURE

The area A will be a function of ℓ/a, m/b, and n/c, where ℓ, m, and n are the direction cosines of the line-of-sight with the three coordinate axes, and a, b, c the edge-lengths of the ellipses along these axes. Because of the symmetry of the optical model, it is necessary to consider only the range of parameters

$$\ell/a \geq m/b \geq n/c, \qquad \text{(D.2-1)}$$

where

$$1 > \ell, m, n > 0 . \qquad \text{(D.2-2)}$$

The coordinate system may then be chosen in accordance with

Equation (D. 2-1). Because of the invariance of the optical model under reflections in the coordinate planes, a right-handed system may always be chosen.

Consider the corner reflector of Figure D. 2-1.

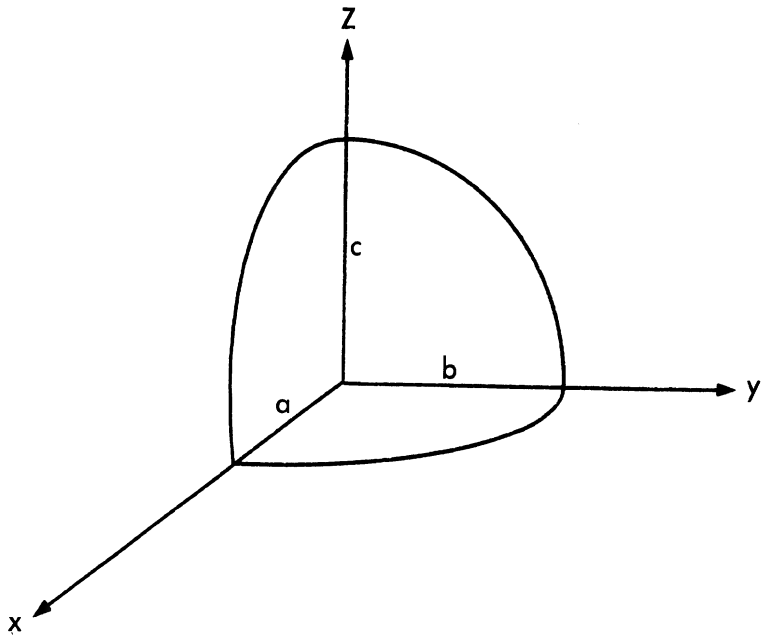

FIG. D.2-1 ORIENTATION OF CORNER REFLECTOR

The equations of the three ellipses are

$$x^2/a^2 + y^2/b^2 = 1$$
$$x^2/a^2 + z^2/c^2 = 1 \qquad \text{(D. 2-3)}$$
$$y^2/b^2 + z^2/c^2 = 1$$

Project these curves onto the X-Y plane along the line-of-sight, or (ℓ, m, n) direction. The equations of these projected curves are

$$x^2/a^2 + y^2/b^2 = 1$$

$$x^2 - \frac{2\ell}{m}xy + y^2 \frac{(\ell^2 c^2 + n^2 a^2)}{m^2 c^2} = a^2 \qquad \text{(D. 2-4)}$$

$$\frac{m^2c^2 + n^2b^2}{\ell^2 c^2} x^2 - \frac{2m}{\ell} xy + y^2 = b^2 .$$

The area common to the three curves is to be determined, and then projected onto the plane normal to the line-of-sight. A is therefore the common area in the X-Y plane multiplied by n, the cosine of the angle between the normals to the two planes.

The procedure is simplified by an additional projection which transforms the first ellipse into a circle. If $b < a$, the projection introduces the transformation

$$x' = x \cos \psi = x \frac{b}{a} , \qquad \text{(D. 2-5)}$$

where ψ is the projecting angle. If $b > a$, use

$$y' = y \cos \chi = y \frac{a}{b} . \qquad \text{(D. 2-6)}$$

Either of these will lead to the same final result for A. The first is employed.

Equation (D. 2-4) then becomes (dropping the primes on x and y)

$$x^2 + y^2 = b^2$$

$$x^2 - \frac{2\ell b}{m a} xy + y^2 \left[\frac{\ell^2 b^2 c^2 + n^2 a^2 b^2}{m^2 a^2 c^2} \right] = b^2 \qquad \text{(D. 2-7)}$$

$$\frac{m^2 a^2 c^2 + n^2 a^2 b^2}{\ell^2 b^2 c^2} x^2 - \frac{2ma}{\ell} xy + y^2 = b^2 \ .$$

The area common to these three curves must be found, and multiplied by na/b to yield A.

D. 3 THE INTERSECTIONS, SEMI-AXES, AND ORIENTATIONS OF THE CURVES

Using the condensation symbols

$$L = \ell^2 b^2 c^2 \ , \ M = m^2 a^2 c^2, \ N = n^2 a^2 b^2 , \qquad \text{(D. 3-1)}$$

Equations (D. 2-7) become

$$\text{(a)} \ x^2 + y^2 = b^2$$

$$\text{(b)} \ x^2 - 2\sqrt{\frac{L}{M}}\, xy + \frac{L+N}{M}\, y^2 = b^2 \qquad \text{(D. 3-2)}$$

$$\text{(c)} \ \frac{M+N}{L} x^2 - 2\sqrt{\frac{M}{L}}\, xy + y^2 = b^2 \ .$$

The intersection points of these three curves are displayed in Table D. 3-2, the key to which is Table D. 3-1. In each block, the upper intersection is encountered first in a counter-clockwise circuit.

TABLE D. 3-1

NOMENCLATURE FOR INTERSECTION POINTS

	1	2	3
1		P B	E F
2	C D		I J
3	G H	K L	

TABLE D. 3-2

LOCATION OF INTERSECTION POINTS

	$\theta = 0$ $\theta = \pi$ $\rho = b$	$\theta = \frac{\pi}{2}$ $\theta = \frac{3\pi}{2}$ $\rho = b$
$\tan\theta = \frac{2\sqrt{LM}}{L-M+N}$ $\rho = b$		$\tan\theta = \sqrt{M/L}$ $= \sqrt{\frac{M+L}{N}}\ B$
$\tan\theta = -\frac{L-(M+N)}{2\sqrt{LM}}$	$\tan\theta = \sqrt{M/L}\left[\frac{L-M-N}{L-M+N}\right]$ $\rho^2 = \frac{b^2}{N}\ \frac{(L+M)(L-M)^2+2N(L-M)^2+N^2(L+M)}{(L-M)^2+2N(L+M)+N^2}$	

It follows from the inequality [Equation (D. 2-1)] which may be written

$$L \geq M \geq N \qquad \text{(D. 3-3)}$$

that the intersection points are ordered in the following fashion:

TABLE D. 3-3

ORDERING OF INTERSECTION POINTS

Case 1 $L < M + N$

Quadrant	1				2		3				4	
Point:	P	G	I	C	E	K	B	H	J	D	F	L
ρ:	b	a	>b	b	b	<b	b	b	>b	b	b	<b

TABLE D. 3-3 (Continued)

Case 2 $L > M + N$

Quadrant	1				2		3				4	
Point:	P	K	I	C	E	G	B	L	J	D	F	H
ρ:	b	b	$>\rho_k$	b	b	b	b	$>b$	$>\rho_L$	b	b	b

The curves may, therefore, be drawn as shown in Figures D. 3-1 and D. 3-2. Now the area of a sector of an ellipse of semi-major axis r and semi-minor axis s between the angles α and β is given by

$$\text{Area} = \frac{rs}{2}\left[\arctan\left(\frac{r}{s}\tan\phi\right)\right]_{\alpha}^{\beta} . \qquad \text{(D. 3-4)}$$

The semi-axes and orientation of the semi-major axes in our coordinate system must therefore be obtained. For the circle, of course,

$$r = s = b; \qquad \text{(D. 3-5)}$$

for ellipse (b) of Equation (D. 3-2)

$$\frac{r^2}{s^2} = \frac{2\,b^2\,M}{L+N+M \mp \sqrt{(L+N-M)^2 + 4LM}} ; \qquad \text{(D. 3-6)}$$

for ellipse (c)

$$\frac{r^2}{s^2} = \frac{2\,b^2\,L}{L+N+M \mp \sqrt{(L-M-N)^2 + 4ML}} . \qquad \text{(D. 3-7)}$$

The angle between the semi-major axes of ellipse (b) and the x-axis is the first quadrant root of

$$\theta_2 = \frac{1}{2}\tan^{-1}\frac{2\sqrt{ML}}{L+N-M} . \qquad \text{(D. 3-8)}$$

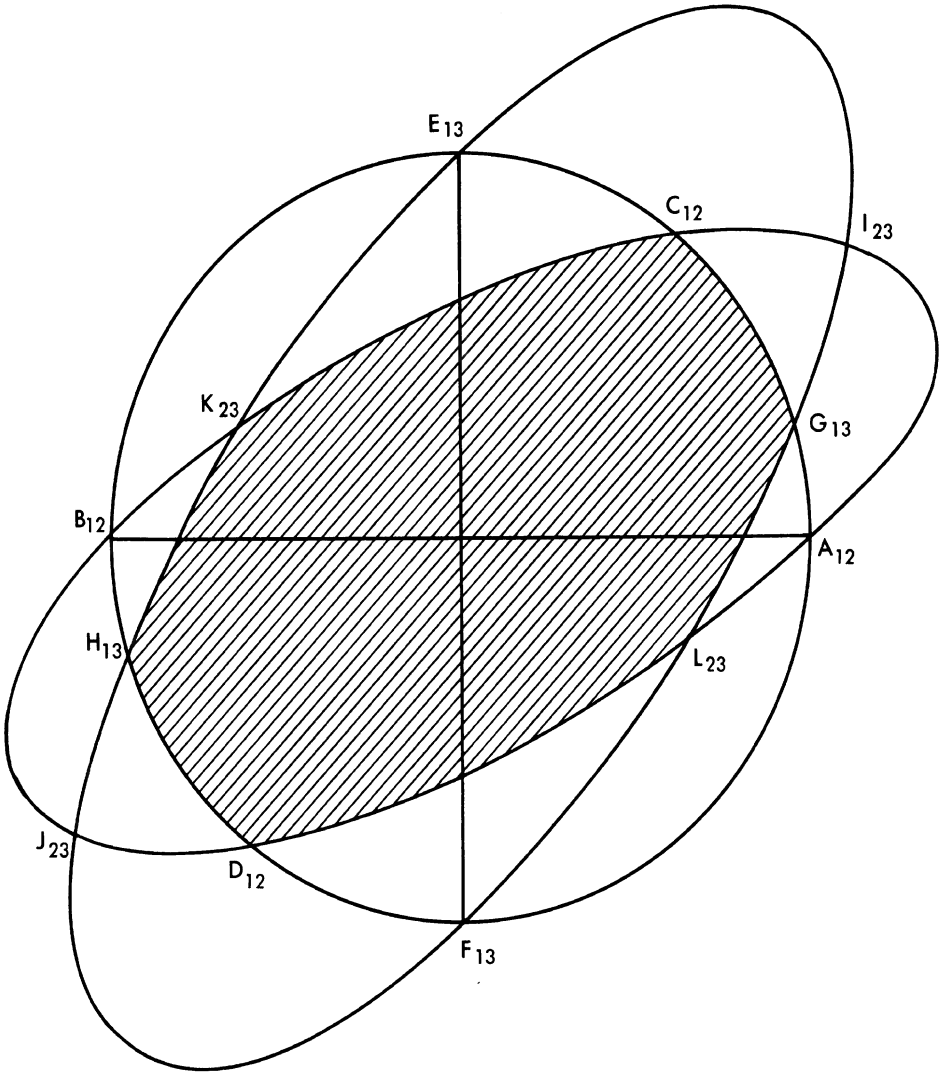

FIG. D.3-1 SIX-SIDED AREA FOR L < M + N

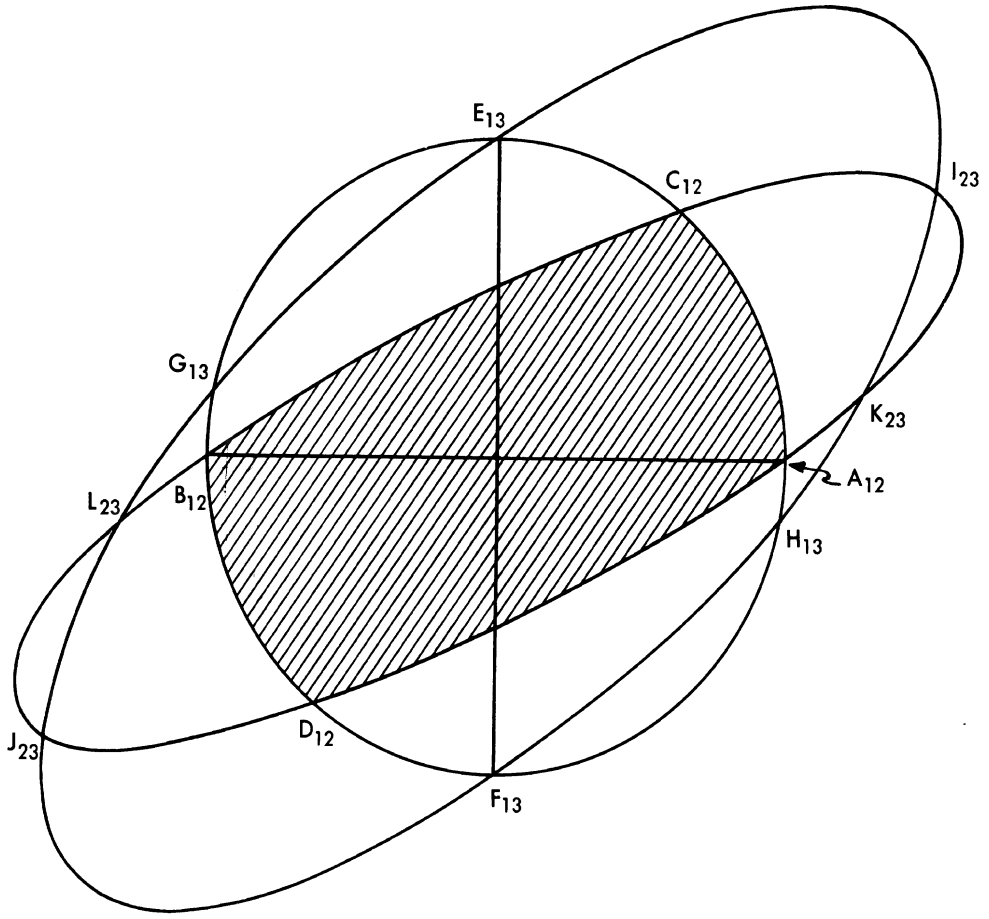

FIG. D.3-2 FOUR-SIDED AREA FOR L > M + N

The similar quantity for ellipse (c) is given by the first quadrant root of

$$\theta_3 = \frac{1}{2}\tan^{-1}\frac{2\sqrt{ML}}{L-M-N} \quad . \qquad \text{(D. 3-9)}$$

The final expressions for A, the shaded areas in Figures D. 3-1 and D. 3-2, may also be given. They are, for $L < M+N$:

$$A = nab\,(C-G) + nab\sqrt{\frac{M}{N}}\arctan\frac{2\sqrt{MN}\tan\phi}{L+M+N-\sqrt{(L-M+N)^2+4LM}}\Bigg|_{C-\theta_2}^{K-\theta_2} + nab\sqrt{\frac{L}{N}}\arctan\frac{2\sqrt{LN}\tan\phi}{L+M+N-\sqrt{(L-M-N)^2+4LM}}\Bigg|_{K-\theta_3}^{H-\theta_3} ; \qquad \text{(D. 3-10)}$$

for $L > M+N$:

$$A = nab\,(C-P) + nab\sqrt{M/N}\arctan\left(\frac{2\sqrt{MN}\tan\phi}{L+M+N-\sqrt{(L-M+N)^2+4LM}}\right)\Bigg|_{C-\theta_2}^{B-\theta_2} . \qquad \text{(D. 3-11)}$$

When the values of P, B, C, G, H, and K from Tables D. 3-1 and D. 3-2 and the expressions for θ_2 and θ_3 from Equations (D. 3-8) and (D. 3-9) are utilized in Equations (D. 3-10) and (D. 3-11), these expressions for the common area become:

$$L > M+N,\ \frac{A}{abc} = \sqrt{M}\tan^{-1}\left(\frac{2\sqrt{LN}}{L+M-N}\right) + \sqrt{N}\tan^{-1}\left(\frac{2\sqrt{LM}}{L+N-M}\right) ; \qquad \text{(D. 3-12)}$$

$$L < M+N, \quad \frac{A}{abc} = \sqrt{L}\tan^{-1}\left(\frac{(M+N)^2-L^2}{4L\sqrt{MN}}\right) + \sqrt{M}\tan^{-1}\left(\frac{(L+N)^2-M^2}{4M\sqrt{LN}}\right)$$

$$+ \sqrt{N}\tan^{-1}\left(\frac{(L+M)^2-N^2}{4N\sqrt{LM}}\right) . \qquad \text{(D. 3-13)}$$

We may simplify the form of these equations by making use of the symmetric functions

$$S = \frac{1}{2}(L+M+N)$$

$$T = LMN .$$

Then we have

$$L \geq M+N, \quad \frac{A}{abc} = \sqrt{M}\tan^{-1}\left(\frac{\sqrt{\frac{T}{M}}}{S-N}\right) + \sqrt{N}\tan^{-1}\left(\frac{\sqrt{\frac{T}{N}}}{S-M}\right); \qquad \text{(D. 3-14)}$$

$$L \leq M+N, \quad \frac{A}{abc} = \sqrt{L}\tan^{-1}\left(\frac{S(S-L)}{\sqrt{LT}}\right) + \sqrt{M}\tan^{-1}\left(\frac{S(S-M)}{\sqrt{MT}}\right) +$$

$$\sqrt{N}\tan^{-1}\left(\frac{S(S-N)}{\sqrt{NT}}\right) . \qquad \text{(D. 3-15)}$$

This form is the easiest for numerical computation.

D. 4 DISCUSSION OF RESULTS

It is to be noted that for the transition point $L = M+N$, $G = P = 0$ and $E = B = H = \pi$, so that Equations (D. 3-12) and (D. 3-13) become identical, as they should.

Further, the transition point corresponds to that of $\ell^2 = 1/2$ for a circular reflector. For a circular corner reflector of edge length R,

Equations (D. 3-12) and (D. 3-13) reduce to

$$\ell^2 \geq \frac{1}{2}, \quad \frac{A}{R^2} = m \tan^{-1}\left(\frac{2\ell n}{1-2n^2}\right) + n \tan^{-1}\left(\frac{2\ell m}{1-2m^2}\right) . \qquad \text{(D. 4-1)}$$

$$\ell^2 \leq \frac{1}{2}, \quad \frac{A}{R^2} = \ell \tan^{-1}\left(\frac{1-2\ell^2}{4\ell^2 mn}\right) + m \tan^{-1}\left(\frac{1-2m^2}{4\ell m^2 n}\right) + n \tan^{-1}\left(\frac{1-2n^2}{4\ell m n^2}\right) . \qquad \text{(D. 4-2)}$$

The values of A/R^2 for a circular corner reflector of unit radius have been computed from Equations (D. 4-1) and D. 4-2). A is plotted as a function of m^2 (or n^2) for fixed values of ℓ^2 from 0. 01 to 0. 99 in steps of 0. 01 (Figs. D. 4-1 ff). Of course, ℓ^2, m^2, and $n^2 = 1 - \ell^2 - m^2$ may be permuted in any convenient way in using these graphs. σ is determined from the graphs as

$$\sigma = \frac{4\pi A^2}{\lambda^2} . \qquad \text{(D. 4-3)}$$

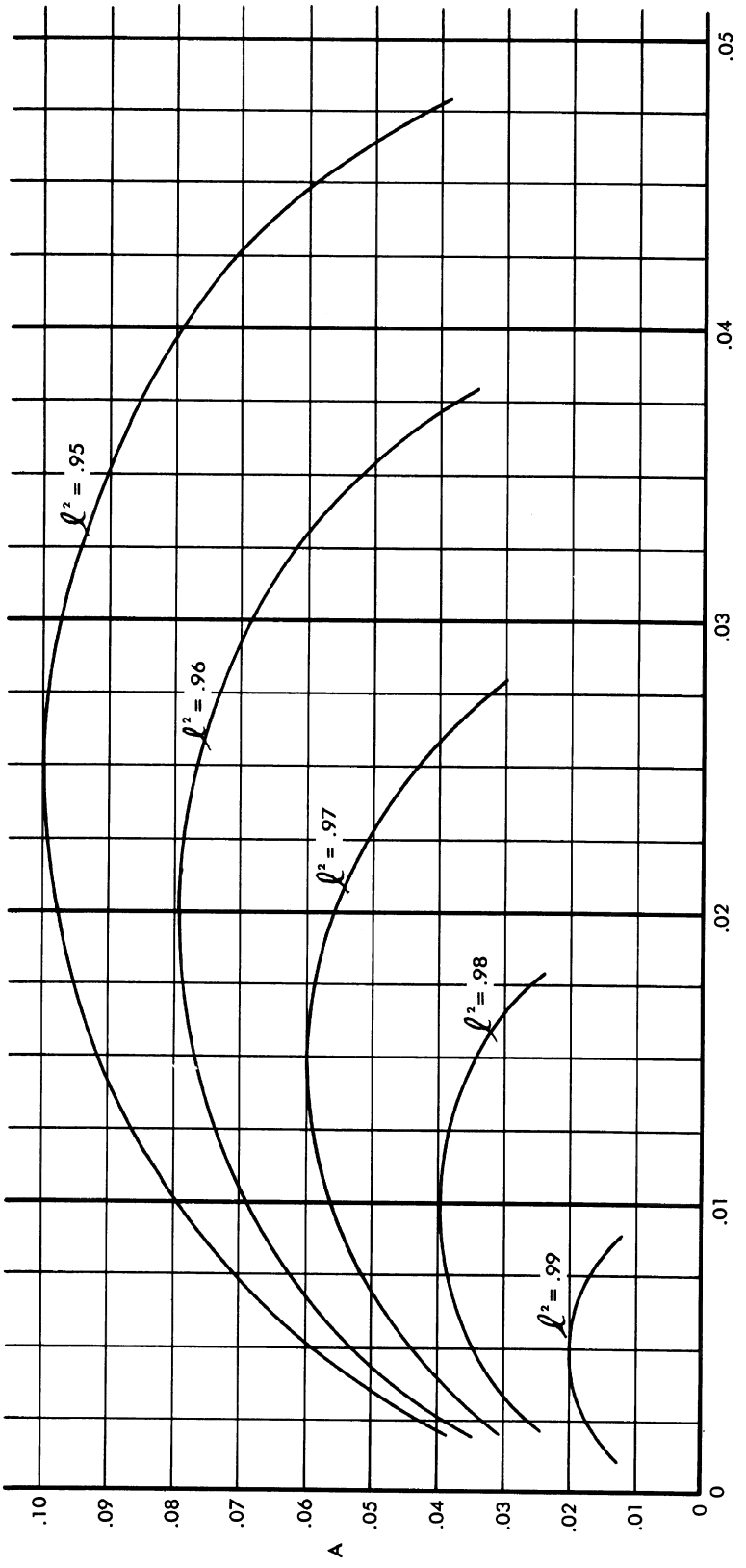

FIG. D.4-1 A, FOR UNIT EDGE CIRCULAR CORNER REFLECTOR, vs. m^2 or n^2 FOR ℓ^2=.99(.01).95

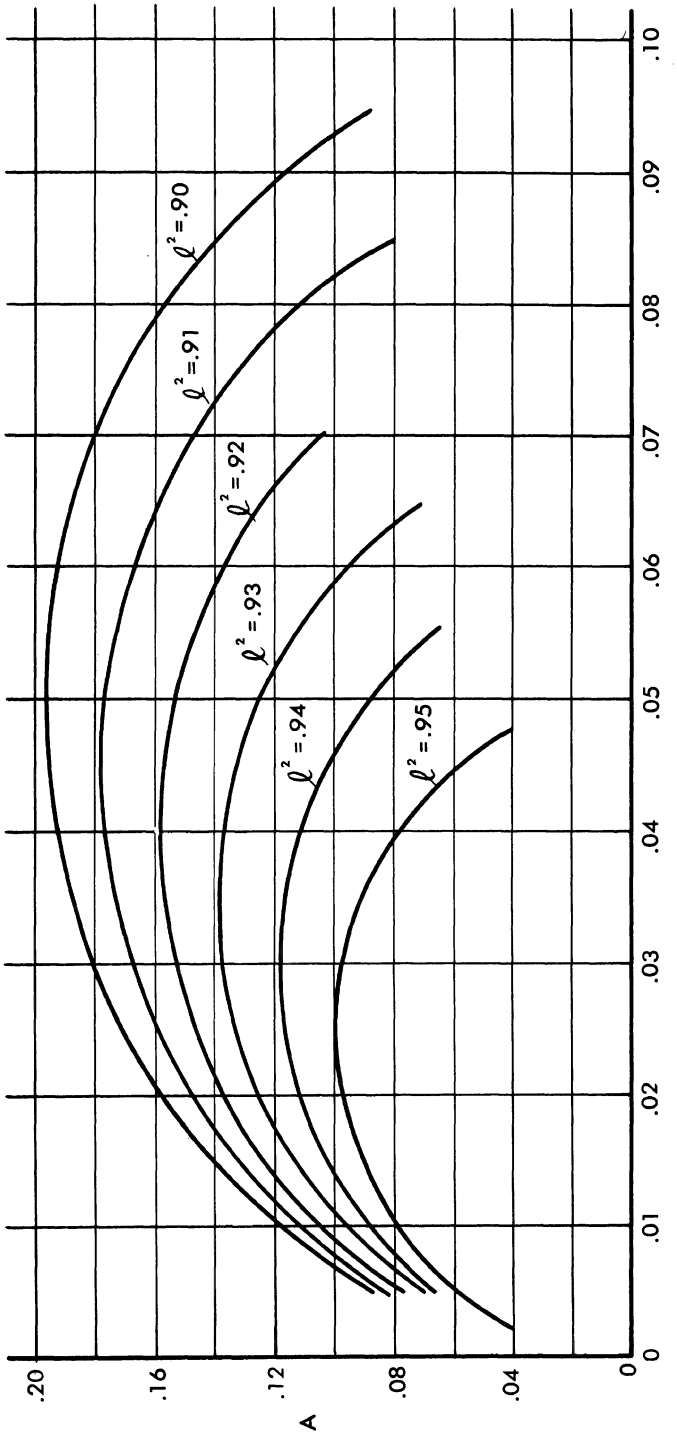

FIG. D.4-2 A, FOR UNIT EDGE CIRCULAR CORNER REFLECTOR, vs. m^2 or n^2 FOR ℓ^2=.95(.01).90

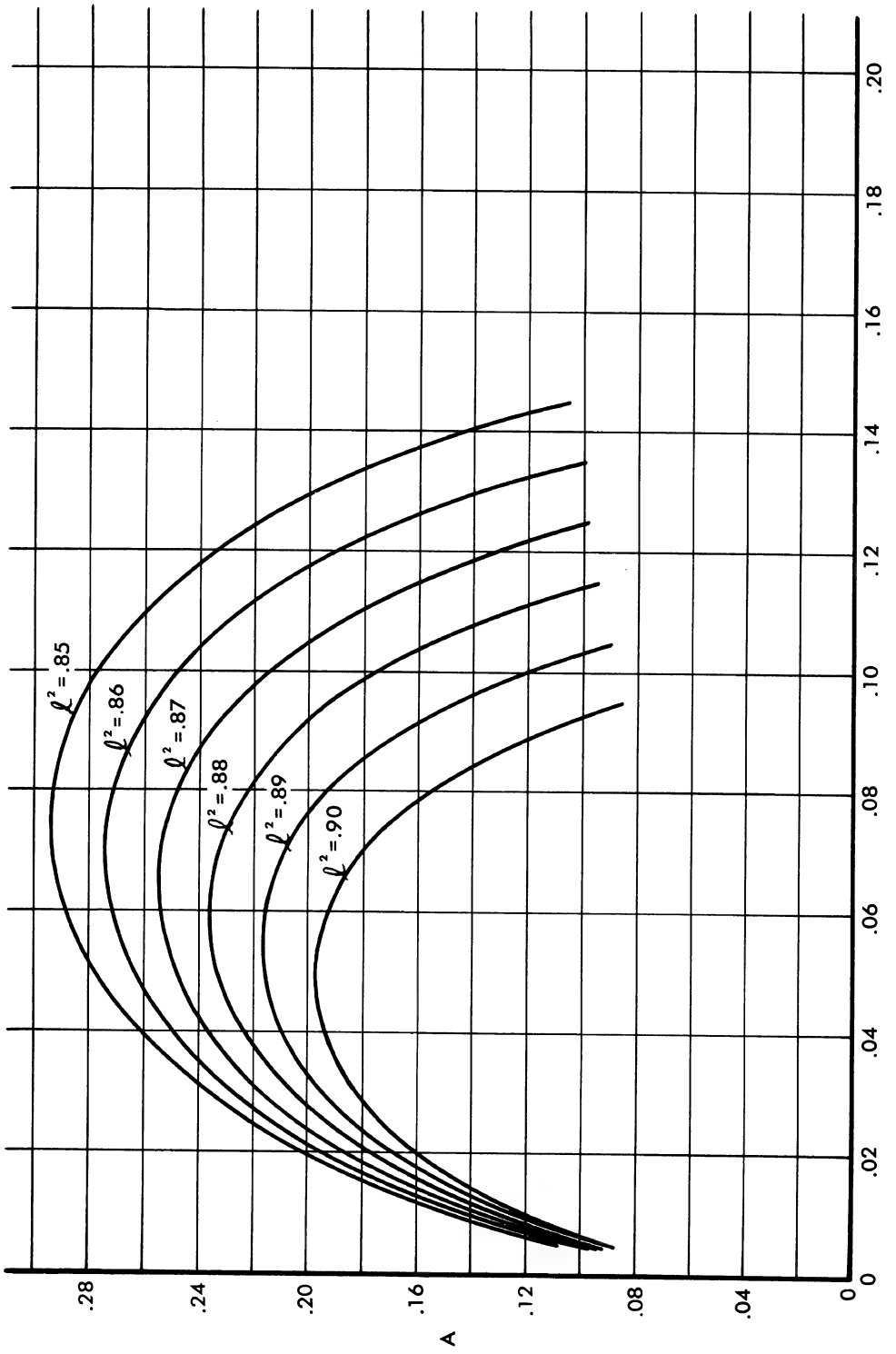

FIG. D.4 - 3 A, FOR UNIT EDGE CIRCULAR CORNER REFLECTOR, vs. m^2 or n^2 FOR ρ^2=.90(.01).85

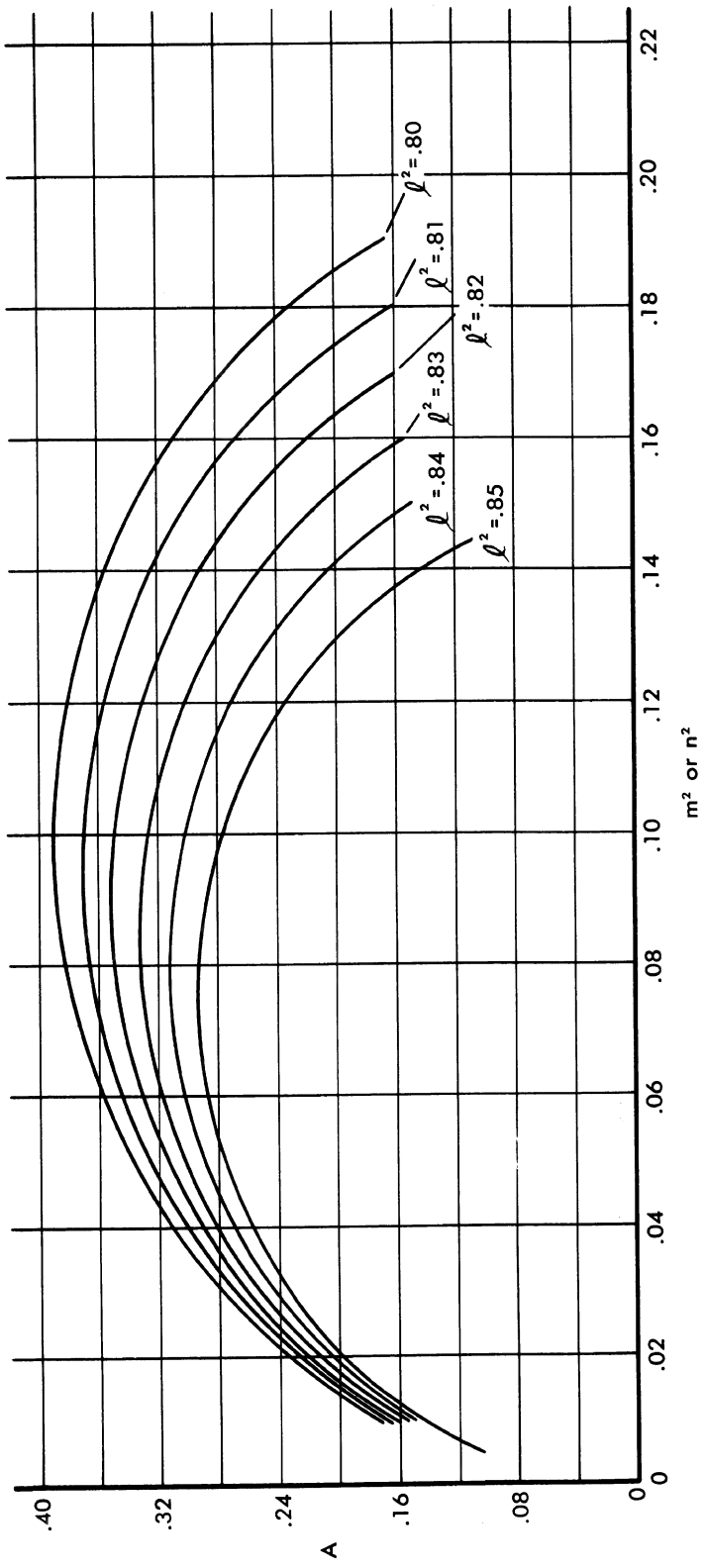

FIG. D.4 - 4 A, FOR UNIT EDGE CIRCULAR CORNER REFLECTOR, vs. m^2 or n^2 FOR ρ^2=.85(.01).80

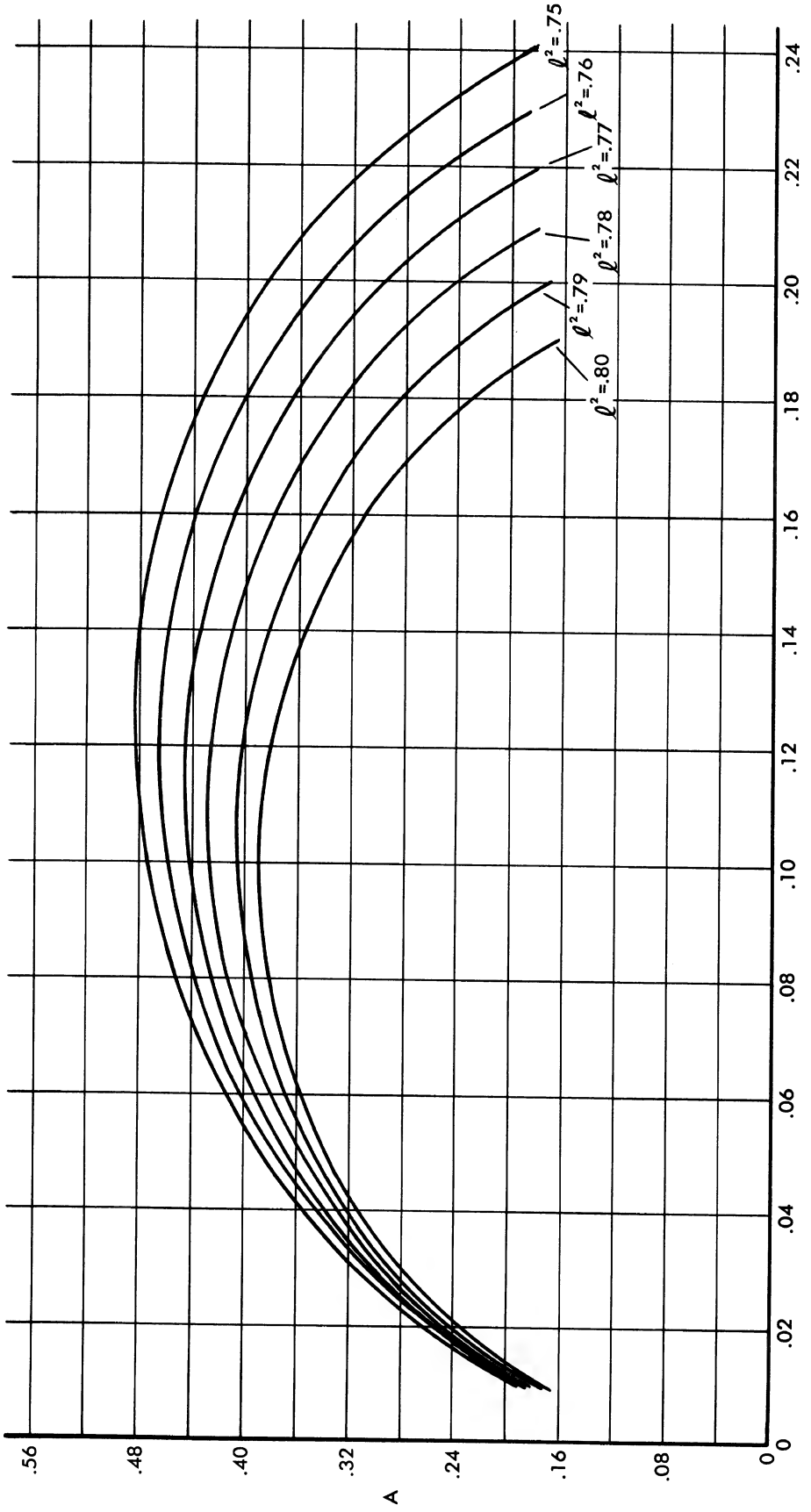

FIG. D.4 - 5 A, FOR UNIT EDGE CIRCULAR CORNER REFLECTOR, vs. m^2 or n^2 FOR ℓ^2=.80(.01).75

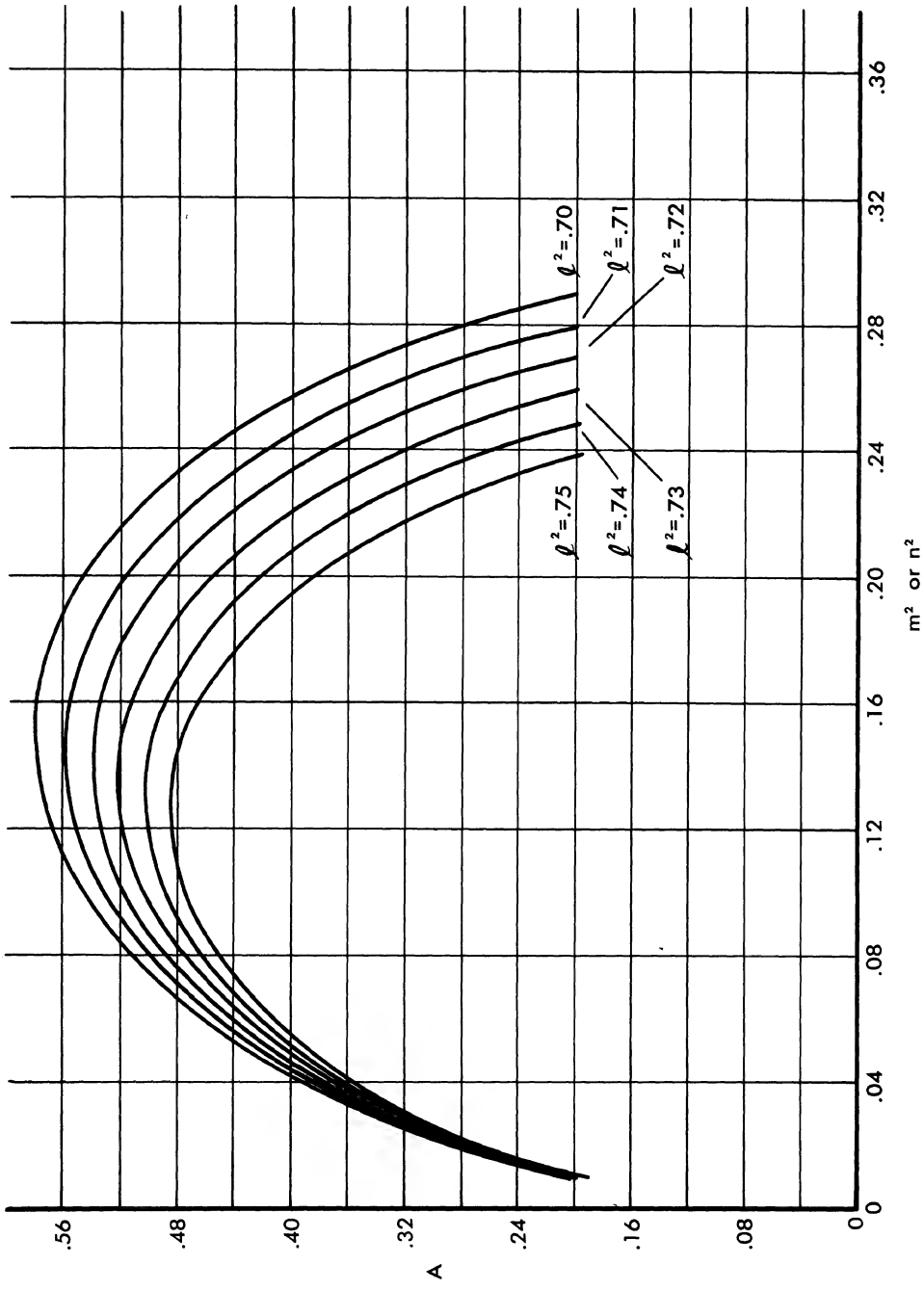

FIG. D.4-6 A, FOR UNIT EDGE CIRCULAR CORNER REFLECTOR, vs. m^2 or n^2 FOR ℓ^2=.75(.01).70

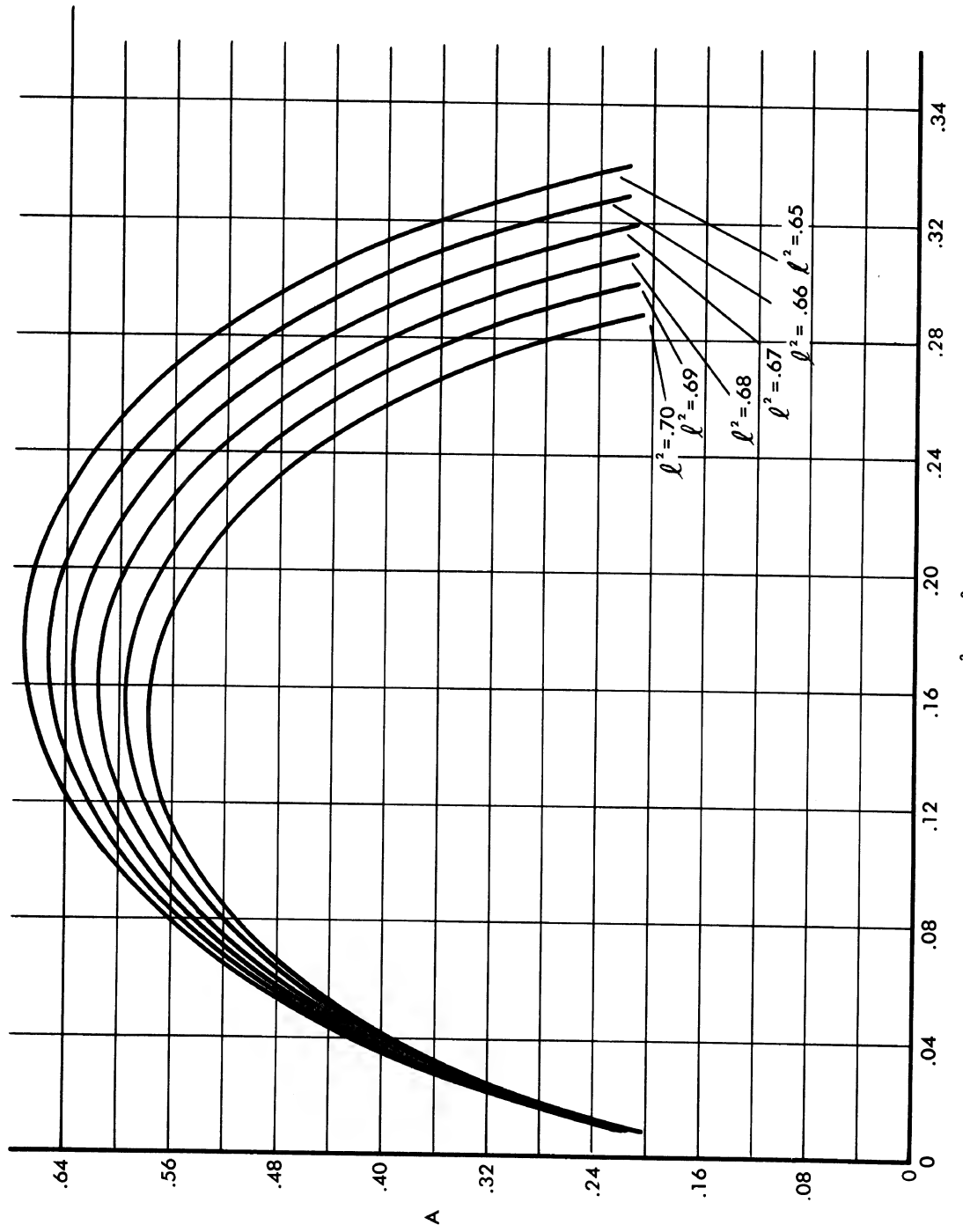

FIG. D.4 - 7 A, FOR UNIT EDGE CIRCULAR CORNER REFLECTOR, vs. m^2 or n^2 FOR ℓ^2=.70(.01).65

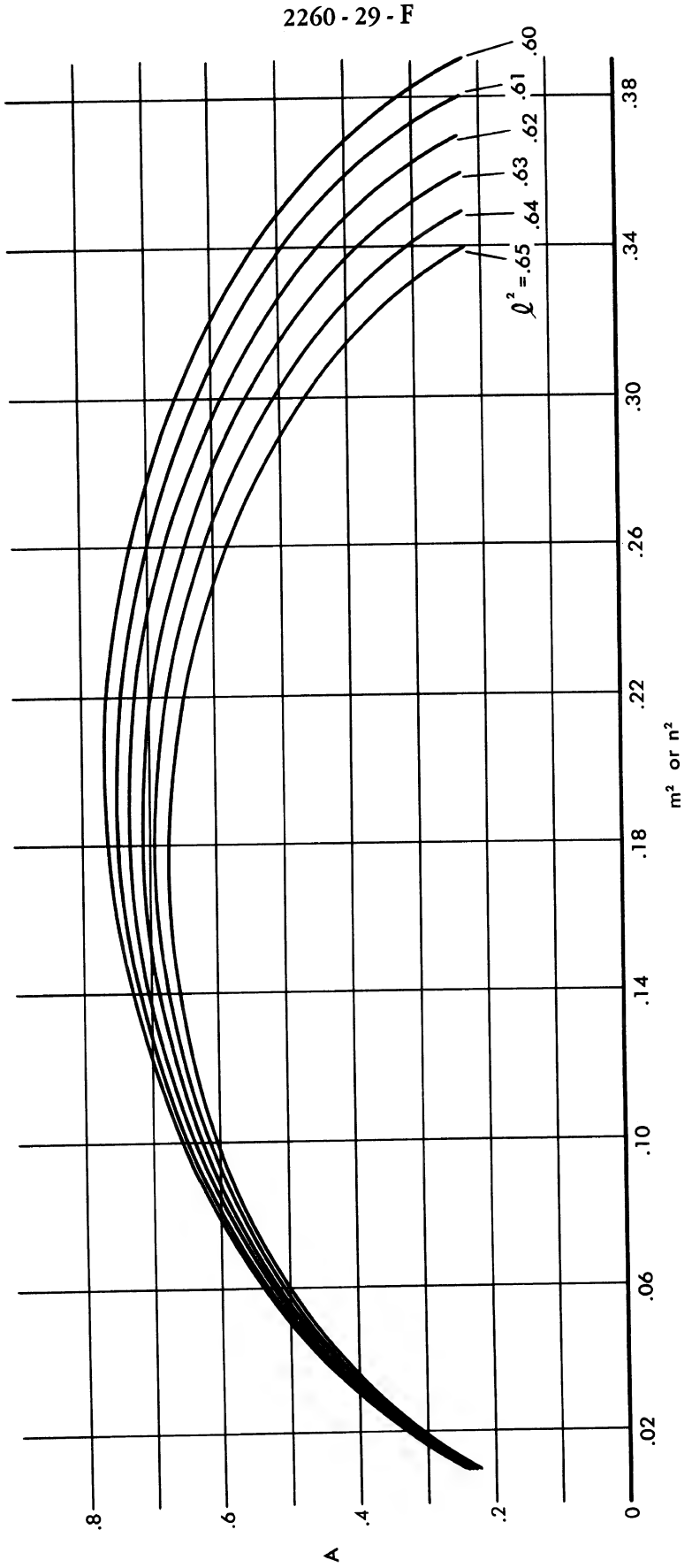

FIG. D.4-8 A, FOR UNIT EDGE CIRCULAR CORNER REFLECTOR, vs. m^2 or n^2 FOR ℓ^2=.65(.01).60

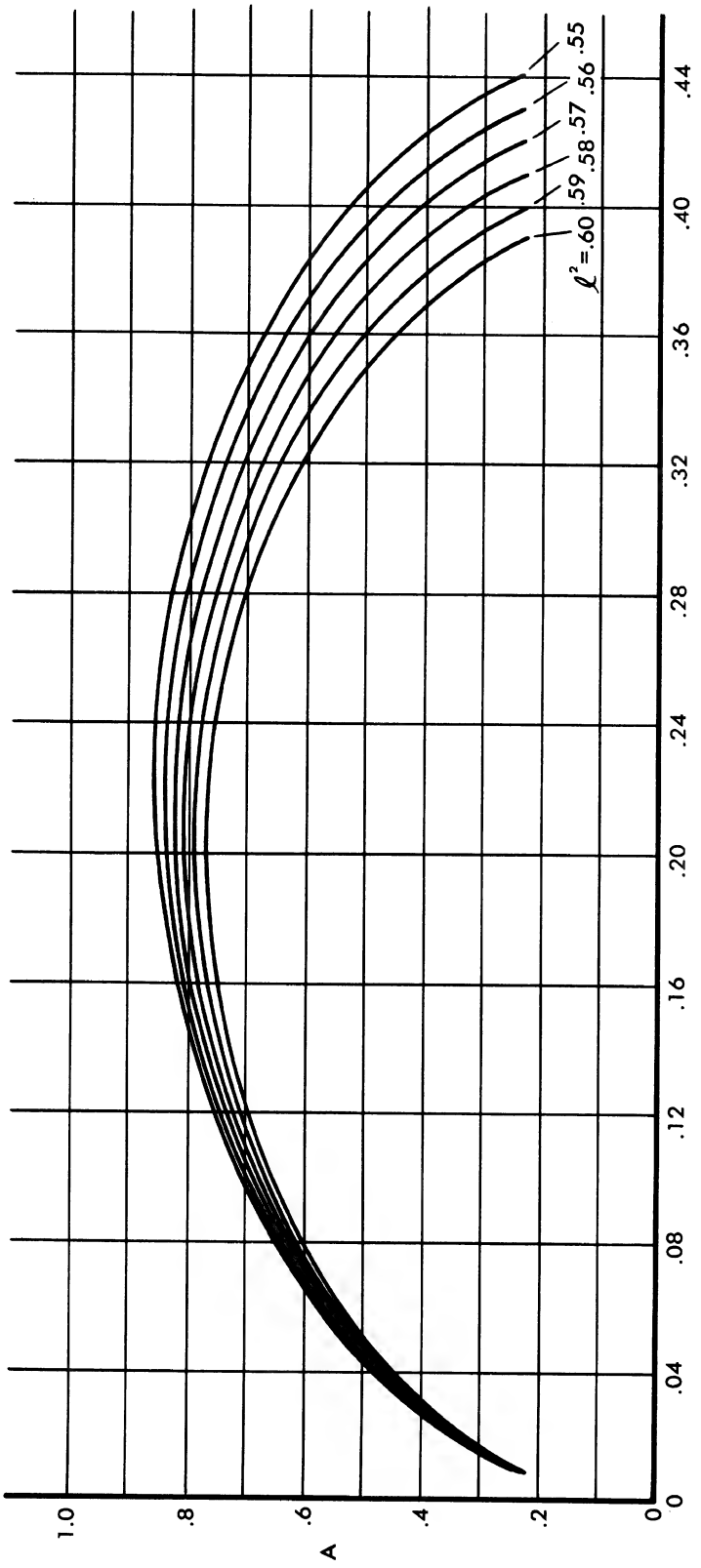

FIG. D.4-9 A, FOR UNIT EDGE CIRCULAR CORNER REFLECTOR, vs. m^2 or n^2 FOR ℓ^2=.60(.01).55

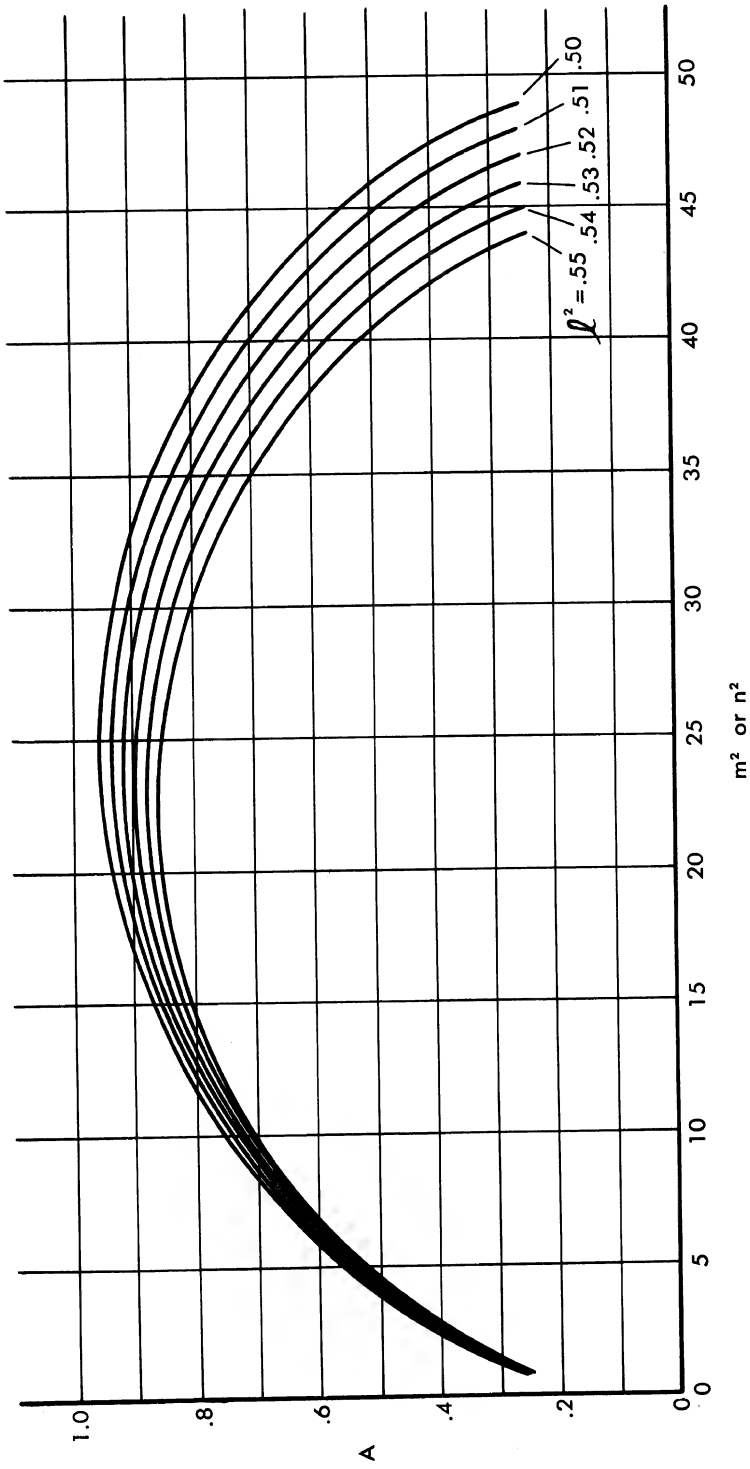

FIG. D.4-10 A, FOR UNIT EDGE CIRCULAR CORNER REFLECTOR, vs. m^2 or n^2 FOR $\ell^2 = .55(.01).50$

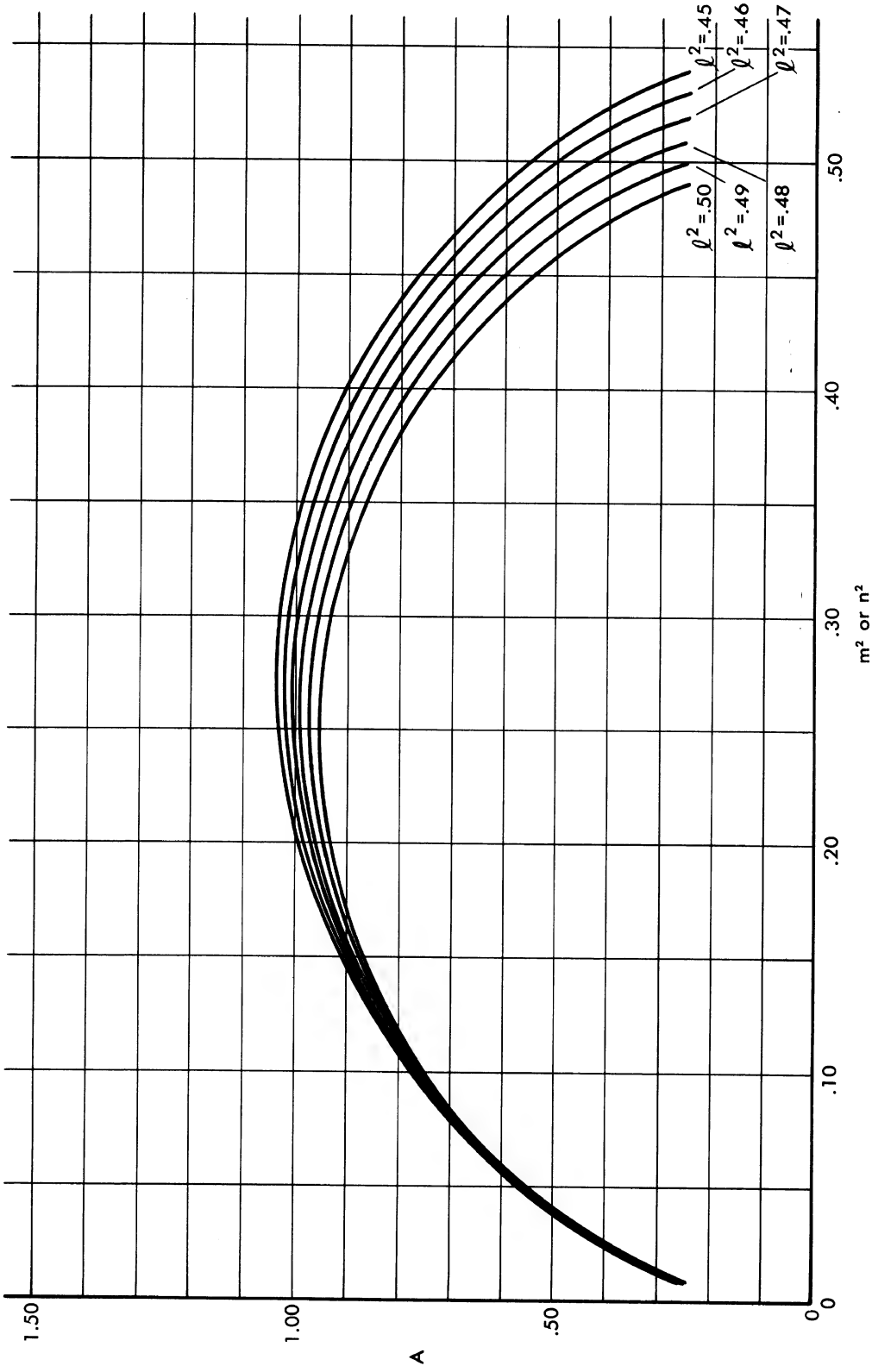

FIG. D.4-11 A, FOR UNIT EDGE CIRCULAR CORNER REFLECTOR, vs. m^2 or n^2 FOR ℓ^2=.50(.01).45

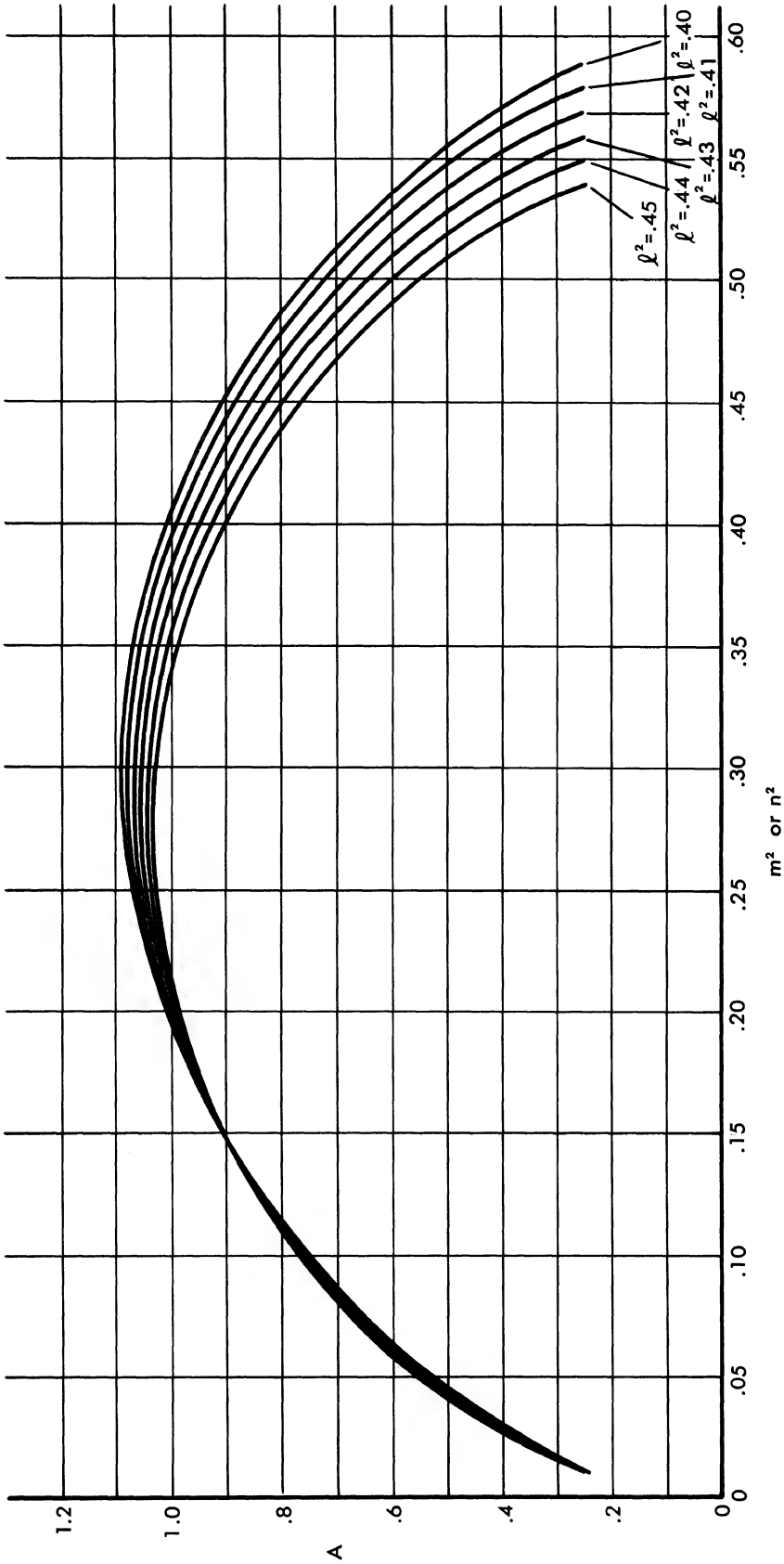

FIG. D.4-12 A, FOR UNIT EDGE CIRCULAR CORNER REFLECTOR, vs. m^2 or n^2 FOR ℓ^2 = .45(.01).40

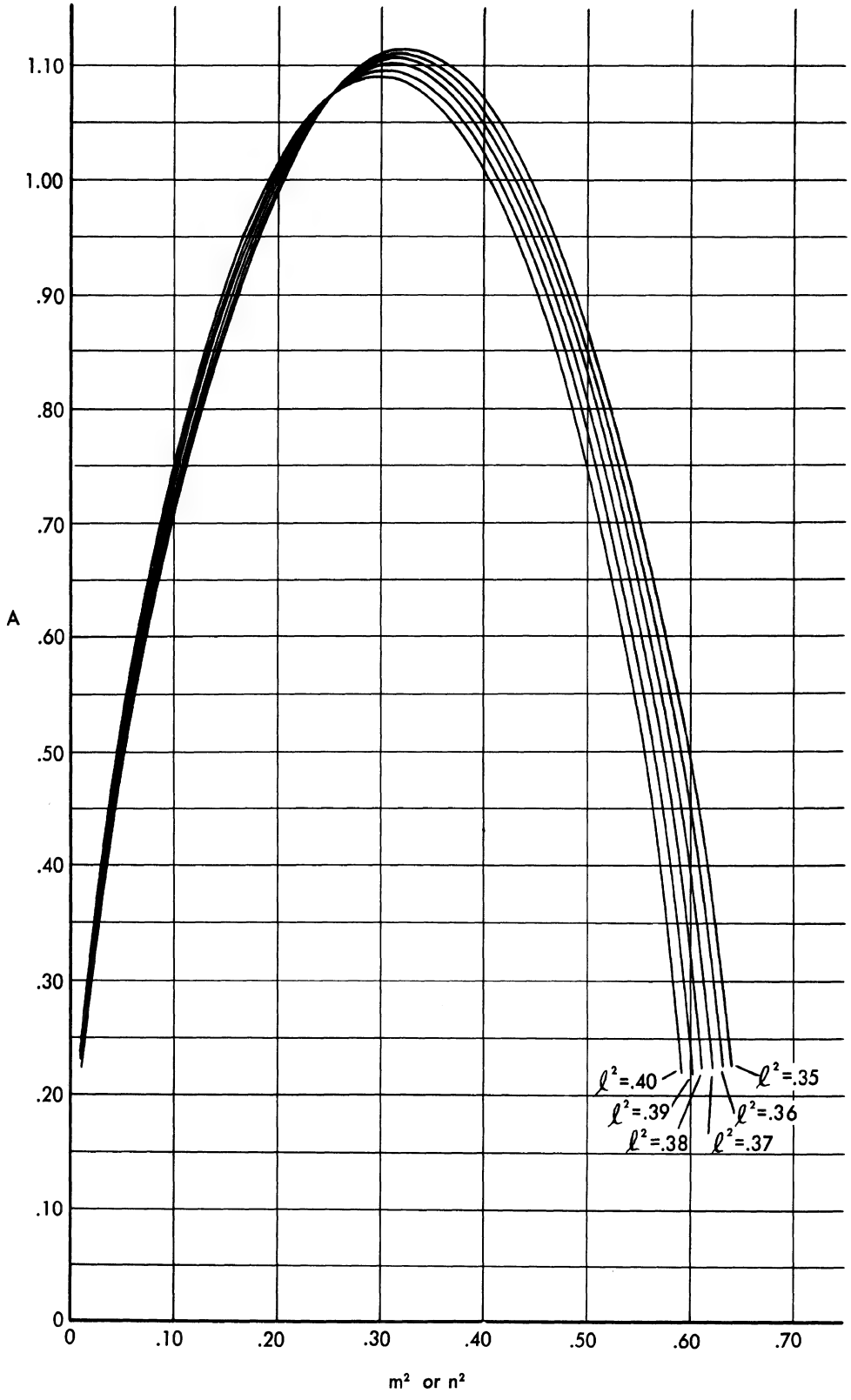

FIG. D.4-13 A, FOR UNIT EDGE CIRCULAR CORNER REFLECTOR, vs. m^2 or n^2 FOR ℓ^2=.40(.01).35

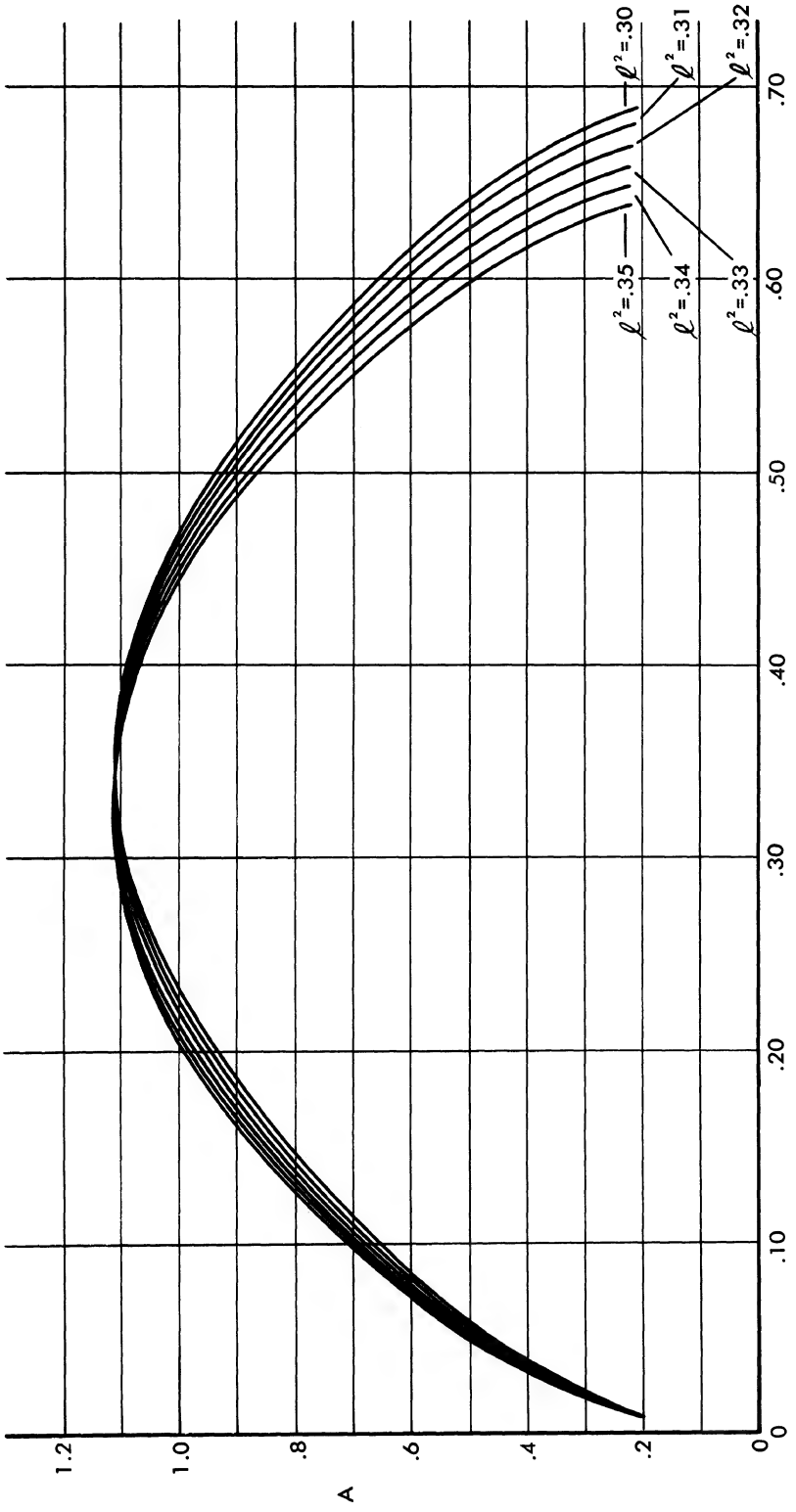

FIG. D.4-14 A, FOR UNIT EDGE CIRCULAR CORNER REFLECTOR, vs. m^2 or n^2 FOR ℓ^2=.35(.01).30

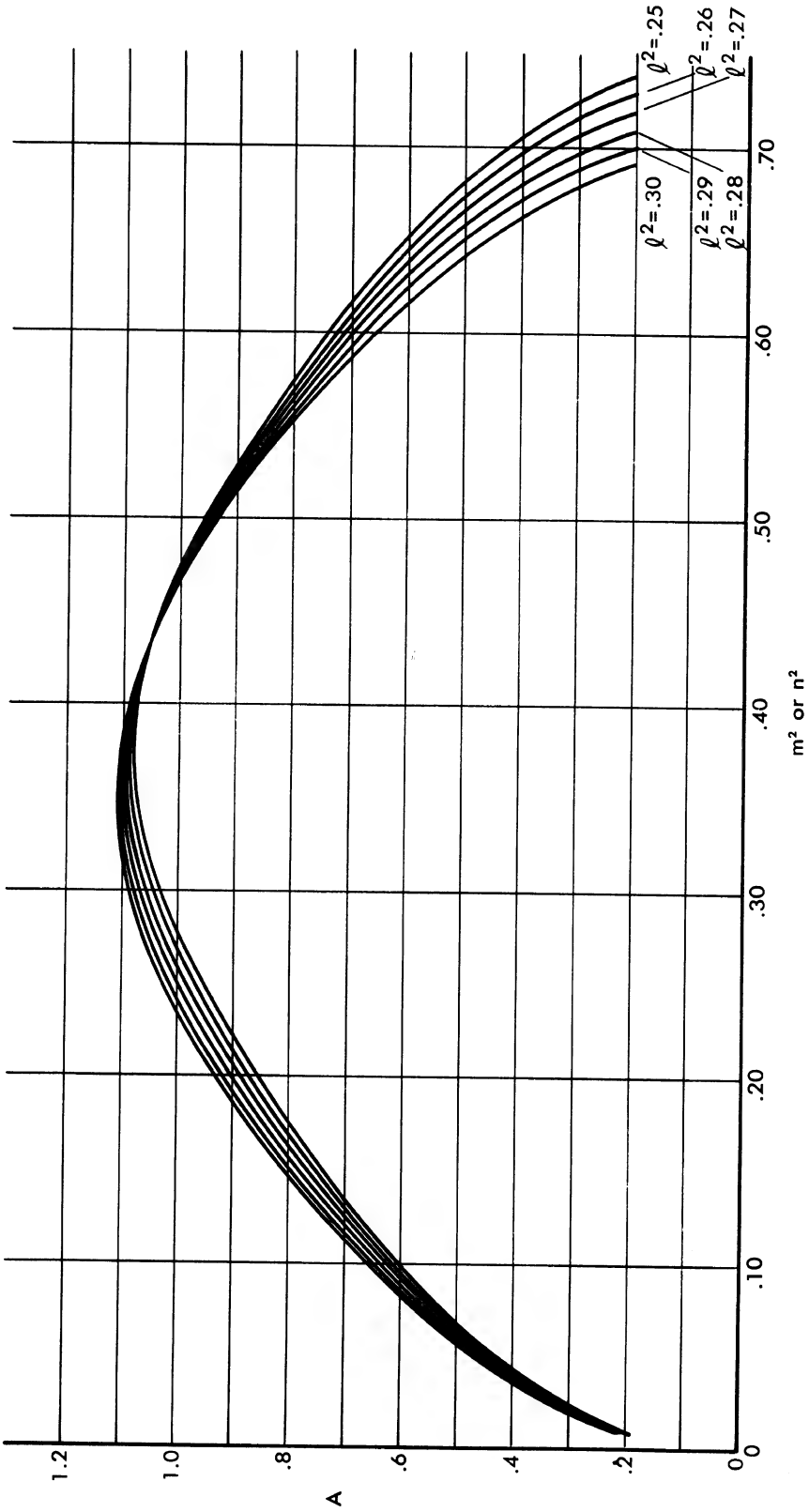

FIG. D.4-15 A, FOR UNIT EDGE CIRCULAR CORNER REFLECTOR, vs. m^2 or n^2 FOR ℓ^2=.30(.01).25

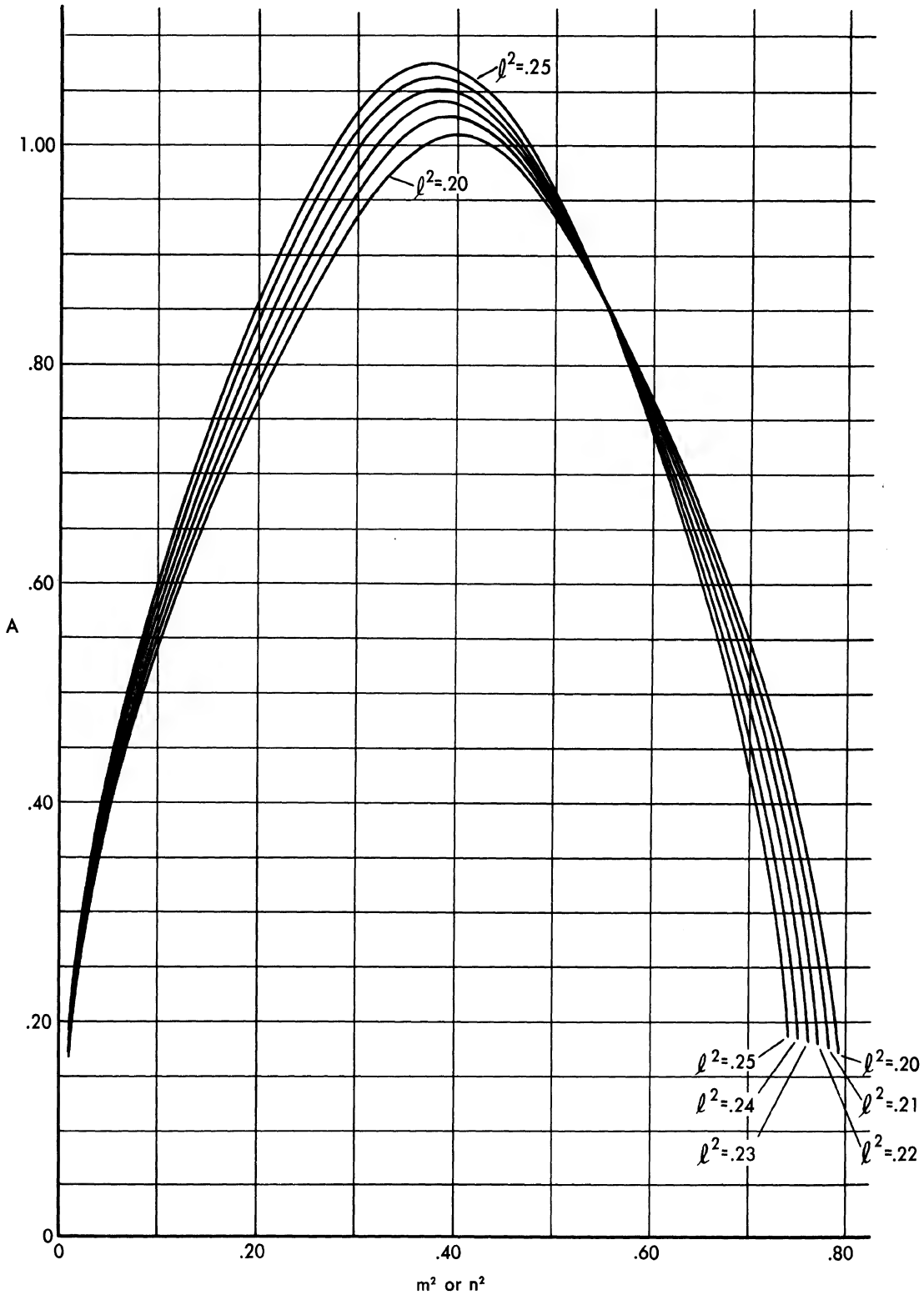

FIG. D.4-16 A, FOR UNIT EDGE CIRCULAR CORNER REFLECTOR, vs. m^2 or n^2 FOR ℓ^2 =.25(.01).20

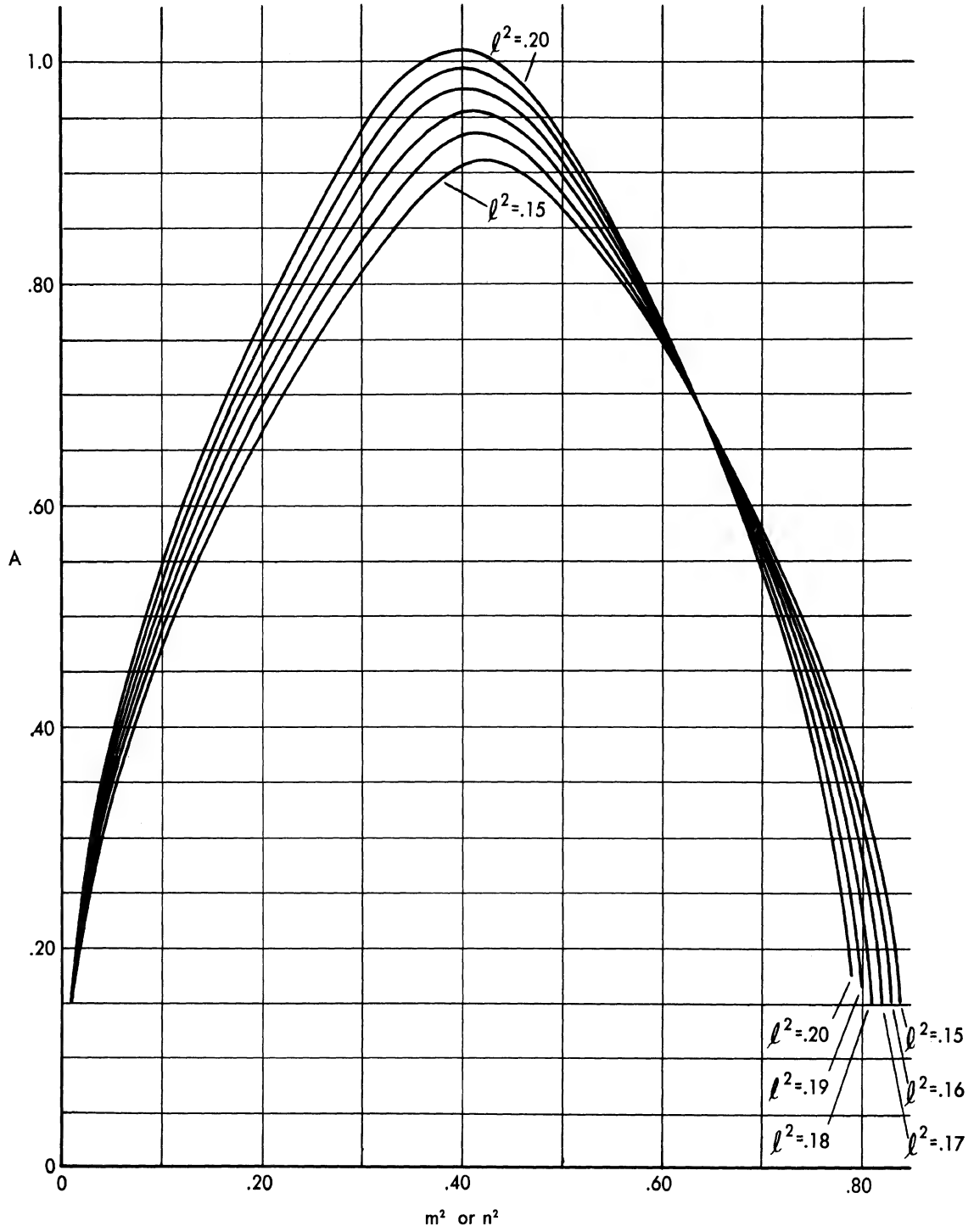

FIG. D.4-17 A, FOR UNIT EDGE CIRCULAR CORNER REFLECTOR, vs. m^2 or n^2 FOR ℓ^2 .20(.01).15

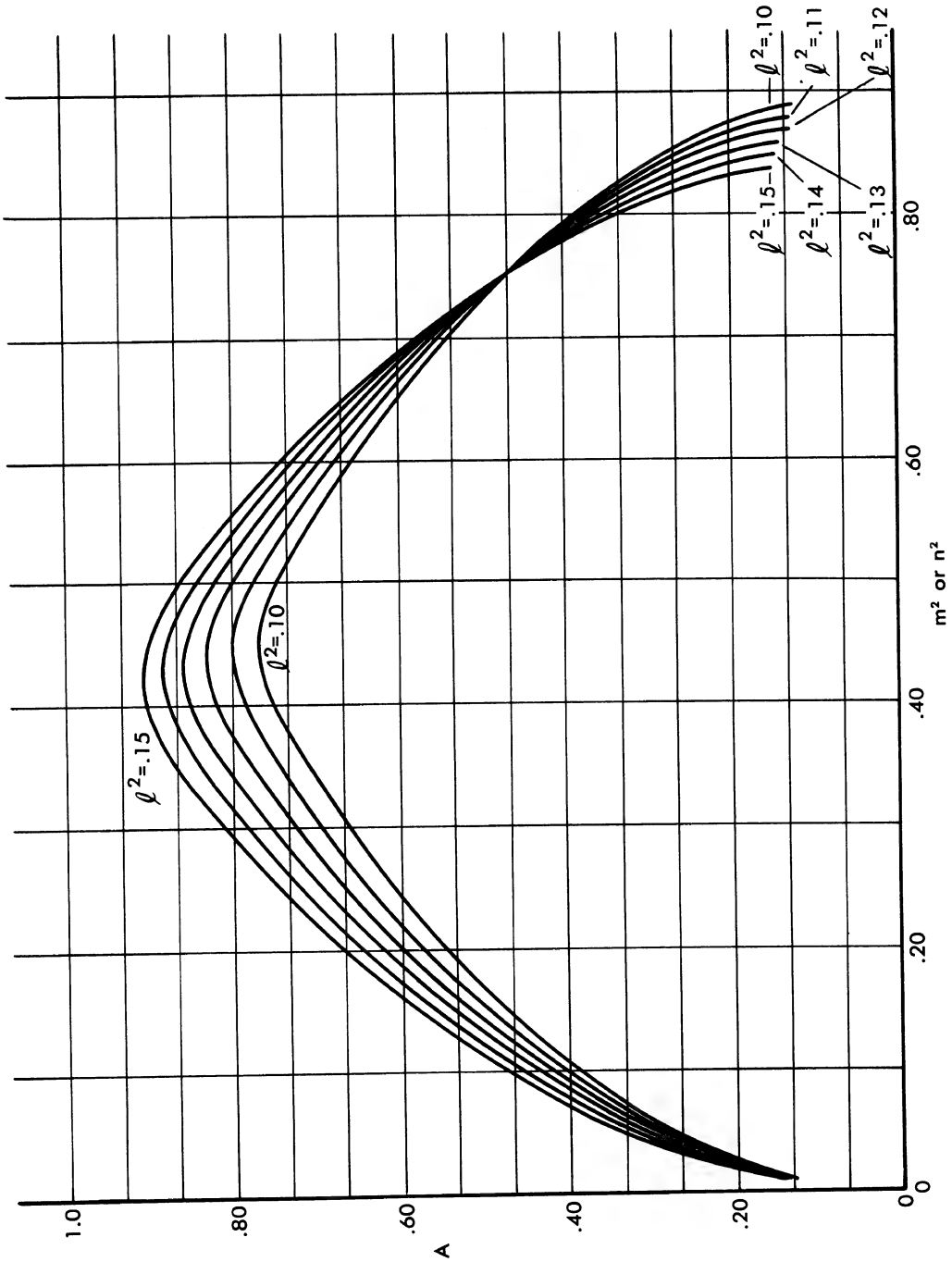

FIG. D.4-18 A, FOR UNIT EDGE CIRCULAR CORNER REFLECTOR, vs. m^2 or n^2 FOR ℓ^2=.15(.01).10

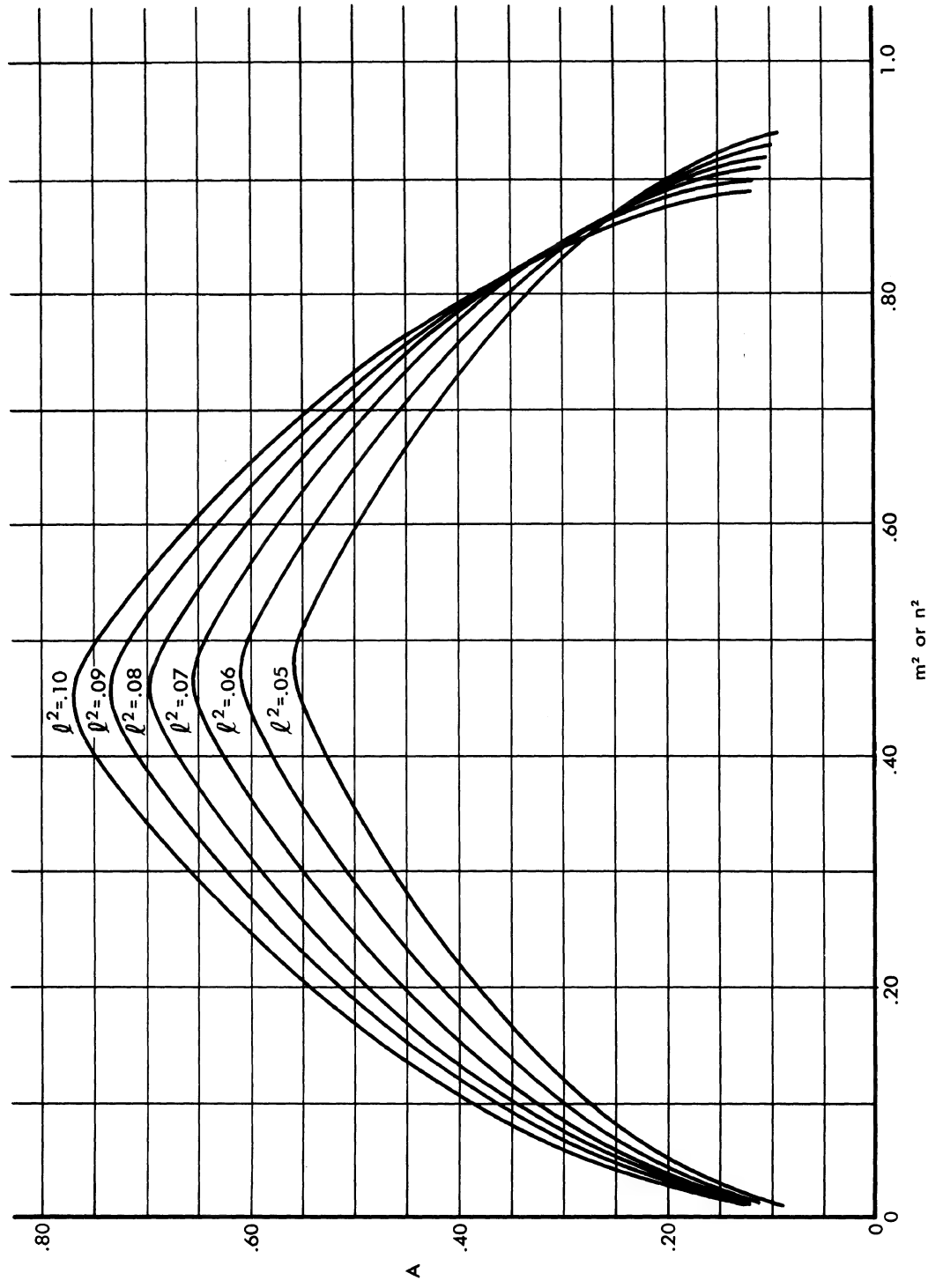

FIG. D.4-19 A, FOR UNIT EDGE CIRCULAR CORNER REFLECTOR, vs. m^2 or n^2 FOR ℓ^2=.10(.01).05

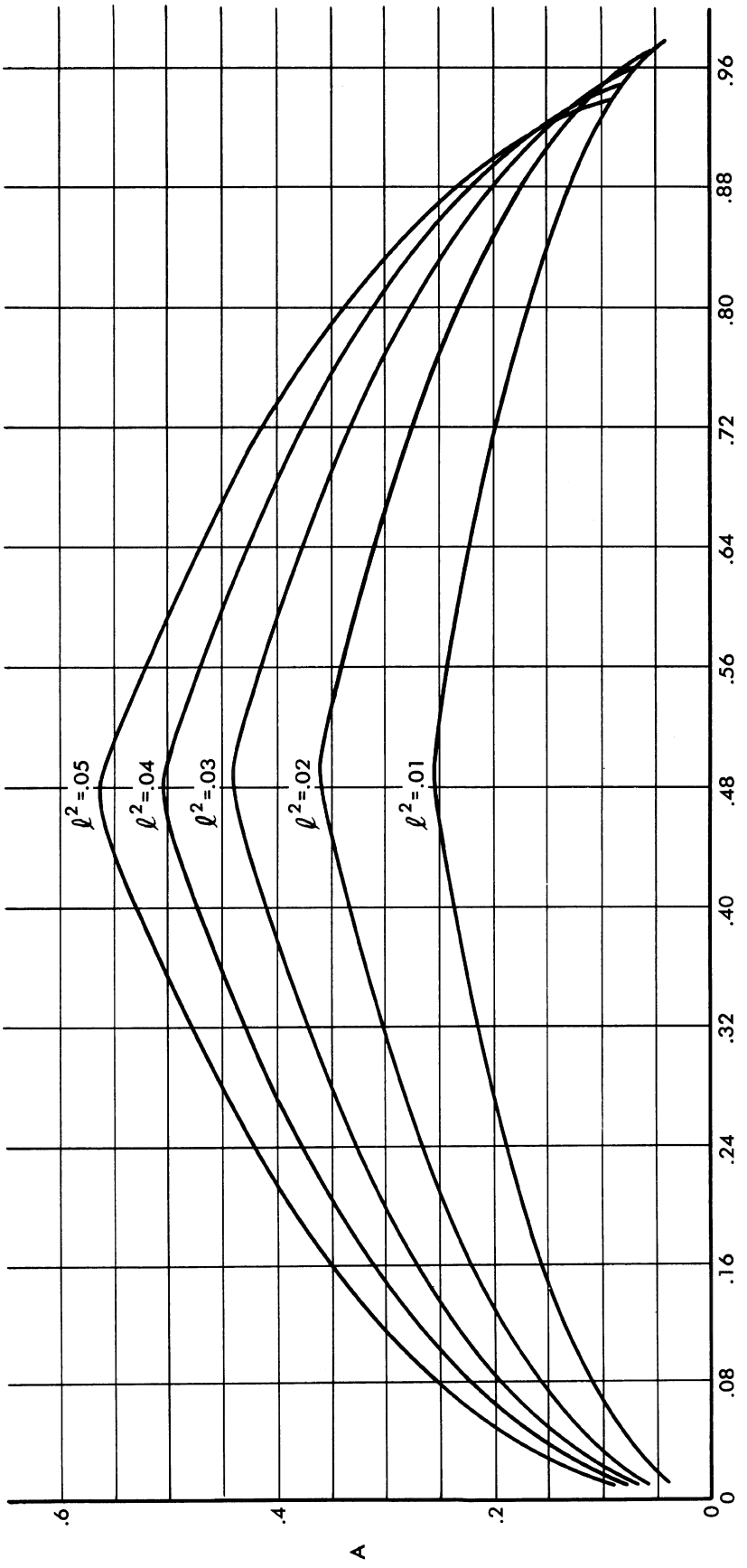

FIG. D.4-20 A, FOR UNIT EDGE CIRCULAR CORNER REFLECTOR, vs. m^2 or n^2 FOR ℓ^2=.05(.01).01

APPENDIX E

GRAPHICAL TECHNIQUES FOR RADAR CROSS-SECTIONS

To present the cross-sections of aircraft, or of corner reflectors in vehicles, in specified coordinate systems, it is advantageous to make use of certain graphical techniques stemming from stereographic projection methods.

In the following sections the stereographic projection and the resulting graphical technique are discussed briefly with an application to triple reflections of a circular corner reflector oriented in a particular manner.

E.1 STEREOGRAPHIC PROJECTION

Let S denote the sphere

$$x^2 + y^2 + (z - 1/2)^2 = 1/4 .$$

The stereographic projection onto the xy-plane is defined as follows: If (x, y, z) is a point on the sphere then the corresponding point (x', y') in the plane is given by

$$x' = \frac{x}{(1-z)}$$

$$y' = \frac{y}{(1-z)}, \quad x^2 + y^2 + (z - 1/2)^2 = 1/4 .$$

The projection can be interpreted geometrically as follows: let N denote the point (0,0,1). Given any point p on S, except N, the projected point p' is the intersection of the line through N and p with the xy-plane.

This projection has strong geometrical invariants; namely, it is a conformal mapping of the sphere into the plane and furthermore it projects circles on the sphere into circles or straight lines on the plane.

Introduce the complex variable $z = x + iy$. As is well known, the linear fractional transformations

$$w = \frac{\alpha z + \beta}{\gamma z + \delta} \quad , \quad \alpha\delta - \beta\gamma \neq 0 \quad ,$$

where α, β, γ, δ are complex numbers, give all conformal mappings of the complex plane onto itself which carry circles onto circles and which can be continuously deformed into the identity transformation.

A sub-group of this group of transformations which is of primary interest here is

$$w = \frac{\alpha z + \beta}{-\bar{\beta} z + \bar{\alpha}} \quad , \quad \alpha\bar{\alpha} + \beta\bar{\beta} = 1 \quad . \qquad \text{(E.1-1)}$$

These transformations correspond, by the stereographic projection, in a 1-to-1 way with the group of proper rotations on the sphere. These transformations, of course, carry circles into circles but also carry circles which correspond to great circles on the sphere into circles which also correspond to great circles on the sphere.

E.2 APPLICATION TO CHANGE OF COORDINATES

The only changes of coordinates of concern here are those in which the new x', y', z' system is positively oriented, rectangular, and has the same origin as the old. Such a change of coordinates can be completely described by three points p, q, r on the sphere S. If the origin of the sphere is s_o the point p is chosen so that the direction $\overrightarrow{s_o p}$ is the same as the direction of the new positive x'-axis; q and r are chosen in a similar fashion. The points p, q, and r are, of course, not arbitrary. Let w_1, w_2, and w_3 be the points in the plane which correspond to p, q, and r respectively. The points which correspond to the positive x, y, and z directions are 1, i, and ∞ respectively. Thus, the mapping in Equation (E.1-1) which corresponds to the change in coordinates must carry 1, i and ∞ into w_1, w_2, and w_3 respectively.

The mapping in Equation (E.1-1) which satisfies these conditions can be written

$$w = \frac{w_3(1 + w_1\bar{w}_3)z - (w_3 - w_1)}{(1 + w_1\bar{w}_3)z + \bar{w}_3(w_3 - w_1)} \quad . \qquad (E.2\text{-}1)$$

Example: Consider the change of coordinates $x' = -z$, $y' = -y$, and $z' = -x$. The points in the plane, w_1, w_2, and w_3 which correspond to the positive x', y', and z' directions are respectively 0, -i, and -1. Thus,

$$w = \frac{1-z}{1+z} \, .$$

The old and new coordinates of any point on the sphere have then the stereographic projections z and $1-z/1+z$ respectively.

E.3 APPLICATION TO POLARIZATION-INDEPENDENT CROSS-SECTIONS

The monostatic cross-section of a closed surface in space can be completely described by a real valued, non-negative function on the sphere S where at each point of S the function has the value which is the cross-section of the surface for the direction corresponding to the point on S. In order to describe this function one could make contour plots on the surface of the sphere, the cross-section constant on each contour. In order to represent these contours more conveniently consider the stereographic projection of the contours into the z-plane. For those cross-sections which are polarization independent a rotation of the sphere takes contours on the sphere into contours with the same constant cross-section. Therefore, the transformations of Equation (E.2-1) will take the projected contours into the projected contours on which the cross-section has the same constant value.

Thus, given the cross-section of a surface with respect to a convenient coordinate system, let its contours be projected into the z-plane. Then the contours can be transformed into the contours with respect to any other coordinate system; i.e., the contours are invariant with respect to the group of transformations of Equation (E.2-1).

E.4 GRAPHICAL TRANSFORMATION OF COORDINATES

Given a right-handed triad of orthogonal unit vectors $\hat{i}$, $\hat{j}$, $\hat{k}$. Given also an arbitrary direction. Let θ be the angle between $\hat{k}$ and the direction. Let ϕ be the angle between $\hat{i}$ and the projection of the direction in the plane spanned by $\hat{i}$ and $\hat{j}$. Given a second system $\hat{i}^*$, $\hat{j}^*$, $\hat{k}^*$, θ^*, ϕ^*. The problem is to graphically relate θ, ϕ to θ^*, ϕ^*.

As a preliminary step let us calculate the Euler angles for the transformation from $\hat{i}$, $\hat{j}$, $\hat{k}$ to $\hat{i}^*$, $\hat{j}^*$, $\hat{k}^*$ since our graphical technique will be given in terms of them. Let $\hat{i}_1$, $\hat{j}_1$, $\hat{k}_1$ be obtained from $\hat{i}$, $\hat{j}$, $\hat{k}$ by a rotation through an angle α about the $\hat{k}$ axis. Then

$$\begin{aligned} \hat{i}_1 &= \hat{i}\cos\alpha + \hat{j}\sin\alpha \\ \hat{j}_1 &= -\hat{i}\sin\alpha + \hat{j}\cos\alpha \\ \hat{k}_1 &= \hat{k} \end{aligned} \qquad \text{(E.4-1)}$$

Now let $\hat{i}_2$, $\hat{j}_2$, $\hat{k}_2$ be obtained from $\hat{i}_1$, $\hat{j}_1$, $\hat{k}_1$ by a rotation through an angle β about the $\hat{j}_1$ axis. Then

$$\begin{aligned} \hat{i}_2 &= \hat{i}_1\cos\beta - \hat{k}_1\sin\beta = \hat{i}\cos\alpha\cos\beta + \hat{j}\sin\alpha\cos\beta - \hat{k}\sin\beta \\ \hat{j}_2 &= \hat{j}_1 = -\hat{i}\sin\alpha + \hat{j}\cos\alpha \\ \hat{k}_2 &= \hat{i}_1\sin\beta + \hat{k}_1\cos\beta = \hat{i}\cos\alpha\sin\beta + \hat{j}\sin\alpha\sin\beta + \hat{k}\cos\beta. \end{aligned} \qquad \text{(E.4-2)}$$

Finally let $\hat{i}^*$, $\hat{j}^*$, $\hat{k}^*$ be obtained from $\hat{i}_2$, $\hat{j}_2$, $\hat{k}_2$ by rotation about the $\hat{k}_2$ axis through an angle γ. Thus

$$\hat{i}^* = \hat{i}_2\cos\gamma + \hat{j}_2\sin\gamma = (\cos\alpha\cos\beta\cos\gamma - \sin\alpha\sin\gamma)\hat{i}$$

$$+ (\sin\alpha\cos\beta\cos\gamma + \cos\alpha\sin\gamma)\hat{j} - \sin\beta\cos\gamma\,\hat{k}$$

$$\hat{j}^* = -\hat{i}_2 \sin\gamma + \hat{j}_2 \cos\gamma = (-\cos\alpha \cos\beta \sin\gamma - \sin\alpha \cos\gamma)\hat{i}$$

$$+ (-\sin\alpha \cos\beta \sin\gamma + \cos\alpha \cos\gamma)\hat{j} + \sin\beta \sin\gamma \hat{k}$$

$$\hat{k}^* = \hat{k}_2 = \cos\alpha \sin\beta \hat{i} + \sin\alpha \sin\beta \hat{j} + \cos\beta \hat{k} . \qquad \text{(E.4-3)}$$

We will require $0 \leq \beta \leq \pi$ so that $\sin\beta \geq 0$. We can obtain $\cos\beta$ from $\hat{k}^* \cdot \hat{k}$, and then compute $\sin\beta = +\sqrt{1 - \cos^2\beta}$. We can then obtain $\sin\alpha$, $\cos\alpha$, $\sin\gamma$, and $\cos\gamma$ from $\hat{k}^* \cdot \hat{j}$, $\hat{k}^* \cdot \hat{i}$, $\hat{k} \cdot \hat{j}^*$, and $\hat{k} \cdot \hat{i}^*$ respectively.

Now the angles θ_1, ϕ_1 and θ_2, ϕ_2 are related to θ, ϕ and θ^*, ϕ^* as follows:

$$\theta = \theta_1 \qquad \theta_2 = \theta^*$$

$$\phi - \alpha = \phi_1 \qquad \phi_2 - \gamma = \phi^* \quad . \qquad \text{(E.4-4)}$$

Thus if we get the relation between θ_1, ϕ_1 and θ_2, ϕ_2 we can obtain the relation between θ, ϕ and θ^*, ϕ^* readily from Equation (E.4-4).

If we draw the lines of constant θ_1 and ϕ_1 on a sphere and make the stereographic projection of the sphere into a plane we get Figure E.4-1. The positions of $\hat{i}_1$, $\hat{j}_1$, $\hat{i}_2$, $\hat{j}_2$, $\hat{k}_2$ are marked for $\beta = 60^\circ$ ($\hat{k}_1$ lies at infinity). The distance from the point $\theta_1 = 180^\circ$ to the circle of constant θ_1 is proportional to $\cot(\theta_1/2)$.

The stereographic projection of the curves of constant θ_2 and ϕ_2 can be drawn easily. Due to the properties of the stereographic projection these curves are all circles or straight lines. Due to the symmetry about the $(x_1 - z_1)$ $(x_2 - z_2)$ plane, the centers of the constant θ_2 circles will lie on the $\phi_1 = 0^\circ$, 180° line. These circles will cut the $\phi_1 = 0^\circ$ line at $\theta_1 = \beta \pm \theta_2$ if these numbers lie in the interval 0° to 180°.

They will cut the line $\phi_1 = 180^\circ$ at $\theta_2 - \beta$ and $2\pi - (\beta + \theta_2)$ if these numbers lie in the interval 0° to 180°. The curve $\theta_2 = \beta$ is a straight line perpendicular to the line $\phi_1 = 0^\circ, 180^\circ$, and is the perpendicular bisector of the segment $\theta_2 = 0^\circ$, $\theta_2 = 180^\circ$. Since all of the curves of constant ϕ_2 go through the points $\theta_2 = 0^\circ$, $\theta_2 = 180^\circ$ the centers of the constant ϕ_2 curves must lie on the line $\theta_2 = \beta$. Since the ϕ_2 = constant curves must go through the points $\theta_2 = 0^\circ, 180^\circ$ at the same angle which the ϕ_1 = constant curves go through $\theta_1 = 180^\circ$, the centers of the ϕ_2 = constant curves lie on a line parallel to the $\phi_1 = \phi_2 \pm 90^\circ$ lines and passing through one of the points $\theta_2 = 0^\circ, 180^\circ$. The curves of constant θ_2, ϕ_2 are shown in Figure E.4-2 for $\beta = 60^\circ$. The positions of $\hat{i}_1$, $\hat{j}_1$, $\hat{i}_2$, $\hat{j}_2$, and $\hat{k}_2$ are also located on Figure E.4-2.

If Figures E.4-1 and E.4-2 are superimposed, then θ_2, ϕ_2 can be read off in terms of θ_1, ϕ_1 and vice versa. The superimposition is best done in two colors to avoid confusion.

This transformation technique is designed for application to obtaining radar cross-sections of complicated shapes. The approximation methods which are used for obtaining such cross-sections involve breaking the complicated shape down into simply shaped pieces and getting the cross-sections of the pieces. The coordinate systems appropriate to each of the pieces and to the total object are generally different. With this technique one can plot the cross-section of the simple shape in a standard orientation on a coordinate system like that in Figure E.4-1 and then make the appropriate coordinate transformation graphically. This procedure is illustrated with the constant cross-section curves for a circular corner reflector in a coordinate system whose axes correspond to edges of the reflector (Fig. E.4-3a) and in a transformed coordinate system (Fig. E.4-3b). (The transformation consisted of a rotation of 45° about the z-axis followed by a rotation of 30° about the new y-axis.)

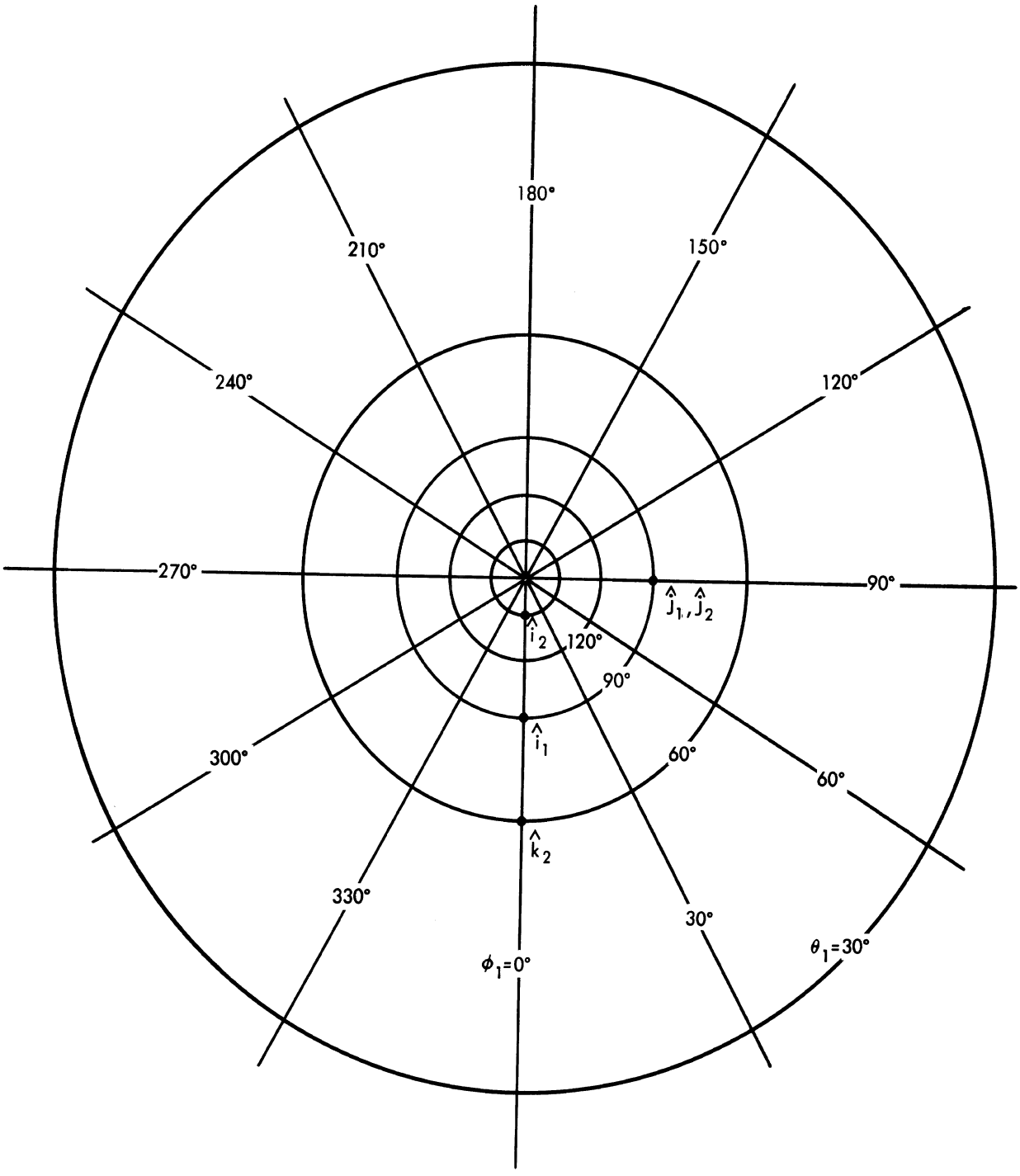

FIG. E.4-1 STEREOGRAPHIC PROJECTION OF SPHERE

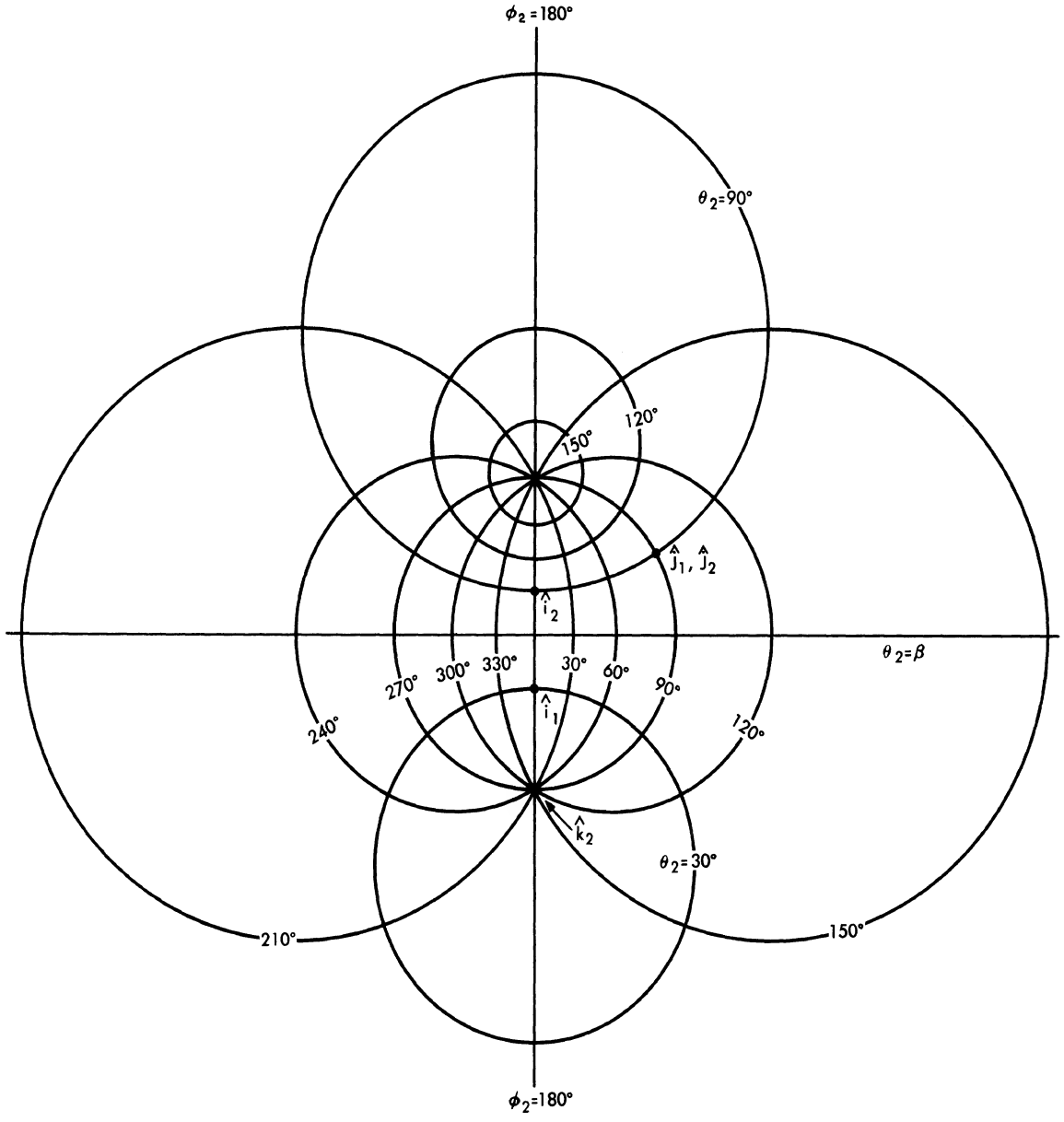

FIG. E.4-2 STEREOGRAPHIC PROJECTION OF ROTATED SPHERE

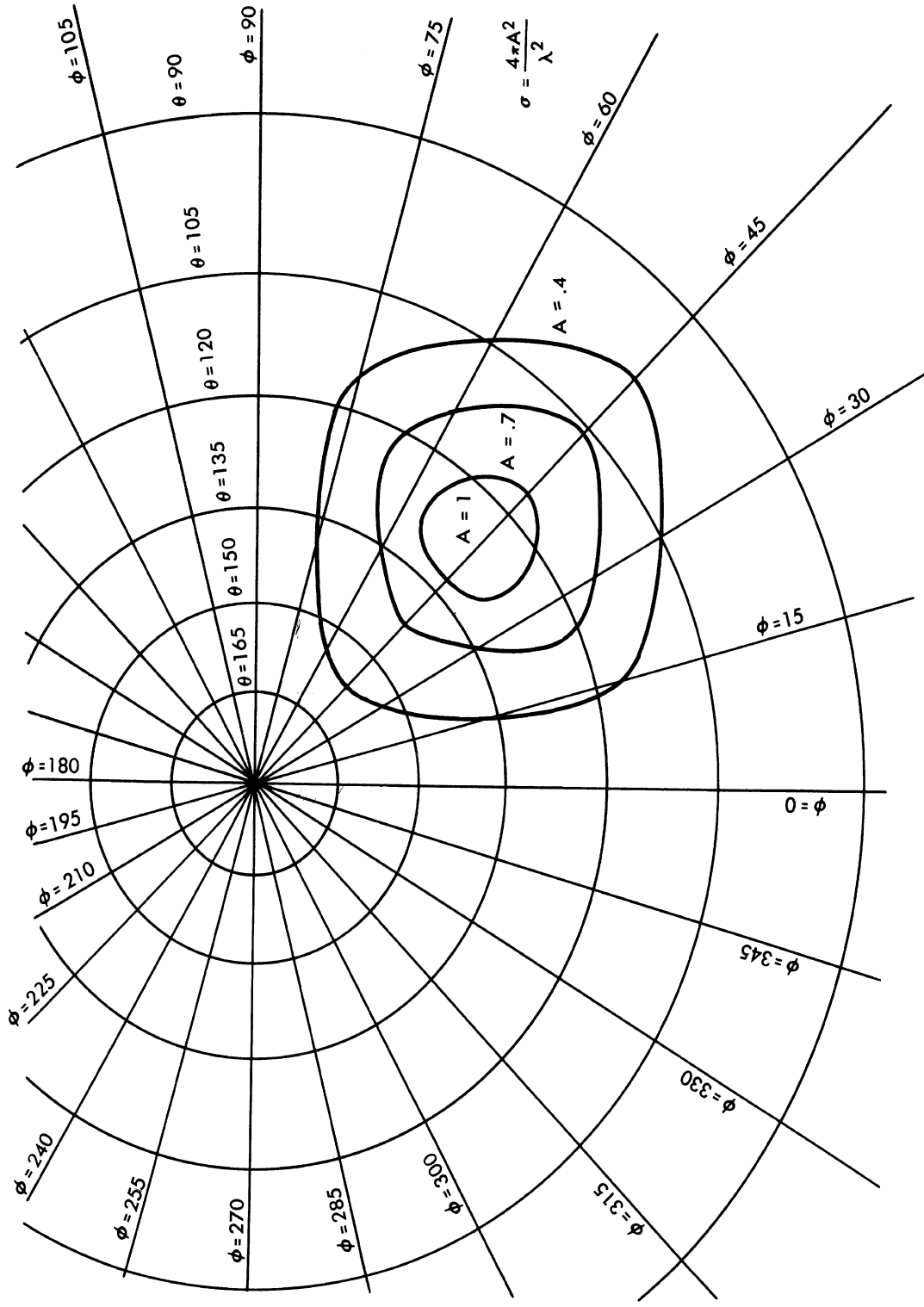

FIG. E.4-3a STEREOGRAPHIC PROJECTION OF UNIT EDGE CIRCULAR CORNER REFLECTOR. (Edges Lie Along Positive x-, Positive y-, and negative z-axes)

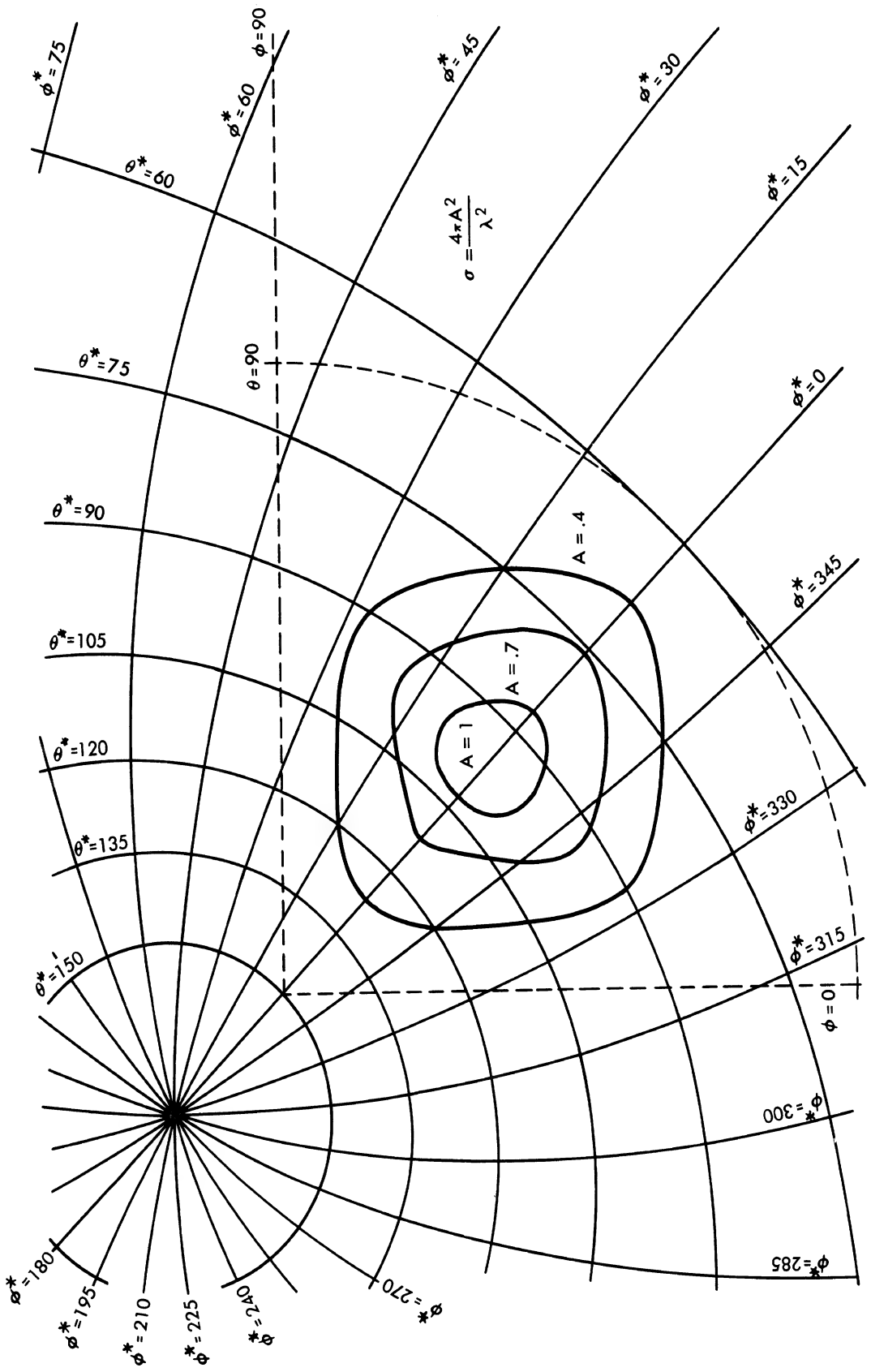

FIG. E.4-3b STEREOGRAPHIC PROJECTION OF CORNER REFLECTOR IN TRANSFORMED COORDINATE SYSTEM

APPENDIX F

EFFECT OF FUEL ON THE RADAR CROSS-SECTION OF CORNER REFLECTORS

The problem of finding the effect on radar cross-section of fuel of different types at various levels in differently shaped corner reflectors with many sorts of coverings is in general difficult. An approach to the problem has been made by finding the radar cross-section for a circular corner reflector covered with a spherical cap and filled with fuel of index of refraction $n < 2$. These results are compared to certain experimental data (Ref. 33).

F.1 RADAR CROSS-SECTION OF FUEL-FILLED CIRCULAR CORNER REFLECTOR

The simplest approach is to let the circular corner reflector of edge R be an octant of a sphere of radius R. With this arrangement incident rays may be traced through the sphere as through it were a lens since the action of the corner reflector would simply reverse the directions of the traced rays. Thus for a cylindrical tube of rays of given cross-sectional area incident on the sphere the cross-sectional area of the emitted tube (or cone) of rays may be calculated at some distance r from the sphere. Under the assumption that there is no absorption in the fuel, the amount of energy in the incident and emitted tubes must be the same, and since the square of the field is proportional to this energy, the transmitted field (or at least its magnitude) may be obtained.

Let the radius of the cylinder of incident rays be a. The cross-sectional area of the emitted cone of rays must be found at large distance r from the sphere. This is the problem of finding b in Figure F-1a. To do this consider the simplified two-dimensional picture of Figure F-1b.

From Snell's law,

$$\frac{\sin\theta}{\sin\theta'} = n, \quad \text{or,} \quad \theta' \cong \frac{\theta}{n} ,$$

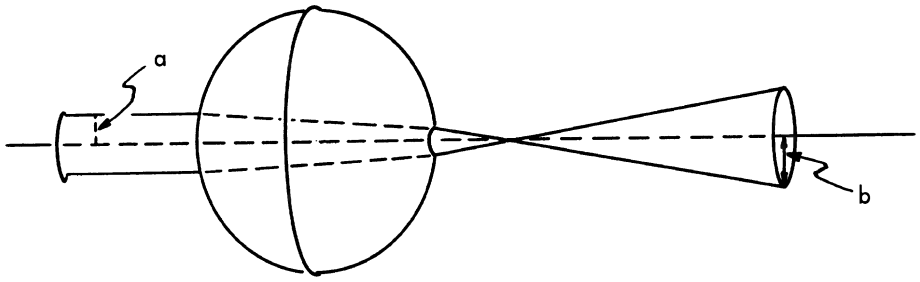

FIG. F-1a RAY PATHS THROUGH A SPHERICAL LENS

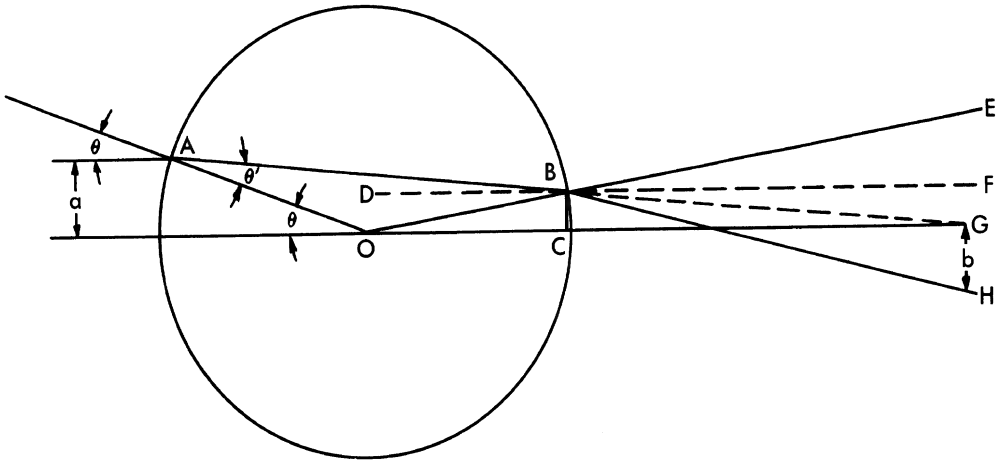

FIG. F-1b SECTIONAL VIEW OF RAY PATHS THROUGH A SPHERICAL LENS

for small angles θ and θ'. The geometry of triangle AGO indicates that angle ABD is approximately,

$$\theta\left(\frac{n-1}{n}\right).$$

From this the distance a' is found to be (again making use of the fact that the angles involved are small)

$$a' \cong a\left(\frac{2-n}{n}\right),$$

whence angle DBO is given approximately by,

$$\frac{a'}{R} = \theta\left(\frac{2-n}{n}\right);$$

this is also the value of angle EBF. Now using the value θ/n for angle ABO and reapplying Snell's law, angle EBH is found to be θ. Finally angle FBH is

$$\theta - \theta\left(\frac{2-n}{n}\right) = \frac{2a(n-1)}{Rn},$$

so that,

$$b \cong \frac{2ar(n-1)}{Rn}.$$

The cross-sectional area of the cone of rays at a large distance r from the sphere is approximately,

$$\text{Area} = \pi\left[\frac{2ar(n-1)}{Rn}\right]^2.$$

Since the cross-sectional area of the incident tube of rays is πa^2, the transmitted field has the form,

$$\text{Field} = \vec{E}_0 \frac{e^{ikr}}{r} \frac{Rn}{2(n-1)} e^{i\gamma} ,$$

where $\vec{E}_0$ is the incident field and $e^{i\gamma}$ is some undetermined phase factor.

Consequently the radar cross-section σ of the fuel-filled corner reflector being considered is[1],

$$\sigma = \frac{\pi R^2 n^2}{(n-1)^2} .$$

F.2 COMPARISON OF RESULTS WITH EXPERIMENT

As an example consider a circular corner reflector (empty) whose radar cross-section along the axis of symmetry is 35 sq.m for a frequency of 9375 Mc (λ = 3.2 cm). From the formula (D.1-1 , App. D),

$$\sigma = 15.61 \frac{R^4}{\lambda^2} ,$$

the edge of this reflector will be

$$R = \sqrt[4]{\frac{(35)(.032)^2}{15.61}} .$$

[1]Reflections from the spherical face of the fuel have been neglected since the reflection coefficient is about 0.03. Moreover, the covering of the fuel has been neglected entirely. This formula is not valid if it predicts a cross-section greater than that given by the corner reflector formula.

Thus for such a reflector full of fuel of index of refraction $n \cong \sqrt{2}$ [1] the radar cross-section will be

$$\sigma = \frac{\pi R^2 n^2}{(n-1)^2} = \frac{\pi \sqrt{\frac{35}{15.61}}\,(.032)\,(2)}{(\sqrt{2}-1)^2} = 1.76 \text{ sq. m.}$$

This example was chosen in order to be able to effect a comparison with experiment. In experiments of the Microwave Radiation Company, Inc. of Gardena, California (Ref. 33), the 35 sq. m nose-on cross-section (along its symmetry axis) of an empty reflector (or pod of reflectors) dropped to 1.1 sq. m for the reflector 2/3 full of fuel and to 3.3 sq. m for the reflector 5/6 full.[2]

Although the levels of fuel considered in the experiment differ somewhat from that considered theoretically, the above example seems to indicate good agreement between theory and experiment.

A fairly simple discussion may also be given for a diheral partially covered by fuel (see sketch below) when the direction of incident rays is perpendicular to the edge of the dihedral.

Let a be that fraction of the length of the dihedral edge not covered by fuel.

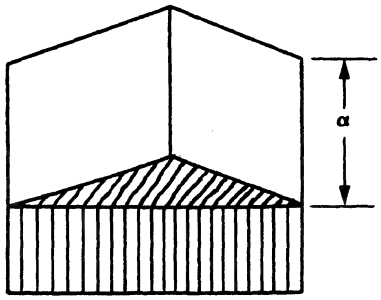

[1] This is a realistic number for 91 and 100 octane gas, kerosene, JP-1, and JP-3 fuels.

[2] In these cases the corner of the reflector was completely covered by fuel.

Then the emitted field is given by an expression of the form,

$$\vec{E} = \frac{a\,\hat{a} + (1-a)\,\hat{a}\,e^{i\phi}}{2\sqrt{\pi}\,r}\sqrt{\sigma_o} \quad ,$$

where ϕ is some phase difference depending on the index of refraction of the fuel and the wavelength of the incident radiation, and σ_o is the radar cross-section of the empty dihedral.

The radar cross-section is then,

$$\sigma = \sigma_o\left[a^2 + (1-a)^2 + 2a(1-a)\cos\phi\right]$$

$$= \sigma_o\left[1 - 2a(1-a)\,(1-\cos\phi)\right] \quad .$$

In the graph below σ is plotted vs. a for certain fixed values of ϕ.

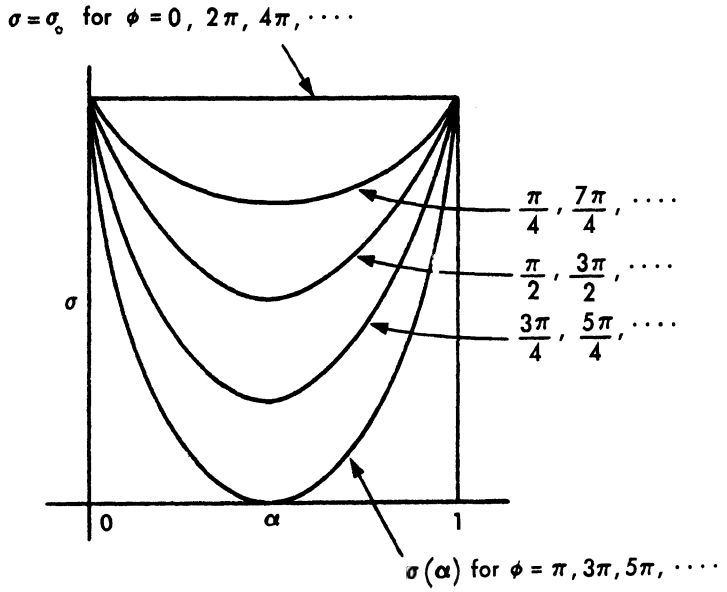

F.3 RESUME OF EXPERIMENTAL RESULTS FOR RADAR CROSS-SECTION OF CORNER REFLECTORS AS A FUNCTION OF FUEL LEVEL[1]

In Reference 33 a description was given of experimental results for the radar back-scattering cross-section of the XQ-4 reflector assembly measured at a frequency of 9375 Mc as a function of JP-4 fuel level in the .080 inch fiberglas-laminated pod housing the reflector assembly.

The following six paragraphs are direct quotes from Reference 33:

"The work was performed several months ago as a portion of our development of the passive reflector system for the XQ-4. The reflector assembly used was the final model of the reflector assembly delivered to Radioplane for the XQ-4 program.

"In Figure 1, the change in back-scattering cross-section for the nose reflector assembly is given in increments of liquid level where the total capacity of the tank was 60 gallons and fuel was added in 10 gallon increments.

"In Figure 2, the change in the return of the broad side reflector assembly was measured simultaneously with that of the nose reflector under the same conditions. (The modulation present in the back-scattering return of the broad side reflector was a specific feature of the design of the reflector assembly. A more detailed discussion of the reflector assembly design, as such, is given in the XQ-4 report.)

"The last series of measurements on each of the two figures represents the change in the back-scattering cross-section when the pod was drained, five gallons of fuel put in, the tank vigorously agitated as to thoroughly wet all surfaces, the fuel drained and the back-scattering cross-section measured in the next few moments.

---

[1]Microwave Radiation Company, Inc. This section gives a resume of Reference 33.

"There are two striking features in Figures 1 and 2 [Figs. F-2a and F-2b] . First, the marked reduction in cross-section as the fuel level approached the 1/3 full mark and, second, the minor change in back-scattering cross-section for the wetted but empty tank.

"These data are more than adequate to provide a semi-quantitative measure of the effects of the JP-4 fuel on the back-scattering cross-section of the reflector assembly at X-band. If a more general picture were desired, a further systematic study would have to be made."

It was pointed out in Reference 33 that the graphically presented measurements were made in the plane of maximum return, which here was the azimuthal plane, for azimuths 0^{o}, 5^{o}, 10^{o}, and 85^{o}, 90^{o}, 95^{o} for each indicated fuel level.

Since the corner of the reflector was covered for levels of 2/3 full and 5/6 full it was felt that it would be feasible to compare these experimental curves with a curve (which happens to be a constant) determined theoretically for a full reflector. This theoretical value is indicated on the Figure 1 graph of Reference 33 (Fig. F-2a) in the 5/6 full column.

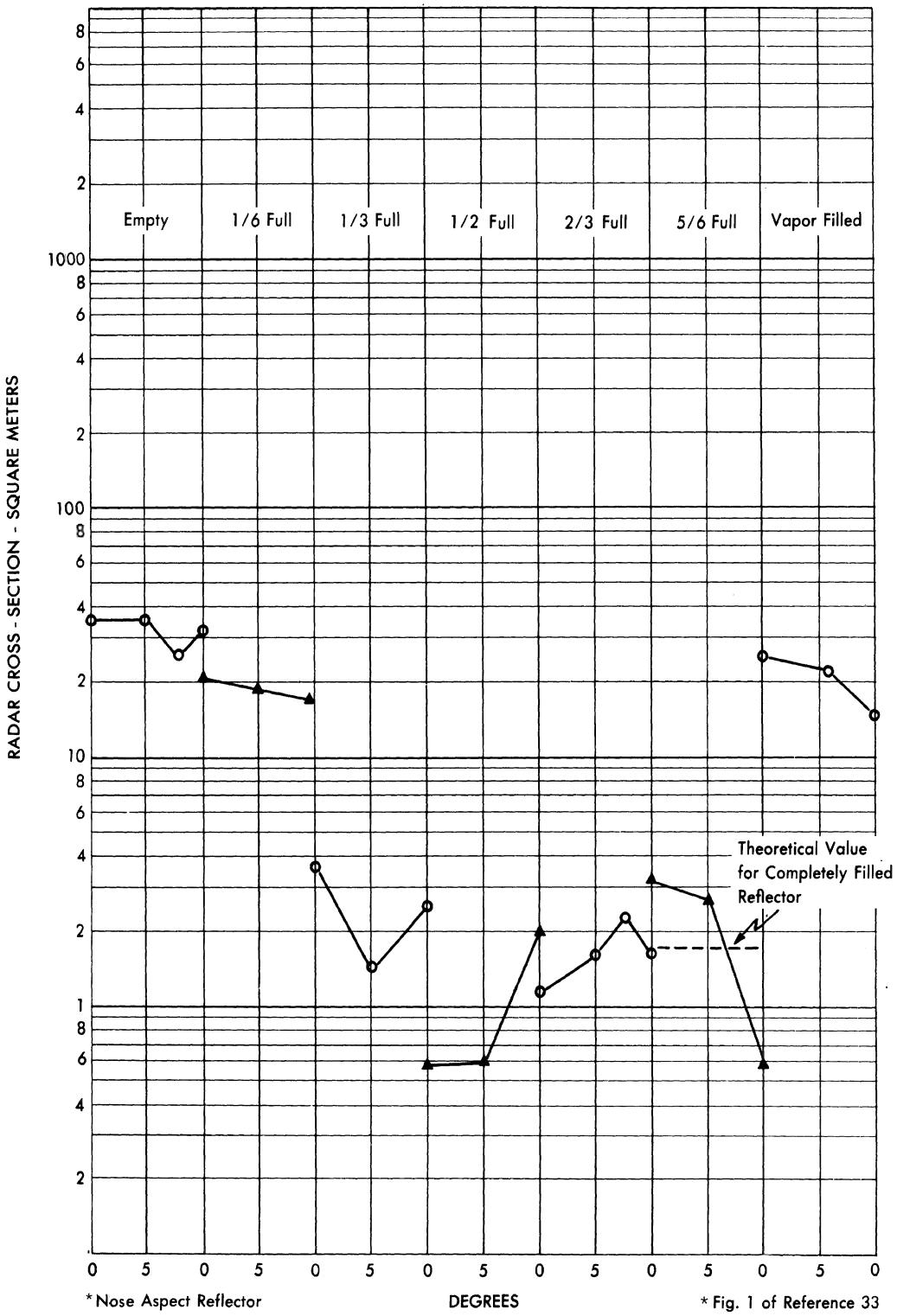

FIG. F-2a RADAR BACK SCATTERING CROSS - SECTION OF XQ-4 REFLECTOR ASSEMBLY AS A FUNCTION OF AMOUNT OF JP-4 FUEL IN REFLECTOR POD*

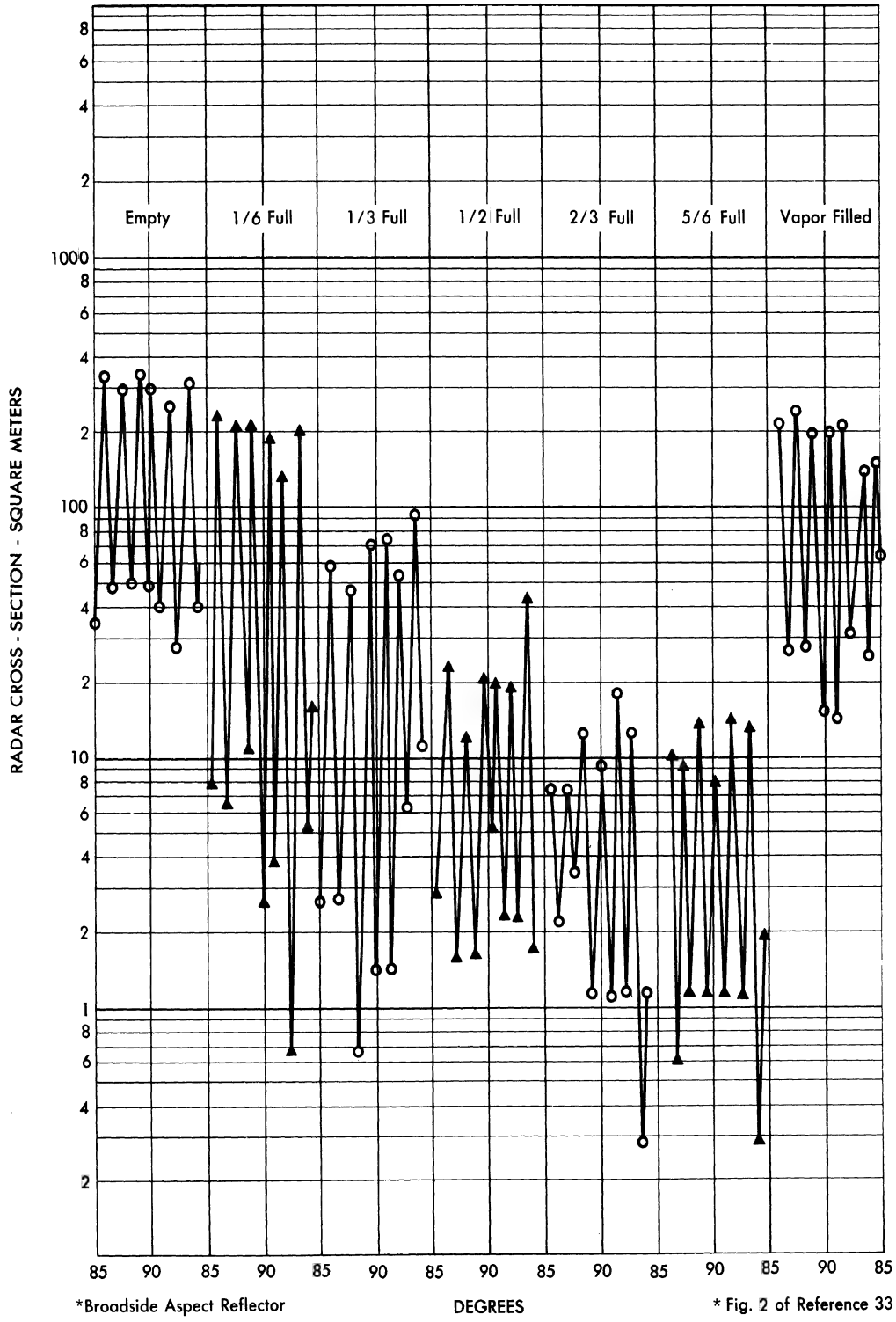

FIG. F-2b RADAR BACK SCATTERING CROSS - SECTION OF XQ-4 REFLECTOR ASSEMBLY AS A FUNCTION OF AMOUNT OF JP-4 FUEL IN REFLECTOR POD*

APPENDIX G

CIRCULAR POLARIZATION ANALYSIS FOR A SQUARE CORNER REFLECTOR

A corner reflector was chosen to match the theoretical nose-on value of σ (RL) for a B-47 (12 sq. m). Since the theoretical value of σ(RL) is sharply peaked near nose-on, a square corner reflector was chosen (the square corner reflector has a sharper peak than the triangular or the circular corner reflector). The wavelength of interest was 12 cm and the edge length of the corner reflector was taken to be 26 cm. The axis of symmetry of the corner reflector was taken to point straight ahead. More details of the orientation of the corner reflector appear below.

A right-handed x, y, z coordinate system was used with the xy-plane horizontal, and the x-axis the axis of the B-47. The edges of the corner reflector were taken to have the directions

$$\hat{e}_1 = \frac{1}{\sqrt{3}}\hat{i} - \sqrt{\frac{2}{3}}\hat{k},$$

$$e_2 = \frac{1}{\sqrt{3}}\hat{i} + \frac{1}{\sqrt{2}}\hat{j} + \frac{1}{\sqrt{6}}\hat{k},$$

$$\hat{e}_3 = \frac{1}{\sqrt{3}}\hat{i} - \frac{1}{\sqrt{2}}\hat{j} + \frac{1}{\sqrt{6}}\hat{k}.$$

The direction to the radar was taken to be

$$\hat{d} = \sin\theta^* \cos\phi^* \hat{i} + \sin\theta^* \sin\phi^* \hat{j} + \cos\theta^* \hat{k}.$$

The vectors specifying horizontal and vertical polarization were taken to be

$$\hat{p}(H) = -\sin\phi^* \hat{i} + \cos\phi^* \hat{j}$$

$$\hat{p}(V) = -\cos\theta^* \cos\phi^* \hat{i} - \cos\theta^* \sin\phi^* \hat{j} + \sin\theta^* \hat{k},$$

while those specifying right and left-hand circular polarization were taken to be

$$\hat{p}(R) = -\frac{1}{\sqrt{2}}\hat{p}(H) + \frac{i}{\sqrt{2}}\hat{p}(V)$$

$$\hat{p}(L) = \frac{1}{\sqrt{2}}\hat{p}(H) + \frac{i}{\sqrt{2}}\hat{p}(V) .$$

The cross-sections were computed by physical optics (Ref. 2). Flat plate, dihedral, and trihedral contributions were taken into account. The cross-sections of the various contributions were added, thus obtaining phase-averaged cross-sections.

In order to compute the flat plate contributions, the faces were approximated by circular flat plates having the same area as the faces. The flat plate contribution is then

$$\sigma_{(1)}(RR) = 0$$

$$\sigma_{(1)}(RL) = \sigma_{(1)}(HH) = \sigma_{(1)}(VV)$$

$$= \frac{b\lambda}{4\pi^{3/2}}\left[\frac{n^2}{(\ell^2+m^2)^{3/2}} + \frac{m^2}{(\ell^2+n^2)^{3/2}} + \frac{\ell^2}{(m^2+n^2)^{3/2}}\right] \qquad (G.1\text{-}1)$$

where any of the terms in the square brackets that exceed

$$\frac{16\pi^{5/2}b^3}{\lambda^3}$$

are to be replaced by this value. Here $b = 0.26$ m is the side length of the corner reflector, $\lambda = 0.12$ m is the wavelength, ℓ is the smallest (in magnitude) of L, M, and N, m is the next in magnitude, and n is the largest.

L, M, and N are given by

$$L = \hat{e}_1 \cdot \hat{d} = \frac{1}{\sqrt{3}} \sin\theta^* \cos\phi^* - \sqrt{\frac{2}{3}} \cos\theta^*$$

$$M = \hat{e}_2 \cdot \hat{d} = \frac{1}{\sqrt{3}} \sin\theta^* \cos\phi^* + \frac{1}{\sqrt{2}} \sin\theta^* \sin\phi^* + \frac{1}{\sqrt{6}} \cos\theta^*$$

$$N = \hat{e}_3 \cdot \hat{d} = \frac{1}{\sqrt{3}} \sin\theta^* \cos\phi^* - \frac{1}{\sqrt{2}} \sin\theta^* \sin\phi^* + \frac{1}{\sqrt{6}} \cos\theta^* .$$

The three terms of Equation (G.1-1) in square brackets represent the three flat plates and the limiting value is the normal incidence value.

The trihedral contribution is zero if any of L, M, and N are negative. When L, M, and N are all positive the trihedral contribution is

$$\sigma_{(3)}(RR) = 0$$

$$\sigma_{(3)}(RL) = \sigma_{(3)}(HH) = \sigma_{(3)}(VV) = \frac{4\pi A^2}{\lambda^2}$$

where

$$A = \begin{cases} 4 \dfrac{\ell m}{n} b^2 & \left(m \leq \dfrac{n}{2}\right) \\ \ell\left(4 - \dfrac{n}{m}\right) b^2 & \left(m \geq \dfrac{n}{2}\right) \end{cases} .$$

The dihedral contribution is

$$\sigma_{(2)}(RL) = 0$$

$$\sigma_{(2)}(RR) = \frac{2m^2b^2}{\pi\ell^2} + \frac{2\ell^2b^2}{\pi m^2} + \frac{2\ell^2b^2}{\pi n^2}$$

where the first term is replaced by $16\pi m^2b^4/\lambda^2$ if it gets bigger than this, and the second and third terms are limited by $16\pi \ell^2b^4/\lambda^2$. $\sigma_{(2)}(HH)$ and $\sigma_{(2)}(VV)$ are obtained by multiplying one of the terms in the formula for $\sigma_{(2)}(RR)$ by

$$\left(\frac{4}{3\sin^2\theta^*} - 1\right)^2$$

and multiplying the other two terms by

$$\left(\frac{1}{3\sin^2\theta^*} - 1\right)^2 .$$

The factor

$$\left(\frac{4}{3\sin^2\theta^*} - 1\right)^2$$

goes with first, second, or third term as L = ℓ, m, or n respectively.

The total effective cross-sections are:

$$\sigma(RL) = \sigma_{(1)}(RL) + \sigma_{(3)}(RL) ,$$

$$\sigma(RR) = \sigma_{(2)}(RR) ,$$

$$\sigma(HH) = \sigma(VV) = \sigma_{(1)}(HH) + \sigma_{(2)}(HH) + \sigma_{(3)}(HH) .$$

Comparisons of the cross-sections of the square corner reflectors described above and the theoretically determined cross-sections of the B-47 at S-band (λ = 12 cm) are given in Figures G-2 ff. The geometry defining the parameters θ^* and ϕ^* used in these figures is given in Figure G-1.

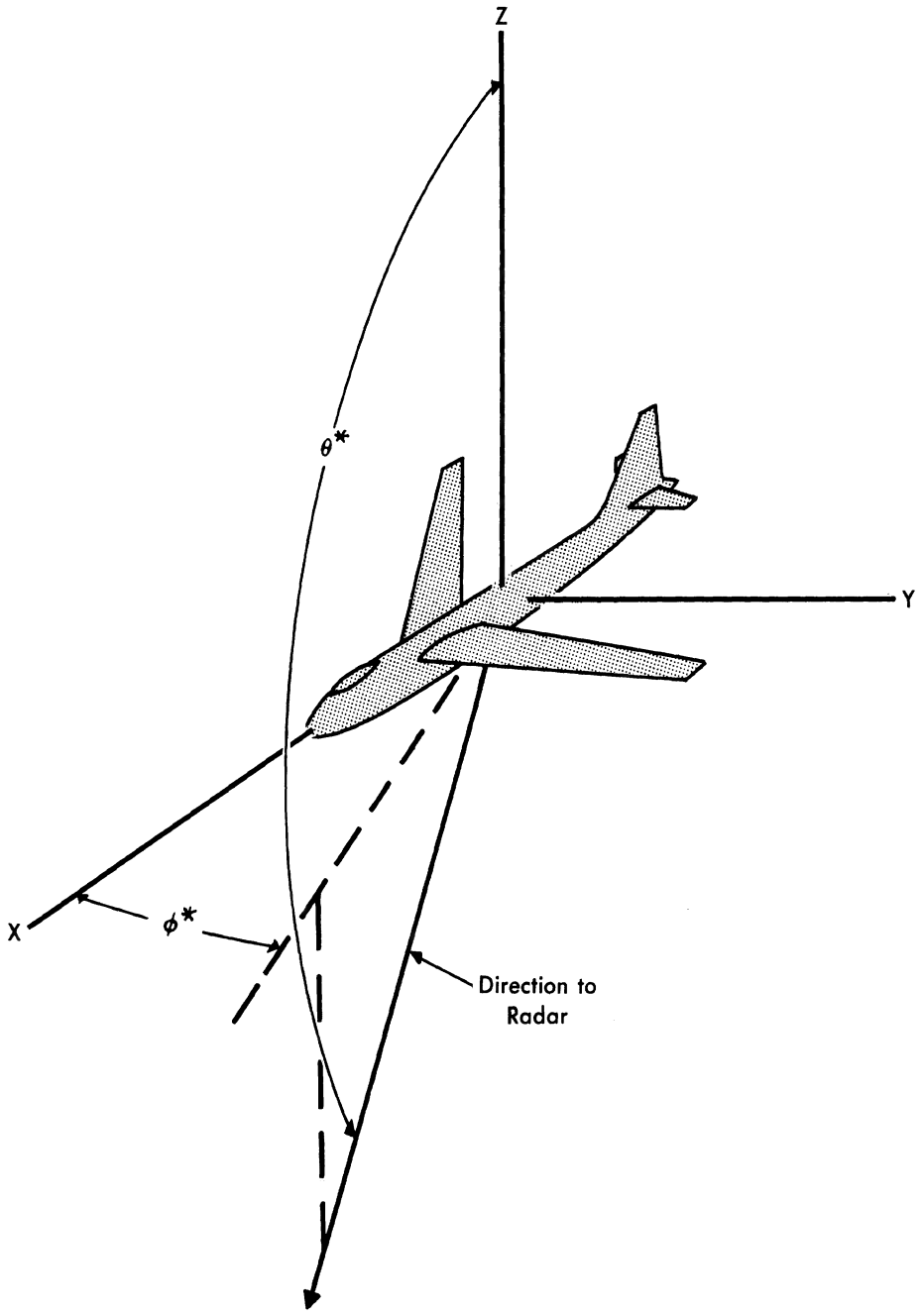

FIG. G - 1 BASIC COORDINATE SYSTEM USED IN DETERMINING THE CROSS-SECTIONS

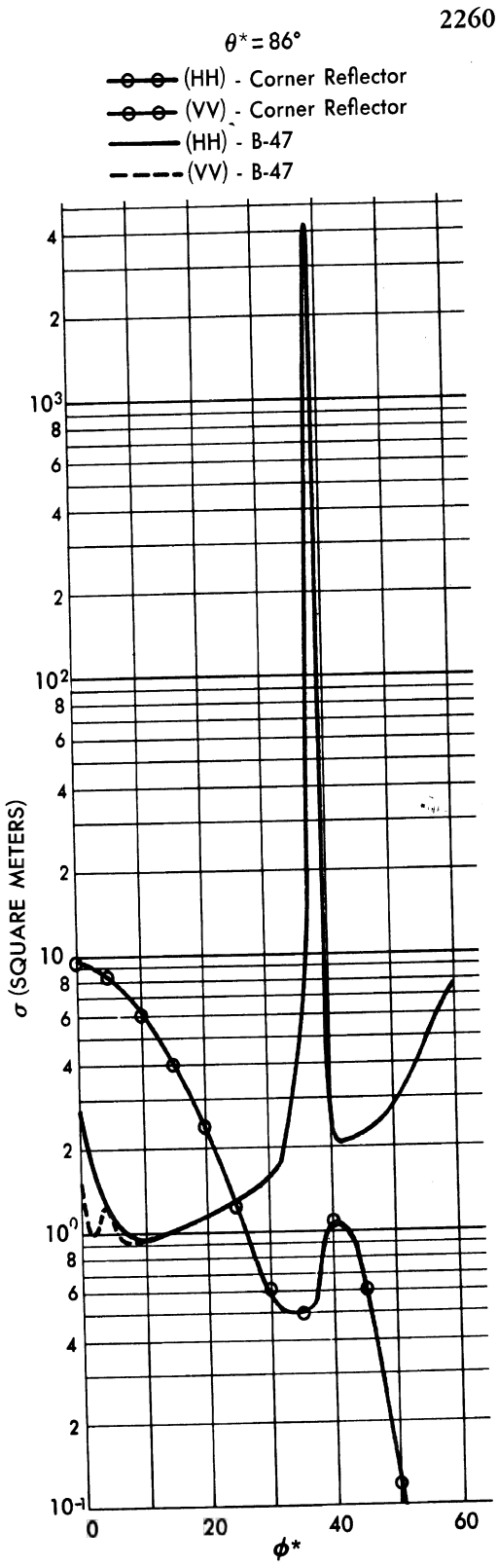

FIG. G-2

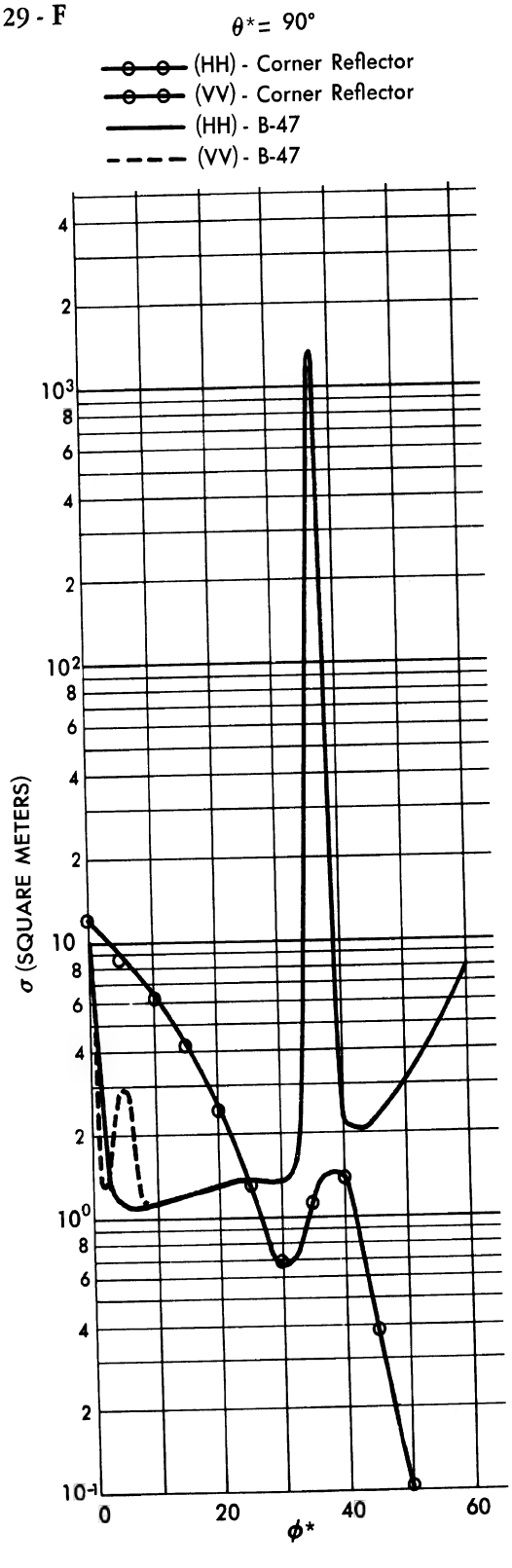

FIG. G-3

COMPARISON OF CROSS-SECTIONS OF THE B-47 AND SQUARE CORNER REFLECTORS AT S-BAND Linear Polarization

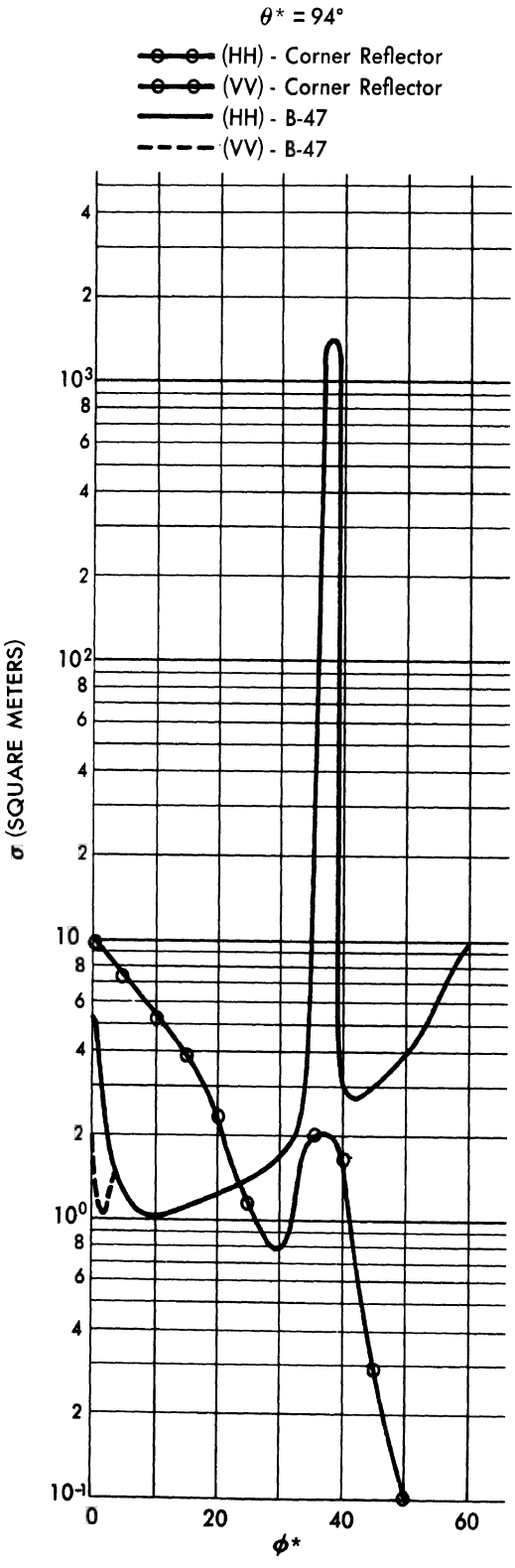

FIG. G-4 Linear Polarization

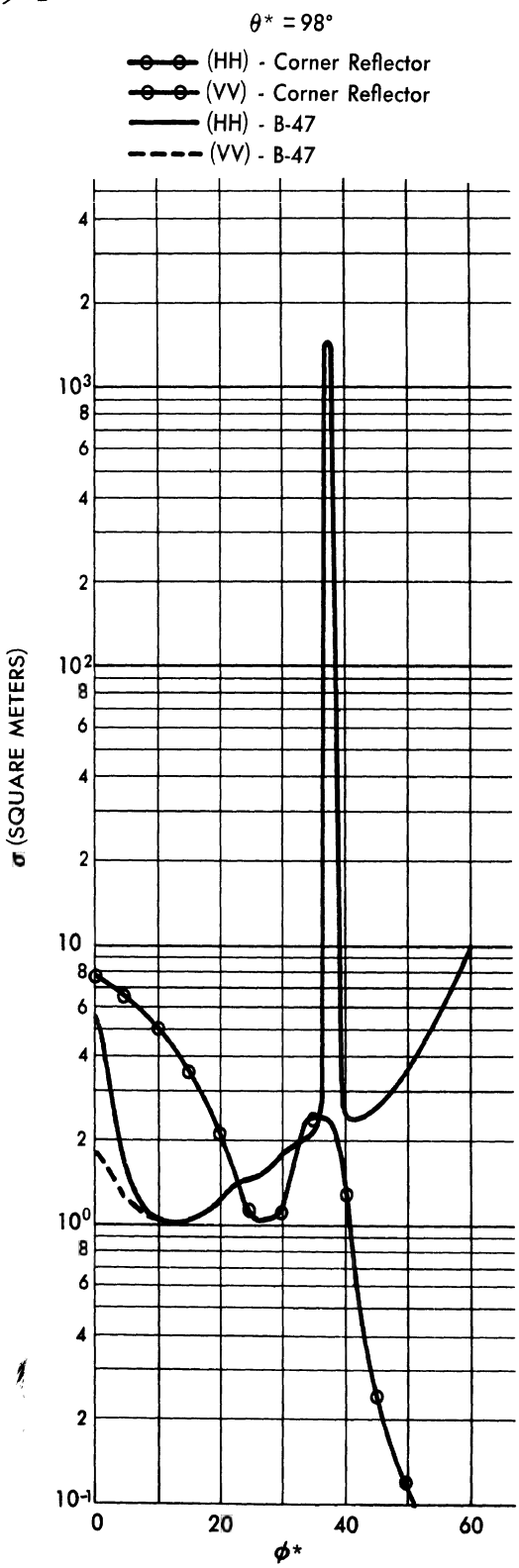

FIG. G-5 Linear Polarization

COMPARISON OF CROSS-SECTIONS OF THE
B-47 AND SQUARE CORNER REFLECTORS AT S-BAND

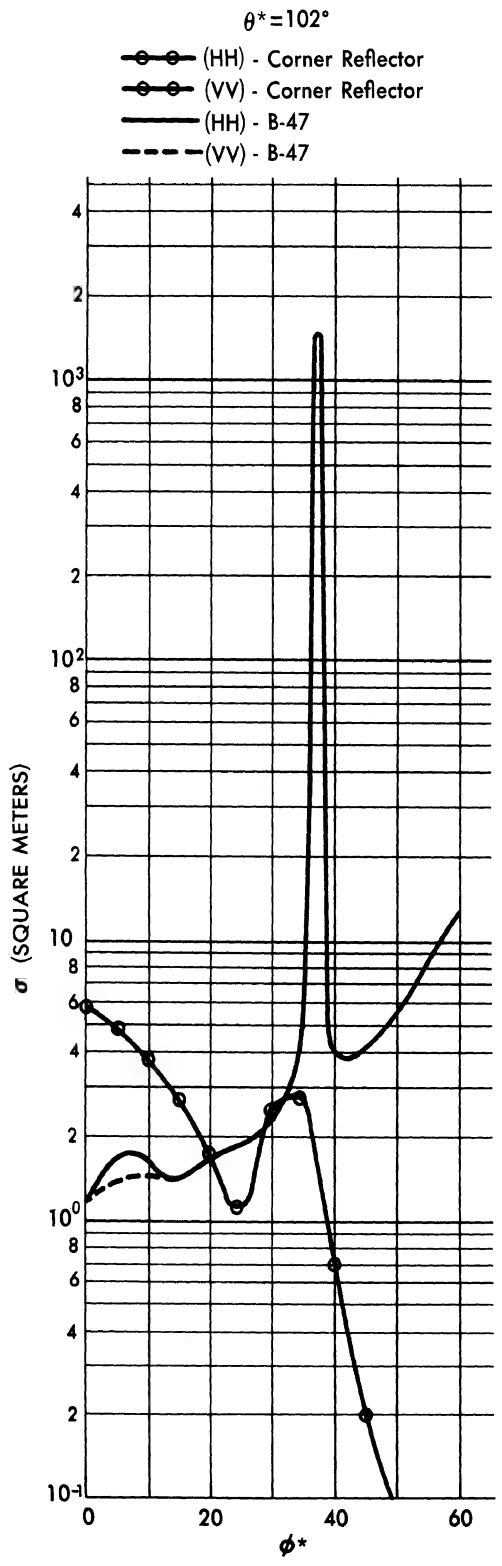

FIG. G-6 Linear Polarization

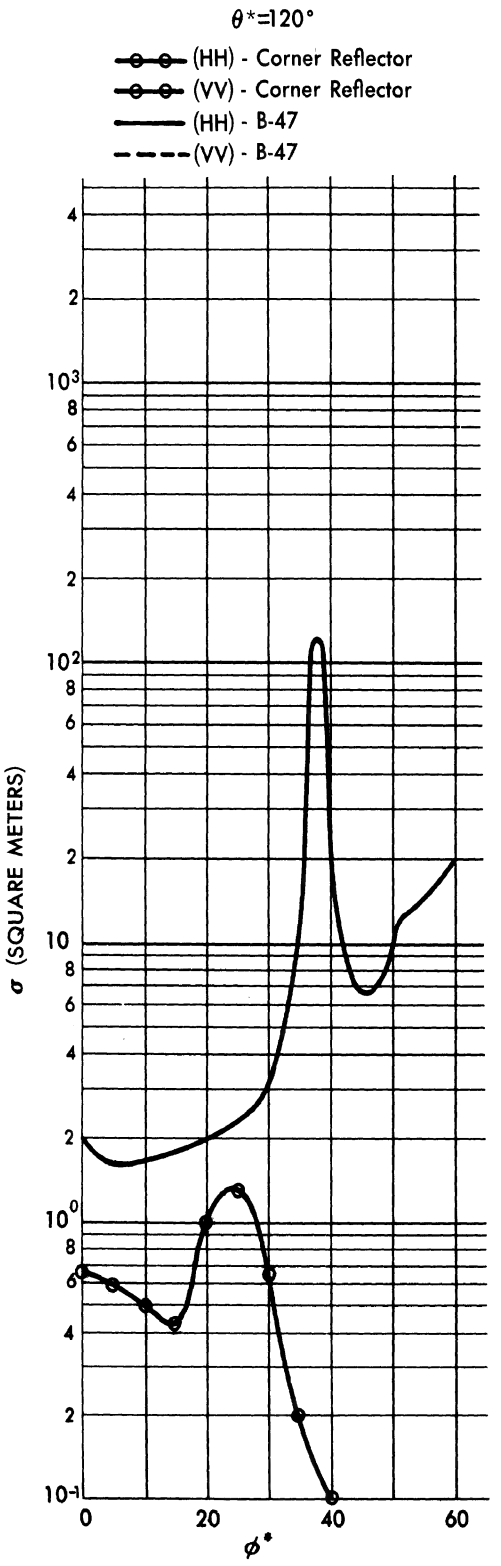

FIG. G-7 Linear Polarization

COMPARISON OF CROSS-SECTIONS OF THE
B-47 AND SQUARE CORNER REFLECTORS AT S-BAND

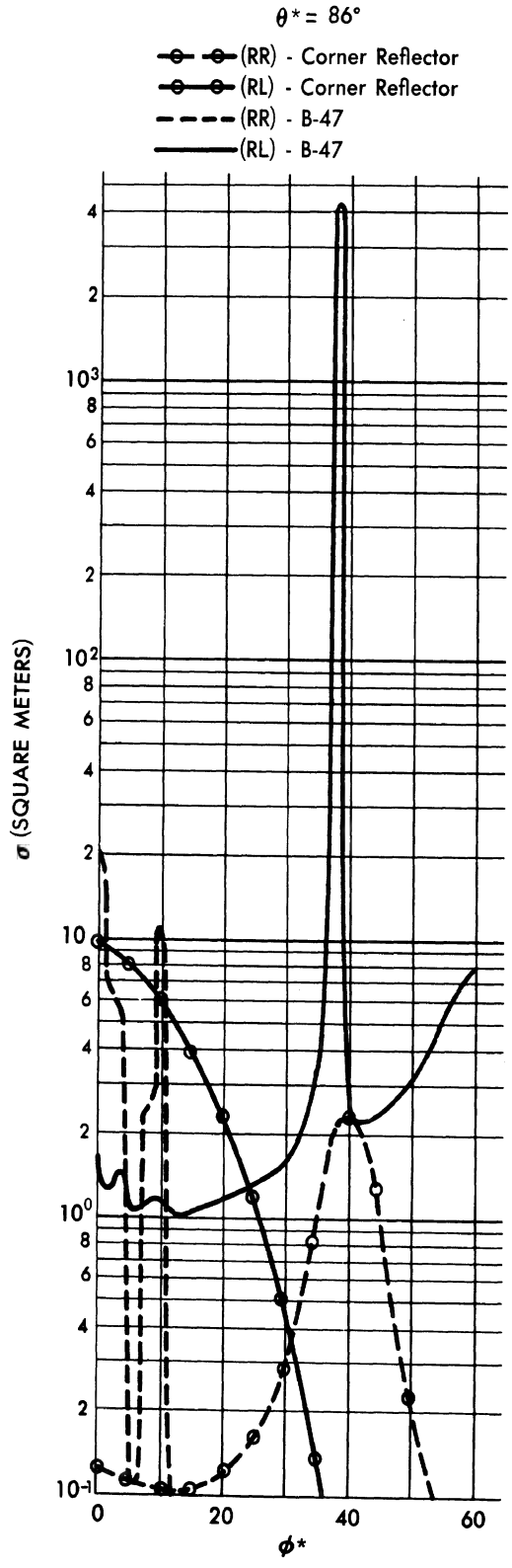

FIG. G-8 Circular Polarization

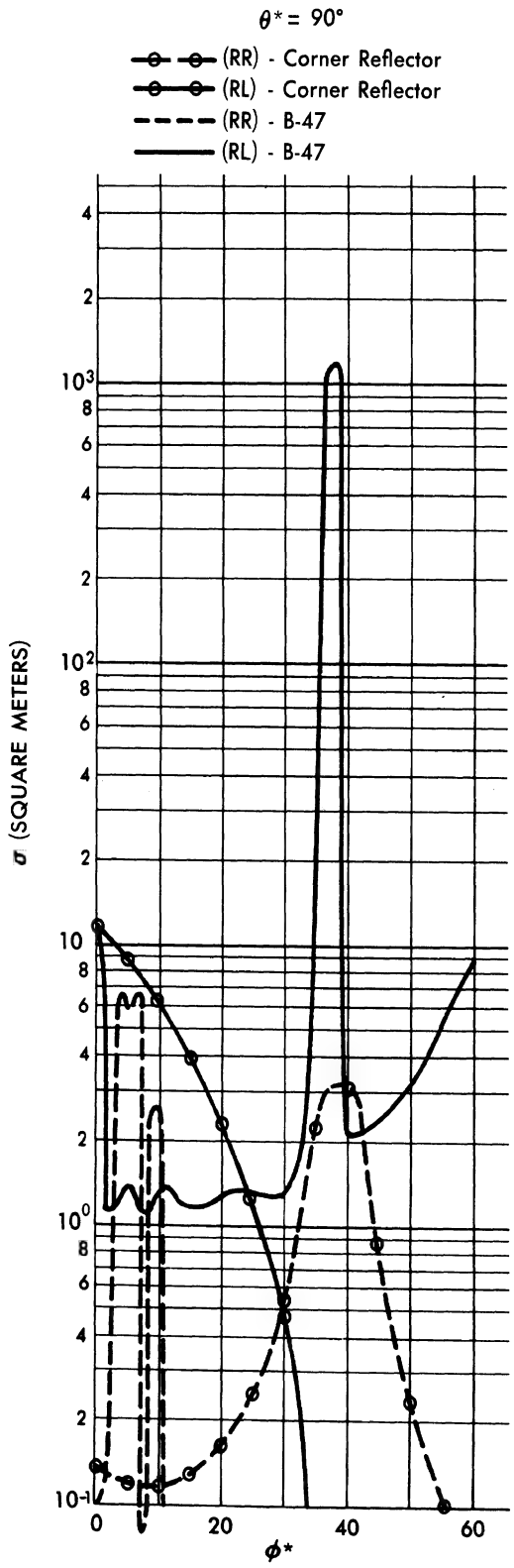

FIG. G-9 Circular Polarization

COMPARISON OF CROSS-SECTIONS OF THE
B-47 AND SQUARE CORNER REFLECTORS AT S-BAND

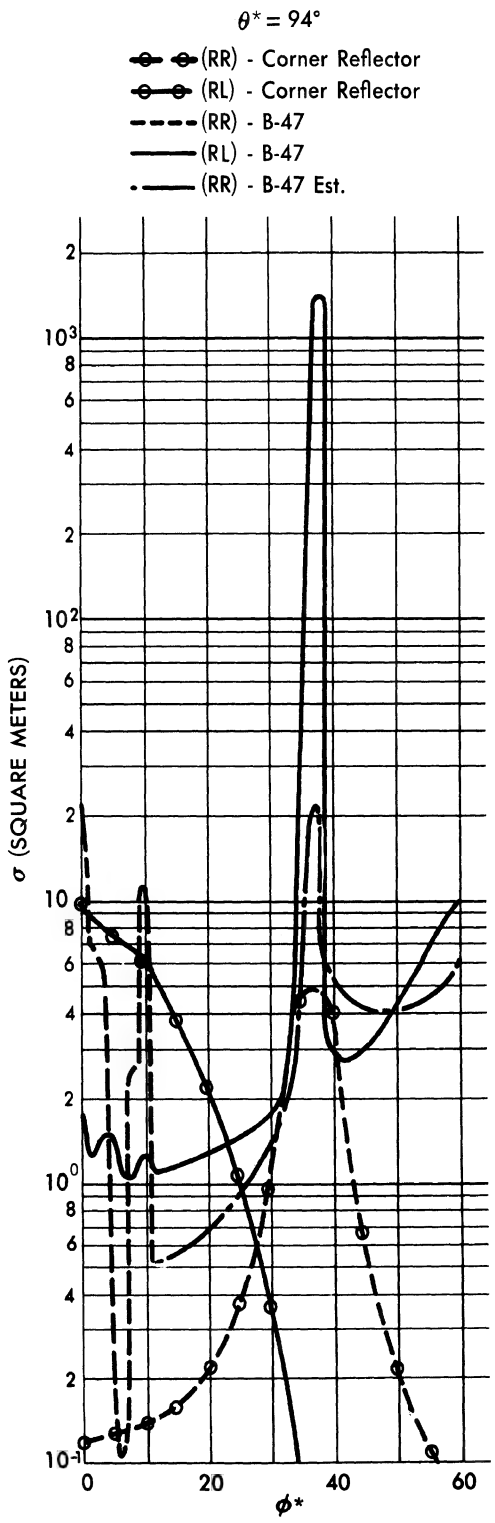

FIG. G-10

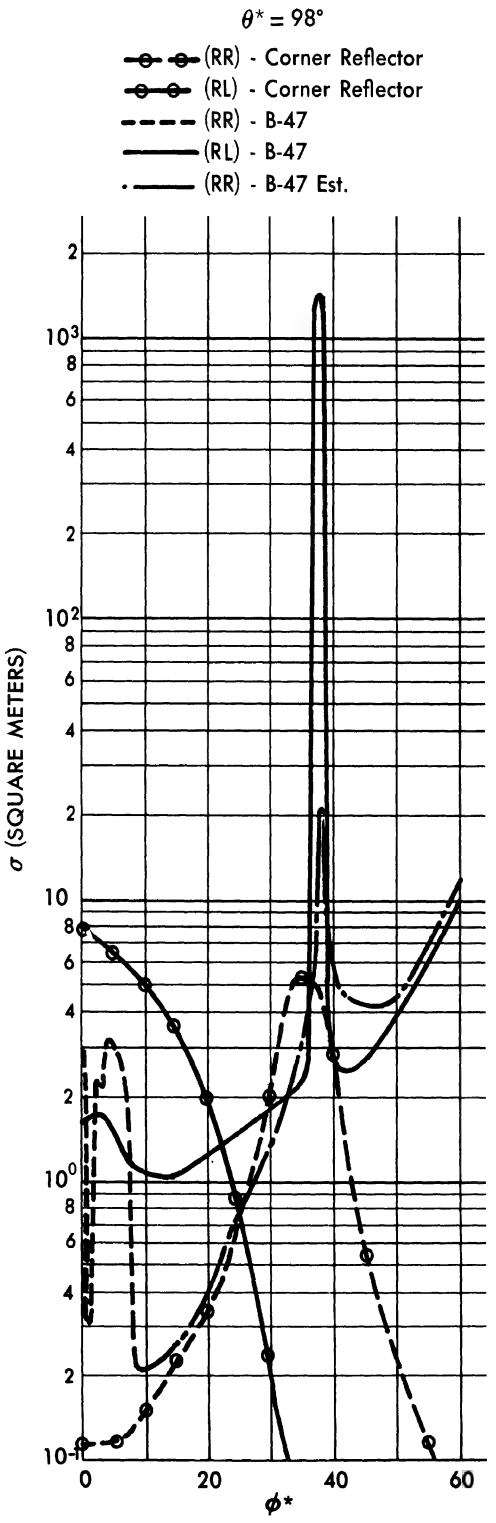

FIG. G-11

COMPARISON OF CROSS-SECTIONS OF THE B-47 AND SQUARE CORNER REFLECTORS AT S-BAND Circular Polarization

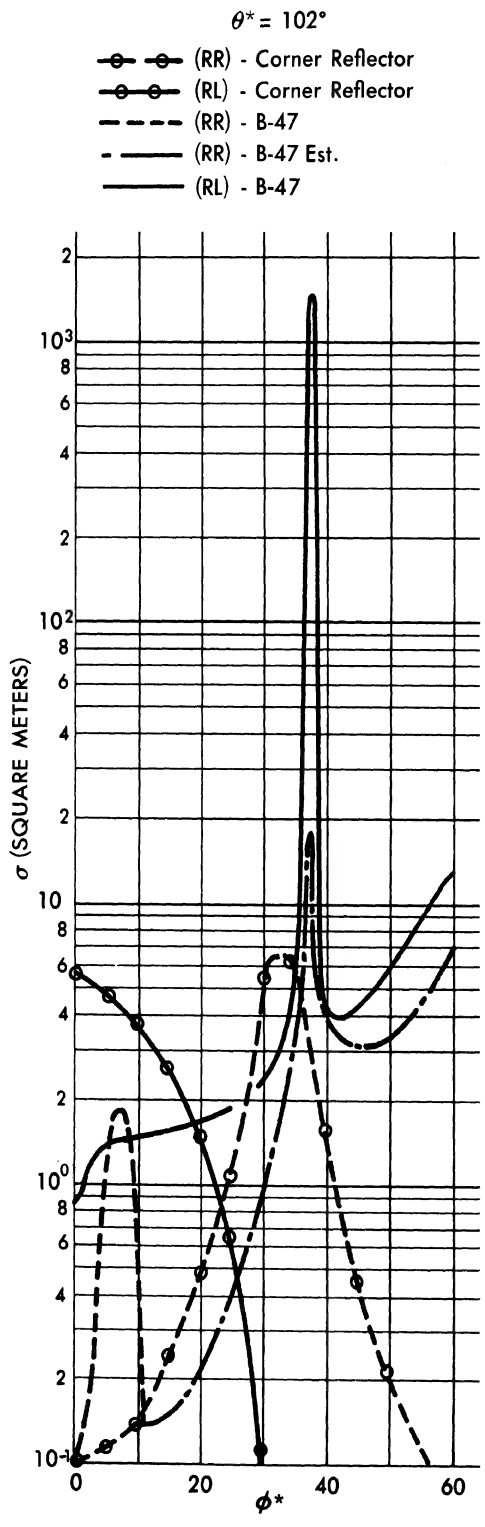

FIG. G-12

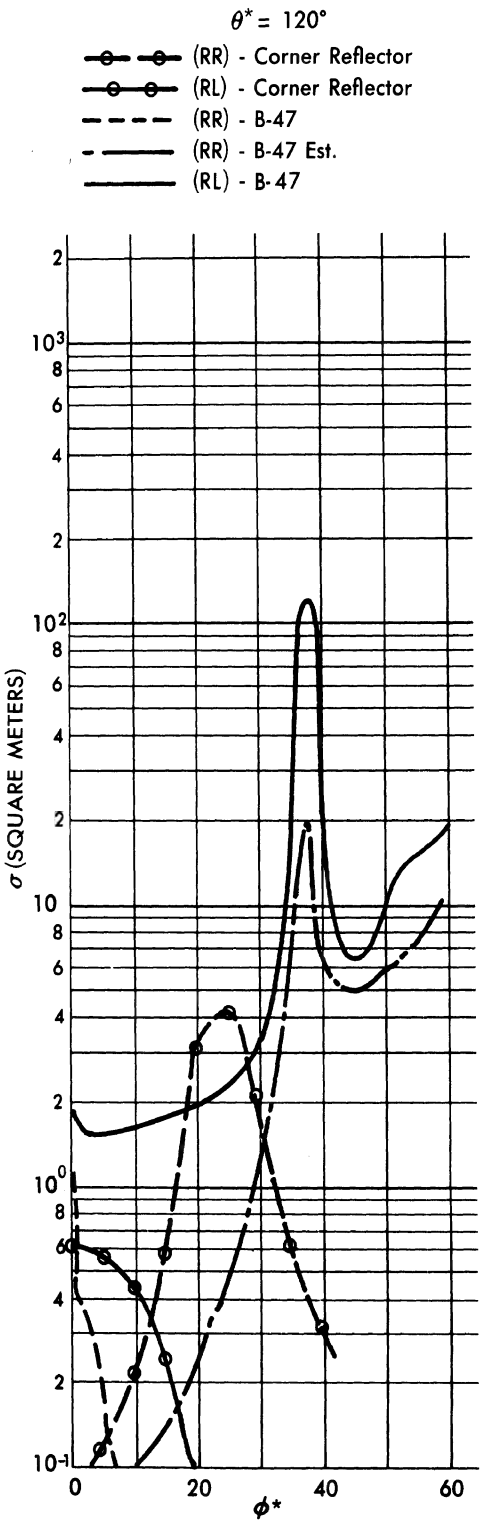

FIG. G-13

COMPARISON OF CROSS-SECTIONS OF THE B-47 AND SQUARE CORNER REFLECTORS AT S-BAND Circular Polarization

APPENDIX H

BISTATIC RADAR CROSS-SECTION OF THE B-47 AIRCRAFT AT S-BAND

The dimensions of the fuselage, nacelles, and wing tanks are such that geometrical optics gives a good estimate of their cross-section for many aspects. With the exception of their trailing edges, the wing and the horizontal and vertical tail are amenable to the physical optics approximation. The contributions from the trailing edge of the wing, horizontal and vertical tail, engine and wing-tank supports, and jet intake and exhaust can be better approximated by formulas based on thin-wire theory. The actual estimation of the radar cross-section is predicated upon the assumption that the aircraft may be replaced by a configuration of simple geometrical shapes with only a negligible change in cross-section. Two such substitute configurations may be found in Reference 2.

The geometric optics cross-sections, where applicable, were computed from the relation $\sigma = \pi R_1 R_2$ for all but the forward, and near-forward, scattering. In this formula, R_1 and R_2 represent the principle radii of curvature at the specular reflection point.

In particular, for the ogive the value of σ is given by

$$\sigma = \pi a^2 \left(1 - \frac{\cos\beta}{|\cos\eta|}\right),$$

where a is the radius of curvature of the generating arc, β is the half-angle corresponding to the generating arc, and η is the angle between the equatorial plane and the line OS to the specular reflection point as shown in Figure H-1. In terms of the incident and reflecting directions,

$$\cos\eta = \left[\frac{(\sin\theta_T + \sin\theta_R)^2 + (\cos\theta_T \sin\phi_T + \cos\theta_R \sin\phi_R)^2}{2\left[1 + \sin\theta_T \sin\theta_R + \cos\theta_T \cos\theta_R \cos(\phi_T - \phi_R)\right]}\right]^{\frac{1}{2}}$$

where the transmitter and receiver positions must be such that $1 \geq \cos\eta \geq \cos\beta$.

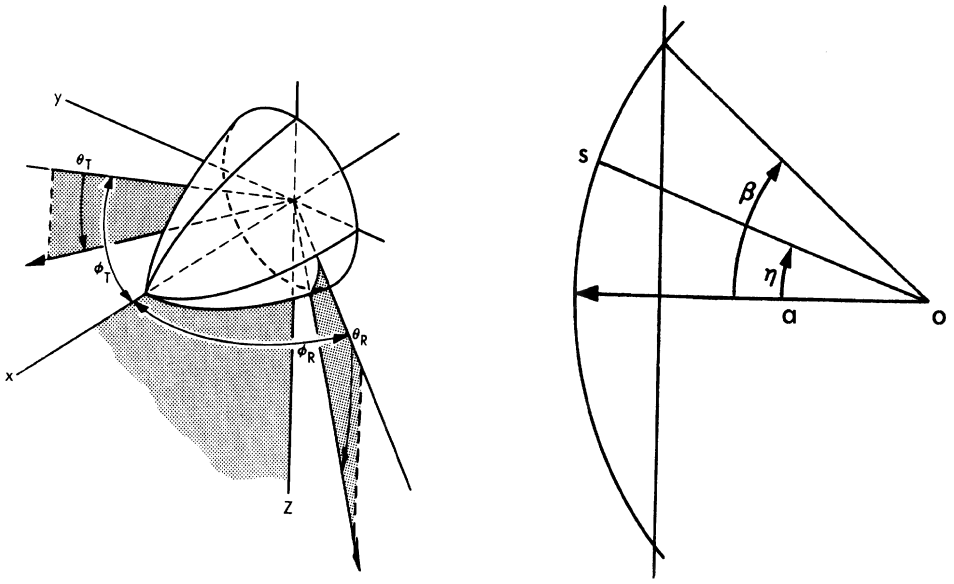

FIG. H-1 COORDINATE SYSTEM FOR THE OGIVE

The prolate spheroid cross-section is given by

$$\sigma = \pi a^2 \left[\frac{\eta^2 + \tan^2 \theta}{\eta^4 + \tan^2 \theta} \right]^2 \quad ; \quad \eta = a/b \ ,$$

where a is the semi-major axis and b the semi-minor axis. Again in terms of transmitter and receiver directions,

$$\tan^2 \theta = \eta^2 \frac{1 - \cos^2 \theta_A \cos^2 \phi_A}{\cos^2 \theta_A \cos^2 \phi_A} \quad , \text{ where}$$

$$\cos^2 \theta_A = \frac{2 \cos \theta_T \cos \theta_R \cos (\phi_R + \phi_T) + \cos^2 \theta_T + \cos^2 \theta_R}{2 \left[1 + \cos \theta_T \cos \theta_R \cos (\phi_T + \phi_R) + \sin \theta_T \sin \theta_R \right]}$$

$$\text{and} \quad \cos^2\phi_A = \frac{(\cos\theta_T \cos\phi_T + \cos\theta_R \cos\phi_R)^2}{2\cos\theta_T \cos\theta_R \cos(\phi_T+\phi_R) + \cos^2\theta_T + \cos^2\theta_R} \ .$$

In these expressions θ_R, ϕ_R, and θ_T, ϕ_T denote the receiver and transmitter directions respectively.

A physical-optics approximation to the cross-section of a truncated elliptic cone is given by

$$\sigma = \frac{\lambda L_2}{\pi} \frac{\tan^2\beta}{\tan\alpha} \frac{K^2(\hat{n}_o, \hat{k})}{\gamma^3(\gamma\tan\alpha+\nu)^2} \left\{ 1 + \frac{L_1}{L_2} + 2\sqrt{\frac{L_1}{L_2}} \cos\left[k(\gamma\tan\alpha+\nu)(L_2-L_1)\right] \right\} ,$$

where

$$\frac{x^2}{\tan^2\alpha} + \frac{y^2}{\tan^2\beta} = z^2$$

is the equation of the elliptic cone; $\hat{k}(\theta_T, \phi_T)$ and $\hat{n}_o(\theta_R, \phi_R)$ are unit vectors directed toward the transmitter and receiver respectively;

$$K(\hat{n}_o, \hat{k}) = \Big[(\gamma\tan\alpha+\nu)\sin(\phi_T+\delta) - \sin\theta_R \sin\theta_T - (1+\cos\theta_T\cos\theta_R)\cos(\phi_T-\phi_R) \Big] \ ;$$

$$\gamma = \left\{ \Big[\sin\theta_T \cos(\phi_T+\delta) + \sin\theta_R \cos(\phi_R+\delta) \Big]^2 + \frac{\tan^2\beta}{\tan^2\alpha} (\cos\theta_T + \cos\theta_R)^2 \right\}^{\frac{1}{2}} \ ;$$

$$\nu = \sin\theta_T \sin(\phi_T+\delta) + \sin\theta_R \sin(\phi_R+\delta) \ ;$$

δ is the angle between aircraft y-axis and wing-axis; and L_1 and L_2 are respectively the smaller and greater truncation distances measured from the tip of the full cone. The above is for the starboard wing. For the port wing, let $\delta \rightarrow \pi - \delta$. The port wing is in the positive y-direction.

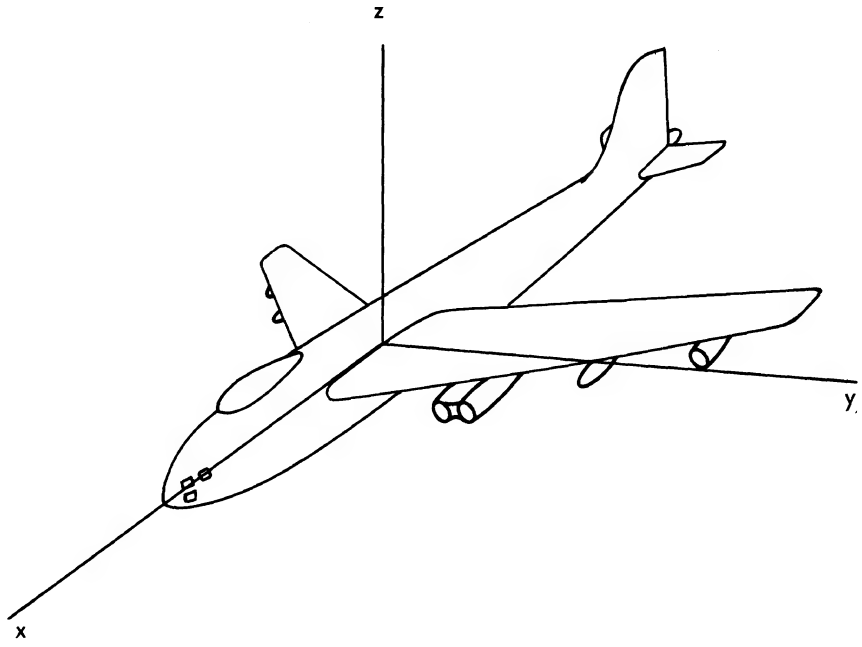

FIG. H-2 COORDINATE SYSTEM FOR THE B-47 AIRCRAFT

The cylinder cross-section was calculated from the formula (Ref. 34, p. 1381)

$$\sigma = \frac{2\pi L^2}{\lambda}\left\{ a \sin\left(\frac{\theta_T+\theta_R}{2}\right) + \frac{\lambda}{2\pi^2}\cot^2\left(\frac{\theta_R+\theta_T}{2}\right)\sin^2\left[ka\,(\theta_R+\theta_T)\right]\right\},$$

which is valid for the broadside case and which contains a forward scattering term, unlike the preceeding formulas (Fig. H-1). In fact the forward scattering term here and the forward scattering as given in the exact solution to the sphere problem were used to approximate the beam width of the forward lobe of similar geometrical shapes.

The straight thin wire cross-section was obtained from the current distribution suggested in Reference 31, that is,

$$I(z) = -\frac{i\omega E_o \cos\phi}{k^2 \Omega \sin\theta_T}\left[\frac{\cos q z \cos k\ell - \cos k z \cos q\ell}{\cos k\ell + \frac{i}{\Omega}A} + i\,\frac{\sin q z \sin k\ell - \sin k z \sin q\ell}{\sin k\ell + \frac{i}{\Omega}B}\right],$$

where $\Omega = 2\left[\ln\frac{2}{\gamma ka} + Ci(2k\ell)\right]$,

$\omega = kc$,

$k = 2\pi/\lambda$,

c = velocity of light,

$q = k\cos\theta_T$,

$$A = \zeta \cos k\ell + \frac{1}{\xi_1}\left\{ Cin(4k\ell)\cos^2 q\ell - \xi_2 \left[\frac{1+\cos^2\theta_T}{2\cos\theta_T} \cos^2 k\ell \cos 2q\ell + \frac{1}{2}\sin 2k\ell \sin 2q\ell \right] - \left[(1+\cos\theta_T)\sin^2 k\ell (1-\cos\theta_T) + (1+\cos\theta_T)\sin^2 k\ell (1+\cos\theta_T) \right] \cos^2 k\ell \right\},$$

$$\xi_1 = \sin^2\theta_T \left[k\ell + \frac{\sin 2q\ell}{2\cos\theta_T} \right] \cos k\ell - \left\{ (1+\cos\theta_T)\sin k\ell (1-\cos\theta_T) + (1-\cos\theta_T)\sin k\ell (1+\cos\theta_T) \right\} \cos q\ell ,$$

$$\xi_2 = \ln\left(\frac{(1+\cos\theta_T)}{(1-\cos\theta_T)} \right) - Ci\left[2k\ell (1+\cos\theta_T) \right] + Ci\left[2k\ell (1-\cos\theta_T) \right],$$

$$B = \zeta \sin k\ell + \frac{1}{\xi_3}\left\{ Cin(4k\ell)\sin^2 q\ell + \xi_2 \left[\frac{1+\cos^2\theta_T}{2\cos\theta_T} \sin^2 k\ell \cos 2q\ell - \frac{1}{2}\sin 2k\ell \sin 2q\ell \right] - \left[(1+\cos\theta_T)\sin^2 k\ell (1-\cos\theta_T) + (1-\cos\theta_T)\sin^2 k\ell (1+\cos\theta_T) \right] \sin^2 k\ell \right\},$$

$$\xi_3 = \sin^2\theta_T \left[k\ell - \frac{\sin 2q\ell}{2\cos\theta_T} \right] \sin k\ell - \left\{ (1+\cos\theta_T)\sin\left[k\ell (1-\cos\theta_T) \right] - (1-\cos\theta_T)\sin\left[k\ell (1+\cos\theta_T) \right] \right\} \sin q\ell ,$$

$$\zeta = \mathrm{Si}\left[2k\ell(1+\cos\theta_T)\right] + \mathrm{Si}\left[2k\ell(1-\cos\theta_T)\right] \quad ,$$

and a = radius of wire,

γ = 1.781072 (Euler's number),

2ℓ = length of the wire,

ϕ = angle between $|\bar{E}_o|$ and plane defined by the wire and the direction of incidence,

E_o = the incident electric field,

θ_T = angle defined by the wire and the direction of incidence,

θ_R = angle defined by the wire and the direction of reflection,

Si(x) and Ci(x) are the sine and cosine integrals, respectively, of x as defined in Jahnke and Emde (Ref. 32) and

$$\mathrm{Cin}(x) = \ln x + 0.577 - \mathrm{Ci}(x).$$

The scattered field is given by

$$E_s = \frac{ik\sin\theta_R}{cR}\int_{-\ell}^{\ell} I(z)\, e^{ikz\cos\theta_R}\, dz \quad ,$$

from which the value of σ is obtained through

$$\sigma = \lim_{R\to\infty} 4\pi R^2 \left|\frac{E_s}{E_o}\right|^2 \quad ;$$

that is, $$\sigma = \frac{4\lambda^2\cos^2\phi}{\pi\sin^2\theta_R\sin^2\theta_T}\left[\frac{\rho^2+\mu^2}{\Omega^2+B^2}\right] \quad ,$$

where,

$$\rho = \frac{\cos(k\ell\cos\theta_T)\cos(k\ell\cos\theta_R)}{A}\,\Omega\,,$$

$$\mu = \frac{1}{\cos^2\theta_T - \cos^2\theta_R}\left\{\cos\theta_T \sin^2\theta_R \cos(k\ell\cos\theta_T)\sin(k\ell\cos\theta_R) - \cos\theta_R \sin^2\theta_T \cos(k\ell\cos\theta_R)\sin(k\ell\cos\theta_T)\right\} - \frac{B\cos(k\ell\cos\theta_T)\cos(k\ell\cos\theta_R)}{A}\,,$$

which applies when $\theta_R \neq \theta_T$. For the case where $\theta_R = \theta_T = \theta$ the cross-section is given by

$$\sigma = \frac{4\pi\ell^2 \sin^2\theta \left(\frac{\sin k\ell}{k\ell}\right)^2}{(\pi/2)^2 + \left[\ln\left(\frac{\lambda}{\gamma\pi a \sin\theta}\right)\right]^2}\,.$$

In this report the average value of σ over the polarization angle is used, i.e.,

$$\frac{1}{2\pi}\int_0^{2\pi} \sigma\, d\phi\,.$$

The wire loop cross-section may be estimated as in Reference 2, ignoring the current induced in the wire by the scattered field from all other segments of the wire.

Consider the loop to lie in the xy-plane and the transmitter and

receiver directions to be indicated by the unit vectors $\hat{p}_T$ and $\hat{p}_R$ as shown in Figure H-3a. By rotating the coordinate system about the z-axis through the angle β given by

$$\cos\beta = \frac{\sin\theta_R + \sin\theta_T}{\sqrt{(\sin\theta_R + \sin\theta_T)^2 + (\cos\theta_R \sin\phi_R - \cos\theta_T \sin\phi_T)^2}}$$

we may express the scattered field by the integral

$$\bar{E}_s = A \int_0^{2\pi} \left[(\bar{p}_R \times \bar{t}) \times \bar{p}_R\right] (\bar{b} \cdot \bar{t})\, e^{(ika\,(\bar{p}_T + \bar{p}_R) \cdot \bar{r})}\, da\,,$$

where $\bar{b}$ is a unit vector in the direction of the incident electric vector, and $\bar{t} = d\bar{r}/da$, where $\bar{r}$ is a unit vector in the direction of the integration element, and a is measured as in Figure H-3a. The complex constant is easily evaluated by referring to Reference 2.

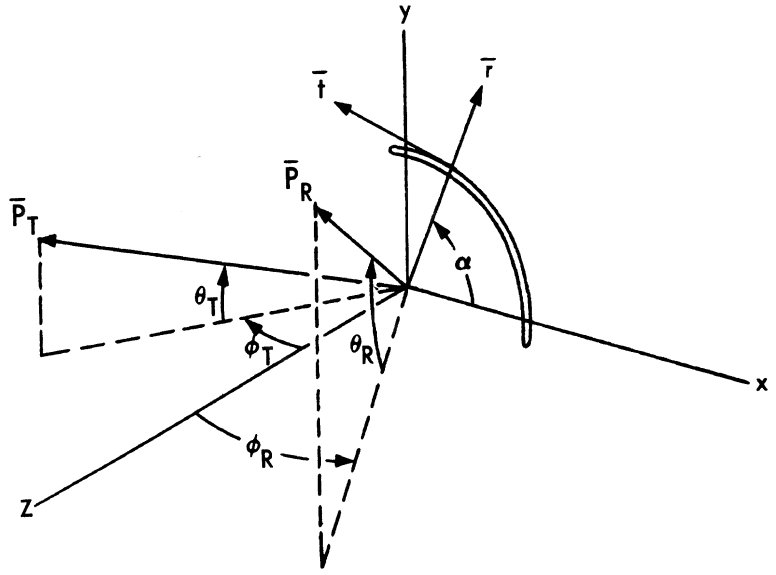

FIG. H-3a COORDINATE SYSTEM FOR THE LOOP

Carrying out the integration, one finds that

$$\sigma = \pi a^2 \left[C_1^2 + C_2^2 + C_3^2 \right] ,$$

where

$$C_1 = b_2\, p_1\, p_2 \left[J_o(\rho) + J_2(\rho) \right] - b_1 (1 - p_1^2) \left[J_o(\rho) - J_2(\rho) \right] ,$$

$$C_2 = b_1\, p_2\, p_1 \left[J_o(\rho) - J_2(\rho) \right] - b_2 (1 - p_2^2) \left[J_o(\rho) + J_2(\rho) \right] ,$$

$$C_3 = b_1\, p_1\, p_3 \left[J_o(\rho) - J_2(\rho) \right] + b_2\, p_2\, p_3 \left[J_o(\rho) + J_2(\rho) \right] ,$$

and

$$p_1 = \cos\theta_R \sin\phi_R \cos\beta - \sin\theta_R \sin\beta ,$$

$$p_2 = \cos\theta_R \sin\phi_R \sin\beta + \sin\theta_R \cos\beta ,$$

$$p_3 = \cos\theta_R \cos\phi_R ,$$

$$b_1 = \frac{1}{q} \left\{ \sin\gamma \cos\theta_T \cos\phi_T + \frac{1}{2} \cos\gamma \left[(\sin^2\theta_T \sin^2\phi_T - 2\cos 2\theta_T) \sin 2\beta + \cos 2\beta \sin 2\theta_T \sin\phi_T \right] \right\} ,$$

$$b_2 = q \cos\gamma$$

$$b_3 = \frac{1}{q} \left\{ \frac{1}{2} \cos\gamma \left(\sin 2\theta_T \cos\phi_T \cos\beta - \cos^2\theta_T \sin\beta \sin 2\phi_T \right) - \sin\gamma \left(\sin\theta_T \sin\beta + \cos\theta_T \cos\beta \sin\phi_T \right) \right\} ,$$

$$\rho = ka \left[(\cos\theta_R \sin\phi_R - \cos\theta_T \sin\phi_T) \sin\beta + (\sin\theta_R + \sin\theta_T) \cos\beta \right] ,$$

$$q^2 = 1 - (\sin\theta_T \cos\beta - \cos\theta_T \sin\beta \sin\phi_T)^2 .$$

This formula reduces to that of the monostatic case when $\phi_R = \phi_T = 0$, and $\theta_T = \theta_R = \theta$, since then $\cos\beta = 1$ and $q = \cos\theta$, to give $p_1 = 0$, $p_2 = \sin\theta$, $p_3 = \cos\theta$, $b_1 = \sin\gamma$, $b_2 = \cos\gamma\cos\theta$, $b_3 = \cos\gamma\sin\theta$.

Using $AA^* = a^2/4\pi^2 R^2$ (A^* is the complex conjugate of A) where a is the radius of the loop, and R the distance to the observation point, and the "effective radar cross-section" is proportional to $\overline{b} \cdot \overline{E_s}$, the formula of Reference 2 is obtained exactly.

As in the case of the straight wire, the average value of σ over the polarization angle is used.

Thus,

$$\sigma = \frac{a^2}{2}\int_0^{2\pi}\left[C_1^2 + C_2^2 + C_3^2\right] d\gamma$$

$$= \frac{\pi a^2}{2}\left\{\frac{q^2 + \frac{1}{4}f^2}{q^2}(1-p_1^2)(J_o - J_2)^2 + q^2(1-p_2)^2(J_o + J_2)^2 - f\,p_1\,p_2\,(J_o^2 - J_2^2)\right\},$$

where the quantities are defined as above, except for f and g, which are

$$f = (\sin^2\theta_T - \cos^2\theta_T \sin^2\phi_T)\sin 2\beta + \sin 2\theta_T \sin\phi_T \cos 2\beta ,$$

$$g = \cos\theta_T \cos\phi_T .$$

The forward scattering cross-section was computed from the relation

$$\sigma = \frac{4\pi A^2}{\lambda^2} ,$$

where A is the area projected upon a plane perpendicular to the direction of propagation. These areas were computed from the following formulas.

For ϕ = 0, 180 degrees the projected area of the airplane is given by

$$A' = \pi(2a_e^2 + a_f b_f + 2a_{de} b_{de} + 2a_p^2) + 2a_{1w}^2 \tan\eta_w \sin\psi_w + 3a_{1HT}^2 \tan\eta_{HT} \sin\psi_{HT},$$

where

a_f, b_f = semi-axes of fuselage ellipse ,

a_{de}, b_{de} = semi-axes of dual nacelles,

a_e = radius of single engine nacelle,

a_p = radius of fuel pod,

a_{1w}, a_{1HT} = "exposed" length of maximum-area plane (Fig. H-3b) of the wing and horizontal tail respectively,

η_w, η_{HT} = half angle of maximum-area plane of wing and horizontal tail respectively,

ψ_w, ψ_{HT} = sweep angle of maximum-area plane for wing and horizontal tail respectively.

(The "exposed" section of the maximum-area plane for the wing has the same projected area as the wing when the airplane is viewed nose-on.)

The projected area for aspects other than those above is the sum of the projected areas of the components given below.

The component cross-sections may be added directly, as pointed out in Reference 2, to obtain the total cross-section for the composite shape.

The formulas for the projected area of these components are given below.

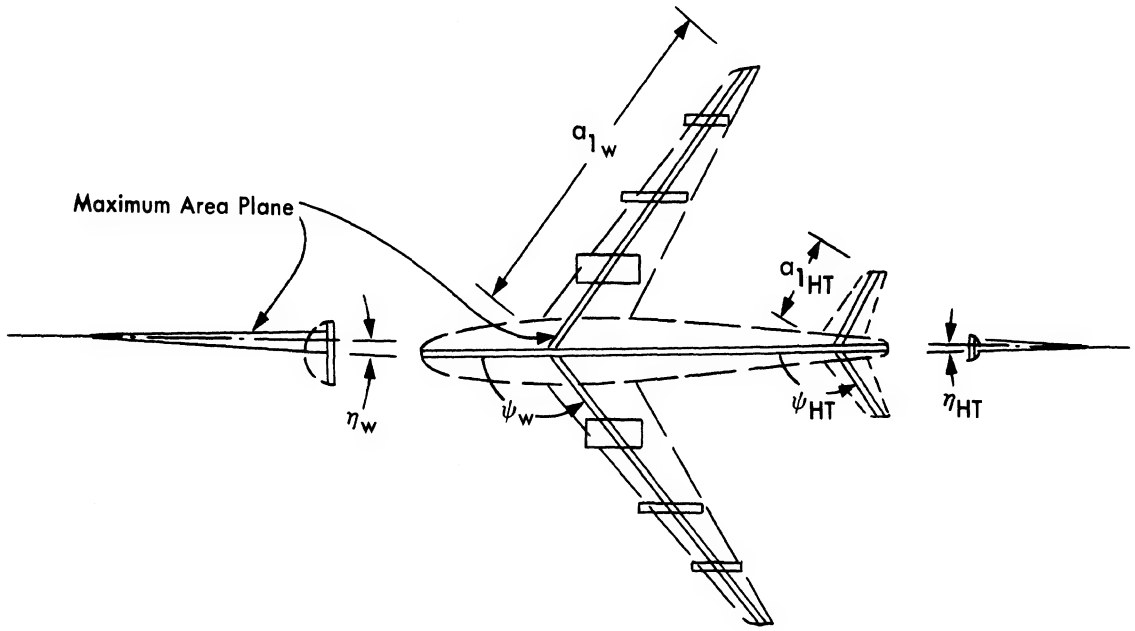

FIG. H - 3b DEFINITION OF PARAMETERS

Starboard wing, W_1

$$A'_{w_1} = \frac{\left[a_o \sin(\phi_T - \psi_w) - \ell_{1w} \sin\phi_T\right]^2}{\sin(\phi_T + \psi_w)} \tan\eta_w \quad (15^o \le \phi_T \le \phi_{T_1})$$

$$\frac{a_o}{\ell_1} = \frac{\sin\phi_{T_1}}{\sin(\phi_{T_1} + \psi_w)}$$

$$A'_{w_1} = -\frac{\left[a_o \sin(\psi_w + \phi_T) + \ell_{2w} \sin\phi_T\right]^2}{\sin(\psi_w + \phi_T)} \tan\eta_w \quad (\pi - \phi_{T_2} \le \phi \le 165^o)$$

$$\frac{a_o}{\ell_2} = \frac{\sin\phi_{T_2}}{\sin(\psi_w - \phi_{T_2})} \quad .$$

Port wing, W_2

$$A'_{w_2} = \frac{\left[a_o \sin(\psi_w - \phi_T) - \ell_{2_w} \sin\phi_T\right]^2}{\sin(\psi_w - \phi_T)} \tan\eta_w \quad (15^o \le \phi_T \le \phi_{T_2}) \, .$$

$$A'_{w_2} = \frac{\left[a_o \sin(\phi_T - \psi_w) - \ell_{1_w} \sin\phi_T\right]^2}{\sin(\phi_T - \psi_w)} \tan\eta_w \quad (\pi - \phi_{T_1} \le \phi_T \le 165^o) \, .$$

Port and starboard horizontal tail projected areas are given by these formulas after replacing ψ_w, ℓ_1, ℓ_2 and η_w by their counterparts.

The fuselage and vertical tail projected area is: $A'_{f+vt} = A_{f+vt} \sin\phi_T$. The formula for the engine supports is of the same form, namely,

$$A'_{es} = A_{es} \sin\phi_T \, . \qquad \text{(H. 1-1)}$$

By modeling the fuel pods and engine nacelles with cylinders, we may approximate their projected areas by

$$A'_e = 2\,RL \sin\phi_T + \pi R^2 \left|\cos\phi_T\right| . \qquad \text{(H. 1-2)}$$

The constants are given below:

$\ell_{1w} = 27$ ft.

$\ell_{2w} = 65$ ft.

$\eta_w = 2^o$

$\psi_w = 125^o$

$a_e = 1.75$ ft.

$a_f, b_f = (5.5)(5)$ ft.^{2}

$a_{de}, b_{de} = (4)(2)$ ft.^{2}

$a_p = 2.5$ ft.

$a_{1_w} = 66$ ft.

$A_{f+vt} = 1122$ ft.^{2}

$\ell_{1_{HT}} = 3$ ft.

$\ell_{2_{HT}} = 3$ ft.

$\eta_{HT} = 2^o$

$\psi_{HT} = 121^o$

$a_{o_w} = 66$ ft.

$a_{o_{HT}} = 19$ ft.

$a_{1_{HT}} = 17.5$ ft.

$L_p = 20$ ft.

$L_e = 13$ ft.

$R_p = 2$ ft.

$R_e = 1.75$ ft.

Equation (H. 1-1) is to be used as follows:

For

$\phi_T = 15^o$, $A'_{es} = (26 + 16) \sin 15^o$;

$\phi_T = 30^o$, $A'_{es} = (16) \sin 30^o$;

$\phi_T = 150^o$, $A'_{es} = (16) \sin 30^o$;

$\phi_T = 165^o$, $A'_{es} = (42) \sin 15^o$;

Equation (H. 1-2) should be applied to the two engine nacelles (the dual and the single) and one fuel pod at $\phi_T = 15^o$; to the fuel pod and single nacelle at 30^o; to the single nacelle at 135^o; to the single nacelle and fuel pod at 150^o; and to two engine nacelles and one fuel pod at 165^o (same as 15^o).

The total area A appearing in the cross-section formula is simply the sum of the projected areas corresponding to the particular aspect.

In adding the component cross-section to obtain the total, the effects of "shadowing" of some components by others were considered in a manner similar to that of Reference 2.

Approximate values of σ were computed for the transmitter in the lower port quadrants and the receiver in the lower starboard quadrants. Transmitter and receiver positions, denoted by (θ_T, ϕ_T) and (θ_R, ϕ_R), were chosen such that θ_T and θ_R ranged from 0 to $\pi/2$ in 15 degree intervals and ϕ_T and ϕ_R ranged from 0 to π in 15 degree intervals; the angle measured as in Figure H-3a (Fig. H-3a is drawn after a rotation of π radians about the z-axis).

For each transmitter position the estimated σ is presented in Tables H-1 through H-7. A graphical representation of σ vs. ϕ_T and ϕ_R for $\theta_T = \theta_R = 15^o$ is given in Figure H-4.

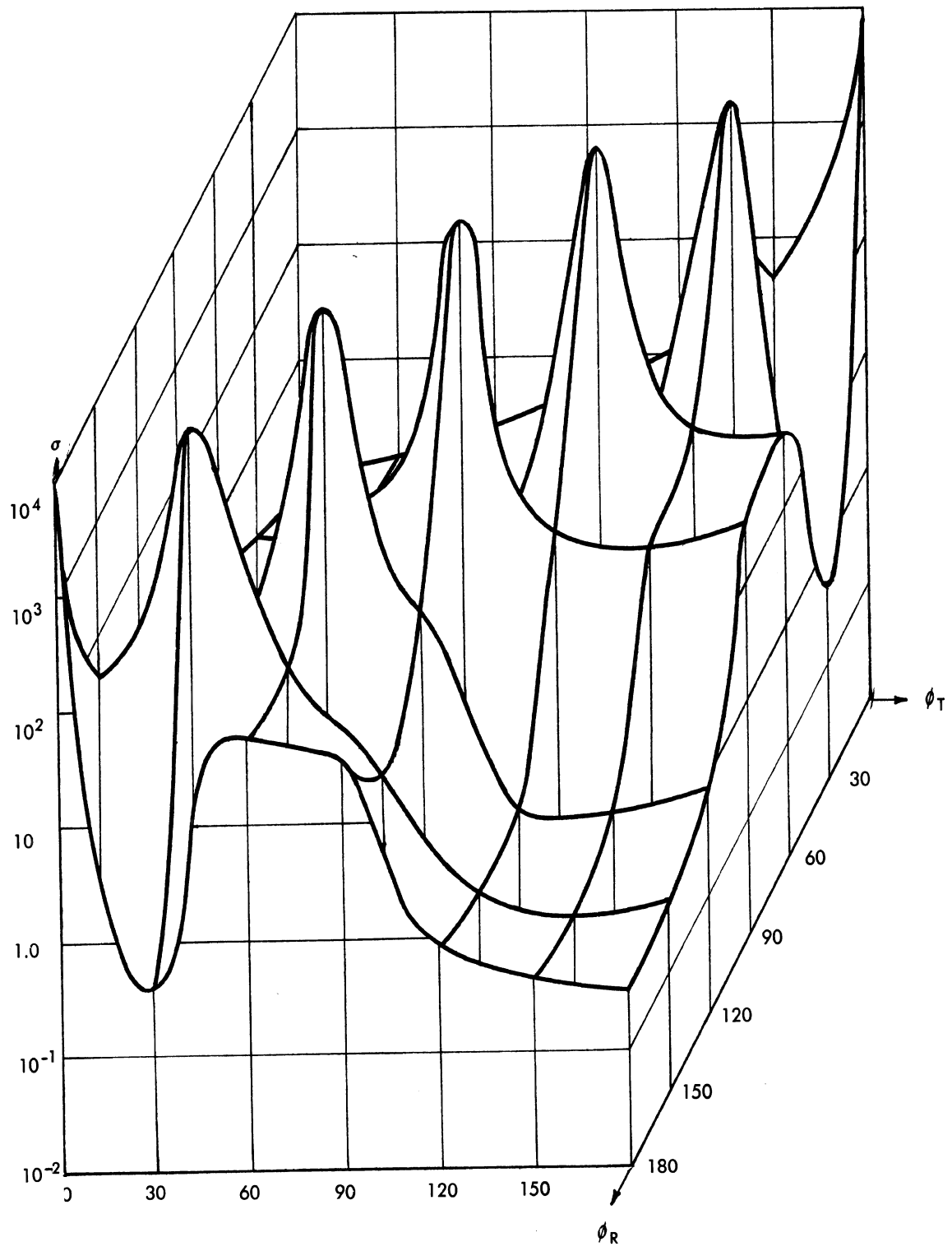

FIG. H-4 BISTATIC RADAR CROSS-SECTION (σ IN m^2) FOR THE B-47 AIRCRAFT FOR $\theta_T = \theta_R = 15°$

θ_R	ϕ_R	ϕ_T=0°	ϕ_T=15°	ϕ_T=30°	ϕ_T=45°	ϕ_T=60°	ϕ_T=75°	ϕ_T=90°	ϕ_T=105°	ϕ_T=120°	ϕ_T=135°	ϕ_T=150°	ϕ_T=165°	ϕ_T=180°
0	0	3.84, 0												
0	15	9.84,-1	9.15,-1											
0	30	1.40, 0	9.81,-1	7.40,-1										
0	45	2.15, 0	1.27, 0	8.30,-1	3.70,-1									
0	60	3.60, 0	1.58, 0	1.39, 0	5.10,-1	5.42,-1								
0	75	8.60, 0	2.63, 0	2.70, 0	2.30, 0	1.70,-1	1.70,-1							
0	90	5.30, 0	1.01, 1	3.40, 0	9.10,-1	1.80,-1	1.70,-1	1.38, 7						
0	105	8.00, 0	5.34, 0	3.29, 0	1.60, 0	2.30,-1	1.29, 7	2.55,-1	2.31,-1					
0	120	1.00, 1	7.41, 0	4.62, 0	4.00,-1	1.04, 7	4.79,-1	3.33,-1	2.55,-1	2.31,-1				
0	135	1.60, 1	1.05, 1	6.17, 0	7.23, 6	1.03, 0	7.08,-1	4.79,-1	3.33,-1	2.55,-1	2.31,-1			
0	150	3.30, 1	1.75, 1	5.65, 6	1.93, 0	1.44, 0	1.03, 0	7.08,-1	4.79,-1	3.33,-1	2.55,-1	2.31,-1		
0	165	7.50, 1	3.21, 5	2.93, 0	2.44, 0	1.93, 0	1.44, 0	1.03, 0	7.08,-1	4.79,-1	3.33,-1	2.55,-1	2.31,-1	
0	180	2.41, 6	4.85,-1	3.34, 0	2.93, 0	2.44, 0	1.93, 0	1.44, 0	1.03, 0	7.09,-1	4.79,-1	3.33,-1	2.55,-1	2.31,-1
15	0	9.80,-1	9.00,-2	1.60, 0	1.40, 0	1.63, 0	3.57, 0	7.12,-1	1.30, 0	3.30, 0	2.80, 2	3.42, 2	2.38, 3	2.18, 2
15	15	1.08, 0	1.01, 0	1.02, 0	1.70, 0	1.15, 0	1.73, 0	1.44, 0	8.60,-1	1.80, 0	5.70, 0	5.60, 1	9.93, 3	9.28,-1
15	30	1.36, 0	1.10, 0	9.20,-1	6.70,-1	8.60,-1	1.26, 0	6.40,-1	6.45,-1	1.32, 0	8.30, 0	1.81, 4	5.86,-2	4.03,-2
15	45	1.80, 0	1.36, 0	1.09, 0	5.70,-1	7.30,-1	1.02, 0	4.25,-1	1.97, 0	2.90, 0	4.90, 2	7.70,-3	3.10,-3	5.90,-3
15	60	2.70, 0	1.87, 0	1.70, 0	9.00,-1	7.20,-1	9.70,-1	4.52,-1	1.48, 0	4.87, 2	1.20,-3	3.71,-1	6.60,-4	4.00,-4
15	75	3.47, 0	2.70, 0	3.00, 0	1.40, 0	8.90,-1	1.28, 0	1.06, 0	4.46, 2	3.74,-1	2.00,-4	2.00,-4	3.00,-4	3.00,-4
15	90	5.30, 0	2.81, 1	4.30, 0	2.00, 0	1.38, 0	3.32, 0	1.79, 3	1.98, 0	6.80,-1	6.17,-1	7.69,-1	1.24, 1	3.33, 1
15	105	7.50, 0	5.40, 0	3.61, 0	2.90,-1	8.30,-1	3.66, 2	8.36,-1	6.43,-1	4.15,-1	4.16,-1	5.26,-1	7.34,-1	1.17, 1
15	120	1.00, 1	6.40, 0	5.20, 0	1.11, 0	5.13, 2	1.59, 0	6.81,-2	4.57,-1	3.31,-1	3.15,-1	3.73,-1	5.07,-1	7.29,-1
15	135	1.50, 1	1.14, 1	7.90, 0	4.63, 3	4.43, 0	1.52,-1	1.73,-2	4.72,-1	3.33,-1	2.80,-1	2.90,-1	3.61,-1	5.03,-1
15	150	2.60, 1	2.60, 1	1.74, 3	4.83, 0	7.01,-1	5.19,-2	7.50,-3	5.93,-1	4.03,-1	3.01,-1	2.64,-1	2.82,-1	3.58,-1
15	165	4.40, 1	4.30, 2	5.64, 0	8.86,-2	6.33,-1	3.61,-2	4.90,-3	8.08,-1	5.45,-1	3.78,-1	2.88,-1	2.51,-1	2.80,-1
15	180	2.62, 2	1.85, 3	6.81,-2	2.87,-2	4.08,-2	7.24,-2	4.70,-3	1.12, 0	7.71,-1	5.24,-1	3.66,-1	2.82,-1	2.55,-1
30	0	1.27, 0	1.38, 0	2.80, 0	1.37, 0	2.10, 0	3.17, 0	1.14, 0	2.78, 0	9.00, 0	3.58, 2	3.50, 3	3.04, 2	2.82, 2
30	15	1.35, 0	1.30, 0	2.00, 0	1.03, 0	1.64, 0	2.97, 0	8.80,-1	1.76, 0	6.51, 0	5.60, 1	3.28, 2	7.11, 1	7.82,-1
30	30	1.62, 0	1.39, 0	1.60, 0	9.90,-1	1.28, 0	2.10, 0	2.74, 0	1.63, 0	8.32, 0	2.11, 2	3.06, 3	3.63,-2	2.80,-3
30	45	2.10, 0	1.66, 0	2.30, 0	9.40,-1	1.17, 0	1.19, 0	9.70,-1	2.55, 0	4.72, 1	9.04, 1	3.20,-3	4.50,-3	5.00,-4
30	60	2.90, 0	2.16, 0	3.00, 0	1.13, 0	1.40, 0	2.25, 0	1.17, 0	3.20, 1	6.35, 1	1.1-,-3	4.00,-4	2.00,-4	1.00,-3
30	75	4.50, 0	1.98, 0	3.60, 0	1.38, 0	1.85, 0	3.28, 0	2.56, 2	4.55, 1	1.57, 0	7.00,-4	1.00,-4	3.00,-4	1.00,-4
30	90	5.50, 0	2.17, 0	3.00, 0	1.98, 0	3.04, 0	8.30, 0	2.78, 3	5.03, 0	3.34, 1	7.29, 0	3.35, 0	1.66, 1	3.33, 1
30	105	7.00, 0	8.20, 0	4.30, 0	6.80,-1	2.90, 0	2.37, 2	5.23, 0	1.71, 0	9.08,-1	6.72,-1	6.70,-1	8.13,-1	1.44, 1
30	120	9.30, 0	7.40, 0	6.10, 0	2.80, 0	1.33, 2	1.31, 1	3.38,-1	1.09, 0	6.67,-1	5.11,-1	4.99,-1	5.93,-1	7.91,-1
30	135	1.41, 1	1.06, 1	8.90, 0	1.50, 2	7.56, 1	1.34, 0	7.54,-2	9.26,-1	5.98,-1	4.46,-1	4.04,-1	4.48,-1	5.78,-1
30	150	2.15, 1	6.70, 0	1.51, 2	1.14, 0	2.93, 0	4.20,-1	3.13,-2	9.58,-1	6.34,-1	4.52,-1	3.71,-1	3.67,-1	4.37,-1
30	165	3.63, 1	6.40, 1	2.30, 2	7.72,-2	5.14,-1	3.40,-1	2.09,-2	1.12, 0	7.58,-1	5.24,-1	3.93,-1	3.41,-1	3.58,-1
30	180	4.85, 1	7.21, 1	3.18, 3	4.00,-4	1.12,-2	2.50,-1	2.37,-2	1.39, 0	5.86, 0	6.66,-1	4.72,-1	3.66,-1	3.33,-1
45	0	1.77, 0	1.92, 0	3.70, 0	1.96, 0	7.35, 0	3.94, 0	2.50, 0	8.50, 0	5.50, 1	5.62, 3	3.02, 2	2.60, 2	2.37, 2
45	15	1.85, 0	1.84, 0	3.30, 0	1.64, 0	2.48, 0	3.84, 0	1.91, 0	6.90, 0	5.50, 1	3.34, 2	8.70,-2	3.02,-2	1.40,-3
45	30	2.11, 0	1.94, 0	3.30, 0	1.50, 0	1.65, 0	4.78, 0	1.80, 0	8.43, 0	1.10, 2	3.26, 2	6.06,-2	1.00,-3	8.50,-3
45	45	2.57, 0	2.91, 0	3.00, 0	1.50, 0	2.15, 0	3.80, 0	2.51, 0	1.82, 1	4.90, 3	5.12,-2	1.90,-3	9.00,-4	1.60,-3
45	60	3.25, 0	3.99, 0	4.50, 0	1.74, 0	2.53, 0	4.13, 0	5.50, 0	1.31, 2	2.18, 1	1.00,-3	1.20,-3	4.63, 1	1.20,-3
45	75	4.19, 0	6.90, 0	2.90, 0	2.12, 0	3.28, 0	7.60, 0	3.19, 1	1.07, 1	2.84, 0	5.00,-4	5.00,-4	1.00,-4	5.00,-4
45	90	7.26, 0	4.90, 0	3.80, 0	3.00, 0	5.50, 0	2.00, 1	4.05, 3	1.13, 1	5.36, 1	3.33, 1	2.06, 1	2.22, 1	3.33, 1
45	105	6.92, 0	7.90, 0	5.00, 0	1.25, 0	9.40, 0	1.73, 2	1.29, 1	3.22, 0	3.78, 1	1.43, 1	9.06,-1	3.69, 0	1.84, 1
45	120	7.04, 0	6.10, 0	6.60, 0	4.70, 0	5.20, 1	4.00, 0	3.25, 0	2.06, 0	2.35, 1	8.65,-1	7.23,-1	7.43,-1	9.00,-1
45	135	1.06, 1	7.80, 0	8.70, 0	2.80, 1	4.90, 3	4.17, 0	7.42,-1	1.69, 0	1.44, 1	7.61,-1	6.17,-1	6.05,-1	7.08,-1
45	150	1.38, 1	1.00, 1	3.07, 1	7.25, 1	4.92,-1	2.18, 0	3.09,-1	1.59, 0	1.31, 1	7.43,-1	5.75,-1	5.26,-1	5.78,-1
45	165	2.10, 1	1.64, 1	6.20, 1	3.00, 2	1.18,-1	7.23,-1	2.24,-1	1.66, 0	1.84, 1	7.98,-1	5.92,-1	5.00,-1	5.03,-1
45	180	9.91, 0	1.77, 1	6.00, 1	5.30, 3	1.15,-2	9.73,-2	2.44,-1	1.84, 0	2.76, 1	2.03, 0	6.66,-1	5.24,-1	4.79,-1
60	0	2.57, 0	4.00, 0	3.12, 0	2.73, 0	4.00, 0	6.30, 0	8.20, 0	5.50, 1	6.46, 3	3.02, 2	2.52, 2	2.04, 2	1.84, 2
60	15	2.63, 0	3.50, 0	3.46, 0	2.46, 0	1.31, 2	5.10, 0	7.30, 0	5.50, 1	1.92,-1	7.37,-1	2.50,-3	4.20,-3	2.00,-4
60	30	2.85, 0	4.30, 0	3.80, 0	2.35, 0	3.84, 0	5.10, 0	8.00, 0	8.61, 1	7.02,-1	1.17,-2	5.00,-3	2.00,-4	1.90,-3
60	45	3.22, 0	3.70, 0	3.00, 0	2.57, 0	3.90, 0	6.50, 0	1.28, 1	1.85, 2	3.28, 0	2.70,-2	5.00,-4	1.40,-3	5.11, 1
60	60	3.75, 0	4.07, 0	3.40, 0	2.72, 0	4.13, 0	8.50, 0	2.92, 1	9.80,-1	1.15, 1	2.90,-3	1.40,-3	2.00,-4	8.00,-4
60	75	4.42, 0	5.50, 0	3.90, 0	3.17, 0	5.70, 0	1.25, 1	1.21, 2	3.65, 0	5.03, 0	1.00,-4	4.00,-4	3.62, 1	4.00,-4
60	90	5.25, 0	4.20, 0	4.60, 0	5.00, 0	1.17, 2	3.00, 1	5.30, 3	1.26, 1	6.27, 1	4.70, 1	3.33, 1	2.80, 1	3.33, 1
60	105	6.16, 0	5.00, 0	5.60, 0	2.60, 0	9.50, 0	1.16, 2	2.31, 0	7.94, 0	5.50, 1	3.78, 1	2.25, 1	1.68, 1	2.33, 1
60	120	7.17, 0	5.90, 0	6.70, 0	6.60, 0	2.56, 1	3.23, 2	3.57, 0	4.10, 0	4.83, 1	2.95, 1	1.22, 1	5.03, 0	1.17, 1
60	135	8.48, 0	6.90, 0	8.00, 0	1.06, 1	9.31, 1	5.70,-1	3.18, 0	2.96, 0	4.36, 1	2.36, 1	4.07, 0	8.44,-1	9.00,-1
60	150	9.60, 0	7.90,-0	1.23, 1	1.59, 1	2.40, 2	3.46,-1	1.85, 0	2.58, 0	4.16, 1	2.14, 1	9.02,-1	7.75,-1	7.91,-1
60	165	1.07, 1	8.00, 0	1.28, 1	2.51, 1	3.21, 2	1.35,-1	8.21,-1	2.49, 0	4.25, 1	2.30, 1	9.09,-1	7.51,-1	7.29,-1
60	180	1.91, 0	6.02, 0	9.40, 0	6.00, 1	6.46, 3	3.17,-2	2.24,-1	2.55, 0	4.56, 1	2.76, 1	5.86, 0	7.71,-1	7.08,-1
75	0	3.74, 0	3.60, 0	4.50, 0	4.40, 1	6.40, 0	1.32, 1	5.50, 1	6.82, 3	4.39,-1	2.50, 2	1.90, 2	1.47, 2	1.31, 2
75	15	3.36, 0	3.55, 0	4.40, 0	3.90, 0	6.30, 0	1.30, 1	5.50, 1	9.35,-2	1.17, 0	1.50,-3	1.90,-3	4.65,-2	8.00,-4
75	30	3.89, 0	3.64, 0	4.40, 0	3.89, 0	5.30, 0	1.34, 1	6.58, 1	2.03,-1	2.26, 0	1.13,-2	1.40,-3	8.00,-4	3.00,-4
75	45	4.12, 0	3.66, 0	4.50, 0	3.99, 0	6.60, 0	1.40, 1	9.11, 1	4.21,-1	5.02, 0	6.30,-3	3.00,-4	7.00,-4	5.43, 1
75	60	4.41, 0	3.96, 0	4.70, 0	4.10, 0	7.00, 0	1.80, 1	1.59, 2	8.30,-1	8.00, 0	1.00,-3	1.00,-4	2.00,-4	2.00,-4
75	75	4.89, 0	4.26, 0	5.00, 0	4.20, 0	7.70, 0	2.70, 1	2.57, 2	9.59, 0	7.25, 0	1.30,-3	7.00,-4	1.00,-4	3.00,-4
75	90	5.23, 0	4.63, 0	5.40, 0	5.60, 0	1.04, 1	4.60, 1	6.45, 3	6.12, 0	6.99, 1	5.47, 1	4.21, 1	3.33, 1	3.33, 1
75	105	5.68, 0	5.05, 0	6.00, 0	2.01, 1	8.40, 0	7.72, 1	4.99,-1	6.99, 0	6.52, 1	5.13, 1	3.78, 1	2.84, 1	2.84, 1
75	120	6.18, 0	5.52, 0	6.50, 0	6.80, 0	1.35, 1	1.55, 2	5.23,-1	6.79, 0	6.20, 1	4.82, 1	3.39, 1	2.37, 1	2.33, 1
75	135	7.65, 0	6.00, 0	7.30, 0	4.87, 0	2.31, 1	3.35, 2	4.45,-1	5.83, 0	5.98, 1	4.60, 1	3.10, 1	1.98, 1	1.84, 1
75	150	7.10, 0	6.46, 0	6.87, 0	5.62, 0	3.41, 1	3.00, 2	1.77, 0	4.74, 0	5.86, 1	4.49, 1	2.95, 1	1.71, 1	1.44, 1
75	165	7.36, 0	6.17, 0	2.30, 1	7.13, 0	4.80, 1	3.22, 2	4.13,-1	3.88, 0	5.84, 1	4.50, 1	2.94, 1	1.61, 1	1.17, 1
75	180	1.40, 0	3.20, 0	6.20, 0	8.14, 0	6.20, 1	6.82, 3	1.89,-1	3.37, 0	5.91, 1	4.62, 1	3.09, 1	1.68, 1	1.08, 1
90	all	5.20, 0	5.10, 0	6.00, 0	6.30, 0	1.34, 1	6.30, 1	7.50, 3	1.84, 0	7.11, 1	5.70, 1	4.63, 1	3.62, 1	3.19, 1

BISTATIC CROSS-SECTION (σ IN m^2) FOR THE B-47 AIRCRAFT

(The numbers following comma indicate multiplication by that power of 10)

θ_T = 0°

TABLE H - 2

θ_R	ϕ_R	ϕ_T=0°	ϕ_T=15°	ϕ_T=30°	ϕ_T=45°	ϕ_T=60°	ϕ_T=75°	ϕ_T=90°	ϕ_T=105°	ϕ_T=120°	ϕ_T=135°	ϕ_T=150°	ϕ_T=165°	ϕ_T=180°
15	0	1.26, 0												
15	15	1.36, 0	1.28, 0											
15	30	1.58, 0	1.41, 0	1.39, 0										
15	45	2.26, 0	1.80, 0	1.56, 0	1.62, 0									
15	60	3.24, 0	2.48, 0	2.04, 0	2.04, 0	2.37, 0								
15	75	9.77, 0	3.47, 0	2.91, 0	2.30, 0	3.47, 0	5.63, 0							
15	90	5.76, 0	1.09, 1	7.26, 0	4.36, 0	6.73, 0	1.40, 1	1.95, 4						
15	105	9.60, 0	6.95, 0	1.98, 1	7.30, 0	1.62, 1	1.66, 4	6.32, 1	3.58, 1					
15	120	1.28, 1	1.54, 1	1.24, 1	4.17, 2	1.68, 4	6.98, 1	3.83, 1	3,85, 0	6.67,-1				
15	135	2.30, 1	1.93, 1	3.07, 2	1.69, 4	7.35, 1	4.78, 1	2.09, 1	8.41,-1	5.66,-1	4.52,-1			
15	150	4.70, 1	5.70, 1	6.96, 3	7.45, 1	5.82, 1	4.15, 1	2.50, 1	1.01, 0	6.07,-1	4.40,-1	3.79,-1		
15	165	3.13, 2	8.37, 3	1.27, 0	6.60, 1	5.74, 1	4.50, 1	2.80, 1	4.72, 0	6.69,-1	4.83,-1	3.80,-1	3.44,-1	
15	180	8.53, 3	2.86, 0	4.27,-1	6.86, 1	6.09, 1	5.22, 1	3.97, 1	2.32, 1	8.76,-1	6.20,-1	4.55,-1	3.64,-1	3.38,-1
30	0	1.83, 0	1.97, 0	2.36, 0	3.13, 0	4.35, 0	5.78, 0	1.69, 0	3.15, 0	1.11, 1	3.71, 1	3.22, 2	8.96, 0	2.37, 2
30	15	1.84, 0	1.83, 0	2.04, 0	2.69, 0	3.58, 0	5.38, 0	1.01, 0	2.73, 0	9.79, 0	4.27, 1	5.78, 3	3.58, 3	1.11, 1
30	30	2.25, 0	1.94, 0	2.14, 0	2.47, 0	3.26, 0	4.61, 0	2.73, 0	3.08, 0	1.57, 1	3.08, 2	6.16, 3	8.39, 0	2.41, 0
30	45	2.82, 0	2.38, 0	2.26, 0	2.59, 0	3.37, 0	4.98, 0	1.33, 0	7.25, 0	5.48, 1	2.47, 2	6.49, 2	9.38,-1	9.09,-1
30	60	3.58, 0	3.13, 0	2.92, 0	3.14, 0	4.15, 0	6.79, 0	9.52, 0	3.48, 1	1.48, 2	1.56, 1	5.66,-1	7.64,-2	2.19,-1
30	75	6.62, 0	4.04, 0	3.91, 0	4.26, 0	5.69, 0	9.90, 0	2.90, 1	1.28, 2	6.11, 0	1.20, 0	3.56,-1	4.68,-2	2.32,-2
30	90	7.86, 0	5.64, 0	1.10, 1	6.77, 0	8.70, 0	2.40, 1	4.56, 3	8.31, 1	5.65, 1	4.18, 1	3.45, 1	3.67, 1	4.42, 1
30	105	8.60, 0	8.20, 0	8.20, 0	1.01, 1	2.50, 1	4.55, 2	7.68, 2	5.75, 1	3.80, 1	2.08, 1	1.37, 1	1.88, 1	2.96, 1
30	120	1.25, 1	1.07, 1	1.45, 1	2.80, 1	4.39, 2	8.48, 1	6.01, 1	4.19, 1	1.88, 1	8.94,-1	8.17,-1	9.57, 0	1.36, 1
30	135	1.95, 1	1.78, 1	5.10, 1	1.43, 3	8.34, 1	6.45, 1	4.91, 1	8.07, 1	4.44, 0	7.40,-1	6.50,-1	6.81,-1	1.57, 0
30	150	3.20, 1	4.90, 1	5.00, 2	7.92, 1	7.00, 1	5.86, 1	4.43, 1	2.66, 1	1.06, 0	7.00,-1	5.76,-1	5.55,-1	6.36,-1
30	165	6.20, 1	1.94, 2	5.78, 3	7.10, 1	6.64, 1	5.78, 1	4.55, 1	3.00, 1	6.87, 0	7.18,-1	5.65,-1	5.01,-1	5.19,-1
30	180	1.23, 2	1.21, 2	3.82,-2	7.04,-1	6.66, 1	6.01, 1	5.03, 1	3.83, 1	1.91, 1	8.42,-1	6.34,-1	5.19,-1	4.85,-1
45	0	2.49, 0	2.72, 0	3.36, 0	4.26, 0	8.36, 0	8.30, 0	3.42, 0	1.21, 1	4.01, 1	3.22, 2	2.06, 0	1.02, 1	1.73, 1
45	15	2.60, 0	2.70, 0	3.03, 0	3.97, 0	5.29, 0	8.10, 0	7.17, 0	9.64, 0	4.74, 1	6.94, 3	1.17, 1	4.92, 1	4.74, 1
45	30	2.73, 0	2.81, 0	3.14, 0	3.91, 0	5.18, 0	7.10, 0	2.97, 0	1.17, 0	7.95, 1	7.72, 0	1.59, 3	4.34, 1	1.97, 0
45	45	3.48, 0	3.26, 0	3.46, 0	4.14, 0	5.44, 0	8.30, 0	6.70, 0	2.52, 1	3.29, 2	2.86, 1	5.15, 0	7.58, 1	5.67,-1
45	60	4.07, 0	3.92, 0	4.04, 0	4.73, 0	5.85, 0	9.80, 0	1.72, 1	1.29, 2	2.48, 1	7.81, 0	1.29, 0	3.04,-1	1.04,-1
45	75	5.52, 0	4.94, 0	5.07, 0	5.74, 0	8.50, 0	1.72, 1	4.04, 1	1.73, 1	2.30, 2	5.88,-1	1.46,-1	5.51,-1	3.57,-2
45	90	2.60, 1	5.78, 0	6.84, 0	8.30, 0	1.36, 1	8.00, 1	5.73, 3	8.59, 1	6.45, 1	5.24, 1	4.39, 1	4.21, 1	4.63, 1
45	105	8.60, 0	8.30, 0	8.60, 0	1.24, 1	2.56, 1	2.70, 2	8.34, 1	1.48, 2	5.39, 1	4.04, 1	3.09, 1	3.02, 1	3.74, 1
45	120	1.17, 1	1.06, 1	1.26, 1	2.40, 1	1.06, 2	8.01, 1	6.97, 1	6.05, 1	4.39, 1	2.83, 1	1.71, 1	1.52, 1	2.25, 1
45	135	1.51, 1	1.72, 1	2.40, 1	1.07, 2	7.79, 1	7.35, 1	6.27, 1	5.26, 1	3.62, 1	1.85, 1	4.49, 0	9.26,-1	7.65, 0
45	150	2.25, 1	2.44, 1	9.00, 1	2.18, 2	7.27, 1	6.88, 1	5.92, 1	4.89, 1	3.25, 1	1.35, 1	8.83,-1	8.07,-1	8.63,-1
45	165	3.10, 1	2.62, 1	4.29, 1	6.94, 3	7.08, 1	6.67, 1	5.85, 1	4.89, 1	3.33, 1	1.44, 1	8.55,-1	7.48,-1	7.51,-1
45	180	1.81, 1	3.02, 1	8.01, 1	7.19, 2	7.05, 1	6.66, 1	5.98, 1	5.19, 1	3.80, 1	2.06, 1	9.13,-1	7.62,-1	7.16,-1
60	0	3.69, 0	3.92, 0	4.72, 0	6.72, 0	9.30, 0	1.19, 1	1.12, 1	4.21, 1	3.23, 2	8.81,-1	4.74, 0	2.78, 2	2.77, 0
60	15	3.80, 0	3.92, 0	4.58, 0	6.69, 0	3.32, 1	1.21, 1	1.16, 1	4.22, 1	7,86, 3	5.18, 0	5.66, 0	6.66, 0	4.40, 0
60	30	4.03, 0	4.14, 0	4.60, 0	5.69, 0	8.20, 0	1.12, 1	7.13, 1	3.11, 2	1.26, 0	9.62, 0	4.09, 2	1.84, 0	6.66, 0
60	45	4.48, 0	4.37, 0	4.95, 0	6.76, 0	8.50, 0	1.40, 1	1.53, 1	1.21, 2	4.29, 0	8.62, 0	4.26, 0	8.73,-1	1.98, 1
60	60	5.18, 0	5.06, 0	5.43, 0	6.97, 0	1.00, 1	1.73, 1	2.84, 2	3.25, 2	1.14, 1	2.82, 2	6.90,-1	3.23,-1	2.00,-1
60	75	6.73, 0	6.18, 0	6.81, 0	7.30, 0	1.33, 1	3.00, 1	7.81, 1	6.52, 3	6.35, 0	2.50, 2	1.63,-1	4.38,-2	9.64,-1
60	90	6.98, 0	6.99, 0	8.00, 0	9.10, 0	1.12, 1	5.30, 1	6.90, 3	8.30, 1	7.11, 1	5.86, 1	5.01, 1	4.60, 1	4.84, 1
60	105	8.50, 0	8.40, 0	2.30, 1	1.28, 1	3.50, 1	1.55, 2	7.55, 1	7.48, 1	8.34, 1	5.21, 1	4.29, 1	3.85, 1	4.07, 1
60	120	1.01, 1	9.10, 0	1.21, 1	2.47, 1	4.01, 1	6.52, 3	7.56, 1	6.86, 1	6.40, 1	4.60, 1	3.57, 1	3.06, 1	3.45, 1
60	135	1.31, 1	1.23, 1	1.64, 1	3.05, 1	1.34, 2	7.30, 1	7.09, 1	6.47, 1	5.45, 1	4.13, 1	2.97, 1	2.33, 1	2.48, 1
60	150	1.43, 1	1.48, 1	2.19, 1	3.41, 1	3.11, 2	7.17, 1	6.83, 1	6.25, 1	5.16, 1	3.93, 1	2.58, 1	1.76, 1	1.77, 1
60	165	1.54, 1	8.01, 0	1.98, 1	4.12, 1	7.86, 3	7.08, 1	6.69, 1	6.19, 1	5.11, 1	3.81, 1	2.47, 1	1.48, 1	1.26, 1
60	180	6.57, 0	2.86, 1	1.64, 1	7.40, 1	7.20, 1	7.06, 1	6.67, 1	6.26, 1	5.26, 1	4.02, 1	2.67, 1	1.54, 1	1.08, 1
75	0	5.30, 0	5.55, 0	6.85, 0	3.30, 0	1.16, 1	2.10, 1	4.11, 1	3.23, 2	4.90,-1	3.26, 0	1.62, 0	2.98, 2	7.20,-1
75	15	5.32, 0	5.55, 0	4.84, 0	9.50, 0	1.15, 1	2.10, 1	4.12, 1	1.88, 1	2.05, 0	4.44, 0	3.33, 0	1.64, 0	6.68,-1
75	30	5.54, 0	5.67, 0	6.85, 0	8.50, 0	1.26, 1	2.30, 1	5.74, 1	4.27,-1	5.08, 0	4.41, 0	1.31, 2	8.01,-1	5.24,-1
75	45	5.68, 0	5.72, 0	1.97, 0	8,60, 0	1.30, 1	2.70, 1	7.88, 1	8.08,-1	4.53, 0	3.40, 0	5.55, 0	4.26,-1	3.24,-1
75	60	6.76, 0	6.77, 0	7.10, 0	8.90, 0	1.47, 1	3.00, 1	8.31, 1	1.39, 0	6.19, 0	2.52, 0	2.06, 3	1.96,-1	1.29,-1
75	75	6.89, 0	7.94, 0	8.20, 0	1.03, 1	1.73, 1	4.90, 1	3.01, 2	2.20, 0	5.67, 0	2.39, 0	6.12,-1	6.93,-2	1.94,-2
75	90	7.10, 0	7.10, 0	8.50, 0	1.29, 1	2.32, 1	5.00, 1	8.03, 3	7.93, 1	7.25, 1	6.45, 1	5.44, 1	4.90, 1	4.84, 1
75	105	7.30, 0	7.30, 0	1.00, 1	3.52, 1	2.90, 1	8.21, 1	7.30, 1	7.63, 1	6.90, 1	6.73, 1	5.13, 1	4.56, 1	4.50, 1
75	120	8.50, 0	8.60, 0	1.14, 1	2.97, 1	2.90, 2	2.11, 2	7.25, 1	7.48, 1	6.63, 1	5.90, 1	4.84, 1	4.23, 1	4.15, 1
75	135	8.70, 0	1.01, 1	1.34, 1	1.28, 1	2.99, 2	3.10, 2	7.19, 1	7.28, 1	6.45, 1	5.69, 1	4.62, 1	3.95, 1	3.83, 1
75	150	1.01, 1	1.04, 1	7.17, 0	1.56, 1	3.04, 2	3.22, 2	7.27, 1	7.13, 1	6.33, 1	5.50, 1	4.50, 1	3.75, 1	3.57, 1
75	165	1.03, 1	7.94, 0	5.24, 1	1.33, 1	3.01, 2	8.46, 3	7.40, 1	7.03, 1	6.29, 1	5.38, 1	4.41, 1	3.64, 1	3.39, 1
75	180	2.53, 0	3.14, 0	1.40, 1	1.51, 1	3.09, 2	7.20, 1	7.47, 1	7.01, 1	6.32, 1	5.43, 1	4.46, 1	3.65, 1	3.33, 1
90	all	8.20, 0	7.30, 0	1.10, 1	1.50, 1	2.70, 1	9.30, 1	8.98, 3	7.77, 1	7.13, 1	6.27, 1	6.79, 1	4.92, 1	4.68, 1

BISTATIC CROSS-SECTION (σ IN m^2) FOR THE B-47 AIRCRAFT

(The numbers following comma indicate multiplication by that power of 10)

θ_T=15°

θ_R	ϕ_R	ϕ_T=0°	ϕ_T=15°	ϕ_T=30°	ϕ_T=45°	ϕ_T=60°	ϕ_T=75°	ϕ_T=90°	ϕ_T=105°	ϕ_T=120°	ϕ_T=135°	ϕ_T=150°	ϕ_T=165°	ϕ_T=180°
30	0	2.50, 0												
30	15	2.71, 0	2.69, 0											
30	30	3.15, 0	2.67, 0	3.08, 0										
30	45	3.94, 0	2.92, 0	3.50, 0	4.01, 0									
30	60	5.08, 0	3.54, 0	4.47, 0	5.04, 0	6.23, 0								
30	75	1.50, 1	4.50, 0	5.92, 0	6.70, 0	8.77, 0	1.43, 1							
30	90	8.31, 0	5.99, 0	7.06, 0	1.18, 1	1.50, 1	4.66, 1	1.42, 4						
30	105	2.22, 1	1.27, 1	2.62, 1	2.06, 1	6.37, 1	8.58, 3	9.40, 1	6.62, 1					
30	120	2.03, 1	1.13, 1	9.54, 1	6.04, 5	8.63, 3	2.33, 2	6.48, 1	5.53, 1	4.24, 1				
30	135	3.28, 1	1.93, 1	8.58, 3	8.67, 3	1.40, 2	1.81, 2	5.64, 1	4.56, 1	3.08, 1	1.68, 1			
30	150	1.36, 2	3.52, 1	8.63, 3	9.41, 1	7.04, 1	6.14, 1	5.20, 1	4.01, 1	2.42, 1	7.85, 0	8.71,-1		
30	165	2.70, 2	4.28, 3	7.96, 0	7.23, 1	6.66, 1	5.97, 1	5.04, 1	3.98, 1	2.44, 1	7.07, 0	8.19,-1	7.47,-1	
30	180	4.33, 3	5.15, 0	4.91,-1	7.00, 1	6.65, 1	6.09, 1	5.31, 1	4.43, 1	3.05, 1	1.41, 1	8.71,-1	7.52,-1	7.16,-1
45	0	3.69, 0	3.89, 0	4.45, 0	5.44, 0	7.62, 0	9.30, 0	4.36, 0	1.37, 1	5.02, 1	2.20, 2	2.49, 0	1.96, 1	1.64, 2
45	15	3.44, 0	3.88, 0	4.31, 0	5.17, 0	6.59, 0	1.43, 1	3.81, 0	1.26, 1	5.60, 1	2.53, 2	1.75, 1	2.24, 3	2.72, 1
45	30	4.27, 0	4.71, 0	4.47, 0	4.91, 0	6.68, 0	8.99, 0	4.58, 0	1.81, 1	1.02, 2	8.42, 3	3.86, 3	1.67, 3	5.99, 0
45	45	4.95, 0	4.74, 0	5.01, 0	5.82, 0	7.32, 0	1.01, 1	7.57, 1	4.56, 1	2.77, 2	1.46, 2	9.15, 1	4.19, 0	1.35, 0
45	60	6.01, 0	5.65, 0	5.90, 0	6.92, 0	8.90, 0	1.31, 1	2.13, 2	1.81, 2	8.21, 1	2.49, 1	1.94, 1	4.32,-1	2.76,-1
45	75	7.79, 0	6.98, 0	7.30, 0	8.74, 0	1.17, 1	2.34, 1	2.06, 2	6.94, 1	8.54, 1	2.73, 0	1.35, 0	2.34,-2	3.78,-2
45	90	1.02, 1	8.90, 0	9.56, 0	1.19, 1	1.77, 1	1.32, 2	6.96, 3	1.80, 3	7.11, 1	6.32, 1	6.05, 1	5.83, 1	5.73, 1
45	105	1.23, 1	1.26, 1	1.30, 1	2.14, 1	5.07, 1	8.11, 1	1.06, 2	1.34, 2	6.30, 1	5.51, 1	5.00, 1	4.75, 1	4.98, 1
45	120	1.68, 1	2.28, 1	2.88, 1	4.68, 1	1.32, 2	9.41, 1	7.87, 1	6.76, 1	5.57, 1	4.66, 1	3.99, 1	3.77, 1	4.11, 1
45	135	2.78, 1	9.03, 1	5.26, 1	7.95, 1	8.98, 1	7.50, 1	6.59, 1	5.95, 1	4.93, 1	3.90, 1	3.09, 1	2.77, 1	5.24, 1
45	150	4.25, 1	1.37, 2	1.14, 2	8.42, 3	8.94, 1	7.50, 1	6.93, 1	6.21, 1	5.80, 1	4.76, 1	3.39, 1	2.42, 1	1.92, 1
45	165	7.89, 1	6.84, 1	7.88, 0	7.30, 1	7.32, 1	6.72, 1	6.09, 1	5.49, 1	4.43, 1	3.25, 1	2.15, 1	1.43, 1	1.35, 1
45	180	1.13, 2	1.25, 1	1.98, 0	7.19, 1	7.17, 1	6.70, 1	6.16, 1	5.64, 1	4.65, 1	3.51, 1	2.35, 1	1.43, 1	1.08, 1
60	0	5.24, 0	5.48, 0	6.23, 0	7.72, 0	1.22, 1	1.38, 1	1.51, 1	6.51, 1	2.80, 2	1.05, 0	5.35, 0	5.21, 1	1.15, 1
60	15	5.37, 0	5.50, 0	6.14, 0	7.44, 0	1.07, 1	1.38, 1	1.47, 1	7.15, 1	2.96, 2	3.61, 0	1.39, 1	3.40, 1	2.64, 2
60	30	5.69, 0	5.73, 0	6.37, 0	7.57, 0	1.21, 1	1.49, 1	1.91, 1	1.01, 2	9.18, 3	1.02, 1	1.12, 3	7.27, 0	2.81, 2
60	45	6.26, 0	6.02, 0	6.95, 0	8.17, 0	1.07, 1	1.71, 1	3.07, 1	1.73, 2	7.53, 0	2.18, 1	1.08, 1	5.45, 0	2.29, 0
60	60	7.13, 0	7.05, 0	7.65, 0	9.28, 0	1.26, 1	2.74, 1	6.88, 1	3.25, 2	1.48, 1	2.02, 2	2.11, 0	5.79, 1	2.67,-1
60	75	8.37, 0	8.16, 0	8.90, 0	1.08, 1	1.54, 1	4.01, 1	1.79, 2	1.16, 1	1.53, 1	5.12, 0	5.09,-1	9.78, 3	4.09,-2
60	90	9.80, 0	9.64, 0	1.08, 1	1.40, 1	3.11, 1	5.86, 1	8.03, 3	9.01, 1	3.59, 2	6.62, 1	6.10, 1	5.82, 1	6.37, 1
60	105	1.17, 1	1.22, 1	1.49, 1	1.96, 1	1.20, 2	1.18, 1	8.03, 1	7.79, 1	7.25, 1	6.14, 1	5.59, 1	5.30, 1	5.41, 1
60	120	1.71, 1	1.10, 1	1.95, 1	4.31, 1	1.66, 1	7.85, 1	7.91, 1	7.18, 1	6.43, 1	5.69, 1	5.08, 1	4.75, 1	4.98, 1
60	135	3.36, 1	2.08, 1	3.03, 1	4.88, 1	7.49, 0	7.49, 1	7.18, 1	6.80, 1	6.07, 1	5.30, 1	4.62, 1	4.23, 1	4.27, 1
60	150	3.27, 1	2.96, 1	4.77, 1	1.06, 1	9.18, 3	7.25, 1	6.92, 1	6.59, 1	6.34, 1	5.12, 1	4.29, 1	3.82, 1	3.78, 1
60	165	2.87, 1	5.66, 0	1.11, 1	7.77,-1	7.23, 1	7.65, 1	6.78, 1	6.51, 1	5.77, 1	4.94, 1	4.14, 1	3.58, 1	3.45, 1
60	180	2.52, 1	1.10, 2	9.88,-1	2.90,-1	7.19, 1	7.40, 1	6.75, 1	6.53, 1	6.12, 1	5.01, 1	4.20, 1	3.57, 1	3.33, 1
75	0	7.24, 0	6.66, 0	8.80, 0	2.03, 1	1.52, 1	2.66, 1	8.81, 1	3.13, 2	5.98,-1	2.92, 0	3.05, 0	2.88, 1	1.99, 0
75	15	7.35, 0	6.68, 0	8.72, 0	1.17, 1	1.52, 1	2.69, 1	9.03, 1	3.21, 2	1.38, 0	4.54, 0	7.18, 0	4.94, 0	1.02, 0
75	30	7.56, 0	6.77, 0	8.87, 0	1.12, 1	1.56, 1	2.94, 1	1.09, 2	9.36, 3	2.84, 0	5.49, 0	3.13, 2	2.12, 0	1.59, 0
75	45	7.92, 0	8.15, 0	9.18, 0	1.13, 1	1.71, 1	2.25, 1	1.39, 2	1.51, 0	6.46, 0	5.49, 0	1.36, 1	1.09, 0	1.13, 0
75	60	8.48, 0	8.67, 0	9.86, 0	1.24, 1	2.03, 1	3.69, 1	2.02, 2	2.53, 0	7.97, 0	5.47, 0	1.41, 1	4.91,-1	5.46,-1
75	75	9.20, 0	9.45, 0	1.08, 1	1.43, 1	2.71, 1	4.45, 1	2.82, 2	3.65, 0	5.90, 0	9.02, 0	1.10, 0	1.16,-1	7.14,-2
75	90	1.01, 1	1.01, 1	1.23, 1	1.74, 1	3.13, 1	7.18, 1	8.98, 3	7.89, 1	7.55, 1	1.43, 2	6.31, 1	5.98, 1	5.92, 1
75	105	1.10, 1	1.14, 1	1.39, 1	3.74, 1	3.82, 1	3.76, 0	7.42, 1	7.84, 1	7.23, 1	8.23, 1	6.07, 1	5.74, 1	5.68, 1
75	120	1.23, 1	1.27, 1	1.74, 1	1.09, 2	6.55, 0	2.51, 0	7.35, 1	7.59, 1	6.98, 1	6.43, 1	4.86, 1	5.50, 1	5.44, 1
75	135	1.38, 1	1.46, 1	1.95, 1	9.54, 0	4.87, 0	1.61, 0	7.26, 1	7.39, 1	6.81, 1	6.50, 1	5.69, 1	5.30, 1	5.22, 1
75	150	1.63, 1	1.59, 1	8.93, 0	6.20, 0	2.85, 0	9.36, 3	8.77, 1	7.25, 1	6.71, 1	7.22, 1	5.59, 1	5.15, 1	5.04, 1
75	165	1.67, 1	9.73,-1	6.36, 1	6.78,-1	2.28,-1	8.17, 1	7.30, 1	7.16, 1	6.66, 1	6.07, 1	5.49, 1	5.05, 1	4.91, 1
75	180	6.92, 0	1.41, 0	8.91, 0	2.36,-1	1.71,-1	7.20, 1	7.76, 1	7.14, 1	6.67, 1	6.09, 1	5.50, 1	5.04, 1	4.87, 1
90	all	1.05, 1	1.18, 1	1.61, 1	2.13, 1	4.00, 1	1.22, 2	9.80, 3	7.26, 1	7.26, 1	6.68, 1	1.07, 2	5.87, 1	5.72, 1

BISTATIC CROSS-SECTION (σ IN m^2) FOR THE B-47 AIRCRAFT

(The numbers following comma indicate multiplication by that power of 10)

θ_T=30°

TABLE H - 4

θ_R	ϕ_R	ϕ_T=0°	ϕ_T=15°	ϕ_T=30°	ϕ_T=45°	ϕ_T=60°	ϕ_T=75°	ϕ_T=90°	ϕ_T=105°	ϕ_T=120°	ϕ_T=135°	ϕ_T=150°	ϕ_T=165°	ϕ_T=180°
45	0	5.24, 0												
45	15	5.39, 0	5.47, 0											
45	30	5.94, 0	5.90, 0	6.25, 0										
45	45	6.93, 0	6.77, 0	7.08, 0	8.07, 0									
45	60	8.50, 0	8.08, 0	8.48, 0	9.62, 0	1.21, 1								
45	75	2.59, 1	1.01, 1	1.07, 1	1.27, 1	1.76, 1	4.96, 1							
45	90	1.39, 1	1.51, 1	1.52, 1	2.05, 1	3.42, 1	3.77, 2	1.40, 4						
45	105	2.12, 1	2.14, 1	4.80, 2	6.68, 1	9.86, 1	6.09, 3	2.25, 2	7.87, 1					
45	120	3.31, 1	3.46, 1	6.91, 1	1.67, 4	6.11, 3	1.21, 3	8.84, 1	6.90, 1	6.33, 1				
45	135	7.26, 1	8.16, 1	2.92, 2	6.13, 3	3.32, 2	7.42, 2	7.14, 1	6.43, 1	5.82, 1	5.23, 1			
45	150	1.58, 2	2.28, 2	6.07, 3	1.45, 2	8.60, 1	7.09, 1	7.17, 1	6.10, 1	5.44, 1	4.78, 1	4.24, 1		
45	165	3.52, 2	3.02, 3	2.14, 1	7.54, 1	7.11, 1	6.71, 1	6.25, 1	5.94, 1	5.26, 1	4.56, 1	3.95, 1	3.57, 1	
45	180	3.04, 3	2.06, 1	2.76, 0	7.19, 1	6.99, 1	6.69, 1	6.27, 1	5.99, 1	5.34, 1	4.63, 1	3.98, 1	3.51, 1	3.33, 1
60	0	7.31, 0	7.50, 0	8.36, 0	9.82, 0	3.07, 1	1.62, 1	1.50, 1	3.05, 1	1.05, 2	7.50, 3	8.26, 0	5.07, 1	1.23, 2
60	15	7.44, 0	8.60, 0	8.33, 0	9.62, 0	1.27, 1	1.66, 1	1.57, 1	3.73, 1	1.20, 2	1.30, 1	3.01, 1	1.71, 3	2.10, 3
60	30	7.88, 0	8.07, 0	8.62, 0	9.99, 0	1.26, 1	1.73, 1	1.92, 1	4.53, 1	3.20, 2	2.61, 1	2.97, 3	2.96, 2	1.92, 1
60	45	8.78, 0	8.75, 0	9.48, 0	1.09, 1	1.40, 1	2.29, 1	3.07, 1	8.00, 1	8.42, 3	1.09, 2	5.27, 1	1.37, 3	2.83, 0
60	60	1.01, 1	9.98, 0	1.07, 1	1.27, 1	1.74, 1	3.46, 1	6.99, 1	3.41, 2	5.99, 1	2.89, 2	1.97, 1	2.06, 2	6.12,-1
60	75	1.19, 1	1.18, 1	1.28, 1	1.62, 1	3.17, 1	1.26, 2	1.63, 2	5.01, 1	2.13, 3	1.03, 1	4.98, 0	1.20, 2	7.92,-2
60	90	1.66, 1	1.47, 1	1.67, 1	2.33, 1	4.12, 1	3.54, 2	9.02, 3	1.32, 2	2.32, 2	7.22, 1	6.85, 1	6.65, 1	6.65, 1
60	105	1.96, 1	2.08, 1	2.54, 1	3.81, 1	2.40, 2	3.78, 2	1.04, 2	1.90, 2	7.52, 1	6.78, 1	6.46, 1	9.10, 1	8.02, 1
60	120	2.71, 1	3.55, 1	3.98, 1	8.31, 1	2.77, 2	9.88, 1	9.43, 1	2.86, 2	6.90, 1	6.43, 1	6.09, 1	5.91, 1	5.99, 1
60	135	3.98, 1	5.95, 1	7.40, 1	8.80, 2	8.42, 3	8.14, 1	7.37, 1	7.58, 1	7.34, 1	6.13, 1	5.75, 1	5.53, 1	5.64, 1
60	150	1.37, 2	8.64, 1	4.21, 2	3.41, 2	7.96, 1	7.48, 1	6.98, 1	6.85, 1	6.41, 1	5.91, 1	5.49, 1	5.23, 1	5.19, 1
60	165	7.04, 1	1.14, 2	1.36, 2	3.25, 2	7.31, 1	7.16, 1	6.83, 1	6.75, 1	6.28, 1	5.78, 1	5.33, 1	5.03, 1	4.96, 1
60	180	8.43, 1	3.15, 2	1.30, 2	7.50, 3	7.19, 1	7.06, 1	6.80, 1	6.75, 1	6.29, 1	5.79, 1	5.33, 1	4.99, 1	4.87, 1
75	0	1.02, 1	1.07, 1	1.21, 1	1.97, 1	2.08, 1	2.96, 1	5.47, 1	3.11, 2	9.46,-1	3.55, 0	7.24, 0	6.26, 1	9.09, 0
75	15	1.04, 1	1.08, 1	1.20, 1	1.53, 1	2.09, 1	2.99, 1	6.09, 1	3.21, 2	2.37, 0	2.49, 1	1.97, 1	2.73, 1	9.52, 0
75	30	1.08, 1	1.10, 1	1.24, 1	1.51, 1	2.16, 1	3.32, 1	6.52, 1	3.24, 2	5.00, 0	1.10, 1	9.15, 2	8.64, 0	1.21, 1
75	45	1.12, 1	1.16, 1	1.29, 1	1.60, 1	2.66, 1	3.55, 1	8.17, 1	8.42, 3	8.56, 0	1.43, 1	6.77, 1	4.30, 0	2.37, 2
75	60	1.24, 1	1.26, 1	1.41, 1	1.79, 1	5.37, 1	4.74, 1	1.24, 2	6.61, 0	1.11, 1	2.66, 1	1.18, 1	1.93, 0	7.10, 0
75	75	1.36, 1	1.37, 1	1.56, 1	2.18, 1	5.71, 1	7.28, 1	2.26, 2	8.71, 0	1.80, 1	4.90, 2	2.59, 0	6.21,-1	6.92,-1
75	90	1.49, 1	1.44, 1	1.87, 1	2.87, 1	5.31, 1	9.93, 1	9.80, 3	8.39, 1	8.13, 1	1.03, 2	6.94, 1	6.73, 1	9.09, 1
75	105	1.71, 1	1.86, 1	2.29, 1	4.71, 1	6.51, 1	1.48, 2	7.86, 1	9.96, 1	7.71, 1	7.38, 1	6.74, 1	6.55, 1	6.58, 1
75	120	2.12, 1	2.25, 1	2.91, 1	5.17, 3	7.12, 1	3.27, 2	7.66, 1	7.81, 1	7.34, 1	6.90, 1	6.58, 1	6.39, 1	6.38, 1
75	135	2.56, 1	2.72, 1	3.81, 1	6.85, 1	7.73, 1	8.42, 3	7.44, 1	7.52, 1	7.11, 1	6.76, 1	6.45, 1	6.25, 1	6.22, 1
75	150	2.89, 1	3.19, 1	6.03, 1	5.09, 1	1.34, 2	7.39, 1	7.26, 1	7.36, 1	7.00, 1	7.15, 1	6.38, 1	6.14, 1	6.09, 1
75	165	2.95, 1	2.22, 1	1.38, 3	5.64, 1	2.45, 2	7.24, 1	7.67, 1	7.27, 1	6.95, 1	6.61, 1	6.29, 1	6.06, 1	5.99, 1
75	180	2.00, 1	2.63, 1	3.71, 1	5.76, 1	2.94, 2	7.20, 1	7.65, 1	7.25, 1	6.95, 1	6.61, 1	6.28, 1	6.04, 1	5.96, 1
90	all	1.54, 1	1.67, 1	2.56, 1	2.86, 1	3.93, 1	9.32, 1	1.04, 4	7.42, 1	7.44, 1	7.07, 1	2.69, 2	6.62, 1	6.48, 1

BISTATIC CROSS-SECTION (σ IN m^2) FOR THE B-47 AIRCRAFT

(The numbers following comma indicate multiplication by that power of 10)

θ_T=45°

TABLE H-5

θ_R	ϕ_R	ϕ_T=0°	ϕ_T=15°	ϕ_T=30°	ϕ_T=45°	ϕ_T=60°	ϕ_T=75°	ϕ_T=90°	ϕ_T=105°	ϕ_T=120°	ϕ_T=135°	ϕ_T=150°	ϕ_T=165°	ϕ_T=180°
60	0	1.00, 1												
60	15	1.04, 1	1.10, 1											
60	30	1.17, 1	1.10, 1	1.30, 1										
60	45	1.38, 1	1.30, 1	1.40, 1	1.50, 1									
60	60	1.56, 1	1.58, 1	1.70, 1	2.00, 1	3.20, 1								
60	75	9.60, 1	2.00, 1	2.30, 1	2.90, 1	3.80, 1	1.13, 2							
60	90	2.60, 1	7.20, 1	3.60, 1	4.30, 1	8.70, 1	2.93, 2	1.47, 4						
60	105	3.50, 1	4.10, 1	5.70, 5	2.38, 2	4.77, 2	4.98, 3	1.94, 3	1.36, 2					
60	120	7.10, 1	8.30, 1	3.24, 2	6.49, 3	4.99, 3	2.40, 4	4.23, 2	8.12, 1	7.23, 1				
60	135	9.30, 1	1.77, 2	1.35, 3	5.01, 3	7.32, 2	1.73, 3	1.24, 2	7.42, 1	6.95, 1	6.72, 1			
60	150	2.83, 2	5.75, 2	4.94, 3	2.84, 2	1.22, 2	9.84, 1	1.82, 2	7.07, 1	6.79, 1	6.54, 1	6.34, 1		
60	165	3.76, 2	2.47, 3	6.52, 1	8.30, 1	7.48, 1	7.12, 1	6.87, 1	6.94, 1	6.68, 1	6.42, 1	6.19, 1	6.05, 1	
60	180	2.47, 3	7.77, 1	1.01, 1	7.46, 1	7.21, 1	7.03, 1	6.83, 1	6.93, 1	6.67, 1	6.40, 1	6.17, 1	6.01, 1	5.96, 1
75	0	1.70, 1	1.70, 1	1.80, 1	2.70, 1	4.00, 1	4.10, 1	5.20, 1	1.16, 2	2.45, 0	7.57, 0	2.23, 1	2.20, 3	1.05, 2
75	15	1.70, 1	1.70, 1	1.80, 1	2.50, 1	3.50, 1	4.20, 1	5.30, 1	1.23, 2	1.05, 4	1.81, 1	6.97, 1	1.47, 3	7.12, 2
75	30	1.80, 1	1.80, 1	1.90, 1	2.30, 1	2.90, 1	4.40, 1	6.80, 1	1.38, 2	2.29, 1	3.86, 1	2.55, 3	7.63, 1	8.85, 2
75	45	2.00, 1	1.90, 1	2.20, 1	2.55, 1	3.20, 1	6.50, 1	8.80, 1	1.78, 2	3.27, 1	9.27, 1	7.07, 2	6.76, 1	6.79, 2
75	60	2.10, 1	2.05, 1	2.35, 1	2.80, 1	4.50, 1	1.25, 2	1.56, 2	1.04, 4	5.02, 1	2.22, 3	4.66, 1	4.45, 1	6.75, 1
75	75	2.10, 1	2.50, 1	2.75, 1	3.50, 1	8.80, 1	1.59, 2	1.68, 2	4.18, 1	7.28, 1	3.68, 2	1.14, 1	1.44, 1	2.86, 1
75	90	2.15, 1	2.80, 1	3.30, 1	5.45, 1	7.65, 2	1.95, 2	1.05, 4	1.15, 2	2.21, 2	1.16, 2	7.56, 1	7.31, 1	7.42, 1
75	105	3.40, 1	5.20, 1	4.20, 1	7.90, 1	5.69, 2	1.69, 2	1.05, 2	1.04, 2	7.67, 2	7.95, 1	7.22, 1	7.10, 1	7.35, 1
75	120	5.00, 1	7.20, 1	6.80, 1	3.15, 2	2.03, 2	1.05, 4	9.18, 1	8.93, 1	5.12, 3	7.30, 1	7.07, 1	7.01, 1	5.92, 2
75	135	9.00, 1	1.10, 2	1.14, 2	4.64, 2	2.07, 2	9.26, 1	8.09, 1	8.65, 1	1.03, 2	7.14, 1	7.00, 1	6.93, 1	7.09, 1
75	150	1.19, 2	1.87, 2	8.70, 1	6.10, 1	2.02, 2	7.95, 1	7.48, 1	7.49, 1	7.25, 1	7.54, 1	6.98, 1	6.87, 1	6.90, 1
75	165	8.10, 1	9.43, 1	2.20, 2	9.21, 1	1.05, 4	7.35, 1	7.18, 1	7.36, 1	7.19, 1	7.02, 1	6.87, 1	6.78, 1	6.78, 1
75	180	7.60, 1	2.42, 2	8.50, 1	8.40, 1	2.46, 2	7.22, 1	7.12, 1	7.35, 1	7.19, 1	7.02, 1	6.87, 1	6.76. 1	6.74, 1
90	all	3.00, 1	3.50, 1	6.80, 1	8.10, 1	1.05, 2	1.69, 2	1.09, 4	7.88, 1	7.87, 1	7.70, 1	8.21, 2	7.96, 1	7.31, 1

BISTATIC CROSS-SECTION (σ IN m^2) FOR THE B-47 AIRCRAFT
(The numbers following comma indicate multiplication by that power of 10)

θ_T=60°

TABLE H-6

θ_R	ϕ_R	$\phi_T=0°$	$\phi_T=15°$	$\phi_T=30°$	$\phi_T=45°$	$\phi_T=60°$	$\phi_T=75°$	$\phi_T=90°$	$\phi_T=105°$	$\phi_T=120°$	$\phi_T=135°$	$\phi_T=150°$	$\phi_T=165°$	$\phi_T=180°$
75	0	2.30, 1												
75	15	3.20, 1	3.30, 1											
75	30	3.60, 1	3.30, 1	3.40, 1										
75	45	3.80, 1	3.50, 1	3.40, 1	3.90, 1									
75	60	4.70, 1	3.50, 1	4.10, 1	5.10, 1	9.00, 1								
75	75	2.02, 6	5.00, 1	5.40, 1	9.50, 1	1.32, 2	2.22, 2							
75	90	4.70, 1	1.71, 3	1.52, 2	1.81, 2	2.76, 2	8.53, 2	1.53, 4						
75	105	9.50, 1	2.18, 2	4.31, 3	7.75, 2	1.21, 3	4.47, 3	1.45, 6	7.80, 2					
75	120	1.27, 2	2.72, 2	3.07, 3	3.89, 3	4.48, 3	1.35, 4	1.87, 3	2.36, 2	9.59, 1				
75	135	2.18, 2	5.85, 2	8.38, 4	4.49, 3	1.87, 3	2.39, 3	1.48, 3	3.32, 2	8.96, 1	7.39, 1			
75	150	4.93, 2	1.53, 4	4.43, 3	9.97, 2	3.44, 2	2.51, 2	6.79, 2	9.65, 1	7.43, 1	7.49, 1	7.56, 1		
75	165	4.64, 2	2.20, 3	5.03, 2	1.32, 2	8.84, 1	7.68, 1	7.24, 1	8.50, 1	7.37, 1	7.36, 1	7.38, 1	7.46, 1	
75	180	2.22, 3	6.35, 2	6.68, 1	8.76, 1	7.66, 1	7.27, 1	7.12, 1	7.90, 1	7.40, 1	7.40, 1	7.38, 1	7.40, 1	7.49, 1
90	all	1.25, 2	1.44, 2	3.80, 2	7.41, 2	3.39, 2	3.79, 2	1.13, 4	1.80, 2	1.07, 2	1.16, 2	2.37, 3	1.37, 3	1.36, 2

BISTATIC CROSS-SECTION (σ IN m^2) FOR THE B-47 AIRCRAFT
(The numbers following comma indicate multiplication by that power of 10)

$\theta_T = 75°$

SECRET

TABLE H-7

θ_R	ϕ_R=0°	ϕ_R=15°	ϕ_R=30°	ϕ_R=45°	ϕ_R=60°	ϕ_R=75°	ϕ_R=90°	ϕ_R=105°	ϕ_R=120°	ϕ_R=135°	ϕ_R=150°	ϕ_R=165°	ϕ_R=180°
90	1.55, 4	1.55, 4	1.55, 4	1.55, 4	1.55, 4	1.55, 4	1.55, 4	1.55, 4	1.55, 4	1.55, 4	1.55, 4	1.55, 4	1.55, 4

BISTATIC CROSS-SECTION (σ IN m^2) FOR THE B-47 AIRCRAFT
(The numbers following comma indicate multiplication by that power of 10)
$\theta_T = 90°$ and ALL ϕ_T

The values omitted from the preceding tables can be obtained by reading the entries corresponding to an interchange of the subscripts R and T

APPENDIX I

CORNER REFLECTOR EXPERIMENTS AT OHIO STATE UNIVERSITY

Under Contract AF 30(635)-2811 the Antenna Laboratory of the Ohio State University Research Foundation is investigating the design of reflectors suitable for use with cross-linear and circularly polarized radar systems where maximum discrimination against rain clutter is desired. In their Quarterly Progress Report for the period ending 31 March 1955 (Ref. 17) some of the results obtained for modified corner reflectors are reported. As of that date all of the patterns of reflectors investigated were measured using linear polarization; in that report (i.e., Ref. 17) it is stated that analysis and measurement of circularly polarized return from modified corner reflectors was planned for the next reporting interval. [1]

Of the modifications on corner reflectors being studied at Ohio State the one which is of interest in this paper is the one in which one or more of the surfaces of the corner is lined with a layer of dielectric. This modification is examined in Reference 17 for two types of corners: a "double-double bounce" corner (Fig. I-1) and a triangular corner reflector.

Reflection patterns were obtained for two double-double bounce corners using horizontal polarization at K-band (λ=1/2 inch). Both double-double bounce corners had four-inch square apertures and the "modified corner" differed from the "standard" one only in that the upper and lower surfaces were lined with 1/16-inch thickness lucite sheets. The reflection patterns obtained are reproduced in Figure I-2. It will be observed that the null obtained along the axis of the "standard" corner is completely eliminated by using the indicated modification with little change in the remainder of the pattern being obtained.

---

[1]At the time of the writing of this report the O.S.U. Progress Report dated 16 June 1955 was being bound and thus no copies were available. Information received in a letter from the Antenna Laboratory of O.S.U. indicates that they are preparing a technical report on the subject which will be completed in the near future.

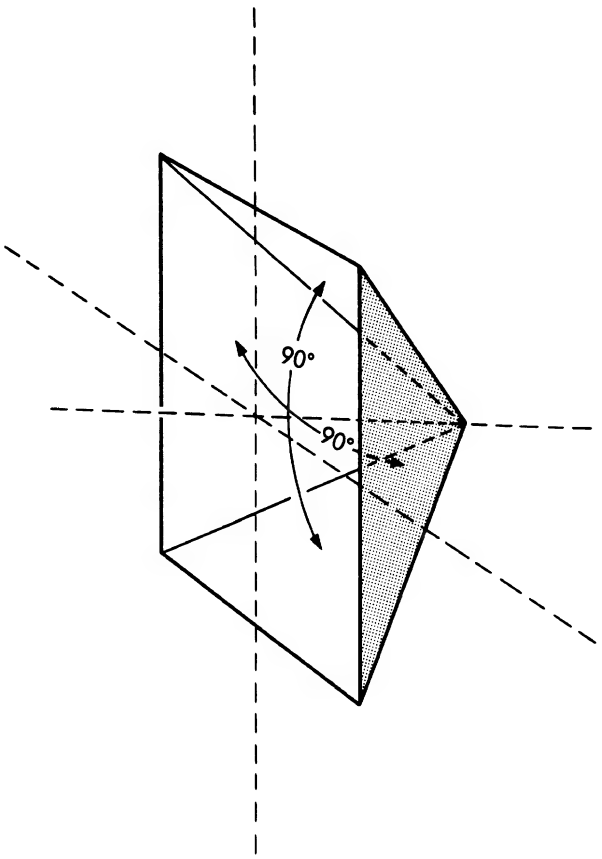

FIG. I-1 DOUBLE - DOUBLE BOUNCE CORNER USED IN OHIO STATE UNIVERSITY MEASUREMENTS

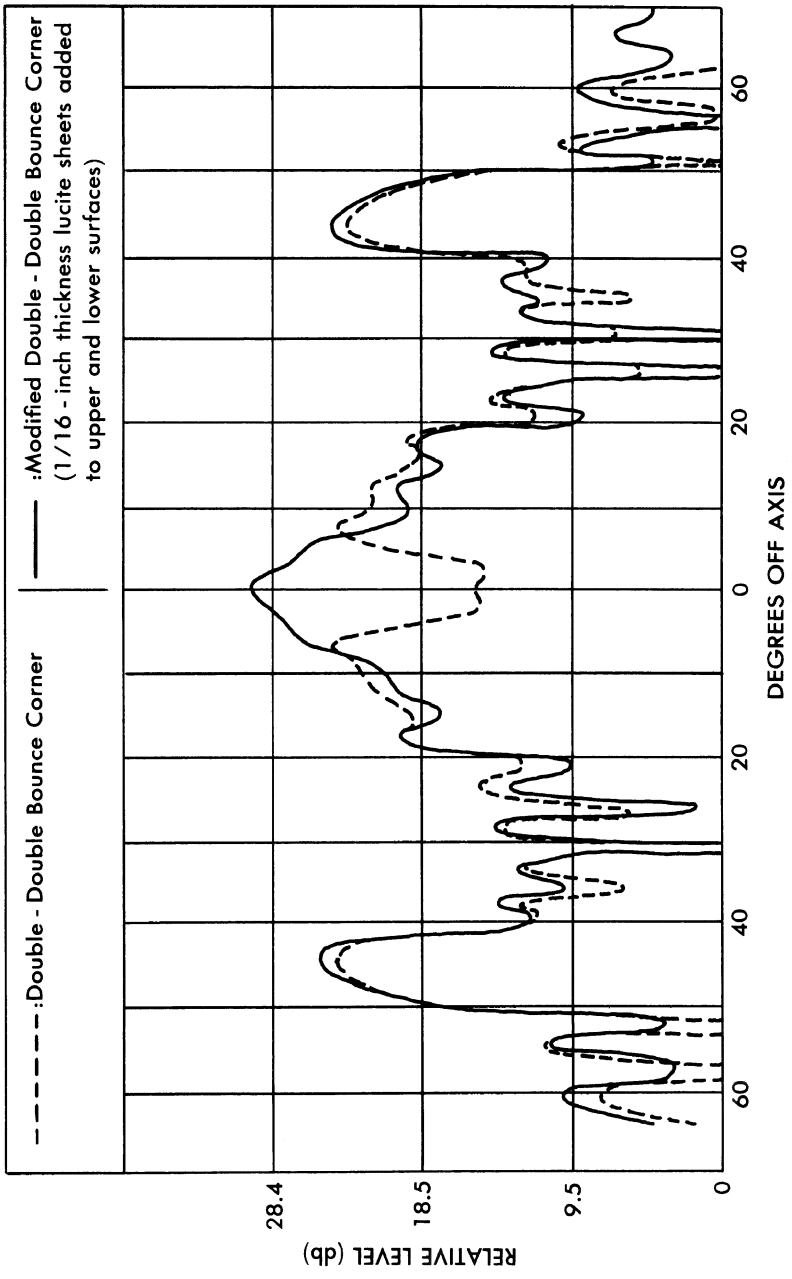

FIG. I-2 REFLECTION PATTERNS OF "DOUBLE - DOUBLE BOUNCE" CORNERS (four-inch square aperture, horizontal polarization, measured at K-band ($\lambda = \frac{1}{2}$ inch))

For the triangular corner reflector, only theoretical considerations are reported in Reference 17. A brief resume of these theoretical considerations is as follows:

For an unmodified corner reflector the S-matrix, referred to a linear polarization basis, is of the form

$$\begin{pmatrix} 1 & 0 \\ 0 & 1 \end{pmatrix},$$

i.e., there is no cross-polarization return and the phase difference between the orthogonal components is not changed. However, on introducing a dielectric coating on one or more of the faces, in general there will be a change in the phase difference of the two components while there still will be no cross-polarization return. The S-matrix then will be of the form

$$\begin{pmatrix} e^{i\theta} & 0 \\ 0 & e^{-i\theta} \end{pmatrix}$$

where 2θ is the change in phase difference between the two components and θ will depend upon the dielectric constant, the thickness of the coating, and the angle of incidence. It is to be noted that the ray picture is unaltered by the introduction of the dielectric coating, that is, the effect of the dielectric on the ray picture is a parallel displacement of the rays.

Referred to a circular polarization basis, the S-matrix in the unmodified corner reflector in triple reflections is of the form

$$\begin{pmatrix} 0 & 1 \\ 1 & 0 \end{pmatrix},$$

i.e., for right-circular incident radiation, left-circular emerges and vice versa. Upon modification, however, the S-matrix takes the form

$$\begin{pmatrix} \sin\theta & \cos\theta \\ \cos\theta & -\sin\theta \end{pmatrix}$$

which, for $\sin\theta \neq 0$, indicates a non-vanishing return for the same emergent and incident circular polarization. Since the latter form of the S-

matrix was obtained by a coordinate transformation of the linear basis S-matrix, it is again noted that the ray pictures remain the same.

Coverage diagrams were computed for a triangular corner reflector for linear polarization and for a triangular corner reflector with a sheet of polystyrene of thickness ($\lambda/16$) on one face for circular polarization. These coverage diagrams are repeated, in part, in Figure I-3a, and the coordinate system involved is shown in Figure I-3b.[1] With reference to these coverage diagrams, it is stated in Reference 17 that:

> "The echo contours are drawn for 1 db variations in echo area relative to the maximum obtained with the unmodified triple-bounce corner. It is seen that the peak return for circularly polarized waves is about 5 db below that for linear polarizations. The 3-db down points for the circularly polarized return enclose a region approximately 40 degrees wide in azimuth and 20 degrees in climb angle. The center of this region is 15 degrees below the symmetry axis of the corner. The improvements to be obtained by use of coatings on more than one face, or several layers of different dielectric material in each coating, are under study. A special report on the polarization properties of a corner with such modifications is in preparation."

[1] In Reference 17 the coverage diagrams are drawn for 1 db variations in echo area; only "odd-numbered" db variations are shown in Figure I-3a.

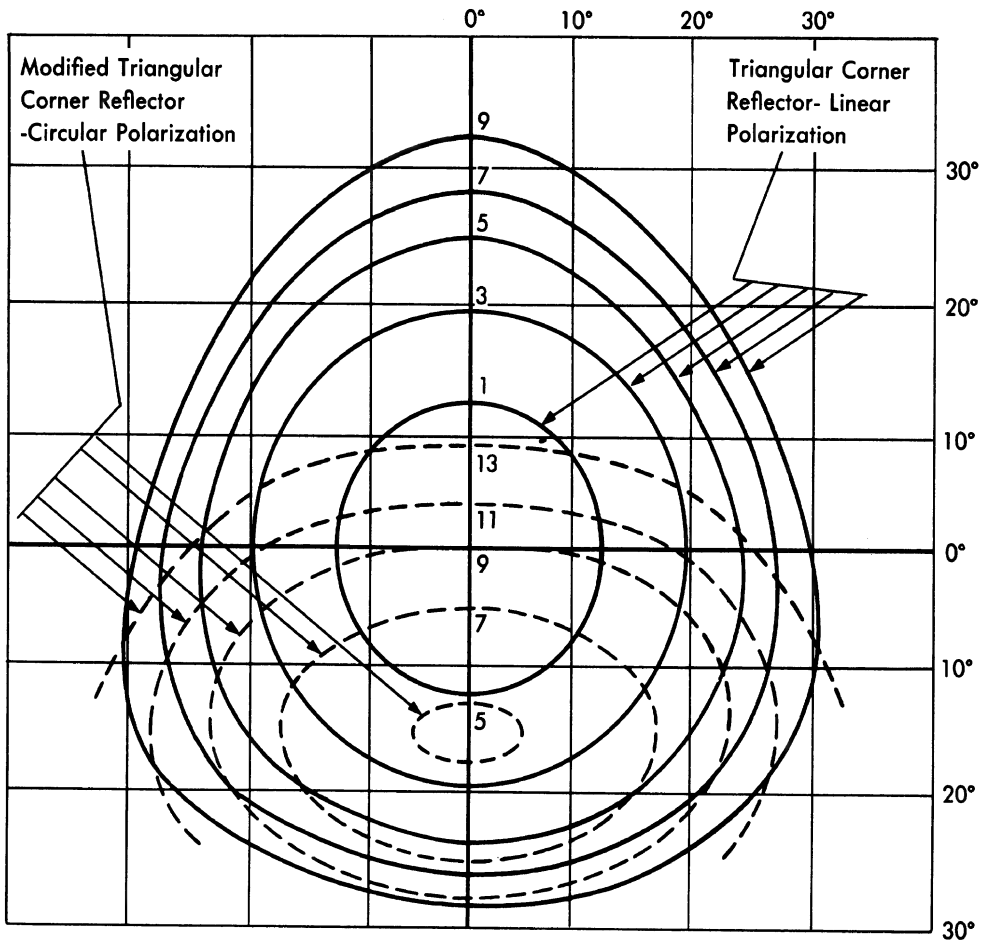

FIG. I-3a COVERAGE DIAGRAM - TRIANGULAR CORNER REFLECTOR

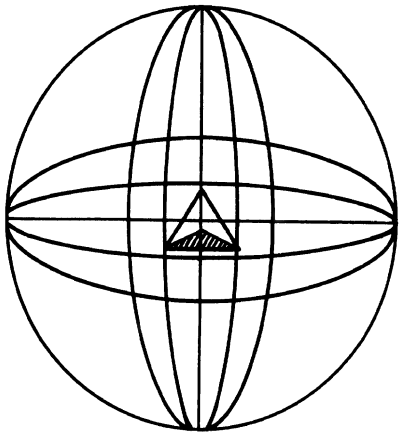

FIG. I-3b COORDINATE SYSTEM FOR COVERAGE DIAGRAMS OF FIG. I-3a

REFERENCES

Number

1. (a) RM-1080, Research Memorandum, "Electronic Countermeasures Against U. S. Air Defense: 1953-1960," Barlow, E. J., Rand Corporation (1 May 1953). SECRET

(b) RM-1090, Research Memorandum, "Electronic Countermeasures Against Air Defense Systems," Hult, J. L., Rand Corporation (1 June 1953). SECRET

(c) RM-1144, Research Memorandum, "Some Promising Counter-measures Against Enemy Air Defense Systems," Hult, J. L., and Graham, W. B., Rand Corporation (14 September 1953). SECRET

(d) RM-1176, Research Memorandum, "The Detection of Aerial Decoys by Air Defense Radars," Hult, J. L., Rand Corporation (20 December 1953). SECRET

(e) RM-1295, Research Memorandum, "Influence of Certain Offense Countermeasures on the Comparison of High and Low Altitude Capabilities of Strategic Bombers," Schamberg, R., Rand Corporation (23 April 1954). SECRET

2. 2260-1-T, "Studies in Radar Cross-Sections XV — Radar Cross-Sections of B-47 and B-52 Aircraft," Schensted, C. E., Crispin, J. W., and Siegel, K. M., University of Michigan, Engineering Research Institute (August 1954). CONFIDENTIAL

3. UMM-106, "Studies in Radar Cross-Sections VI — Cross-Sections of Corner Reflectors and Other Multiple Scatterers at Microwave Frequencies," Bonkowski, R. R., Lubitz, C. R., and Schensted, C. E., University of Michigan, Engineering Research Institute, AF 30(602)-9 (October 1953). SECRET (UNCLASSIFIED when Appendix is removed.)

REFERENCES (Continued)

4. NADC-EL-5340, "Proposed Military Specification for Triangular Corner Reflectors for Drone Aircraft," U. S. Naval Air Development Center, Bureau of Aeronautics (29 April 1953). CONFIDENTIAL

5. NRL-MR-148, "Target Drone Reflectivity Radar Characteristics Measurement and Simulation Studies," Lewis, B. L., Naval Research Laboratory Radio Division III, (13 March 1953). CONFIDENTIAL

6. 35M-967, "Monthly Progress Report for May 1954, Contract AF 30(602)-978, Lightweight Collapsible Spherical Radar Reflector," Fairchild Aircraft Corporation (10 June 1954). CONFIDENTIAL

7. "Balloon-Borne ECM," Memorandum, Headquarters Air Defense Command, Ent Air Force Base (11 April 1952). SECRET

8. ADC-SAB-52-C1, "Military Characteristics for Balloon Radar Reflectors," Department of the Air Force, Deputy Chief of Staff, Development Directorate of Requirements, (11 March 1952). SECRET

9. RM-1436, Research Memorandum, "Strategic Bombardment Campaigns and the Effects of Some Electronic Countermeasures — Abridged Edition," Rand Corporation (15 March 1955). SECRET

10. APG-SAB-28-A, "Tactical Employment of Chaff – Phase I," Eglin Air Force Base (10 July 1952). SECRET

11. 1044-1, Interim Engineering Report, "Echo Amplitude Comparisons of Chaff at 200 MC – Radar Reflectivity Measurement," Radiation, Incorporated, Contract AF 33(616)-2577 (27 April 1955). SECRET

REFERENCES (Continued)

12. AF-15, "MX-2223 Simulation Studies — Part Two," Brodwin M. E., Frey, G. W., Glaser, E. M., Smith, C. W., The Johns Hopkins University Radiation Laboratory (September 1955). SECRET

13. Project A-400, Report 4, "Analysis of Window and Related Matters," Chu, L. J., Radio Research Laboratory, Harvard University (22 October 1952). UNCLASSIFIED

14. 2260-6-T, "Studies in Radar Cross-Sections XVII - Complete Scattering Matrices and Circular Polarization Cross-Sections for the B-47 Aircraft at S-Band," Maffett, A. L., Barasch, M. L., Burdick, W. E., Goodrich, R. F., Orthwein, W. C., Schensted, C. E., and Siegel, K. M., University of Michigan, Engineering Research Institute (June 1955). CONFIDENTIAL

15. TRE-TN-170, Technical Note, "The Effect of Cross-Polarization on Radar Echoes From Aircraft, Precipitation and Land Targets at 8mms Wavelengths," Robinson, N. P., Telecommunications Research Establishment (September 1952). SECRET

16. TRE-TN-183, Technical Note, "Radar Echoes From Aircraft, Precipitation and Land Targets Illuminated by Circularly Polarized Radiation at 8mms Wavelength," Robinson, N. P., Telecommunications Research Establishment (April 1953). SECRET

17. 612-2, "Quarterly Progress Report–Polarization Dependence of Radar Echoes, Contract AF 30(635)-2811, Period ending 31 March 1955," Antenna Laboratory, The Ohio State University Research Foundation (16 March 1955). UNCLASSIFIED

18. Informal Communication, Ehrlich, Morris J., President, Microwave Radiation Company, Inc., to K. M. Siegel. UNCLASSIFIED

REFERENCES (Continued)

19. NRL-4258, "The Coherence of Radar Echoes," Boyd, F. E., Special Research Branch, Radio Division III, Naval Research Laboratory (8 December 1953). CONFIDENTIAL

20. S-10, "Detection of Propeller and Sambo Modulations," Ming-Chen, W., Uhlenbeck, G. E., Allred, C. M., et al, Massachusetts Institute of Technology (16 May 1944).

21. Hughes TM-377, "Amplitude Scintillation Spectra of Aircraft Targets," Jackob, D. M., Muchmore, R. B., and Wanlass S. D., Hughes Aircraft Company (1 August 1954). CONFIDENTIAL

22. "Radar Characteristics of Jet Exhaust Gases," Lewis B. L., Tracking Branch, Radar Division of the Naval Research Laboratory (2 December 1954).

23. Report No. 1, "Quarterly Engineering Report," Electrical Engineering Research Laboratory, The University of Texas (15 May 1955). UNCLASSIFIED

24. RM-1217, Research Memorandum, "Probability of Detection for Fluctuating Targets," Swerling, P., Rand Corporation (17 March 1954). UNCLASSIFIED

25. P-2186-12, "Fourth Quarterly Engineering Report on Research on Radar Terrain Return Theory, Instrumentation, and Techniques," The Franklin Institute (June 1951). CONFIDENTIAL

26. "The Calculation of the Echo Area of Several Scatterers of Simple Geometry by the Variational Method," Kouyoumjian, R. G., Symposium on Microwave Optics, McGill University (22-25 June 1953).

REFERENCES (Continued)

27. TR-AF-15, "MX-2223 Simulation Studies, Part One," Thomas, R. K., Smith, C., Glaser, E., Brodwin, M., Johns Hopkins University Radiation Laboratory (March 1955). SECRET

28. FZM-377, "MX-2224A Flight Test Program Report," Convair Division, General Dynamics, Contract AF 33(600)-27337 (1 February 1955). SECRET

29. TM-341, Technical Memorandum, "X-band Radar Cross-Section Measurements," Wanlass, S. D., Muchmore, R. B., Jacob, D. M., Hughes Aircraft Company (1 March 1954). CONFIDENTIAL

30. C-3460-94A/51, "Quantitative Measurements of Radar Echoes From Aircraft III—B-36 Amplitude Distributions and Aspect Dependence," Naval Research Laboratory (19 June 1951). CONFIDENTIAL

31. "Theory of Radar Reflection From Wires or Thin Metallic Strips," Van Vleck, J. H., Bloch, F., Hamermesh, M., Journal of Applied Physics, Volume 18, No. 3, pp. 274-294 (March 1947).

32. Tables of Functions, Jahnke and Emde, Dover Publishing Company (1945).

33. Informal Communication, Ehrlich, Morris J., President, Microwave Radiation Company, Inc., to K. M. Siegel (3 May 1955). SECRET

34. Methods of Theoretical Physics, Part II, Morse, P. M., Feshbach, H., McGraw-Hill Book Company, Inc. (1953).

35. UMM-134, "Studies in Radar Cross-Section XIV—Radar Cross-Section of a Ballistic Missile," Siegel, K. M., Barasch, M. L., Crispin, J. W., Schensted, C. E., Orthwein, W. C., Weil, H., University of Michigan (September 1954). SECRET

DISTRIBUTION LIST

COPY NO.	
1-2	Commander, Wright Air Development Center ATTN: WCLRE-5, R. Rawhouser Wright-Patterson Air Force Base, Ohio
3	Commander, Wright Air Development Center ATTN: WCSG, Major F. Porter Wright-Patterson Air Force Base, Ohio
4	Rheem Manufacturing Company Research and Development Laboratories ATTN: J. Joerger Downey, California
5	McDonnell Aircraft Company ATTN: G. G. McKee St. Louis, Missouri
6	Fairchild Aircraft Division ATTN: Walter Tydon Hagerstown, Maryland
7-12	Armed Services Technical Information Agency Document Service Center Knott Building Dayton 2, Ohio
13	Commander, Wright Air Development Center ATTN: WCLRC-1, G. W. Schivley Wright-Patterson Air Force Base, Ohio
14	Commander, Wright Air Development Center ATTN: WCLGB, A. L. Brothers Wright-Patterson Air Force Base, Ohio
15	Commander, Wright Air Development Center ATTN: WCOSI Wright-Patterson Air Force Base, Ohio
16	Commander, Wright Air Development Center ATTN: WCSB, J. S. McCollom Wright-Patterson Air Force Base, Ohio
17	Commander, Wright Air Development Center ATTN: WCSM, P. R. Doty Wright-Patterson Air Force Base, Ohio

DISTRIBUTION LIST (Continued)

COPY NO.	
18	Commander, Wright Air Development Center ATTN: WCSM, J. A. Walker Wright-Patterson Air Force Base, Ohio
19	Commander, Wright Air Development Center ATTN: WCSM, J. R. Korosei Wright-Patterson Air Force Base, Ohio
20	Commander, Wright Air Development Center ATTN: WCSP, E. B. Bell Wright-Patterson Air Force Base, Ohio
21	Commander, Air Materiel Command ATTN: ATIAE, R. L. James Wright-Patterson Air Force Base, Ohio
22	Commander, Wright Air Development Center ATTN: WCLRO, Major G. J. Akerland Aircraft Radiation Laboratory Wright-Patterson Air Force Base, Ohio
23	Commander, Wright Air Development Center ATTN: WCLRD, G. B. Fanning Wright-Patterson Air Force Base, Ohio
24	Director of Research and Development Headquarters, USAF ATTN: AF-DRD-EL Washington 25, D. C.
25	Commander, Air Research and Development Command ATTN: RDDE, Major D. L. Deal P. O. Box 1395, Baltimore 3, Maryland
26	Commander Rome Air Development Center ATTN: Research Library, RCRES-4C Griffiss Air Force Base, Rome, New York
27	Commander, U. S. Naval Air Missile Test Center ATTN: L. S. Marquardt Point Mugu, California
28	Commander, Air Force Cambridge Research Center ATTN: CRRDG, Ralph Hiatt L. G. Hanscom Field, Bedford, Massachusetts
29	Commander, Air Force Cambridge Research Center ATTN: Electronics Research Library L. G. Hanscom Field, Bedford, Massachusetts

DISTRIBUTION LIST (Continued)

COPY NO.	
30	Commander, U. S. Naval Air Missile Test Center ATTN: Stanley R. Radom Point Mugu, California
31	Commander, Air Force Cambridge Research Center ATTN: CRRDG, Nelson A. Logan L. G. Hanscom Field, Bedford, Massachusetts
32	Commander, Air Force Cambridge Research Center ATTN: CRRDG, C. J. Sletten L. G. Hanscom Field, Bedford, Massachusetts
33	Commander, Air Force Cambridge Research Center ATTN: CRRDA, R. M. Barrett L. G. Hanscom Field, Bedford, Massachusetts
34	Commander, Air Force Missile Test Center ATTN: A. R. Beach Patrick Air Force Base, Cocoa, Florida
35	Commander, Holloman Air Development Center ATTN: Operation and Project Center Alamogordo, New Mexico
36	Research and Development Board, Library Branch Information Offices ATTN: W. H. Plant RE. E1065, The Pentagon Washington 25, D. C.
37	Commander, Rome Air Development Center ATTN: RCECC-1, Louis F. Moses Griffiss Air Force Base, Rome, New York
38	Commander, Air Force Armament Center ATTN: A. J. Wilde Eglin Air Force Base, Florida
39	Commander, Air Proving Ground Command ATTN: Class. Tech. Data Br. D/01 Eglin Air Force Base, Florida
40	Commander, Strategic Air Command ATTN: Operations Analysis Office Offutt Air Force Base, Nebraska
41	Commander, Headquarters Central Air Defense Force Post Office Box 528 Kansas City, Missouri

DISTRIBUTION LIST (Continued)

COPY NO.	
42	Director, Air University Req. CR-3998 Maxwell Air Force Base, Alabama
43	Commander, Rome Air Development Center ATTN: RCER, Morris Handlesman Griffiss Air Force Base, Rome, New York
44	Commander, Rome Air Development Center ATTN: RCDE, Joseph Vogelman Griffiss Air Force Base, Rome, New York
45	Dr. George Adomian, Member Special Studies Group Analysis and Planning Section, Systems Laboratories Hughes Aircraft Company, Culver City, California
46	Director, Naval Research Laboratory ATTN: John E. Meade, Code 5340 Washington 25, D. C.
47	Director, Naval Research Laboratory ATTN: W. S. Ament, Code 5278 Washington 25, D. C.
48	Chief, Bureau of Ships, Department of the Navy ATTN: Code 816 Washington 25, D. C.
49	Chief, Bureau of Aeronautics, Department of the Navy ATTN: Electronics Division Washington 25, D. C.
50	Bureau of Aeronautics, Central District ATTN: Electronics Division Wright-Patterson Air Force Base, Ohio
51	Chief, Bureau of Ordnance, Department of the Navy ATTN: Code AD-3 Washington 25, D. C.
52	Chief of Naval Operations, Department of the Navy ATTN: OP-42-B2 Washington 25, D. C.
53	Commanding Officer and Director U. S. Navy Electronics Laboratory San Diego 52, California
54	Commander, U. S. Naval Air Development Center ATTN: Electronics Laboratory Johnsville, Pennsylvania

DISTRIBUTION LIST (Continued)

COPY NO.	
55	Commander, U. S. Naval Ordnance Laboratory Silver Spring 19, Maryland
56	Commander, U. S. Naval Ordnance Test Station, Inyokern China Lake, California
57	Commander, Rome Air Development Center ATTN: Harry Davis, Technical Director - RCT Griffiss Air Force Base, Rome, New York
58	Chief Signal Officer, Department of the Army ATTN: Engineering Technical Division Washington 25, D. C.
59	Department of the Army, Office of Chief of Ordnance ATTN: ORDTU, Capt. W. O. Fuller Washington 25, D. C.
60	Massachusetts Institute of Technology Project Lincoln, Lincoln Laboratory ATTN: V. A. Nedzel Post Office Box 73, Lexington 73, Massachusetts
61	Hughes Aircraft Company Research and Development Laboratories ATTN: C. H. Wilcox Culver City, California
62	Cornell Aeronautical Laboratory, Incorporated ATTN: R. Kell Buffalo, New York
63	Commander, Signal Engineering Laboratory ATTN: Technical Documents Center Fort Monmouth, New Jersey
64	Cornell Aeronautical Laboratory, Incorporated ATTN: George Richmond Buffalo, New York
65	Document Room, Project Lincoln Massachusetts Institute of Technology ATTN: Ethel R. Brans P. O. Box 390, Cambridge 39, Massachusetts
66	Massachusetts Institute of Technology ATTN: Dr. Dan Dustin, Lincoln Laboratory P. O. Box 73, Lexington 73, Massachusetts

DISTRIBUTION LIST (Continued)

COPY NO.	
67	Massachusetts Institute of Technology ATTN: I. Shapiro, Lincoln Laboratory P. O. Box 73, Lexington 73, Massachusetts
68	Commander, Air Defense Command ATTN: Major Richard J. Lloyd Colorado Springs, Colorado
69	Ohio State University Research Foundation ATTN: Dr. A. Fouty 310 Administration Building, Ohio State University Columbus 10, Ohio
70	Radiation, Incorporated ATTN: M. Cox Melbourne, Florida
71	The University of Texas Electrical Engineering Research Laboratory ATTN: Dr. A. W. Straiton Box 8026, University Station, Austin 12, Texas
72	Franklin Institute Laboratories 20th St. Benjamin Franklin Parkway ATTN: Dr. S. Charp Philadelphia 3, Pennsylvania
73	Boeing Airplane Company ATTN: R. H. Jewett Seattle 14, Washington
74	Hughes Aircraft Company Research and Development Laboratories ATTN: M. D. Adcock Culver City, California
75	Hughes Aircraft Company Research and Development Laboratories ATTN: Dr. L. L. Bailin Culver City, California
76	Hughes Aircraft Company Research and Development Laboratories ATTN: Dr. N. Begovich Culver City, California
77	Hughes Aircraft Company Research and Development Laboratories ATTN: R. S. Wehmer Culver City, California

DISTRIBUTION LIST (Continued)

COPY NO.	
78	The Rand Corporation ATTN: Dr. John L. Hult 1500 4th Street, Santa Monica, California
79	The Rand Corporation ATTN: Dr. Sidney Bertram, Electronics Division 1500 4th Street, Santa Monica, California
80	Ramo-Wooldridge Corporation ATTN: Dr. F. S. Manov 8820 Bellanca Ave., Los Angeles 45, California
81	Stanford University ATTN: Professor L. I. Schiff, Physics Department Palo Alto, California
82	University of Tennessee ATTN: Professor F. V. Schultz Knoxville 16, Tennessee
83	University of California ATTN: Professor Samuel Silver Electrical Engineering Department Berkeley 4, California
84	Philco Radio Corporation ATTN: B. D. Steinberg--Project Engineer Philadelphia 34, Pennsylvania
85	Electronics Defense Laboratory ATTN: Dr. V. Twersky P. O. Box 205, Mountain View, California
86	Bell Telephone Laboratory ATTN: Dr. Allen B. Currie Whippany, New Jersey
87	Ramo-Wooldridge Corporation ATTN: Dr. S. Ramo 8820 Bellanca Ave., Los Angeles 45, California
88	Ramo-Wooldridge Corporation ATTN: Dr. A. D. Wheelon 8820 Bellanca Ave., Los Angeles 45, California
89	Cornell Aeronautical Laboratory, Incorporated ATTN: Dr. Robert A. Wolf Buffalo, New York

DISTRIBUTION LIST (Continued)

COPY NO.	
90	Georgia Institute of Technology State Engineering Experimental Station Atlanta, Georgia
91	Standard Rolling Mills, Incorporated ATTN: Vincent Lane 196 Diamond Street, Brooklyn 22, New York
92	The Johns Hopkins University ATTN: Dr. D. D. King--Radiation Laboratory 1315 St. Paul Street, Baltimore, Maryland
93	The Johns Hopkins University ATTN: E. M. Glaser--Radiation Laboratory 1315 St. Paul Street, Baltimore, Maryland
94	Massachusetts Institute of Technology Research Laboratory of Electronics ATTN: Dr. L. J. Chu Cambridge, Massachusetts
95	Lockheed Missile System Division, Dept. 75-31 7701 Woodley Ave., Van Nuys, California
96	Ryan Aeronautical Company ATTN: J. R. Giantvalley Lindbergh Field, San Diego 12, California
97	Convair, A Division of General Dynamics Corporation ATTN: Orison Wade--Engineering Department San Diego, California
98	Operational Research Group ATTN: G. R. Lindsay Defense Research Board Ottawa, Ontario, Canada
99	McGill University ATTN: Professor G. A. Woonton Eaton Electronics Laboratory Montreal, Quebec, Canada
100	Sylvania Engineering Laboratory ATTN: Dr. L. S. Scheingold 70 Forsythe Street, Boston, Massachusetts
101	William R. Hutchins Raytheon Manufacturing Company Missile and Radar Division Hartwell Road Bedford, Massachusetts

DISTRIBUTION LIST (Continued)

COPY NO.

102 Dr. R. S. Elliott
Research and Development Laboratories
Hughes Aircraft Company
Culver City, California